THESIS FOR THE DEGREE OF LICENTIATE OF ENGINEERING

Combined Electrical Power Generation using Solar and Wind

Ingemar Mathiasson

Department of Electrical Engineering
Division of Electric Power Engineering
CHALMERS UNIVERSITY OF TECHNOLOGY
Göteborg, Sweden 2017

Combined Electrical Power Generation using Solar and Wind
Ingemar Mathiasson

© Ingemar Mathiasson, 2017.

Licentiate Thesis at Chalmers University of Technology

Department of Electrical Engineering
Division of Electric Power Engineering
Chalmers University of Technology
SE-412 96 Göteborg
Sweden
Telephone + 46 (0)31-772 1000

Printed by Chalmers Reproservice
Göteborg, Sweden, 2017

To my daughter Kristina

Combined Electrical Power Generation using Solar and Wind
Ingemar Mathiasson
Department of Electrical Engineering
Division of Electric Power Engineering
Chalmers University of Technology

ABSTRACT

The need for systems for renewable electrical power production is enormous worldwide.This applies to systems of varying size and capacity. From small systems for household purposes up to large systems for regional purposes. If possible, all systems should be linked in a common power grid. From an efficiency perspective, it is also an advantage if a specific power system can be designed for so-called island operation. This means that the present system has the capacity to provide power to its nearest surroundings. An important benefit of island operation is the increased possibility of, by appropriate supervision, evenly distributing the joint production to the overall power grid. It increases the ability to avoid overloading in some power systems. An island system can be equipped with an energy storage or an auxiliary device in the form of for example a diesel generator.

This thesis deals with the analysis of a combined electrical power system for production of wind power and solar power. The total system consists of solar- and wind power generators, energy storage, power back-up and power grids in the form of a local grid and utility grid. The utility grid can be used for export of excess energy or import of deficit energy. The analysis is based on simulation using statistical models regarding solar radiation, wind speed and electrical loads. The solar radiation is calculated as a result of atmospheric transmission, geographic location, time of year and time of day. The atmospheric transmittance has been calculated using the “extinction coefficient”, a parameter which is a function of absorbing molecules and aerosols in the atmosphere. It has been demonstrated that this parameter is a powerful tool in connection with the analysis of the power system that utilizes solar energy. This parameter has in this work a central function in all calculations of solar radiation. The extinction coefficients in existing simulation model is based on performed measurements. However, these parameters can easily be calculated by special software. In this case with atmospheric parameters as input parameters. This has been demonstrated in the work. In the same way the statistical models of wind speed and electrical loads are results of performed measurements. The outputs from simulations are given in the form of statistical parameters. This means that

simulation results are presented in statistical form regarding the combination of wind generators, solar generators, energy storage, power back-up and electrical loads.

The current work has touched on several key issues relating to analysis of power generation using wind and sun. A number of interesting observations made have been noted. As an example of these are the use of the above-mentioned "extinction coefficient" parameter.

The work has contributed to the availability of an effective tool for statistical analysis of various combined power systems with a wide range of applications. The calculation routine used for calculating the effective solar radiation that drives solar power plants has proven to be well established in both practice and theory. The calculation routine in question allows excellent opportunities for detailed analysis regarding the planning of future solar systems. The simulation model has been applied in the work to a large number of cases.

Keywords: Wind turbine, solar cell, silicon solar cell, quantum dots, energy storage, extinction coefficient, atmospheric transmittance, wave length bands, wind speed, electrical load.

Acknowledgements

I want to thank my examiner and supervisor, Prof. Ola Carlson for many interesting conversations and much good advices during the implementation of this work. I want to thank Prof. Tore Undeland for all support and comments. I also want to thank Magnus Ellsén, Robert Karlsson and Aleksander Bartnicki for all their help with the experimental work. I am very grateful to Lars Viksten at Fortum, for all his help in getting access to useful test sites in order to perform the measurements of electrical loads.

Contents

CHAPTER 1

INTRODUCTION

The need for systems for renewable electrical power production is enormous worldwide. This applies to systems of varying size and capacity. From small systems for household purposes up to large systems for regional purposes. If possible, all systems should be linked to a common power grid.
From an efficiency perspective, it is an advantage if a specific power system can be designed for so-called island operation. This means that the system has the capacity to provide power to its nearest surroundings.
An important benefit of island operation is the increased possibility of, by appropriate supervision, evenly distributing the joint production to the overall power grid. It increases the ability to avoid overloading in some power systems.
Another advantage of the opportunity for island operation is the reduced vulnerability in event of any interruption in the public grid.
An island system can be equipped with an energy storage or an auxiliary device in the form of for example a diesel generator.

An interesting option for energy storage is to utilize the storage capacity of electric vehicles. In [50] an example of this on a large scale relating to California. Presuming current annual growth of electric vehicles, California will have 1.7 million electric vehicles by the year 2022. This is equivalent to 8% of California's total passenger vehicle fleet. If these electric vehicles are connected to the grid, when they are not used, the resulting energy storage capacity is enough to use solar and wind to replace all existing coal and nuclear power plants. This example can of course be applied on a smaller scale to provide energy storage for island operation.

A variety of studies relating to combined power systems has been performed. An essential conclusion for the future, pointed out in these studies, is the need to move the infrastructure from large power producing units to grid structures, where the power is produced closer to the location of consumption. [70] gives an overview of such systems with examples of activities around the world. [71] illustrates with Denmark as an example, the development from central to decentralized power production. The document discusses trends of the future grid infrastructure and the most emerging renewable energy sources, wind energy and photovoltaics.

The present thesis deals with a simulation system for detailed analysis of a power system consisting of a combination of solar power, wind power, energy storage and back-up generator. The system is built up as a local unit with local electrical power

consumers and is connected to the utility grid to provide the facility to export/import power.

The intention of the model is to show the potential of systems consisting of renewable energy sources. The systems can be entirely stand alone or connected to utility grids. The model provides the possibility of statistical analysis. This means that basic information that is statistics related such as weather data and electrical consumption data are treated in a statistical manner.

The simulation system is built up by statistical models relating to solar radiation, wind speed and electrical loads. The solar radiation is calculated as a result of atmospheric transmission, cloudiness, geographic location, time of year and time of day. The atmospheric transmission is calculated by using the “extinction coefficient” parameter, that is a result of absorbing molecules and aerosols in the atmosphere. The present statistical model of this parameter has been developed from measurement data. Similarly the statistical models of wind speed and electrical loads are results of performed measurements.
The outputs from simulations are given in the form of statistical parameters. This means that simulation results are presented in statistical form regarding the combination of wind generators, solar generators, energy storage, power back-up and electrical loads.

The simulation system uses two statistical key parameters related to the weather, namely wind speed and cloudiness. Both these parameters are input data to the respective sub module. The modules are developed on the basis of experience from performed measurements.

The wind modul uses input information in the form of “season” or “total year”. Based on this, the program module simulates corresponding statistical wind data.

The module that treats the condition of cloudiness, uses input information in the form of estimated “percentage of cloudiness”. In addition to this input information in the form of “geographical location” and "time of the year" is needed. As a result of this, the program module simulates corresponding statistical solar radiation.

The electrical consumption is treated in a separate sub module, that uses information about “annual power consumption” and type of load. Four categories of load have been modelled: “Industrial area”, “commercial centre”, “residential area” and a “mixture” of these three. The module is developed on the basis of experience from performed measurements.

The thesis describes the simulation system with references to a specific defined combined power system. Two chapters are focused on the basic questions around a combined electrical power system with respect to the principle of the simulation system. Separate chapters focus on the specific simulation modules that handle the extinction coefficient, the wind speed and the electrical power consumption including the development work of these modules.

The simulation system is built up on basis of a flexible module structure. This implies that the system can easily be adapted for an efficient analysis of a combination of a large number of interconnected individually combined power systems into a common larger grid combination. This has been discussed in the thesis in a separate chapter.

Since the solar power production is dependent on the solar cell angles relative to south and zenith, a special chapter is dedicated to this topic. This chapter also deals with the facility for so called “solar tracking”, which is an automatic positioning of the solar cells relative to optimal angles.

Since the intention of the model is to provide an effective tool for statistical analysis of a combined power system, two chapters are focused on this. One chapter describes an analysis of a small power system, intended for single house usage. One chapter deals with the analysis of larger power systems, in different locations, namely Kiruna and Göteborg in Sweden, München in Germany, Malaga in Spain and Nairobi in Kenya. One part of this chapter also deals with the economic aspects.

One chapter in the thesis is focused on the analysis of a small solar power plant intended for household usage. Results from simulations are compared with corresponding measurements.

One chapter is specifically focused on theoretical analysis of some important issues regarding solar power production. A major reason for this part of the thesis is to demonstrate by theoretical analysis the efficiency of the used computational methodology relating to solar radiation in combination with solar cells. This applies particularly in the usage of the parameter extinction coefficient. Another important reason is to identify potential areas for further studies. Among these studies are theoretical calculations of solar radiation, which are dealt with in this part of the thesis.

The presented work shall be regarded as part of a system study. This means that no details regarding, for example, power electronics are involved in the present simulation system. In the chapter about future work, a proposal for an expanded simulation system is described. With this expanded system, it is possible to analyse more detailed functions, e.g. features of power electronics and maximum power point (MPP) tracking.

The current simulation system is consistently developed in Matlab.

1.1 Purpose and contribution

This work is focused on statistical analysis of combined power systems. The systems shall include energy generation in the form of wind power and

photovoltaic power, local electrical load, energy storage and power back-up. The systems shall be able to be connected to the utility grid for energy balance. The purpose and contribution of the work can briefly be summarised as follows:

Purpose of work.

The overall aim of this work is to show the possibility of using a power system with renewable power production. Two main tasks can be defined as:

1. Development of a simulation model for statistical analysis of combined power systems.

2. Development of a calculation routine for statistical calculation of the effective solar radiation that drives a photovoltaic power system. The calculation routine shall be a part of the simulation model.

Contribution of work.

The work has contributed to the availability of an effective tool for statistical analysis of various combined power systems with a wide range of applications. The calculation routine used for calculating the effective solar radiation that drives solar power plants have proven to be well established in both practice and theory. The calculation routine in question allows excellent opportunities for detailed analysis regarding the planning of future solar systems. The simulation model has been applied to a large number of cases.

1.2 Outline of thesis

The thesis is organised as follows:

Chapter 2: Combined Electrical Power System. An overview of a combined power system is given.

Chapter 3: Simulation System. The simulation system is described. Relation to Combined Electrical Power System, described in chapter 2 is given.

Chapter 4: Extinction Coefficient. The extinction coefficient parameter is described. Performed measurements, analysis of measurements and the statistical model of the parameter in combination with cloudiness are described.

Chapter 5: Wind Speed. Performed measurements, analysis of measurements and the statistical model of wind speed are described.

Chapter 6: Electrical Load. Performed measurements, analysis of measurements and statistical models are described.

Chapter 7: Optimum Angle Relative to Zenith and South. Solar Tracking. The simulation model is used to analyse the impact of solar cell direction relative to zenith and south. Solar tracking is studied.

Chapter 8: Small Combined Solar and Wind Power Systems. The simulation model is used to analyse a combined power system intended for use in a private household.

Chapter 9: Large Combined Solar and Wind Power Systems. The simulation model is used to analyse larger power systems in different locations.

Chapter 10: Analysis of a solar power system for household usage. The simulation model is used to analyse a solar power system for household usage. The simulation results are compared with corresponding results regarding measured annual energy production.

Chapter 11: Solar power. Basic analysis. Theoretical analysis is performed in relation to some fundamental topics regarding solar power.

Chapter 12: Interconnection of a number of combined power systems. A combination of a large number of interconnected individually combined power systems into a common larger grid is described.

Chapter 13: Summary of chapter 2 to chapter 12. Summary of the work with references to different chapters.

Chapter 14: Conclusion. A conclusion of the work is given.

Chapter 15: Future Work. Future activities are proposed.

References: Publications with focus on the performed studies are listed.

Appendix A: Calculation of Solar Position. The algorithms used for calculation of solar position in the sky are presented.

1.3 List of publications

Ellsén M, Mathiasson I, Carlson Ola. “Series and Parallel Compensation for the Permanent Magnet Synchronous Generator at Chalmers Test Wind Turbine”. NORDIC WIND POWER CONFERENCE, 2006.

Mathiasson I, Carlson O. ”Prediction of solar power by using the extinction coefficient”. 5th Solar Integration Workshop, International Workshop on Integration of Solar Power into Power Systems, 2015.

CHAPTER 2

COMBINED ELECTRICAL POWER SYSTEM

Fig. 2.1 shows the main components in a Combined Electrical Power System with wind and solar as power sources. The system is adapted for connection to an external power grid. One advantage of such an arrangement is a reduced need for back-up generators (e.g. diesel generator). With this arrangement any surplus energy can be exported in a simple way.

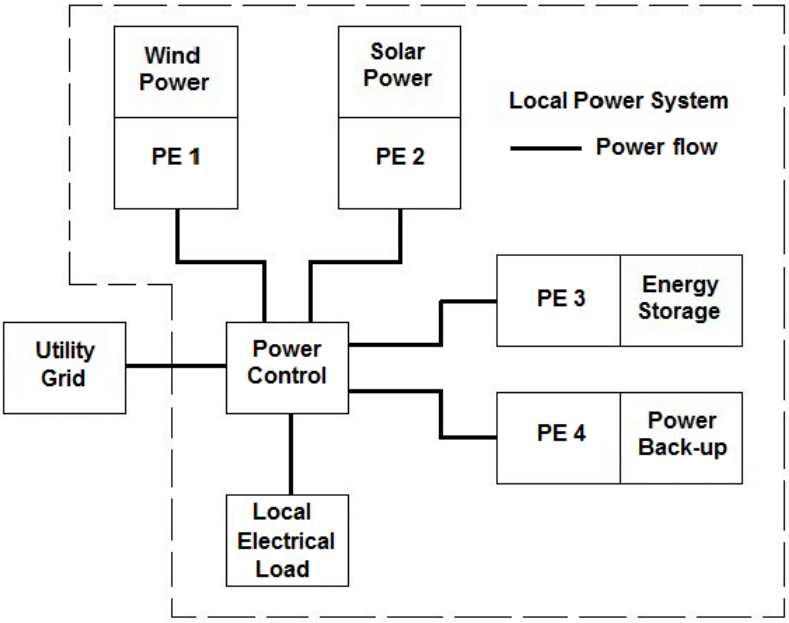

Fig. 2.1 The main components in the Combined Power System. The Local Power System is connected to a utility grid.

Subsystems in Combined Power System are:

Wind Power: Wind power plant.

Solar Power: Solar power plant.

Power Control: Control unit to manage the power flow.

Utility Grid: Utility power grid with facility to handle situations of energy deficit and energy surplus.

Energy Storage: Energy storage device with two purposes: 1) To store surplus energy. 2) To supply energy to the electrical local load to meet an energy deficit.

Power Back-up: Power back-up device e.g. diesel generator.

Local Electrical Load: Local electrical load (active and reactive).

PE 1 – PE 4: Power electronics for electrical adaptation.

2.1 Wind Power

The wind power plant consists of a number of wind power turbines, where the turbines are supposed to be identical regarding technical performance and installation in terms of wind conditions.

Produced power from the plant is:

$$P_F = P_S \times N_T \quad (2.1)$$

Where:

P_F: Produced power from plant
P_S: Produced power from single turbine
N_T: Number of wind power turbines

See Fig. 2.2

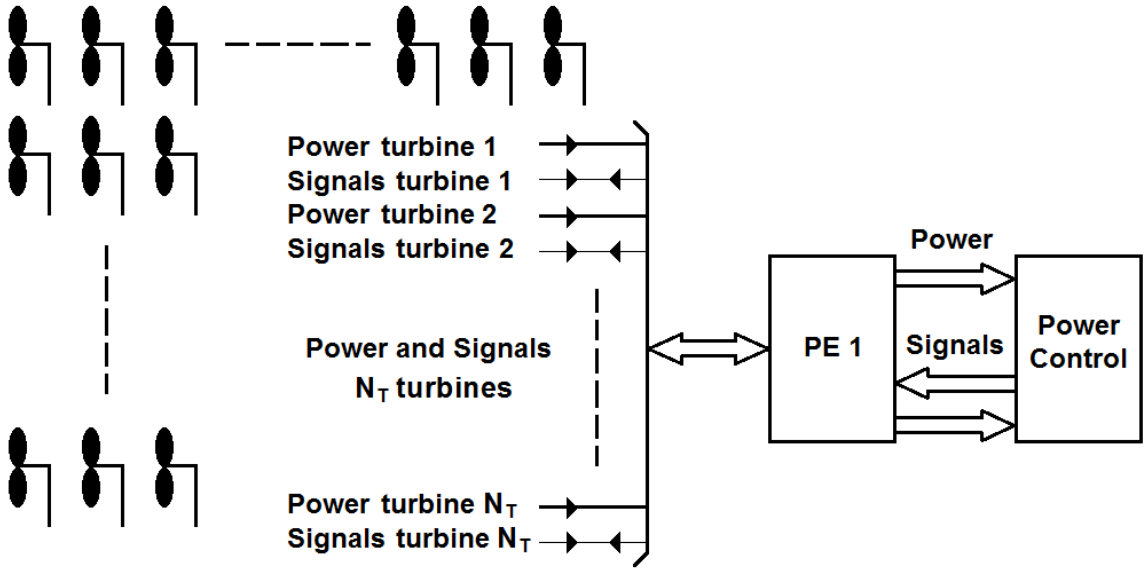

Fig. 2.2. The wind power plant with N_T turbines. The turbines are identical in relation to technical performance and installation regarding wind conditions.

The single turbine is defined by the following parameters:

- Rotation axis, height above sea level
- Rotation blade, diameter
- Rotation blade, maximum rotation speed
- Rotation blade, minimum rotation speed
- Maximum produced power
- Total power efficiency
- Power factor regarding reactive power (phase angle)
- Air temperature
- Air pressure
- Wind speed specification in the form of statistical parameters
- Information regarding power coefficient C_P

Two kinds of wind power turbines are discussed in this work:

- Variable speed controlled turbines
- Aerodynamic stall controlled turbines

The variable speed controlled turbines have been focused on usage in larger power farms, while aerodynamic stall controlled turbines have been focused on usage in smaller systems.

2.1.1 Variable speed controlled turbines. Reference turbine

Chalmers wind power system at Hönö, outside Göteborg with PM-generator "Morley 27/48/1" has been used as reference regarding the principle for systems with variable speed controlled turbines.

A theoretical analysis of the wind power turbine is described in [11] and [12]. These works deal with technical investigations of the wind power system. The works have different goals:

- To increase the theoretical knowledge about some important electromagnetic phenomena e.g. demagnetization, the airgap dependence, the harmonic properties of the coil current and the coil inductance
- To evaluate possibilities of increasing the active power by increasing the coil current
- Reactive power compensation (series and parallel compensation)

See section 3.3.1 regarding simulation of corresponding systems.

2.1.2 Aerodynamic stall controlled turbines. Reference turbine

The wind power turbine "Skystream 3.7", manufactured by Xzeres, USA, has been used as reference regarding the principle for systems with aerodynamic stall controlled turbines.

For more information regarding "Skystream 3.7", see [22] and [23].

See section 3.3.2 regarding simulation of corresponding systems.

2.2 Solar Power

The solar power plant consists of a number of solar cell panels. The power plant can be equipped with so called “sun tracking”. This means that the panels follow the direction of the Sun automatically.

Produced power from the plant is:

$$Ps = G \times A \times Pfs \quad (2.2)$$

$$Pfs = Pf1 \times Pf2 \times Pf3 \quad (2.3)$$

where:

Ps: Generated active solar power (W)
G: Effective incoming solar irradiation (W/m^2)
A: Total solar cell area (m^2) of the plant
Pfs: Power efficiency
Pf1: Solar cell efficiency
Pf2: Maximum Power Point (MPP) efficiency. MPP is the position in the solar cell voltage/current characteristic, where the product voltage × current is maximized.
Pf3: Power electronics efficiency

Fig. 2.3 illustrates a solar power plant with 9 solar cell panels. Each solar cell panel is individually connected to PE 2. This can vary between different power plants. In some cases, it may be preferable to connect all, or some, panels in series regarding the power.

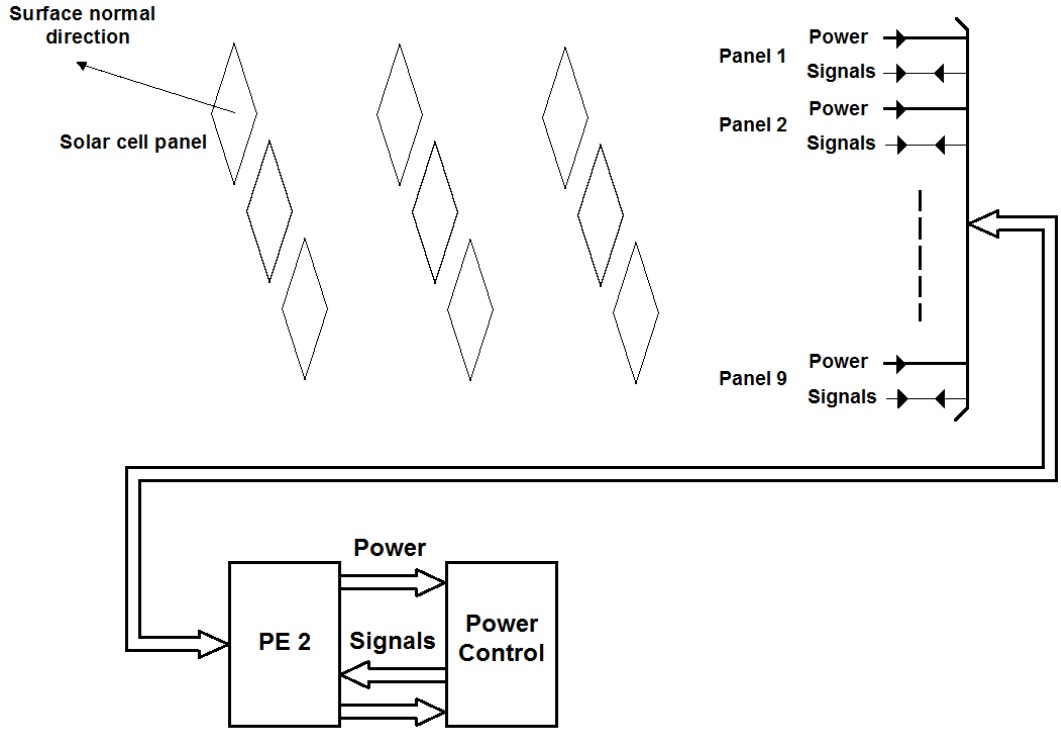

Fig. 2.3. An example of a solar power plant with 9 solar cell panels.

Fig. 2.4 and Fig. 2.5 define the surface normal direction of the solar cell panel relative to zenith and to south respectively.

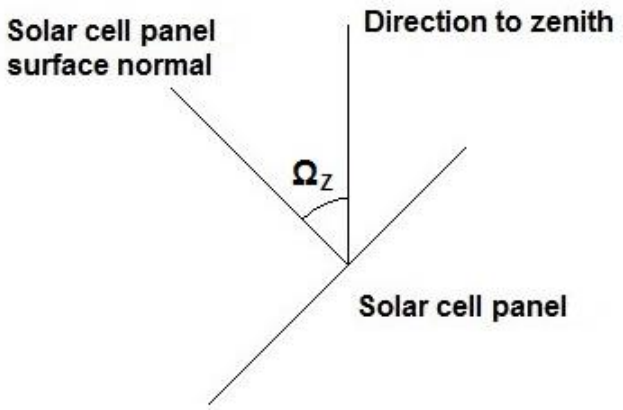

Fig. 2.4. Solar cell panel. Surface normal direction relative to zenith.

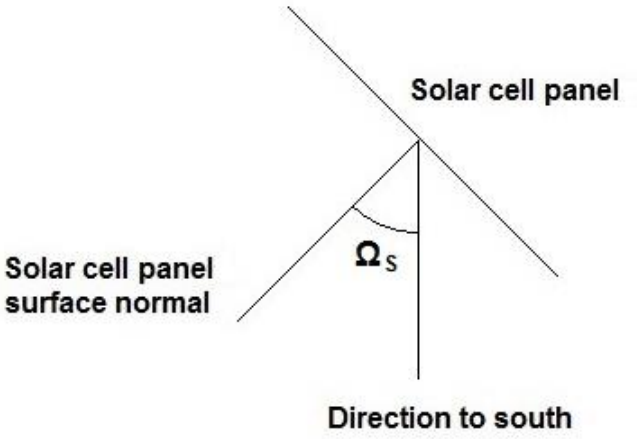

Fig. 2.5. Solar cell panel. Surface normal direction relative to south.

The solar power plant is defined by the following parameters:

- Total solar cell area of the plant
- Power electronics efficiency
- Solar cell efficiency
- Maximum Power Point (MPP) efficiency. MPP is the position in the solar cell voltage/current characteristic, where the product voltage × current is maximized
- Power factor regarding reactive power (phase angle)
- Any sun tracking
- Surface normal direction of the solar cell panels relative to zenith (if there is no sun tracking)

- Surface normal direction of the solar cell panels relative to south (if there is no sun tracking)
- Geographical location
  - Latitude
  - Longitude
- Masking effects against sun radiation

Abundant materials concerning background and application regarding solar energy can be found in, for example, [16] and [17].

2.3 Power Control

The Power Control unit manage the power flow in the power system. Fig. 2.6 shows the power flow and signal flow between Power Control unit and the power electronic units PE 1 – PE 4. The arrows show the power and the signal directions.

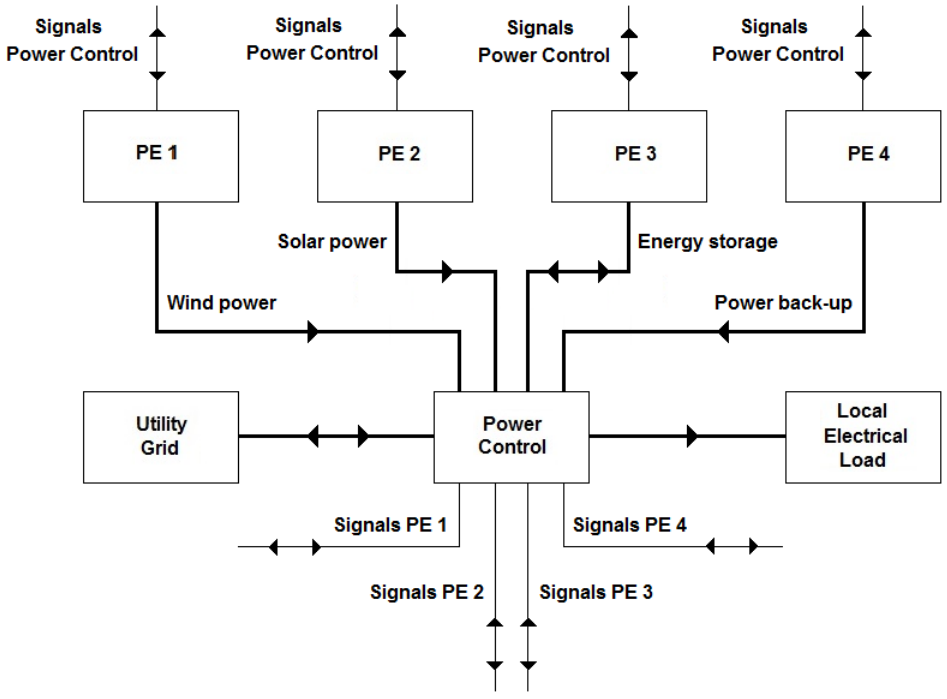

Fig. 2.6. Power Control unit.

2.4 Utility grid

The Utility grid represents an external grid, with the possibility to balance the electrical power in the Local Power System. This means that the Local Power System can export power excess or import power deficit to/from the Utility grid.

2.5 Energy storage

The Energy storage unit represents a power unit with the possibility to balance the electrical power in the Local Power System. The storage can be one of a variety of types, e.g.:

- Battery storage
- Water reservoir (large container or lake)
- Hydrogen

The storage capacity has been defined by parameter “ESC rel” according to:

$$\text{DCE} = \frac{\text{ACE}}{365} \tag{2.4}$$

$$\text{ESC rel} = \frac{\text{ESC abs}}{\text{DCE}} \tag{2.5}$$

Where:

DCE: Mean daily consumed energy from Local Electrical Load (kWh/day)
365: Corresponds to number of days per year
ACE : Annual consumed energy from Local Electrical Load (kWh)
ESC abs: Storage capacity (kWh)
ESC rel: Storage capacity in relation to daily energy consumption

2.6 Power back-up

The Power back-up is an auxiliary unit to be used in case of power deficit. This is typically a diesel generator.

2.7 Electrical load

Four types of power consumers can be used:

- Industrial area
- Residential area
- Commercial centre
- A mix of the consumers above

The loads are specified by the annual electrical power consumption in question. The configurations are described in chapter 6.

2.8 Power electronics

The Power electronics are used for electrical adaptation. In addition to power electronics in the Power Control unit, the following additional devices are defined:

- PE 1. Adaptation between wind power plant and Power Control unit
- PE 2. Adaptation between solar power plant and Power Control unit
- PE 3. Adaptation between Energy storage and Power Control unit
- PE 4. Adaptation between Power back-up unit and Power Control unit

Control and monitoring are performed via signals between PE 1 – PE 4 and Power Control unit.

2.9 The designation “Combined electrical power system”

A combined electrical power system can be designed in different ways and with varying purposes. However, the designations “Combined electrical power system”, or “Combined power system”, refer in this document to the configuration as is described above, which is based on Fig. 2.1.

Note: The “Combined electrical power system” includes the connection between “Utility grid” and “Local power system”. See Fig. 2.1.

CHAPTER 3

SIMULATION SYSTEM

The main purpose of the simulation system, is to facilitate the analysis of a combined power system and to provide quantitative design parameters of key components in the power system. Important elements in this analysis are the statistical treatments of three essential components: incoming solar radiation, wind speed, and the electrical power consumed. The analysis consists of evaluation of the resulted combination of fixed defined parameters, such as properties of wind turbines and solar cells, and statistical properties of wind speed, solar radiation and consumed power.

The simulation system consists of 10 modules according to Table 3.1. The relations between these modules and components in the combined system are listed in Table 3.4, section 3.11.

Table 3.1. Simulation system. Modules.

System Modules	Function
Main program	Control of simulation processes
Wind_make	Stochastic wind speed
Wind_turbine	Electrical wind power
Extinction_make	Stochastic extinction coefficients
Sun_intensity	Solar irradiation
Sun_panel_generator	Electrical solar power
Load_make	Stochastic load
Connect_gen_load	Control of electrical power balance
Storage_distribution	Control of electrical power balance
Power_evaluate	Simulation evaluation

The simulation flowchart is illustrated in Fig. 3.1. The loop is repeated “N” times. Evaluation of the simulation is presented in the form of statistical parameters. To achieve good statistical significance of the final result, “N” should be at least in the order of 100.

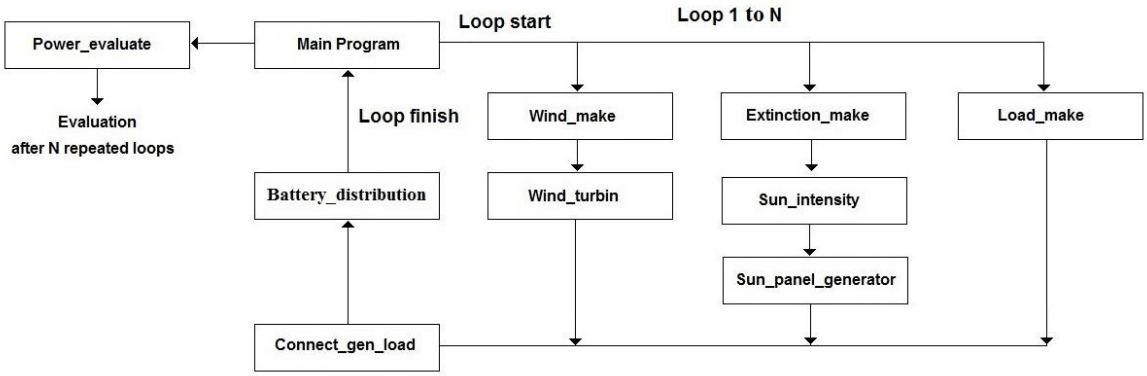

Fig. 3.1. Simulation flowchart. The loop is repeated “N” times.

For more detailed descriptions of the simulation model and simulation applications, see [1] - [10]:

[1]: The simulation system is described.
[2]: Measurements and analysis regarding modelling of the extinction coefficient is described.
[3]: Measurements and analysis regarding modelling of electric load is described.
[4]: Measurements and analysis regarding modelling of wind speed is described.
[5]: Simulation on a small power plant for private usage.
[6]: Simulation with varying solar cell area and storage capacity at three locations.
[7]: Simulation with varying wind power capacity and storage capacity.
[8]: Simulations with combined power systems at five locations and with economic analysis.
[9]: Reference document for presentation at 5th Solar Integration Workshop, International Workshop on Integration of Solar Power into Power Systems, 2015, regarding “Prediction of solar power by using the extinction coefficient”.
[10]: Detailed results regarding measurements for modelling of the extinction coefficient.

3.1 Main Program

Program module “Main Program” implements the administration of the simulation process.

3.2 Module Wind_make

Program module “Wind_make” calculates stochastic wind speeds consisting of two components according to:

$$V = V_B + V_N \quad (3.1)$$

where:

V: Total wind speed
V_B: Base component
V_N: Noise component

V_B is generated by a Weibull process and V_N by a Laplace process.

The wind speed is discussed in Chapter 5.

3.3 Module Wind_turbine

Program module “Wind_turbine” calculates the produced power from a defined number of wind power turbines with given characteristics. To calculate the output power from a single wind power farm, expressions (3.2) - (3.4) are used.

$$P_S = \frac{Cp \times \rho \times A \times V^3 \times Pfw}{2} \quad (3.2)$$

Where:

P_S: Generated active wind power (W)
$C_p(\lambda)$: Power coefficient
ρ: Air density (kg/m^3)
A: Rotor sweeping area (m^2)
V: Wind speed (m/s)
Pfw: Wind power turbine efficiency excluding Cp

The air density (ρ) is calculated according to:

$$\rho = \frac{1.293}{1+0.00367 \times Tair} \times \frac{Pair}{1013} \quad (3.3)$$

Where:

Tair: Air temperature (°C)
Pair: Air pressure (mbar)

Rotor sweeping area (A) is calculated according to:

$$A = \frac{\mathbf{D^2}}{\mathbf{4}} \times \boldsymbol{\pi} \quad (3.4)$$

Where: D: Rotor diameter (m)

Produced power is divided into:

- Active power
- Reactive power

The power coefficient C_p is calculated, depending on whether the turbines are "Variable speed controlled turbines" or "Aerodynamic stall controlled turbines" according to section 3.3.1 – 3.3.2.

3.3.1 Variable speed controlled turbines

The power coefficient is calculated according to:

$$C_p(\lambda) = a0 + a1\lambda + a2\lambda^2 + a3\lambda^3 + a4\lambda^4 + a5\lambda^5 \quad (3.5)$$

Where: λ: Tip speed ratio

The tip speed ratio (λ) is calculated according to:

$$\lambda = \frac{Vt}{V} \quad (3.6)$$

Where:

Vt: Wind turbine blade tip speed (m/s)
V: Wind speed (m/s)

The turbine rotor rotation speed is calculated according to:

$$V_R = \frac{Vt}{\pi \times D} \times 60 \quad (3.7)$$

Where: V_R: Turbine rotor rotation speed (r/min)

Rotation speed is regulated to get optimal value of tip speed ratio for current wind speed. See (3.6). The value is unique to the wind turbine in question and means that $C_p(\lambda)$ is optimized.

In this work the following values of parameters a0 to a5 have been used:

a0 = 1.142515
a1 = - 1.253909
a2 = 4.78158×10^{-1}
a3 = $- 7.554 \times 10^{-2}$
a4 = 5.426×10^{-3}
a5 = $- 1.4623 \times 10^{-4}$

Parameters a0 – a5 are results from a polynomial adaptation to measurements on Chalmers wind power turbine at Hönö outside Göteborg. Fig. 3.2 shows a comparison between measurements and polynomial adaptation.

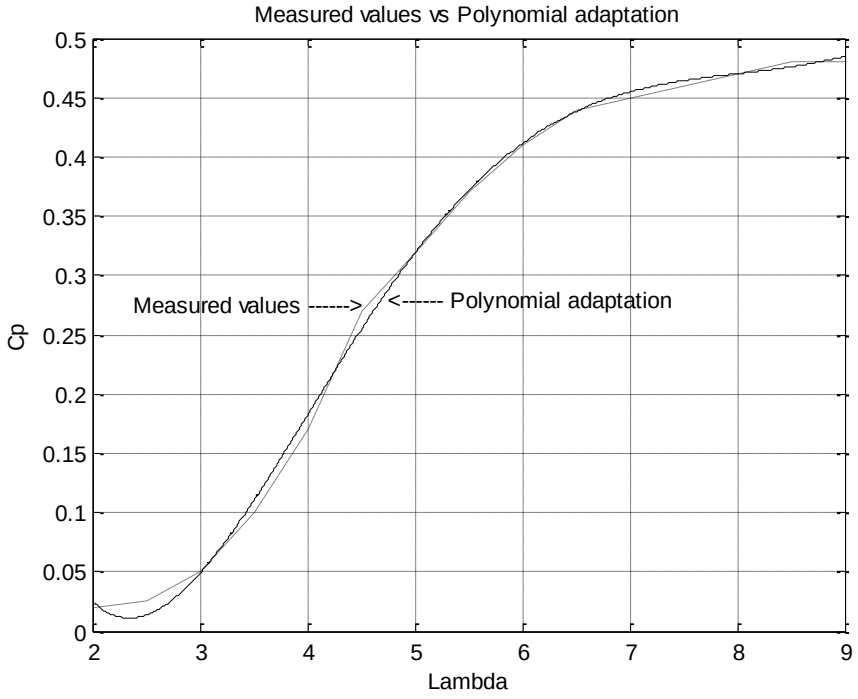

Fig. 3.2. Comparison between measurements and polynomial adaptation regarding coefficient Cp and parameter λ.

The rotation speed is controlled to get the optimal value of tip speed ratio for the current wind speed. See (3.6). This value is unique for the wind turbine in question and means that $C_p(\lambda)$ is optimised. See (3.5) and thereby that Ps is optimised. See (3.2).

If the wind speed exceeds a certain defined maximum level the turbine is stopped, resulting in no output power. If the wind speed is lower than a certain defined minimum level the turbine does not produce any output power.

The rotation speed of a wind turbine is limited by centrifugal forces and in this model limited by an input parameter. That means that the turbine regulation regarding λ only will adjust the rotation speed to give Cp- max up to a certain wind speed. If this wind speed is exceeded the λ-value will be less than the value that corresponds to Cp- max.

Fig. 3.3 illustrates an example of the relation between wind speed and rotor speed. The rotor speed is limited at 85 rpm. Below this limit the control system adjusts the rotor speed to get a λ-value that results in Cp- max. If the rotor speed limit is reached, and if high wind speed condition is present, the λ-value decreases continuously according to Fig. 3.4. On the other hand, this will decrease the Cp-value (following the relation according to Fig. 3.2) as is shown in Fig. 3.5.

Fig. 3.6 shows the electrical output power as a function of wind speed. The electrical output power could be limited by an input parameter, similar to “pitch-control” in reality. The figure illustrates two cases. The red curve represents the case with a power limit of 35 kW. The blue curve represents the case when only “stall control” has impact on the output power.

Other input parameters that have been used in the current examples are:

$\lambda_{ref} = 9.0$

Where λ_{ref} is the λ-value that gives Cp – max

Wind power turbine efficiency, Pfw (excluding Cp) = 0.85.

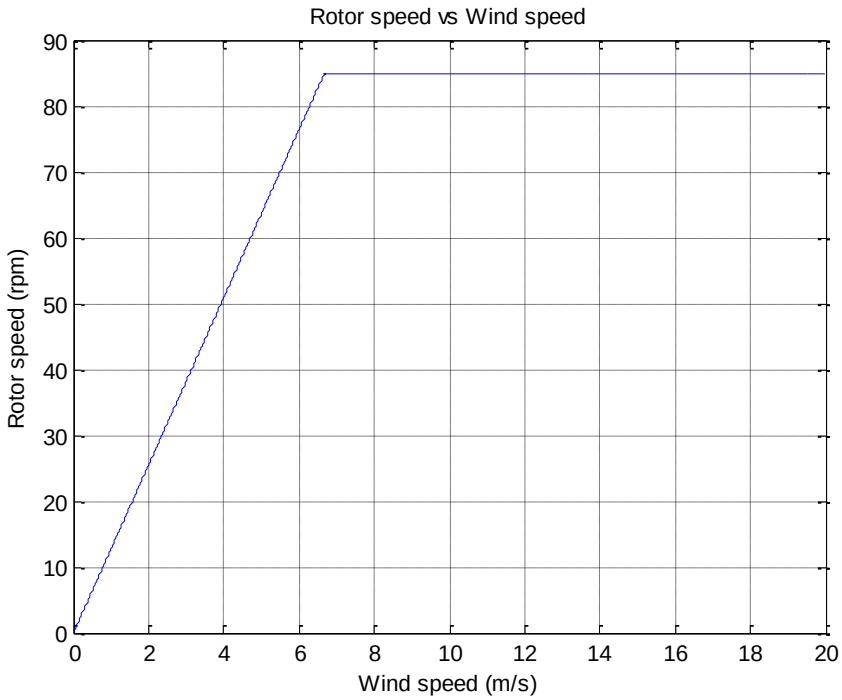

Fig. 3.3. The rotor speed is limited. In this example at 85 rpm.

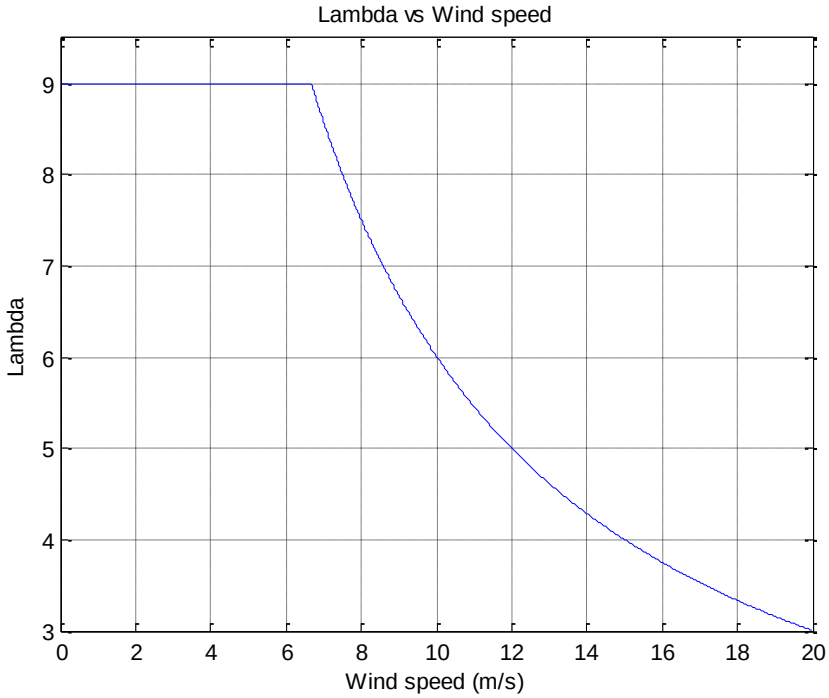

Fig. 3.4. λ as a function of wind speed with a rotor speed limit of 85 rpm. As the rotor speed is limited, the λ - value will decrease for rotor speeds that exceed the limit.

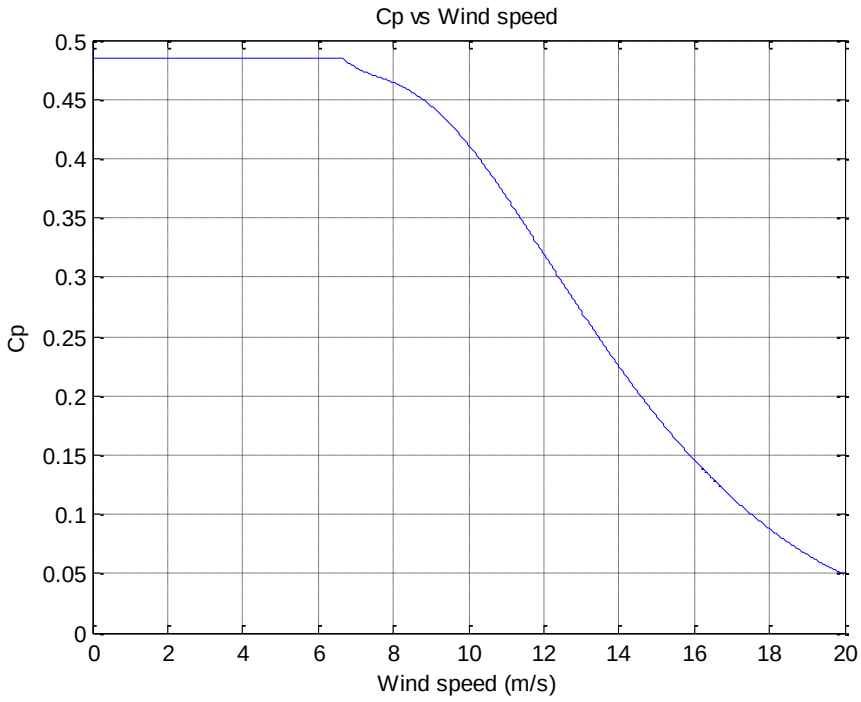

Fig. 3.5. As λ is decreased for rotor speeds at the rotor speed limit and high wind speed conditions, the consequence will be a decreasing C_p - value.

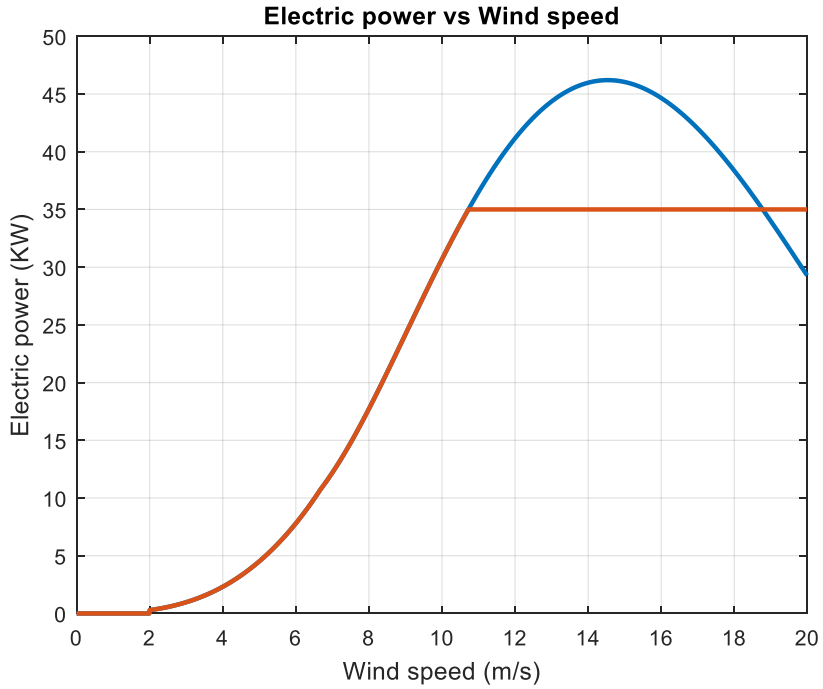

Fig. 3.6. Electrical output power as a function of wind speed. Red curve represents limited power to 35 kW. Blue curve represents the case when only “stall control” has impact on the output power.

3.3.2 Aerodynamic stall controlled turbines

The power coefficient $C_p(\lambda)$ is calculated according to:

$$C_p(V_R) = a0 + a1 \times V + a2 \times V^2 + a3 \times V^3 + \ldots\ldots + a10 \times V^{10} \quad (3.8)$$

Where: V is wind speed (m/s).

Wind turbine Skystream 3.6 has been used as an example in this study.

The following coefficients have been used:

a0 = -0.3095
a1 = 0.7650
a2 = -0.7022
a3 = 0.3120
a4 = -0.0754
a5 = 0.0110
a6 = -0.0010
a7 = 5.9667×10^{-5}
a8 = -2.1963×10^{-6}
a9 = 4.5955×10^{-8}
a10 = -4.1811×10^{-10}

The coefficients are results of polynomial adaptation of measured values. Fig. 3.7 illustrates measured values. Fig. 3.8 illustrates a comparison between measurements and polynomial adaptation.

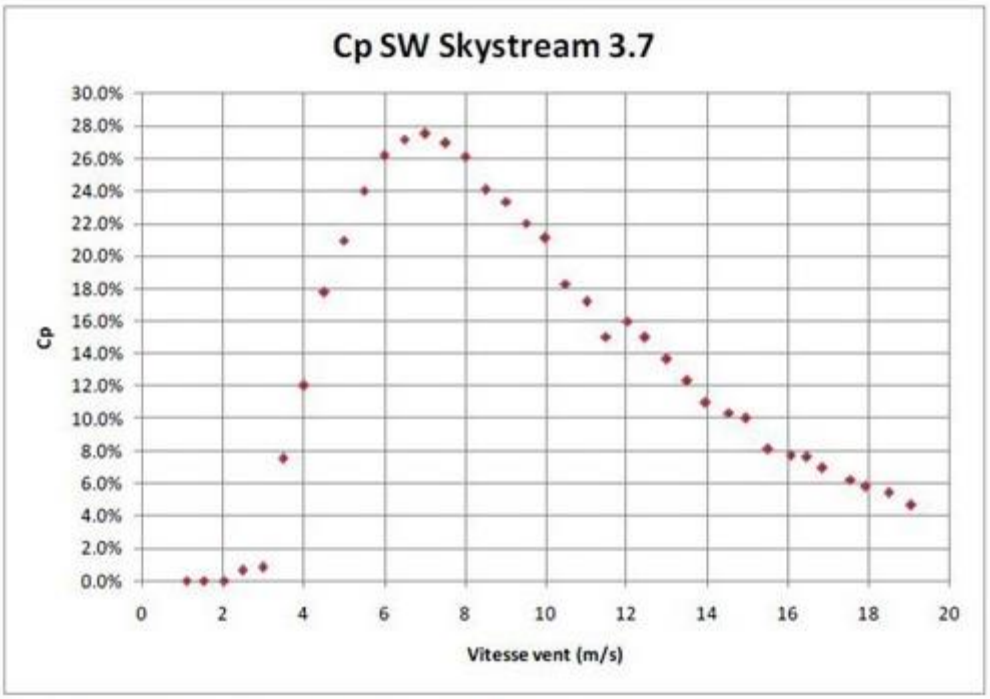

Fig. 3.7. Power coefficient Cp vs wind speed for “Skystream 3.7”. The curve is presented in [22].

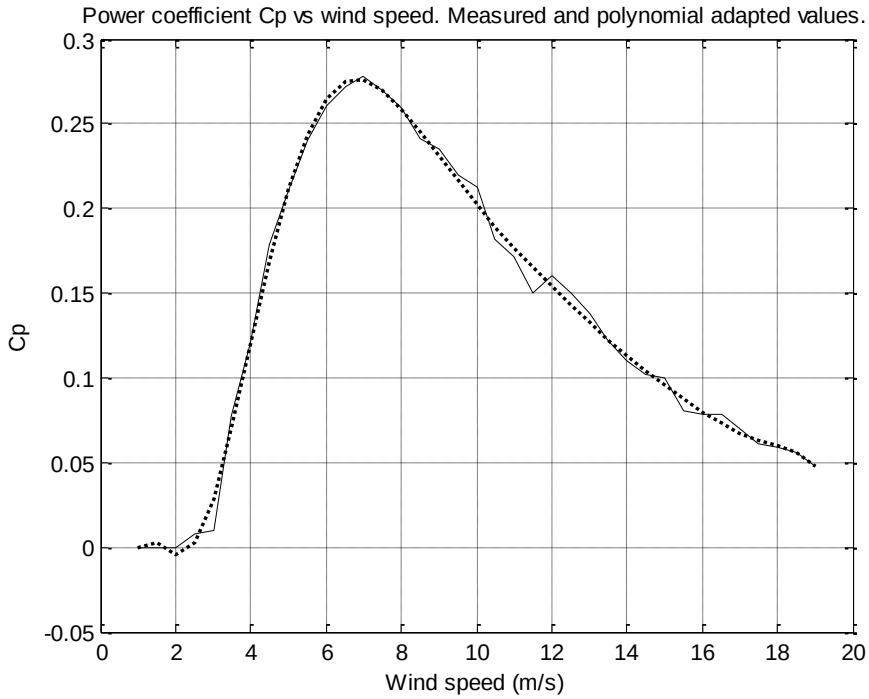

Fig. 3.8. Power coefficient Cp vs wind speed. Measured and polynomial adapted values. Solid curve: Measured values as in Fig. 3.7. Dotted curve: Adapted values.

3.4 Module Extinction_make

Program module “Extinction_make” calculates the extinction coefficients. This parameter is a measure of the atmospheric attenuation regarding the solar radiation. The parameter is given in the form of a statistical quantity. The extinction coefficient is dealt with in Chapter 4.

3.5 Module Sun_intensity

Program module “Sun_intensity” calculates the effective solar irradiation against the solar panels. This is a combination of:

- Sun’s position
- Sun’s position relative to solar cell panels surface normal
- Atmospheric transmission of solar irradiation

3.5.1 Sun’s position in sky

The Sun’s position in the sky is dependent on time of year, time of day and geographic location. A set of algorithms are used for calculation of Sun’s position. These are addressed in Appendix A. The Sun’s position is defined by 2 angles:

- α: Sun angle over horizon
- θ: Sun azimuth

3.5.2 Sun’s position relative to solar cell panels surface normal

Sun’s position relative to solar cell panels surface normal is calculated according to (3.9). See also [18].

$$\cos \beta = \sin \alpha \times \cos \Omega_Z + \cos \alpha \times \sin \Omega_Z \times \cos (\theta - \Omega_S) \quad (3.9)$$

Where:

- β: Angle Sun’s position relative to solar cell panels surface normal
- Ω_Z: Surface normal direction of solar cell panel relative to zenith
- Ω_S: Surface normal direction of solar cell panel relative to south

The angles Ω_Z and Ω_S are defined in Fig. 2.4 and Fig. 2.5.

In the case of so called “Sun tracking”, Ω_Z and Ω_S are automatically controlled, in order to follow the direction of the sun. This implies that $\beta = 0$.

3.5.3 Atmospheric transmission of solar irradiation

The atmospheric transmission of solar irradiation is a function of the extinction coefficient. This parameter is discussed in Chapter 4.

3.5.4 Effective solar irradiation

The effective solar irradiation is calculated according to:

$$\text{Irradiation\_B} = \text{Irradiation\_A} \times \tau \times \cos\beta \qquad (3.10)$$

Where:

- Irradiation_B: Solar irradiation after passing through the atmosphere
- Irradiation_A: Solar irradiation outside the atmosphere
- τ: Atmospheric transmittance

3.5.5 Examples of different geographical locations

Table 3.2 gives three examples of geographic locations for 3 cities, Nairobi in Kenya, Kiruna and Göteborg in Sweden. Calculations with module “Extinction_make” in combination with module “Sun_intensity” give the resulting irradiances according to Table 3.3. The calculations presume in this case a cloudless sky.

Fig. 3.9 shows the integrated irradiance per single month during the year with cloudless sky for Nairobi, Göteborg and Kiruna. As can be observed, the irradiance deviates very little in Nairobi during the year, compared with Kiruna and Göteborg. Presuming "no clouds in sky", the monthly integrated irradiance in Kiruna is higher than in Nairobi from the middle of April to late July.

Table 3.2. Geographic location for 3 cities.

Location	**Latitude (degrees)**	**Longitude (degrees)**
Nairobi	-1.283	36.833
Kiruna	67.850	20.217
Göteborg	57.710	11.968

Table 3.3. Monthly integrated irradiance for 3 cities.

Month	Integrated irradiance (kWh/m^2) Nairobi	Integrated irradiance (kWh/m^2) Göteborg	Integrated irradiance (kWh/m^2) Kiruna
January	260.36	32.06	0.16
February	264.96	91.08	27.43
March	266.68	165.52	111.65
April	263.51	244.25	218.98
May	257.33	302.48	304.27
June	253.12	330.93	348.99
July	255.08	318.29	328.74
August	261.27	269.22	254.84
September	266.08	197.15	153.59
October	266.05	117.67	53.70
November	261.92	47.57	2.42
December	258.61	18.41	0
Total year	3135	2135	1805

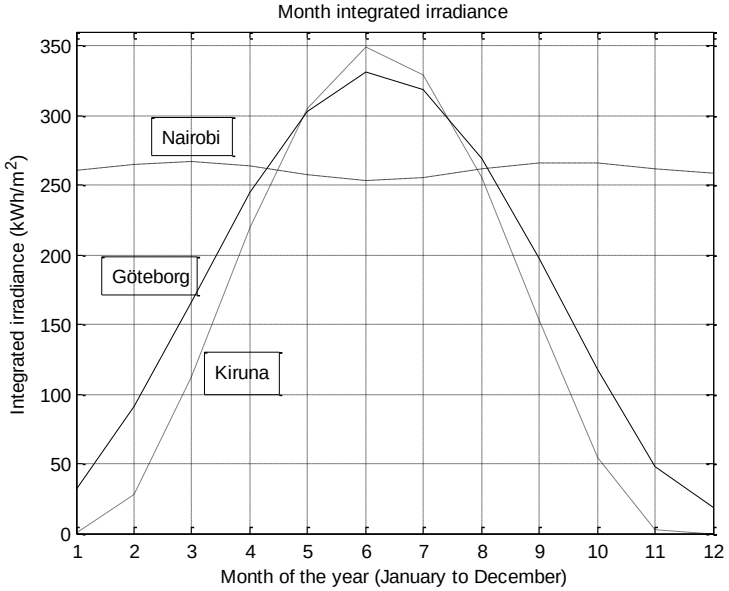

Fig. 3.9. Monthly integrated irradiance with cloudless sky for Nairobi, Göteborg and Kiruna.

3.6 Module Sun_panel_generator

Module “Sun_panel_generator” calculates the produced power from a defined solar cell installation with given characteristics. The power is calculated according to (2.2) and (2.3).

3.7 Module Load_make

Module “Load_make” calculates the local electrical load in the form of a statistical quantity.The load consists of two components, active power and reactive power.

3 different types of power consumers can be used. In combination or individually:

- Industrial area
- Residential area
- Commercial centre

The electrical load is treated in chapter 6.

3.8 Module Connect_Gen_load

Program module “Connect_Gen_load” is a part of the control process regarding the electrical power balance. The module checks “Gross power” and “Net power”, defined according to:

Gross Power = Wind Power + Solar Power (3.11)

Net Power = Gross Power – Load Power (3.12)

where:

- Wind Power: Total generated wind power at a given time
- Solar Power: Total generated solar power at a given time
- Load Power: Total electrical load at a given time

The control process is done in combination with the module “Battery_Distribution”.

3.9 Battery_Distribution

Program module “Battery_Distribution” is a part of the control process regarding the electrical power balance. The module controls the following:

- Charging / Discharging of energy storage
- Exporting/Importing energy via utility grid or usage of Power back-up

The control process is done in combination with the module “Connect_Gen_load”.

3.10 Module Power_evaluate

Program module “Power_evaluate” conducts evaluation of the total simulation process. The result is presented in the form of statistical parameters based on a given number of simulation cycles.

3.11 Relation to the Combined Electrical Power System

The Combined Electrical Power System is modelled in the form of the simulation system described above. Table 3.4 shows the relation between The Combined Electrical Power System and The Simulation System.

The modules in the simulation model reflects the power system at “system level”. This means that, for example, details regarding power electronics are not modelled.

Four functions in the combined power system, namely Power Control, Utility Grid, Energy Storage and Power Back-up, are in the system model administrated by the “Battery_distribution” module. This is for practical programming reasons. Generally, no hardware features have been modeled in detail. According to the proposal in chapter 15 (Future work), some hardware related details will be modelled in order to provide the possibility to fully evaluate dynamic properties of the combined power system.

Table 3.4. Relation between components in Combined Electrical Power system as described above and modules in Simulation system.

Component in Combined Electrical Power system	**Module in Simulation system**
Wind Power	Wind_make, Wind_turbine
Solar Power	Extinction_make, Sun_intensity, Sun_panel_generator
Power Control	Connect_gen_load, Battery_distribution
Utility Grid	Battery_distribution
Energy Storage	Battery_distribution
Power Back-up	Battery_distribution
Local Electrical Load	Load_make

3.12 Summary

This chapter describes a simulation system for modelling of a combined electrical power system with wind and solar as power sources. The combined power system is illustrated in Fig. 2.1. Corresponding simulation system is illustrated in Fig. 3.1. The intention of the simulation system is not to model all hardware functions in detail. In this stage focus has been on providing simulation results in the form of energy conditions and energy flows. The present model has no possibility to analyse dynamic properties in a combined system. For example, transient responses and voltage stability. This is a question for future studies. See chapter 15.

The correlation of the simulation model and the combined electrical power system follows according to 3.11.

The model can be used with different analysis goals. In chapter 7 to 9 some possibilities of usage are exemplified. The model is a mix of deterministic and statistic modelling. The statistical part includes:

- Wind rate
- Cloud condition
- Electrical load

Some key model features and in/out parameters of the present model are:

- Combination wind power farm and solar power farm
- Wind turbine characteristics
- Solar power panel characteristics
- Energy storage characteristics
- Power back-up in the form of power shortage
- Utility grid in the form of power import (power shortage) or power export (power surplus)
- Wind speed conditions (basic statistical parameters)
- Cloud conditions (basic statistical parameters)
- Geographic location
- Time of the year and the day
- Electrical load (load combinations, basic statistical parameters)

CHAPTER 4

EXTINCTION COEFFICIENT

The extinction coefficient is an established parameter for calculation of atmospheric attenuation and is used in different applications. See e.g. [27], [28], [49] and [57].
Parameter extinction coefficient provides information about the atmospheric attenuation for solar radiation and is a key parameter for calculation of the effective radiation to a photovoltaic cell. A statistical model of the parameter has been developed referring to the wave length band of photovoltaic silicon cells. The model is based on measurement data that was collected during 2.5 summer months. The analysis of the measurements is described in more detail in [2]. In [10] an earlier version of analysis regarding the extinction coefficient is documented and contains data from the performed measurements and a lot of figures, illustrating the extinction coefficient during selected days.

The extinction coefficient is dependent on the meteorological conditions relating to:

- Temperature
- Air pressure
- Humidity
- Rain
- Snow
- Cloud conditions

In addition to that there is an influence on the extinction coefficient as an effect of parameters which are not meteorologically dependent:

- Varying conditions regarding aerosols in the air
- Varying conditions regarding the composition of different molecules in the air

Program module “Extinction_make” generates stochastic extinction coefficients.

This chapter deals with the extinction coefficient related to usage as an important component for evaluating the probability for solar radiation at a given location and given time of day and year.

The definition of the extinction coefficient is explained in this chapter. From the basic definition, an expanded definition is given. This is to enable a practical utilization of the parameter.

The objective is to obtain a statistically useful model of the parameter. This is done by means of measurement support in the form of measured short circuit current that is measured under specified conditions.

There is a correlation between the measured short circuit current of a solar cell and corresponding extinction coefficient. This correlation is used for calculation of the current parameter.

The estimated extinctions coefficients are analysed on the basis of a statistical perspective, resulting in a statistical model.

A division into different cloud conditions is made, resulting in a statistical model that utilizes the estimated probability for obscuring cloud cover.

The measurements have provided a basis for the analysis of the occurrence of high-frequency components of the extinction coefficient. This has resulted in statistical modelling of the extinction coefficient divided into two components, a low frequency component and a high frequency component.

To obtain appropriate input data for the model, with respect to the estimated cloud degree, the relationship between locally observed sunshine hours and estimated number of hours with the sun above the horizon, is used.

4.1 General information about the extinction coefficient

The transmission of solar radiation through a homogenous part of the atmosphere can be characterized by the Lambert-Beer law according to:

$$\tau(\lambda) = \exp(-\varepsilon(\lambda) \times R) \qquad (4.1)$$

Where:

$\tau(\lambda)$: Atmospheric transmittance
$\varepsilon(\lambda)$: Extinction coefficient
λ: Wave length
R: Transmission distance

The extinction coefficient is composed of two components according to:

$$\varepsilon(\lambda) = \sigma(\lambda) + k(\lambda) \qquad (4.2)$$

Where:

$\sigma(\lambda)$: Absorption coefficient
$k(\lambda)$: Scattering coefficient

The absorption coefficient is a result of molecular absorption by different gases in the atmosphere, water, carbon dioxide, ozone, nitrous oxide, carbon oxide, methane and so on.

The scattering coefficient is a result of scattering by aerosols, rain, snow, fog. smoke and so on.

In an air mass that is not homogeneous, but with different compositions of scattering and absorbing components between air layers, the extinction coefficient is dependent on wave length band as well as location in the air mass. Fig. 4.1 illustrates an example with an atmosphere column divided into N boxes. Each box has an individual transmittance. An incoming irradiance of G_0 is transmitted through the atmosphere column. Outcoming irradiance from the atmosphere is G. The transmission length through each box is ΔR. The irradiance G illuminates photovoltaic equipment with transfer function H. The output current from the photovoltaic equipment is I.

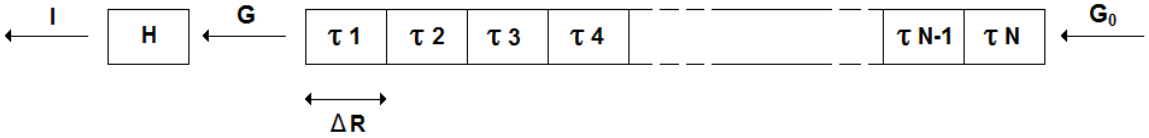

Fig. 4.1. An atmosphere column divided into N boxes with ΔR lengths and different atmospheric transmittances. G_0 and G represent incoming and outcoming irradiances respectively. I is the output current from photovoltaic equipment.

The relation between G_0 and G can be expressed as:

$$G = G_0 \times \tau 1 \times \tau 2 \times \tau 3 \times \tau 4 \times \ldots \times \tau N\text{-}1 \times \tau N \qquad (4.3)$$

Where:

G_0: Incoming Irradiance (W/m^2) before passing the atmosphere column
G: Outcoming Irradiance (W/m^2) after passing the atmosphere column
τk: Transmittance box k, where k = 1, 2, 3, …, N

The relationship between G and I can be expressed as:

$$I = \int_{\lambda 1}^{\lambda 2} H(\lambda) \times G(\lambda)\, d\lambda \quad (4.4)$$

Where:

$H_:$ Transfer function ($Am^2/W\mu m$)
I: Output current (A)
λ_1: Lower wavelength limit of photovoltaic equipment (µm)
λ_2: Upper wavelength limit of photovoltaic equipment (µm)

The transmittance through a single box in the atmosphere column can be expressed as:

$$\tau k = \exp(-\varepsilon k \times \Delta R) \quad (4.5)$$

Where:

εk: Extinction coefficient box k
ΔR: Transmission length through a single box

This gives:

$$G = G_0 \times \exp(-(\varepsilon k+\varepsilon k+\varepsilon k+ \varepsilon k+ \ldots + \varepsilon k+\varepsilon k)\times \Delta R) \quad (4.6)$$

Suppose the following:

- The atmosphere column according to Fig. 4.1 represents an atmosphere column from the ground to the top of the atmosphere
- The atmosphere column is directed to zenith. This means that the length of the column represents the minimum distance from the ground to the top of the atmosphere
- ΔR → infinitely small

Each box has an extinction coefficient, that is a function of both wavelength and level above ground. It means, that the extinction coefficient can be expressed as:

$$\varepsilon k = \varepsilon(\lambda, R) \quad (4.7)$$

In this case, the irradiance G can be expressed according to:

$$G = G_0 \times \exp\left(-\int_{\lambda 1}^{\lambda 2}\int_{L1}^{L2} \varepsilon(\lambda, R)\,d\lambda\,dR\right) \quad (4.8)$$

Where:

L1: Atmosphere column lower limit. That is ground level
L2: Atmosphere column upper limit. That is top of the atmosphere

The distance between L1 and L2 is in this case defined according to:

$$M_0 = L2 - L1 \quad (4.9)$$

Where:

M_0: Minimum distance from ground to the top of the atmosphere

The extinction coefficient is normalised in respect of M_0.

In this case (4.8) can be expressed according to:

$$G = G_0 \times \exp(-\varepsilon_E) \quad (4.10)$$

Where:

$$\varepsilon_E = \int_{\lambda 1}^{\lambda 2}\int_{L1}^{L2} \varepsilon(\lambda, R)\,d\lambda\,dR \quad (4.11)$$

And

ε_E is the “effective” extinction coefficient of the total atmosphere column. Corresponding “effective” extinction coefficient is used in the following analysis in this work. This means that the following applies for future analysis:

$$\varepsilon_E \rightarrow \varepsilon \quad (4.12)$$

The expressions (4.13) to (4.16) in combination with Fig. 4.2. illustrate the relations between some key parameters used in this analysis. In Fig. 4.2, G_0 represents solar radiation outside the atmosphere and G corresponding radiation by atmospheric attenuation.

The length of the atmosphere column is named “atmospheric depth” in the following.

$$\tau = \exp(-\varepsilon \times M) \quad (4.13)$$

$$G = G_0 \times \tau \quad (4.14)$$

$$M = \frac{h}{h0} \quad (4.15)$$

$$M = \frac{1}{\sin \alpha} \quad (4.16)$$

Where:

τ: Atmospheric transmittance
ε: Extinction coefficient
M: Relative atmospheric depth (optical depth) related to the depth when sun is at zenith
$G_{0:}$ Irradiance (W/m^2) before passing the atmosphere. This is the solar constant: 1367 W/m^2
G: Irradiance (W/m^2) after passing the atmosphere
α: Sun altitude above horizon
h0: Atmospheric depth for $\alpha = 90^o$
h: Atmospheric depth

Fig. 4.2 illustrates the relation between some parameters above.

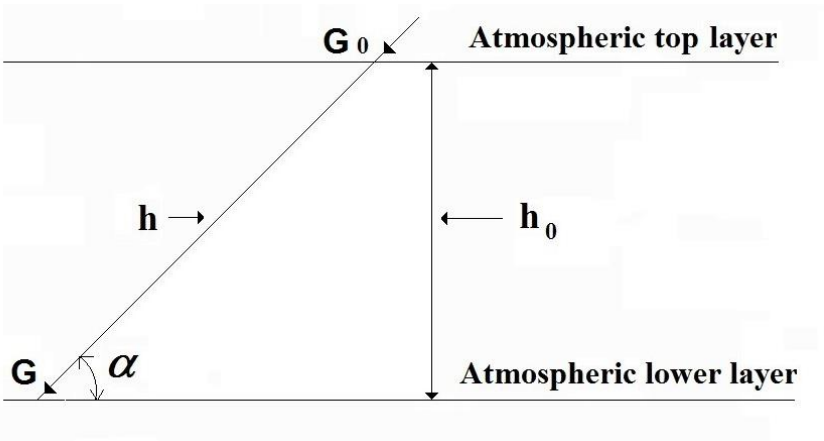

Fig. 4.2. Radiation G as an effect of atmospheric influence.

The extinction coefficient has been divided into two components according to:

$$\varepsilon = \varepsilon_B + \varepsilon_N \quad (4.17)$$

Where: ε: Total extinction coefficient
ε_B: Base component (low frequency component)
ε_N: Noise component (high frequency component)

For more information on atmospheric transmission, wavelength range and extinction coefficient, see sections 11.2, 11.5 and 11.6.

4.2 Cloudiness

This section deals with a simple method to estimate the cloudiness at a specified geographic location in respect of a specified time period. The average number of sunshine hours per day during a time period can be calculated according to:

$$\text{Mean\_sun\_h\_perday\_period} = \frac{\sum_1^{Nm} \text{Mean\_sun\_h\_perday\_month (m)}}{Nm} \quad (4.18)$$

Where:

Mean_sun_h_ perday_period:	Average number of sunshine hours per day during the time period in question
Mean_sun_h_perday_month (m):	Average number of sunshine hours per day during a specific month, m
Nm:	Number of months

Total number of sunshine hours during the time period follows according to:

$$\text{Total\_sun\_h} = Nd \times \text{Mean\_sun\_h\_ perday\_period} \quad (4.19)$$

Where:

Total_sun_h:	Total number of sunshine hours during the time period in question
Nd:	Number of days in the period

The probability of sunshine during the period can be calculated according to:

$$Psun = \frac{Total\_sun\_h}{Sun\_h\_over\_horizon} \times 100 \quad (4.20)$$

Where:

Psun: Probability (%) of sunshine during the period
Sun_h_over_horizon: Calculated number of hours for the location in question when sun is over horizon

An estimated value of the cloudiness can be calculated by combining (4.18), (4.19) and (4.20) according to:

$$Cloudiness = 100 \times \left(1 - \frac{Nd}{Nm} \times \frac{\sum_1^{Nm} Mean\_sun\_h\_perday\_month(m)}{Sun\_h\_over\_horizon}\right) \quad (4.21)$$

Where:

Cloudiness: Estimated value of the probability (%) of cloudiness for location and time period in question

By using (4.21), 5 geographical locations have been investigated in respect of annual estimated cloudiness:

- Kiruna
- Göteborg
- München
- Malaga
- Nairobi

Table 4.1 and Table 4.2 show the parameters used in the calculations. Information in Table 4.1 is derived from [69]. The values in Table 4.2 are results from simulations by using the simulation model according to chapter 3.

Table 4.1 Average number of daily hours of sunshine.

Month	Kiruna Mean sunshine per day (hours)	Göteborg Mean sunshine per day (hours)	München Mean sunshine per day (hours)	Malaga Mean sunshine per day (hours)	Nairobi Mean sunshine per day (hours)
January	0	1	2	5	9
February	1	2	3	6	9
March	3	3	4	7	8
April	5	5	5	7	7
May	8	7	6	9	6
June	9	8	7	11	5
July	8	8	8	11	4
August	5	7	7	11	4
September	4	5	6	8	6
October	2	3	4	7	7
November	1	2	2	6	7
December	0	1	2	5	8
Total	46	52	56	93	80

Table 4.2 Total annual number of hours, when sun is over horizon.

Location	Sun over horizon (hours)
Kiruna	4062
Göteborg	4381
München	4394
Malaga	4369
Nairobi	4377

Table 4.3 lists the estimated annual cloudiness values as a result of using (4.21).

Table 4.3 Estimated annual cloudiness.

Location	Cloudiness (%)
Kiruna	66
Göteborg	64
München	61
Malaga	35
Nairobi	44

4.3 Measurements

Measurements to get statistic foundations to make a survey of the extinction coefficient were performed during the period 21/6 - 7/9 – 2006. The tests were performed on a test facility at Chalmers University of Technology, Göteborg, Sweden.

The principle for the measurement arrangement is illustrated by Fig. 4.3.

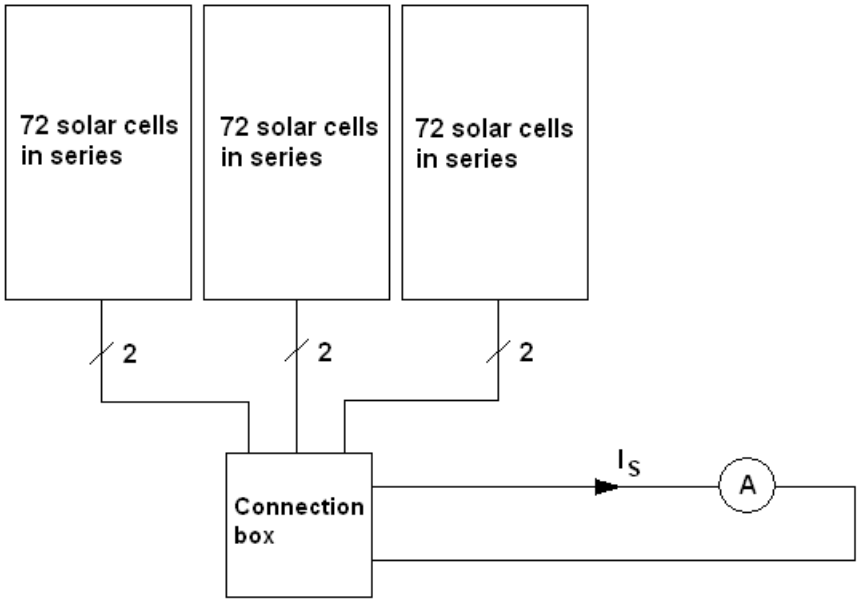

Fig. 4.3. Principle for the measurement arrangement. The connection box connects the three solar cell panels in series. This results in 216 series connected solar cells.

The arrangement shows 216 series connected solar cells (3 × 72). "IS" corresponds to the load current, when all solar cells are short circuited. This is a good measure of the incoming solar radiation, that affects the cells according to:

$$G_1 = G \times \cos \beta \quad (4.22)$$

$$I_S = F \times G_1 \quad (4.23)$$

Where:

G_1: Effective irradiance (W/m^2) to the solar cell panels
I_S: Measured short circuit current

F: Scale factor (Am^2/W). This is a factor which is unique to the relevant solar cells

β: Angle between the surface normal of the measuring surface (solar panel) and the direction of the Sun

Cos β is calculated according to (4.24). See [18].

$$\cos\beta = \sin\alpha \times \cos\Omega_Z + \cos\alpha \times \sin\Omega_Z \times \cos(\theta - \Omega_S) \quad (4.24)$$

Where:

Ω_Z : Normal angle of solar cell surface relative to zenith
Ω_S : Normal angle of solar cell surface relative to south
θ : Sun azimuth

α and θ are calculated by using information regarding time of the year and time of the day and geographic location.

Table 4.4 lists some technical information regarding the solar cells.

Table 4.4. Technical information for used solar cells.

Material	**Polycrystalline silicon**
Wavelength region	0.2 µm - 1.15 µm
Short circuit current at solar irradiance 1000 W/m^2 for polycrystalline silicon	36.6 mA/cm^2
Solar cell area	100 cm^2
Short circuit current for solar cell at solar irradiance 1000 W/m^2	100 cm^2 × 35.4 mA/cm^2 = 3.66 A
Solar cell temperature	Estimated to mean 40º C.

4.4 Direct and diffuse solar radiation

The incoming solar radiation consists of direct radiation and diffuse radiation. With diffuse radiation is meant that radiation which is reflected or spread over the sky before it hits the solar cell. At a cloudless sky, the diffuse radiation is a very small part of the total radiation (global radiation). At a heavy cloudy sky, however, the total radiation consists primarily of diffuse radiation. This implies that incoming solar radiation not follows the relationship according to (4.13) - (4.16) and (4.22) -

(4.23) at the case "totally cloudy sky". The relationship between the different radiation components are according to:

$$G = G_D + G_{diffuse} \quad (4.25)$$

Where:

G: Total irradiance (W/m^2)
G_D: Direct irradiance (W/m^2)
$G_{diffuse}$: Diffuse irradiance (W/m^2)

The method to calculate the extinction coefficient according to (4.13) - (4.16) and (4.22) - (4.23) is not quite correct for the case "totally cloudy sky". This due to the fact that the effective solar irradiance not follows the relationship with angle β according to (4.22) for diffuse radiation. This is illustrated below in Fig. 4.8 and Fig.4.12, where the calculated extinction coefficient partly will be correlated with the direction to the sun. The effect is obvious when estimating high values of the extinction coefficient. However, this effect has just a very marginal influence on the total statistics and is neglected in the analysis. See also section 11.6.2.2.

4.5 Calculation process

Estimated extinction coefficient corresponds to the extinction coefficient for an atmospheric depth of α = 90º. See Fig. 4.2.

The effective irradiance, G1, is calculated by using (4.23).

To calculate cos β and the atmospheric depth, h, is needed information about the angles α and θ at the measurement occasion. This information is calculated by using information regarding time of the year and time of the day and geographic location.

The principle of the calculation follows according to (4.26) and (4.27). See also (4.13) - (4.16) and (4.22) - (4.23).

$$Grel(n) = \frac{G1(n)}{G_0} \times \frac{1}{\cos\beta(n)} \quad (4.26)$$

$$\varepsilon(n) = - \frac{\ln Grel(n)}{M(n)} \quad (4.27)$$

Where:

G1(n): Effective irradiance (W/m^2) to the solar cell panels at sample point n
cos β(n): cos β at sample point n
ε(n): Extinction coefficient at sample point n
M(n): Relative atmospheric depth (optical depth) related to the depth when sun is at zenith at sample point n

The calculation process for the extinction coefficient is illustrated in Fig. 4.4.

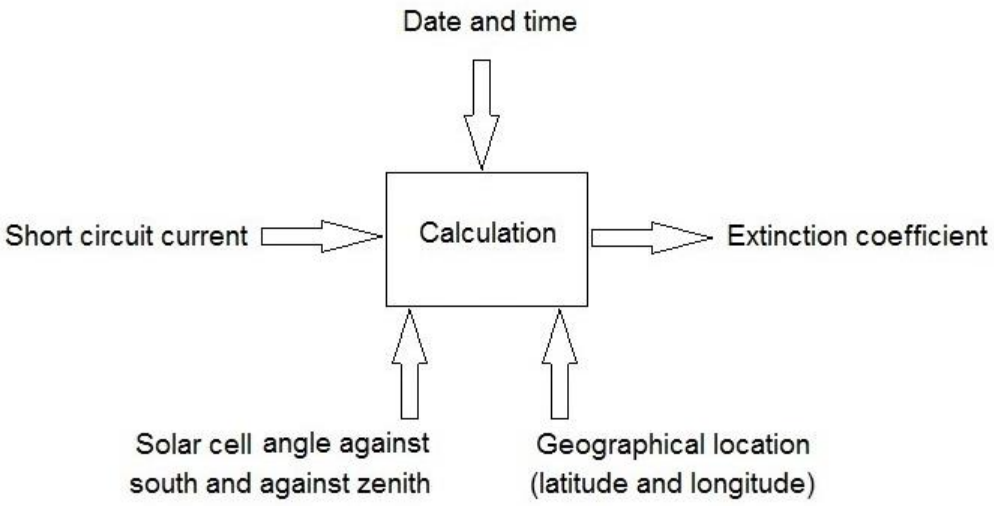

Fig. 4.4. Calculation process to get the extinction coefficient.

4.6 Some results

Fig. 4.5 – Fig. 4.12 illustrate some examples with short circuit currents and corresponding extinction coefficients. The figures show the results for various degrees of cloudiness. Dashed curves represent the short circuit current when incoming solar irradiance is 1000 W/m^2. Note! The time scale for extinction coefficients differs from the time scale for short circuit currents. The reason for this is to limit calculated extinction coefficients to time intervals when no surrounding objects can influence incoming solar radiation.

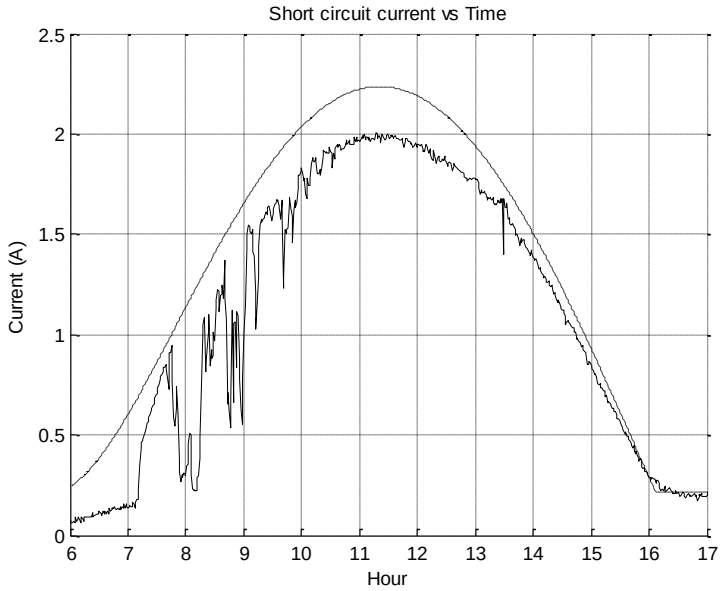

Fig. 4.5. Measured short-circuit current. Low cloudiness.

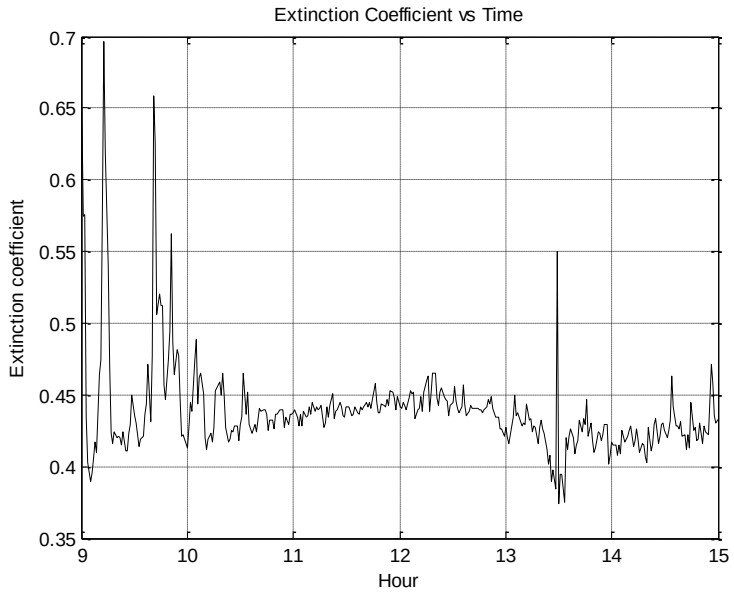

Fig. 4.6. Extinction coefficient corresponding to Fig. 4.5.

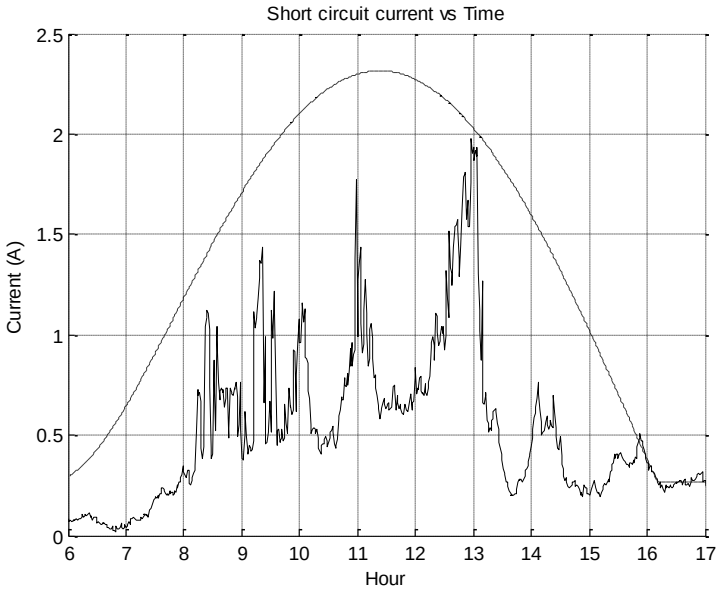

Fig. 4.7. Measured short-circuit current. Heavy cloudiness.

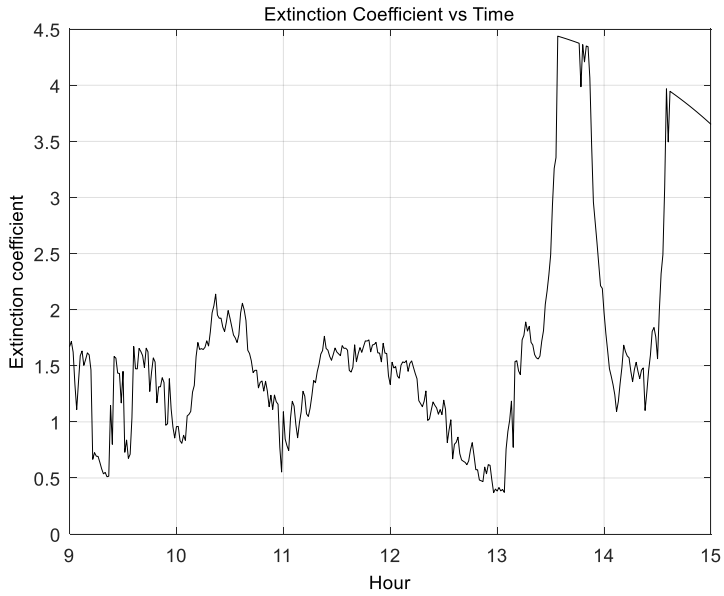

Fig. 4.8. Extinction coefficient corresponding to Fig. 4.7. As an effect of diffuse radiation at a cloudy sky, the calculated extinction coefficient will partly be correlated with the direction to the sun. See section 4.4.

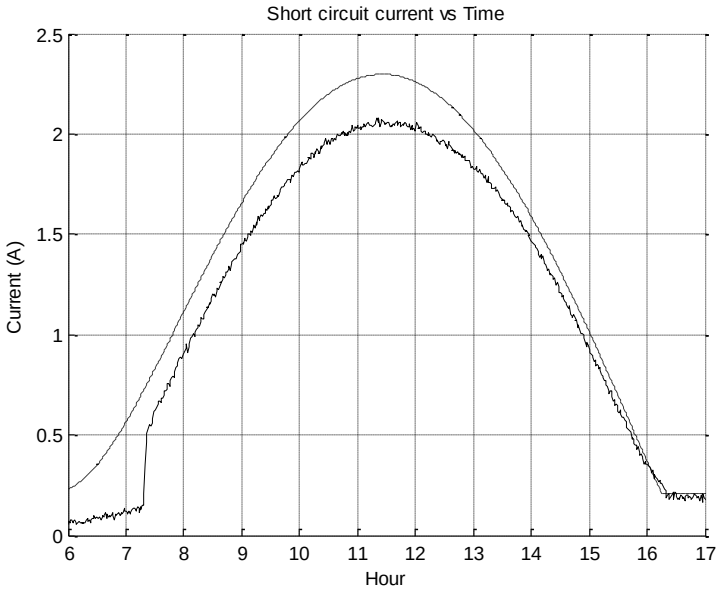

Fig. 4.9. Measured short-circuit current. No cloudiness.

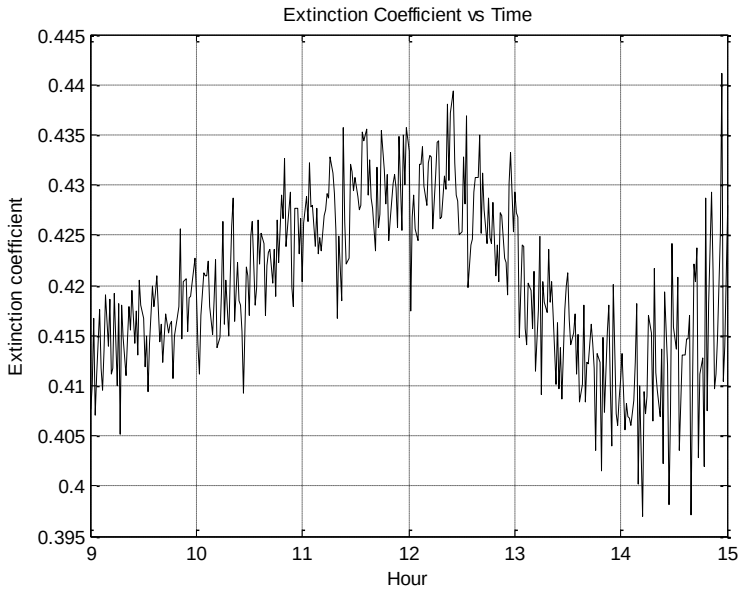

Fig. 4.10. Extinction coefficient corresponding to Fig. 4.9.

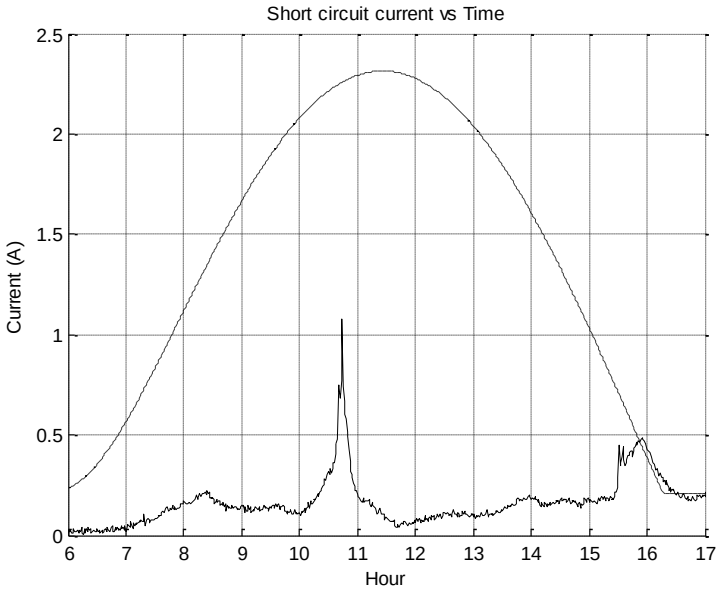

Fig. 4.11. Measured short-circuit current. Total cloudiness.

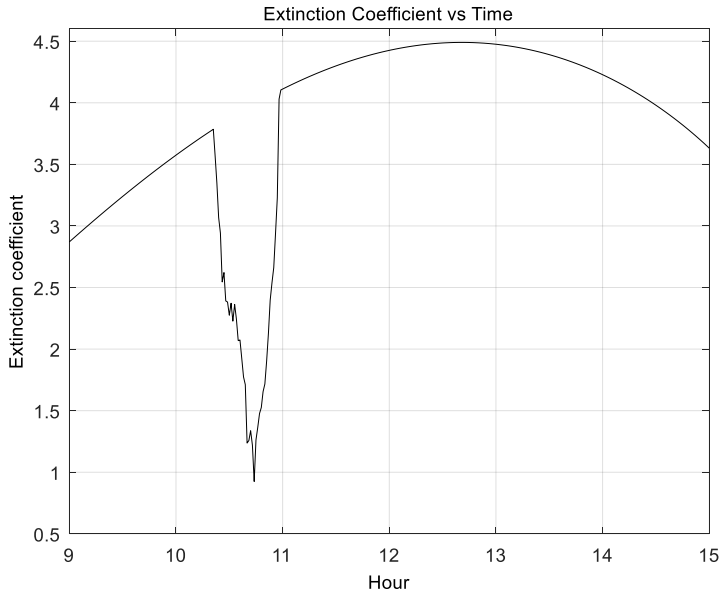

Fig. 4.12. Extinction coefficient corresponding to Fig. 4.11. As an effect of diffuse radiation at a cloudy sky, the calculated extinction coefficient will partly be correlated with the direction to the sun. See section 4.4.

Fig. 4.13 illustrates the mean daily variations of extinction coefficients during the campaign. The values correspond to mean values during each single day between the hours of 9 and 15.

Maximum mean value for a day (between 9 – 15): 3.85
Minimum mean value for a day (between 9 – 15): 0.39

Given these min/max-values and a supposed sun altitude above the horizon of e.g. 50°, this results in a variation of incoming solar radiation from 9 W/m^2 to 822 W/m^2.

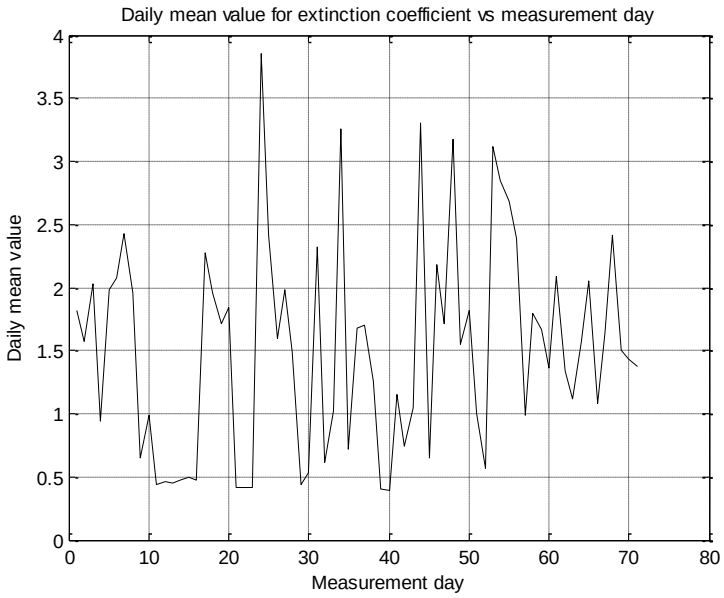

Fig. 4.13. Mean daily extinction coefficient during the campaign.

4.7 Statistical analysis

The goal of the analysis is to find a statistical model to predict a relevant value of the extinction coefficient under defined conditions related to cloud conditions. Fig. 4.14 illustrates the relative distribution for measured extinction coefficients in region 0.31 to 4.5. There is a peak around 0.43. Fig. 4.15 illustrates this peak in more detail. The interval between 0.55 – 4.5 is illustrated in Fig. 4.16. The range up to 0.55 represents conditions when no clouds affect the incoming solar radiation, while the area above represents when clouds influence in varying degrees. Two modes have been defined: “Mode 1, meaning “no clouds affect the solar radiation” and “Mode 2, meaning “clouds affect the solar radiation”.

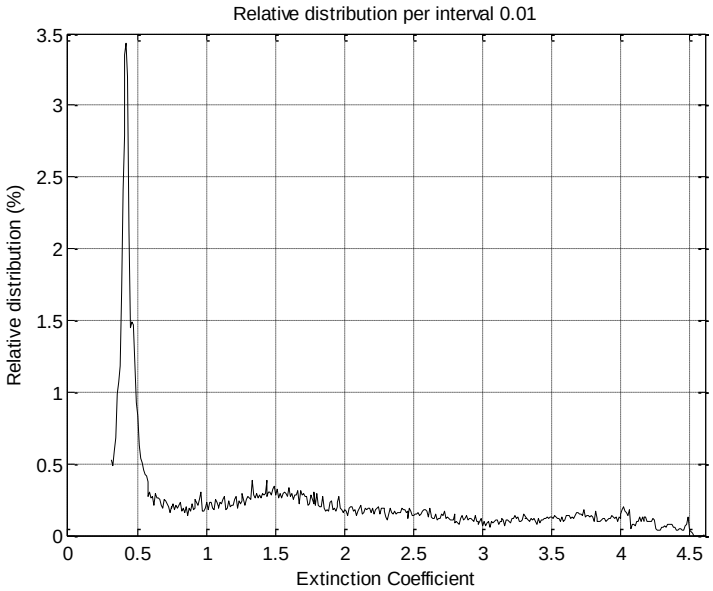

Fig. 4.14. Relative distribution for extinction coefficient per interval 0.01.

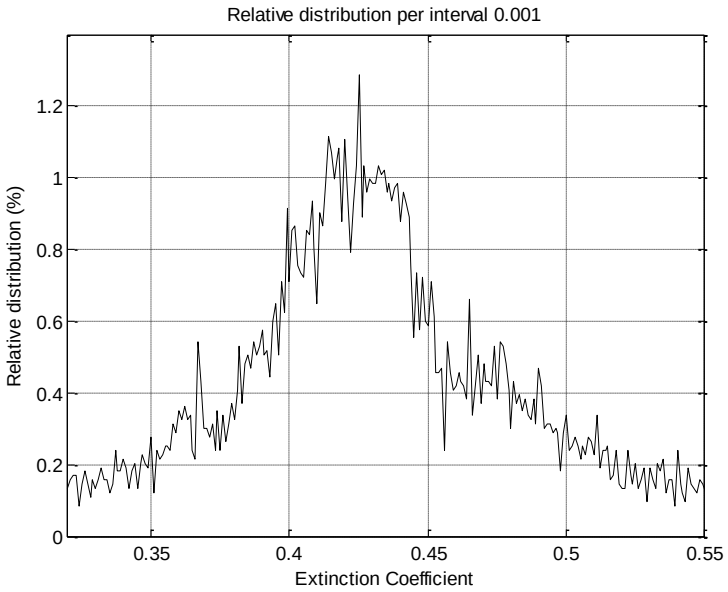

Fig. 4.15. Relative distribution for extinction coefficient per interval 0.001. Interval 0.31 - 0.55.

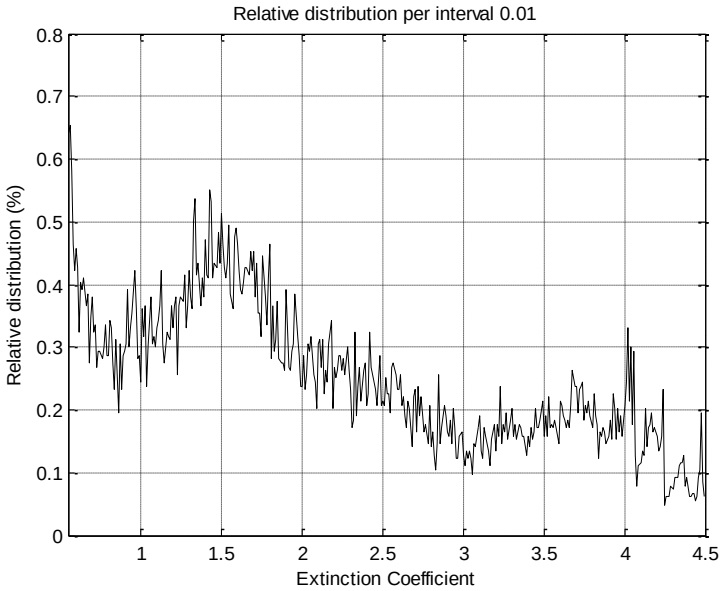

Fig. 4.16. Relative distribution for extinction coefficient per interval 0.01. Interval 0.55 – 4.5.

4.7.1 Mode 1. No clouds affect the solar radiation

In order to get a statistical description of the distribution of the extinction coefficient, in the case of no cloud-influence, the Gaussian distribution has been found to be of special interest. Fig. 4.17 shows the relative distribution of extinction coefficients compared with a perfect Gaussian distribution. The μ-value is the mean between 0.31 – 0.55, that is 0.43. The standard deviation σ, is 0.048. This standard deviation implies that the band limits 0.31 and 0.55 correspond to distances 2.5×σ relative to μ. This means that 98.76 % of the area is within the band limits. The Gaussian distribution is defined according to:

$$p(\mu,\sigma) = \frac{1}{\sigma\sqrt{2\pi}} \times \exp\left(-\frac{(x-\mu)^2}{2\,\sigma^2}\right) \qquad (4.28)$$

Where:

μ: mean value and σ: standard deviation

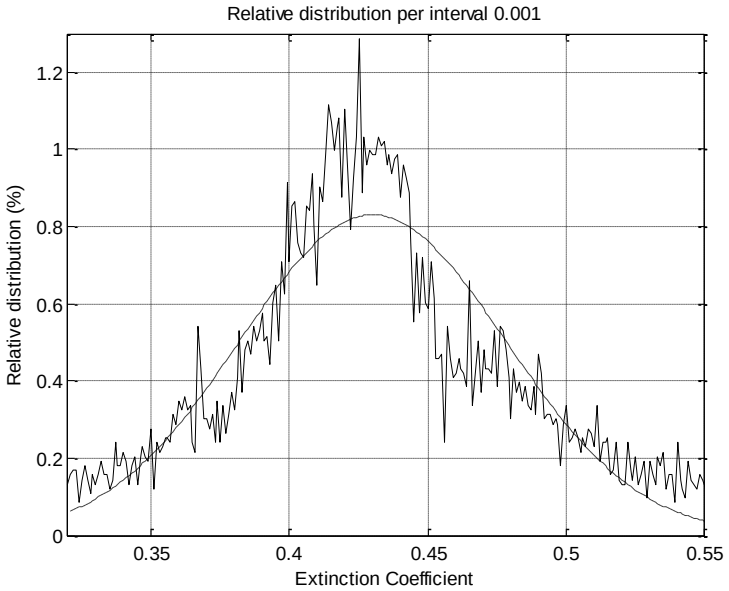

Fig. 4.17. Measured values compared with a perfect Gaussian distribution.
Solid curve: measured values. Dashed curve: Gaussian distribution.

4.7.2 Mode 2. Clouds affect the solar radiation

Depending on variation of the cloud condition, the corresponding extinction coefficient will be varied. In order to get a statistical description of the distribution of the extinction coefficient, in the case of cloud-influence, the trapezoidal distribution has been found to be a relevant function. Fig. 4.18 shows the relative distribution of extinction coefficients compared with a trapezoidal distribution. The trapezoidal distribution with associated parameters is illustrated in Fig. 4.19. The location of the trapezoidal line between p(A) and p(B) is an adaptation to the measured values. The area under the trapezoid is 1. The expected value is 2.00.

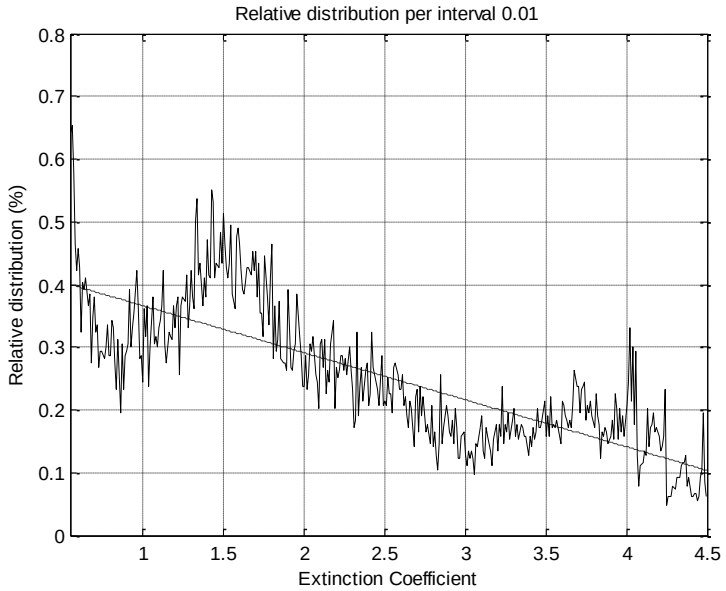

Fig. 4.18. Measured values compared with a trapezoidal distribution.
Solid curve: measured values. Dashed curve: trapezoid distribution.

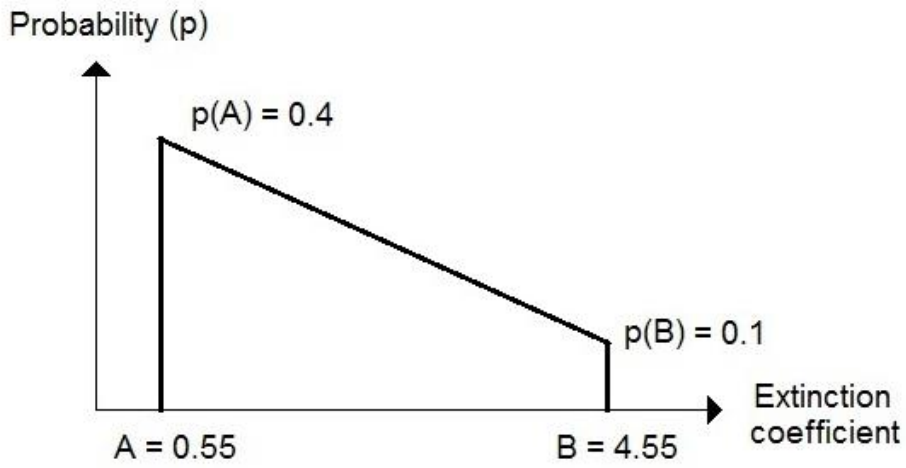

Fig. 4.19. The Trapezoidal distribution with associated parameters. The area under the trapezoid is 1. The expected value is 2.00.

4.7.3 Mode 1 and Mode 2 in combination

During a simulation, a combination of Mode 1 and Mode 2 is used. This is done as follows:

$$t1 = (t1+t2) \times \left(1 - \frac{p(cloud)}{100}\right) \quad (4.29)$$

$$t2 = (t1+t2) \times \frac{p(cloud)}{100} \quad (4.30)$$

Where:

t1: Simulation time according to mode 1
t2: Simulation time according to mode 2
p(cloud): Expected cloudiness in percentage

Fig. 4.20 illustrates the simulation process and continuous update of the modes.

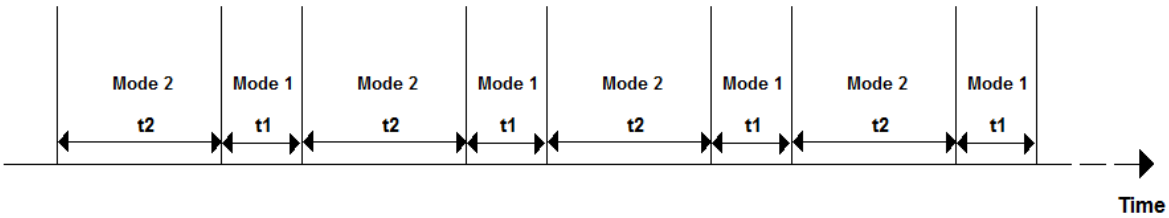

Fig. 4.20. The simulation process and continuous update of the modes.

4.7.4 Low frequency and high frequency components

The total extinction coefficient has been divided into two components:

- Low frequency component
- High frequency component

The low frequency component intends the mean of extinction coefficient during longer time intervals. The high frequency component intends the variation of extinction coefficient during shorter time intervals. The result of the combination of these two components is a statistical variation of the extinction coefficient with each simulation step.

$$\varepsilon = \varepsilon_B + \varepsilon_N \quad (4.31)$$

$$\varepsilon_N = \varepsilon_B \times C\varepsilon \quad (4.32)$$

Where:

ε: Total extinction coefficient
ε_B: Low frequency component
ε_N: High frequency component
$C\varepsilon$: High frequency factor

4.7.5 Low frequency component

The low frequency component is calculated according to sections 4.7.1 to 4.7.3.

4.7.6 High frequency component

4.7.6.1 Extinction coefficient. High frequency gradient

The measured extinction coefficients indicate variations between each measurement sample. This is a result of small variations in atmospheric attenuation of solar radiation. This high frequency component can be modelled by studying the gradients between consecutive samples. The high frequency component is defined according to (4.31) and (4.32). The relative extinction coefficient gradients are here defined according to:

$$G\varepsilon(n) = \frac{\varepsilon(n) - \varepsilon(n+1)}{\varepsilon(n)} \quad (4.33)$$

Where:

n: Measure sample. $1 \leq n \leq N-1$
N: Number of measured samples
$G\varepsilon(n)$: Relative extinction coefficient gradient, sample n
$\varepsilon(n)$: From measurement result calculated extinction coefficient for sample n

4.7.6.2 About the exponential distribution

The exponential distribution follows according to (4.34):

$$p(x) = \frac{1}{\sigma} \times \exp\left(-\frac{x}{\sigma}\right) \quad (4.34)$$

Where σ is the standard deviation

Fig. 4.21 gives an example of an exponential distribution with $\sigma_W = 0.2$. The parameters a and b are x-values, where $0 \leq a < b$. Parameter Δx in the figure is defined as:

$$\Delta x = b - a \tag{4.35}$$

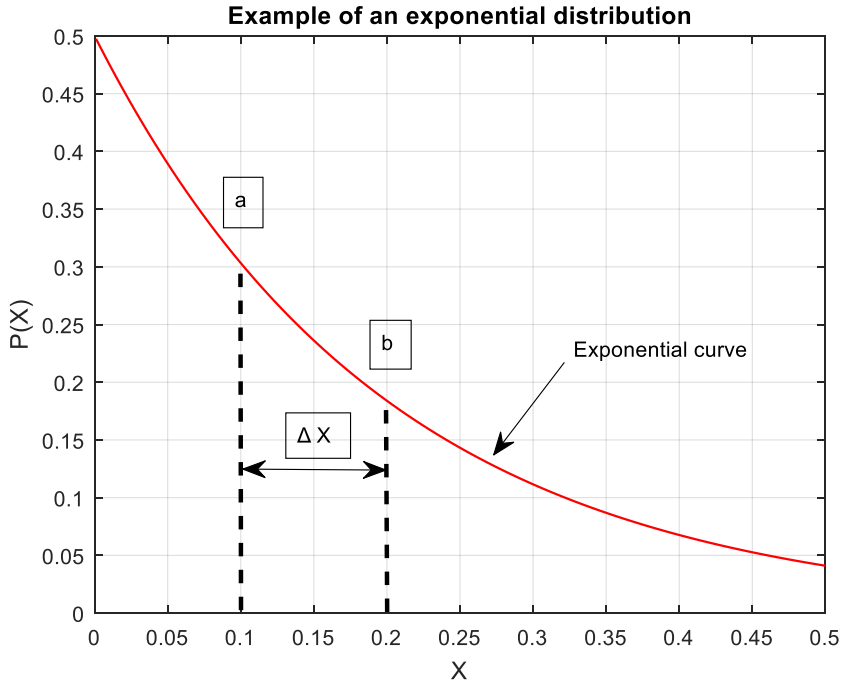

Fig. 4.21. Example of an Exponential distribution with $\sigma_W = 0.2$.

For an exponential distribution, the following is valid:

$$P(x > b \mid x > a) = P(x > \Delta x) \tag{4.36}$$

This implies that given $x > a$, then the probability that $x > b$ is equivalent to $P(x > \Delta x)$. Expression (4.36) can easily be proved according to (4.37) and (4.38):

$$P(x > b \mid x > a) = \frac{\frac{1}{\sigma}\int_b^\infty \exp\left(-\frac{x}{\sigma}\right) dx}{\frac{1}{\sigma}\int_a^\infty \exp(-\frac{x}{\sigma})\, dx} = \frac{\exp(-\frac{b}{\sigma})}{\exp(-\frac{a}{\sigma})} = \exp(-\frac{\Delta x}{\sigma}) \tag{4.37}$$

$$\exp(-\frac{\Delta x}{\sigma}) = \frac{1}{\sigma}\int_{\Delta x}^{\infty} \exp\left(-\frac{x}{\sigma}\right) dx = P(x > \Delta x) \quad (4.38)$$

Thus, (4.36) applies. Also see [67].

The consequence of (4.36) is that P(x > Δ x) is independent of the value of x.

4.7.6.3 High frequency gradients. Statistical modelling

Fig. 4.22 illustrates an example of extinction coefficient gradients with three conditional probabilities, P1, P2 and P3 and corresponding points in the sampling space.

$$P1 = (P(G\varepsilon) > Gr1 \mid G\varepsilon > 0) \quad (4.39)$$

$$P2 = (P(G\varepsilon) > Gr2 \mid G\varepsilon > Gr1) \quad (4.40)$$

$$P3 = (P(G\varepsilon) > Gr3 \mid G\varepsilon > Gr2) \quad (4.41)$$

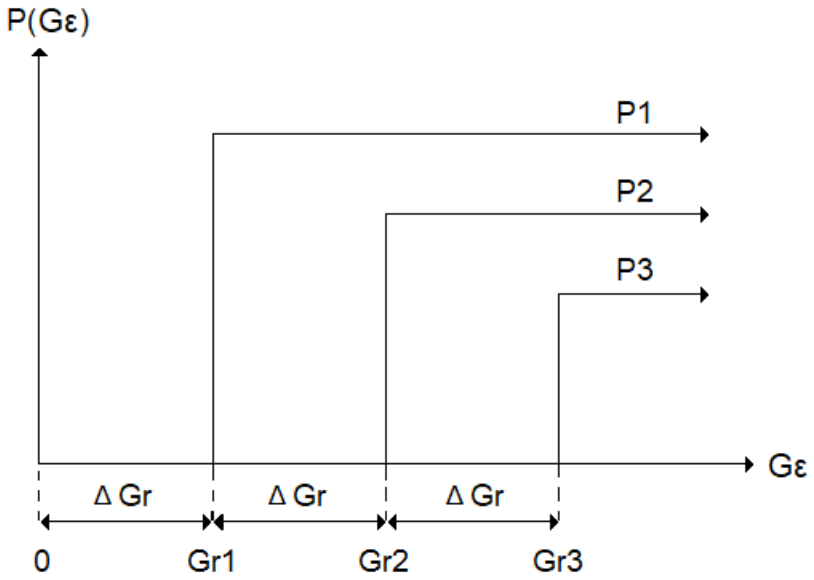

Fig. 4.22. The extinction coefficient gradient with three conditional probabilities, P1, P2 and P3 and corresponding points in the sampling space.

The general assumption according to (4.42) is made for the high frequency gradients:

$$P(G\varepsilon > Gr(n+1) \mid G\varepsilon > Gr(n)) = P(G\varepsilon > \Delta Gr) \quad (4.42)$$

Where:

Gr(n): $n \times \Delta Gr$
n: 0,1,2,3, ….

Fig. 4.23 illustrates an example of the quota ΔGr/Gε with ΔGr = 0.01.

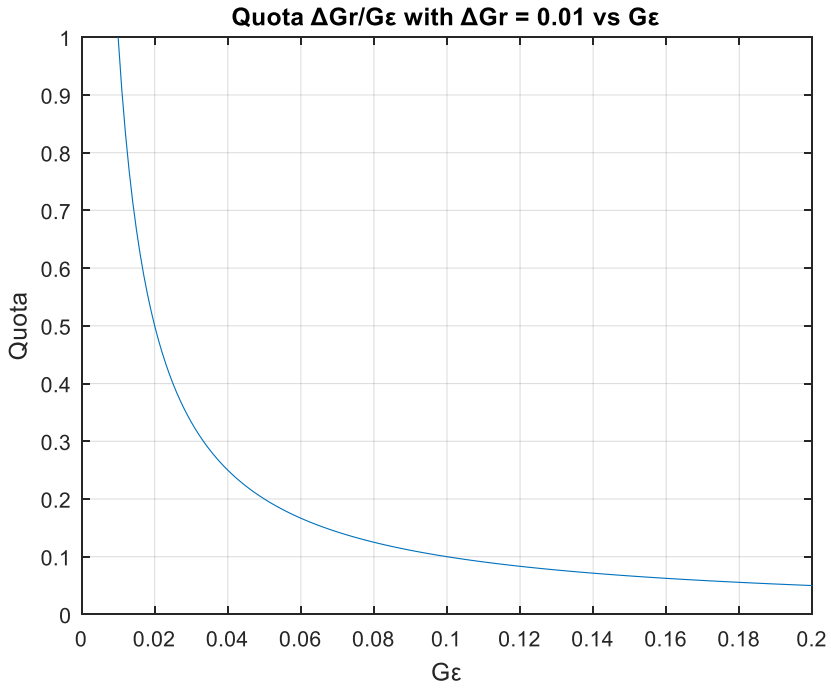

Fig. 4.23. Example of quota ΔGr/Gε with ΔGr = 0.01 vs Gε.

The assumption according to (4.42) seems to be quite reasonable and means that the probability P(Gε > ΔGr) is independent of level Gε. As can be observed in Fig. 4.23, the relation between ΔGr and Gε is dropped down quickly when Gε is increased. This means that although the probability P(Gε > ΔGr) is independent of the x-axis position, its relative significance on the gradient decreases as a function of increasing Gε. This, of course, reinforces the evedence of (4.42) in the present case.

According to section 4.7.6.2, this means that the gradients are exponentially distributed.

The exponential distribution is limited to x-values not less than zero. In the current case however, there is a need to model even negative x-values. To meet this need, the Laplace distribution will be used.

The Laplace distribution is defined according to (4.43). If parameter θ is assigned to value zero, then the Laplace distribution can be seen as two combined functions. The first function is an ordinary exponential distribution function located in the first quadrant. The second function is located in the second quadrant and is a mirror image of the first function along the positive y axis.

$$p(x) = \frac{\mathbf{1}}{\mathbf{2}\cdot \emptyset} \times \exp\left(-\frac{|x-\theta|}{\emptyset}\right) \qquad (4.43)$$

Where ø and θ are Laplace parameters.

Fig. 4.24 illustrates an example of a Laplace distribution with ø = 0.1 and θ = 0.

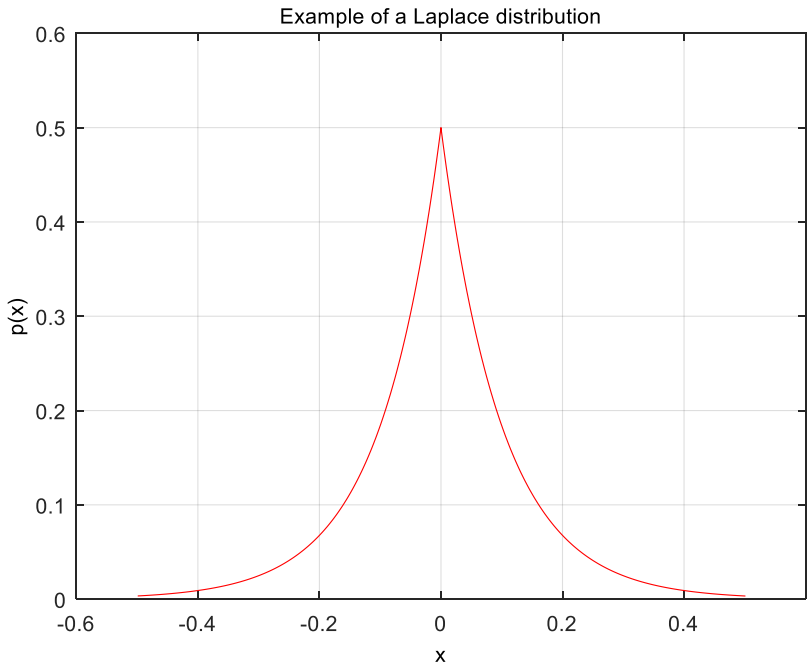

Fig. 4.24. Example of a Laplace distribution with ø = 0.1 and θ = 0.

Expression (4.44) gives the relation between standard deviation and parameter ø for a Laplace distribution.

$$ø = \frac{\sigma}{\sqrt{2}} \tag{4.44}$$

The measurement results according to section 4.3 have been analysed regarding high frequency gradients. Fig. 4.25 illustrates the distribution of gradients between all samples during the measurement period. The y-axis gives the density (%). The x-axis represents the corresponding relative difference between samples. As a comparison, a Laplace distribution is shown in the same figure. The following Laplace parameters have been used:
ø = 0.0631
θ = 0

The selected ø-value is calculated according to (4.44) and corresponds to the obtained standard deviation for measured gradients.

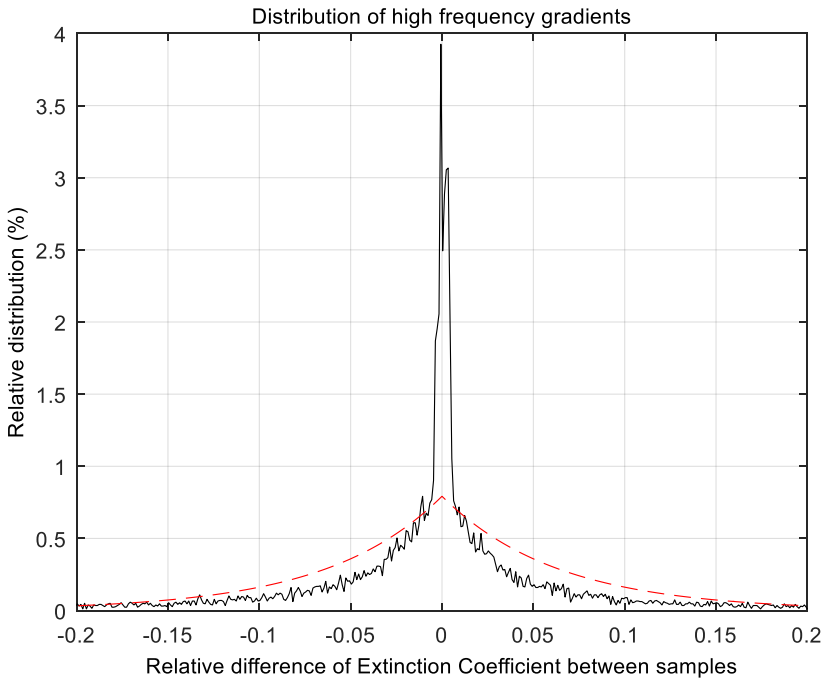

Fig. 4.25. Distribution of high frequency gradients. Black solid curve: Measured values. Red dashed curve: Laplace distribution.

The curves according to Fig. 4.25 illustrate a reasonable correlation between measured gradients and modelled gradients. This is with the exception of the area right around zero. An assessment is made, however, that this deviation can be accepted, because the area in question is quite marginal. One reason for deviation between measured distribution and calculated distribution is probably that the condition according to (4.42) is not quite fulfilled.

The conclusion will be that it is reasonable to use a Laplace distribution for modelling the gradients. The consistency between measured and calculated distributions is sufficiently good for the current work and its intentions and the proposed model appear to be relevant. However, in conjunction with a future expansion of the simulation model in the form of hardware features, it may be appropriate to improve the model regarding high frequency components. See chapter 15.

4.7.6.4 High frequency gradients. Two Laplace distributed functions

As can be noted according to Fig. 4.25, a combination of two Laplace distributed functions can increase the correlation between measured gradients and modelled gradients. The two functions are in that case used in separated regions of the sample space. Regarding to Fig. 4.25 can for example function 1 be in question in the interval - 0.025 to 0.025 and function 2 in the rest of the sample space. This alternative method is not currently used, but may be current in an updated version of the model. See chapter 15.

4.7.6.5 High frequency factor

The Laplace distribution is used for modelling the extinction coefficient gradients. The gradients are the basis for the high frequency factors according to (4.45). Also see (4.32).

$$C\varepsilon(n) = G\varepsilon(n) \qquad (4.45)$$

Where:

Cε(n): High frequency factor, simulation step n
Gε(n): Modelled extinction coefficient gradient, simulation step n

In the simulation model, the parameters Cε and Gε are updated for each simulation step.

4.7.7 Conclusion regarding generation of extinction coefficients

The base component (ε_B) is divided into two modes depending on the external meteorological conditions:

- Mode 1: Solar radiation is not affected by clouds

- Mode 2: Solar radiation is affected by clouds

For stochastic generation in mode 1, the following is applied:

- Gaussian distribution. See (4.28).
- Interval 0.31 – 0.55
- Mean value 0.43
- Standard deviation 0.048

For stochastic generation in mode 2, the following is applied:

- Trapezoidal distribution. See Fig. 4.19.
- Interval 0.55 – 4.55
- A = 0.55, B = 4.55, P(A) = 0.4, P(B) = 0.1
- Expected value 2.00

The high frequency component (ε_N) is generated according to:

$$\varepsilon_N = \varepsilon_B \times C\varepsilon \tag{4.46}$$

Where Cε is a factor that corresponds to the extinction coefficient gradient and is stochastically generated by a Laplace distribution.

The total extinction coefficient consists of 2 components:

$$\varepsilon = \varepsilon_B + \varepsilon_N \tag{4.47}$$

4.7.8 Simulation routines

The routines for stochastic generation of the extinction coefficients are illustrated in Fig. 4.26. The high frequency component is generated for each simulation step. The base components(mode 1 or mode 2) are generated 200 times during a simulation process. This means 100 times per mode and simulation process.

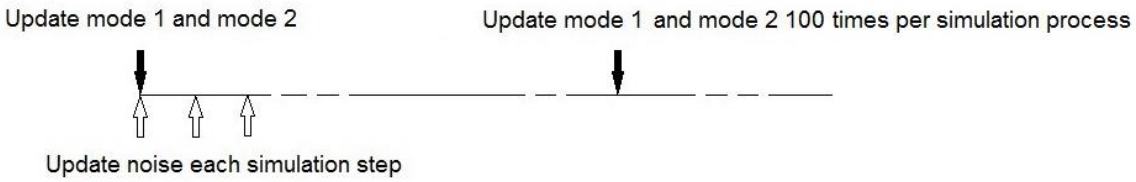

Fig. 4.26. Updating routines for stochastic generation of the extinction coefficients.

4.7.9 Example of simulated extinction coefficients

Fig. 4.27 shows an example (10 days in this case) of extinction coefficients with expected cloudiness of 70%.

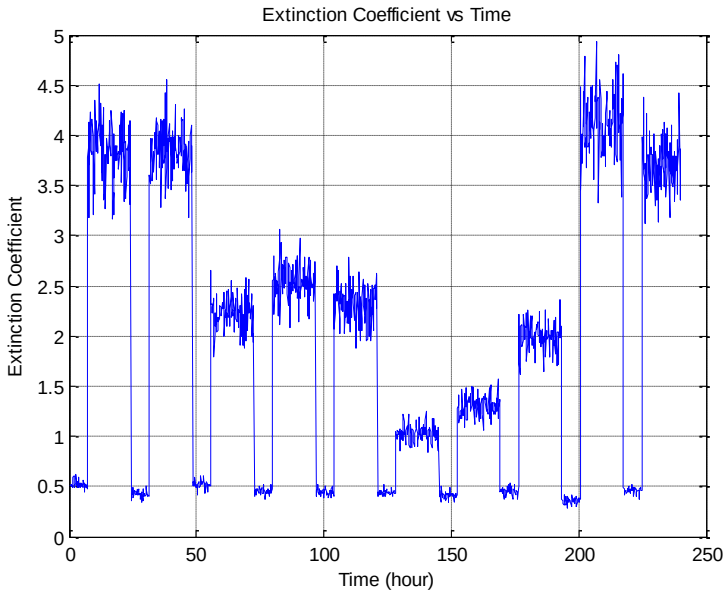

Fig. 4.27. Stochastically generated extinction coefficients with expected cloudiness of 70%.

4.7.10 The model in matrix form

The model can be expressed according to:

$$\mathbf{Ext} = \mathbf{V_B} \times (\mathbf{M_E} + \mathbf{M_G}) \qquad (4.48)$$

Where:

Ext: N elements vector consisting of extinction coefficients. See (4.52)

V_B: N elements vector consisting of low frequency components. See (4.51)
M_E: N × N diagonal matrix. The main diagonal consists of "1". See (4.49)
M_G: N × N diagonal matrix. The main diagonal consists of high frequency factors. See (4.50)
N: Number of simulation steps

Suppose a simulation process corresponding to 365 days and a time resolution of 10 minutes. This means N = 52560.

Also see (4.46) and (4.47).

$$\mathbf{M_E(N\times N)} = \begin{pmatrix} 1 & 0 & 0 & \cdots & 0 & 0 & 0 \\ 0 & 1 & 0 & \cdots & 0 & 0 & 0 \\ 0 & 0 & 1 & \cdots & 0 & 0 & 0 \\ \vdots & \vdots & \vdots & \cdots & \vdots & \vdots & \vdots \\ \vdots & \vdots & \vdots & \cdots & \vdots & \vdots & \vdots \\ \vdots & \vdots & \vdots & \cdots & \vdots & \vdots & \vdots \\ \vdots & \vdots & \vdots & \cdots & \vdots & \vdots & \vdots \\ 0 & 0 & 0 & \cdots & 1 & 0 & 0 \\ 0 & 0 & 0 & \cdots & 0 & 1 & 0 \\ 0 & 0 & 0 & \cdots & 0 & 0 & 1 \end{pmatrix} \tag{4.49}$$

$$\mathbf{M_G(N\times N)} = \begin{pmatrix} C\varepsilon(1) & 0 & 0 & \cdots & 0 & 0 & 0 \\ 0 & C\varepsilon(2) & 0 & \cdots & 0 & 0 & 0 \\ 0 & 0 & C\varepsilon(3) & \cdots & 0 & 0 & 0 \\ \vdots & \vdots & \vdots & \cdots & \vdots & \vdots & \vdots \\ \vdots & \vdots & \vdots & \cdots & \vdots & \vdots & \vdots \\ \vdots & \vdots & \vdots & \cdots & \vdots & \vdots & \vdots \\ \vdots & \vdots & \vdots & \cdots & \vdots & \vdots & \vdots \\ 0 & 0 & 0 & \cdots & C\varepsilon(N-2) & 0 & 0 \\ 0 & 0 & 0 & \cdots & 0 & C\varepsilon(N-1) & 0 \\ 0 & 0 & 0 & \cdots & 0 & 0 & C\varepsilon(N) \end{pmatrix} \tag{4.50}$$

$$\mathbf{V_B(N)} = (\varepsilon_B(1), \varepsilon_B(2), \varepsilon_B(3), \ldots\ldots, \varepsilon_B(N\text{-}2), \varepsilon_B(N\text{-}1), \varepsilon_B(N)) \tag{4.51}$$

$$\mathbf{Ext(N)} = (\varepsilon(1), \varepsilon(2), \varepsilon(3), \ldots\ldots, \varepsilon(N\text{-}2), \varepsilon(N\text{-}1), \varepsilon(N)) \tag{4.52}$$

4.8 Summary

This chapter describes the development work of a module for statistical generation of extinction coefficients and is a part of the simulation system according to chapter 3.

The extinction coefficient is defined by using the Lambert-Beer law. The extinction coefficient is composed of two components, absorption coefficient and scattering coefficient. The absorption coefficient is a result of molecular absorption by different gases in the atmosphere. The scattering coefficient is a result of scattering by aerosols, rain, snow, fog. smoke and so on. These two coefficients are dependent on wave length and level above ground.

In order to enable a practical utilisation of the extinction coefficient, an “effective” extinction coefficient is defined. This is done by using a notional atmosphere column divided into a number of very short boxes. Each box has an individual extinction coefficient that is a function of wave length and level above ground. The “effective” extinction coefficient is a parameter, that reflects the total attenuation of incoming solar radiation after passing all short boxes in the atmosphere column. The column starts at ground level and finishes at the top of the atmosphere. The atmosphere column is directed to zenith.

The atmosphere column, when directed to zenith, is the basic case to define the “effective” extinction coefficient. From this basic case, it is possible to predict the atmospheric transmittance for an atmosphere column that is not directed to zenith. This can be done by using the “effective” extinction coefficient in combination with information about column angle to zenith. The calculation process is used to calculate incoming solar radiation to ground. This is done in combination with information about solar angle over horizon.

The cloudiness is an important parameter when calculating the solar radiation. In order to get useful information about this parameter, a special method hase been used. The method uses the ratio between the number of actual sunshine hours and hours when the sun is above the horizon at a certain place. This is performed on a yearly basis regarding the current location. In this way, an estimated annual cloudiness has been calculated for Kiruna, Göteborg, München, Malaga and Nairobi. The used method makes it possible to calculate the cloudiness in relation to a specific season. However, this has not been done in the present work.

The statistical foundation for analysing the extinction coefficient is based on measurements. These tests were performed during a summer period of 71 days with a sample rate of 1 sample/min and include different weather conditions in respect of cloudiness. The measurement values were converted to corresponding “effective” extinction coefficients by using information about date and time for the day in question.

The total quantity of data was analysed in two main groups, no clouds in sky during test day, and presence of clouds in sky during test day. Regarding the first group (no clouds in sky during test day), the statistical spread was found to follow a Gaussian distribution. For the case when clouds were present in the sky during test day, a trapezoid distribution was found to be the best statistical model.

For statistical prediction in respect of solar radiation, a mix of two modes is used. One mode is focused on the case of no clouds in sky and corresponding statistical distribution (Gaussian). The other mode is focused on the case when clouds are present in sky and corresponding statistical distribution (trapezoidal). The relation between the modes during a simulation process is dependent on predicted cloudiness.

The generated extinction coefficients have, in respect of time, been divided into two time-related components, low frequency components and high frequency components. The low frequency components are randomly updated according to a Gaussian distribution, corresponding to "no clouds affect" the solar radiation, or a trapezoidal distribution, corresponding to "clouds affect" the solar radiation. The low frequency components are normally updated 100 times per simulation process. The high frequency components are updated each simulation step and are added to the low frequency components in the form of gradient functions, proportional to the level of the low frequency components. The high frequency components are randomly generated according to a Laplace distribution.

The generation of extinction coefficients during the simulation process has compactly been described by using matrix formulations.

As has been shown, use of the parameter extinction coefficient will add an important tool when calculating incoming solar radiation to a solar cell.

CHAPTER 5

WIND SPEED

Wind speed is an input parameter to the simulation model, to calculate the output energy from the wind turbines. This chapter deals with the task, of developing and describing a model for statistical simulation of wind speed. The work is based on measurements according to [15]. The measurements were performed during a period of five years in total, from 2008 to 2012. Measurement location was Hönö outside Göteborg, Sweden.

The measurement values have been analysed from a statistical perspective. The given assumption has been that the wind speed can be described based on a Weibull distribution. See (5.3). Based on this assumption, the analysis carried out related to wind speeds during the whole year, as well as wind speeds during the individual seasons.

Weibull parameters for the whole year or for individual seasons were calculated by comparing modeled statistical distributions with measured statistical distributions of wind speeds.

The result was the basis for a statistical model with full year or, alternatively individual season as an input parameter.

The alternative to use Rayleigh distribution instead of Weibull distribution will be discussed.

The measurements have provided a basis for the analysis of the occurrence of high-frequency wind speed components. This has resulted in statistical modelling of wind speed divided into two components, a low frequency component and a high frequency component.

The measurements were made at a given height relative to the ground. Since the model is to be used for simulation at an arbitrary altitude, an algorithm has been introduced for converting the original wind speeds to be valid at the desired height relative to the ground.

5.1 Brief information about the measurements

- Location: Hönö outside Göteborg, Sweden
- Measurement period: 2008 – 2012
- Level above sea: 18.5 m
- Equipment: Wind speed gauge and data logger
- Used sample frequency: 10 minutes

5.2 Analysis

5.2.1 Low frequency and high frequency components

The analysis divides the wind speed into two time related components:

- Low frequency component
- High frequency component

The low frequency component intends the mean of wind speed during longer time intervals. The high frequency component intends the variation of wind speed during a shorter time interval. The result of the combination of these two components is a statistical variation of wind speed in each simulation step.

$$V = V_B + V_N \tag{5.1}$$

$$V_N = V_B \times C_W \tag{5.2}$$

Where:

V: Total wind speed
V_B: Low frequency component
V_N: High frequency component
C_W: High frequency factor

5.2.2 Low frequency component

Regarding the low frequency component, the focus has been to study the Weibull distribution function. This is defined according to:

$$W(V_B) = \frac{C}{A}\left(\frac{V_B}{A}\right)^{C-1} e^{-\left(\frac{V_B}{A}\right)^C} \quad (5.3)$$

where:

V_B: Low frequency component of wind speed
A,C: Weibull parameters. A is the scale parameter, C is the shape parameter

The Weibull parameters have been investigated based on measurement results for the four seasons winter, spring, summer and autumn and for the total year (all seasons).

Comparison between statistical distribution and measured wind speeds resulted in Weibull parameters according to Table 5.1. These values give a good agreement to the measured values over the total speed region in question. The table also shows the relative energy contents of the wind as a result of the Weibull parameters in question. Relations are relative to Weibull parameters for “total year”.

Table 5.1. Weibull parameters for seasons and total year.

Season and Total year	**Weibull parameter**		**Mean wind speed (m/s)**	**Relative energy content of wind. Relation to “total year”**
	A (scale parameter)	**C (shape parameter)**		
Winter	5.9	1.8	5.7	0.98
Spring	5.7	2.0	5.1	0.73
Summer	5.9	2.0	5.2	0.75
Autumn	7.7	2.0	6.5	1.46
Total year	6.3	1.9	5.7	1

Fig. 5.1 - Fig. 5.5 illustrate comparisons between distributions for measured wind speeds and Weibull distributions with parameters according to Table 5.1.

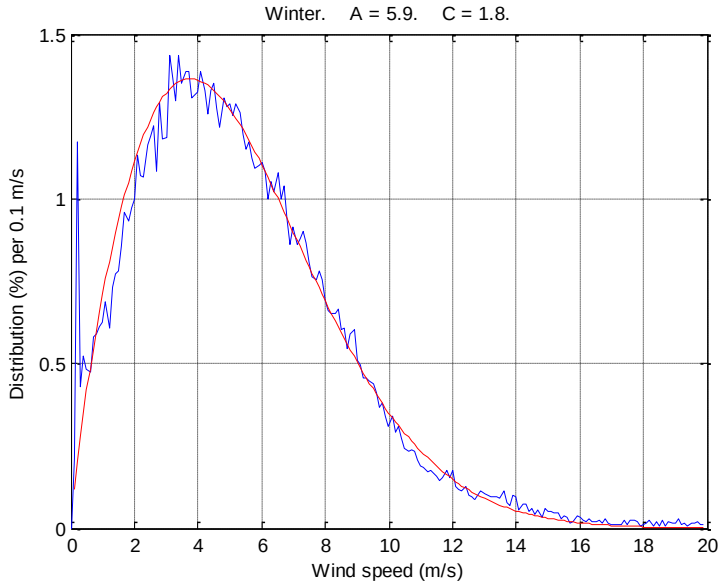

Fig. 5.1. Winter. Measurement – Weibull distribution. A = 5.9, C = 1.8. Blue curve: Measurements. Red curve: Weibull distribution.

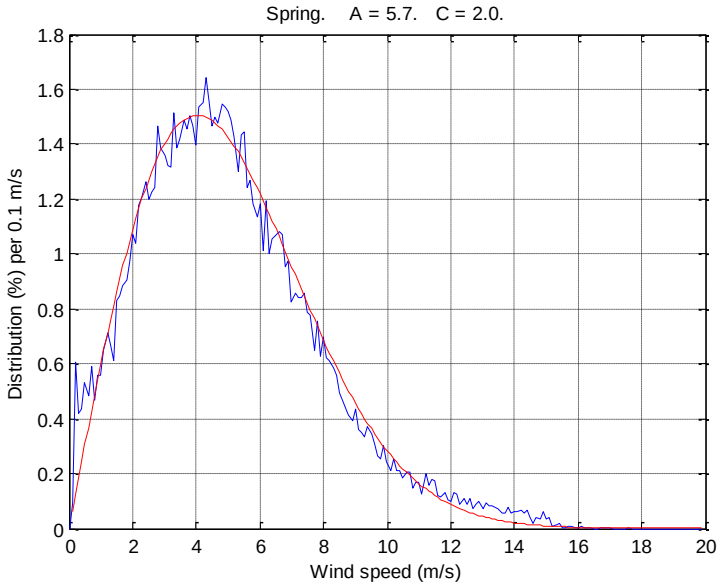

Fig. 5.2. Spring. Measurement – Weibull distribution. A = 5.7, C = 2.0. Blue curve: Measurements. Red curve: Weibull distribution.

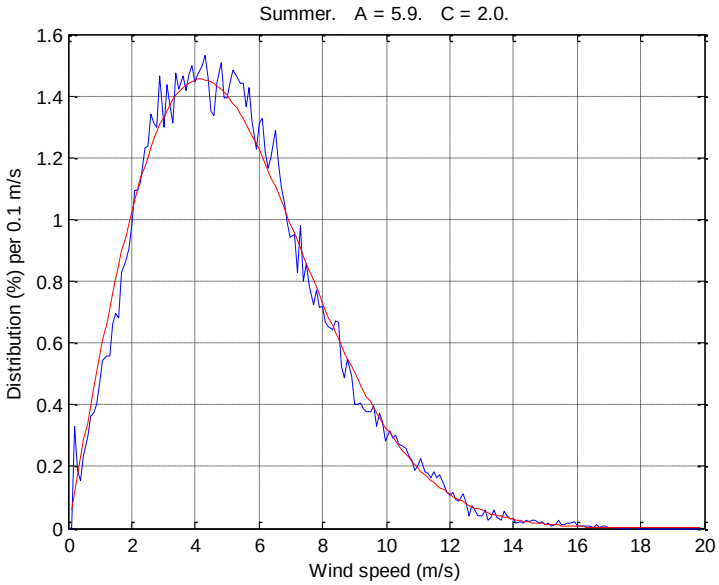

Fig. 5.3. Summer. Measurement – Weibull distribution. A = 5.9, C = 2.0. Blue curve: Measurements. Red curve: Weibull distribution.

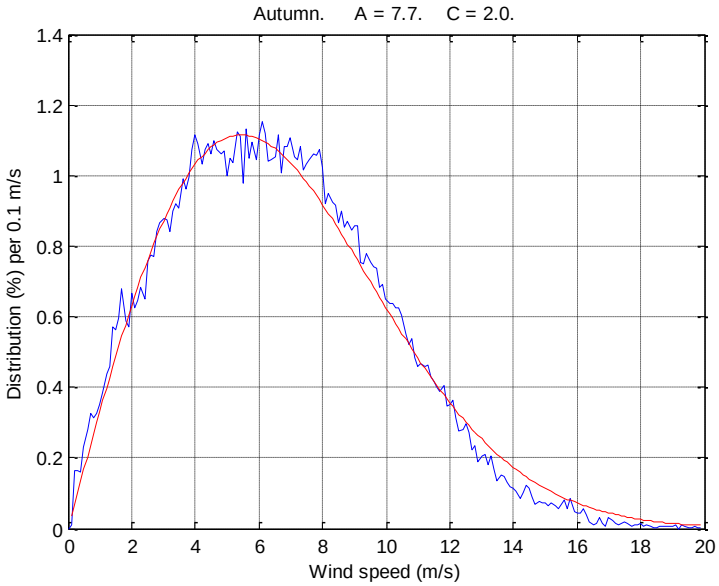

Fig. 5.4. Autumn. Measurement – Weibull distribution. A = 7.7, C = 2.0. Blue curve: Measurements. Red curve: Weibull distribution.

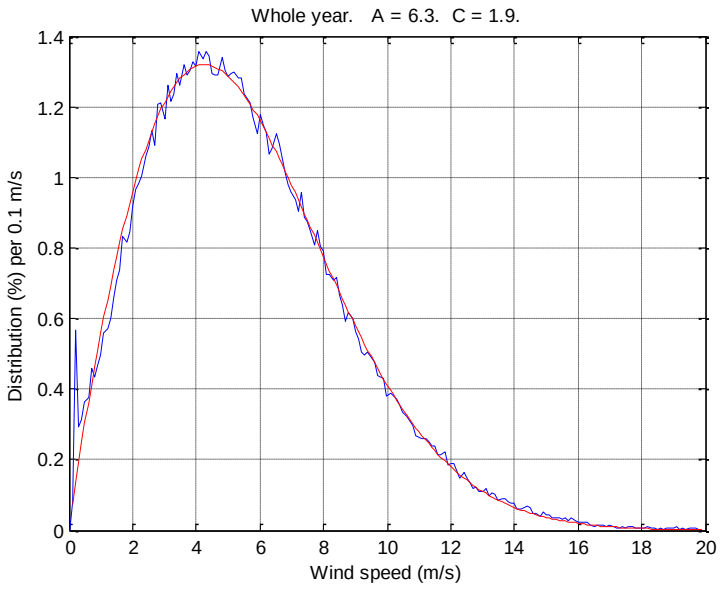

Fig. 5.5. Whole year. Measurement – Weibull distribution. A = 6.3, C = 1.9.
Blue curve: Measurements. Red curve: Weibull distribution.

5.2.3 Rayleigh distribution as an alternative to Weibull distribution

According to [21], it has been assumed that C = 2 is a very realistic value for the shape parameter, in respect of the wind speed at a wind turbine site. For C = 2, the Weibull distribution function is transferred to:

$$R(V_B) = \frac{2\,V_B}{A^2}\; e^{-\left(\frac{V_B}{A}\right)^2} \tag{5.4}$$

Where:

$R(V_B)$ is the Rayleigh distribution

For the Rayleigh distribution, the relation between parameter A and the mean value of the wind speed can be expressed as:

$$A = \frac{2}{\sqrt{\pi}}\,V_{mean} \tag{5.5}$$

Where:

V_{mean}: Mean value of the wind speed

Applying (5.5) in (5.4) results in:

$$R(V_B) = \frac{\pi V_B}{2 V_{mean}^2} e^{-\frac{\pi}{4}\left(\frac{V_B}{V_{mean}}\right)^2} \quad (5.6)$$

See [20] and [21].

Thus, assuming the shape parameter C = 2, then the wind speed can be modelled according to (5.6). In this case, the measured average of wind speeds will be used as input to the model.

Fig. 5.6 illustrates a comparison between Weibull distribution and Rayleigh distribution in relation to a whole year. Weibull parameters: A = 6.3, C = 1.9. Mean wind speed = 5.7 m/s. As is clear, the two curves conform quite well with each other.

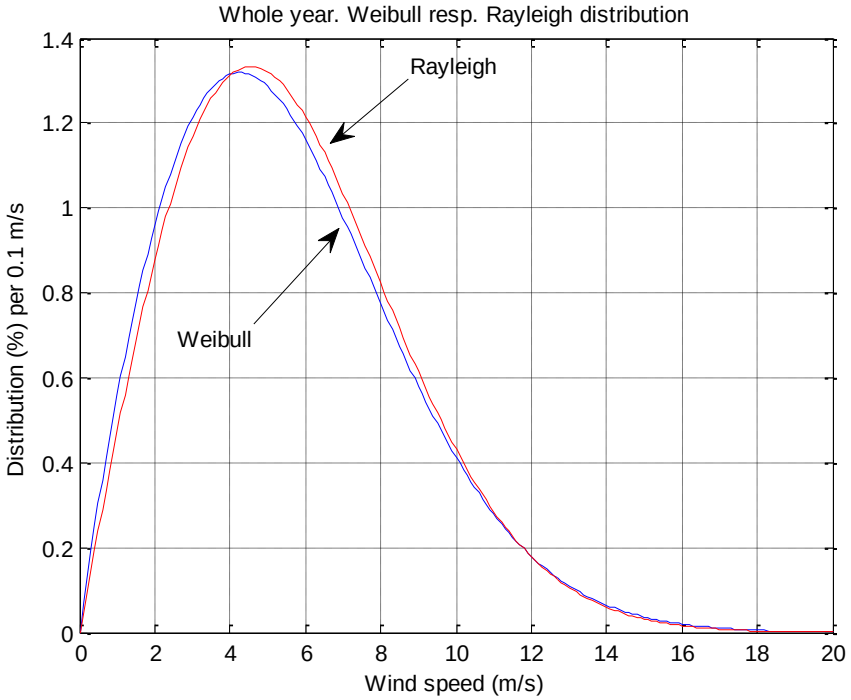

Fig. 5.6. Comparison between Weibull distribution and Rayleigh distribution. Whole year.

In the current case, the shape parameter C is close to 2. See Table 5.1. This means that an application based on the Rayleigh distribution ought to give a satisfactory result. The decision is, however, to continue the work by using the Weibull distribution, and the parameters according to Table 5.1.

For significant deviation from a shape parameter of about 2 at a wind turbine site, a study according to [19] can be referred to as an example. This study has resulted in annual mean values of about 6 - 7 regarding the shape parameter. During a year. Monthly averages varied within the range of about 3 to 11. However, the assumption according to [21] is probably a good starting point, and a good benchmark for general calculation regarding the production capacity of a wind turbine.

5.2.4 High frequency component

5.2.4.1 Wind speed gradients

The high frequency component is defined according to (5.2): $V_N = V_B \times C_W$. The high frequency factor C_W is modelled by using information of the wind speed gradients.

The relative wind speed gradients are here defined according to:

$$Gw(n) = \frac{V(n) - V(n+1)}{V(n)} \qquad (5.7)$$

Where:

n: Measure sample. $1 \leq n \leq N - 1$
N: Number of measure samples
Gw(n): Relative wind speed gradient, sample n
V(n): Wind speed measure for sample n

5.2.4.2 High frequency gradients. Statistical modelling

The Laplace distribution is used for modelling high frequency gradients and wind speeds. This choice is based on similar reasons, which are discussed in relation to the high frequency gradients and extinction coefficients in sections 4.7.6.2. In section 4.7.6.4 is discussed the possibility to use two Laplace functions in combination for modeling the high frequency components. This is even relevant regarding the wind speed gradients. See sections 4.7.6.3 to 4.7.6.4 and chapter 15.

5.2.4.3 High frequency factor

The Laplace distribution is used for modelling the wind speed gradients. The gradients are the basis for the high frequency factors according to (5.8). See also (5.2).

$$Cw(n) = Gw(n) \tag{5.8}$$

Where:

Cw(n): High frequency factor, simulation step n
Gw(n): Modelled wind speed gradient, simulation step n

In the simulation model, the parameters Cw and Gw are updated for each simulation step.

5.2.4.4 Different Laplace parameters in respect of season

The measurement results have been analysed regarding high frequency gradients. Calculated values for standard deviation σ and Laplace parameter ø, divided into seasons and whole year are presented in Table 5.2. Parameter ø is calculated according to (4.44). Laplace parameter θ is assigned to zero.

Table 5.2. σ(g) and ø for seasons and whole year.

Season and Total year	**σ**	**ø**
Winter	0.2398	0.1696
Spring	0.2067	0.1462
Summer	0.1908	0.1349
Autumn	0.1879	0.1329
Whole year	0.2062	0.1458

Fig. 5.7 - Fig. 5.11 illustrate comparisons between distributions for measured wind speed gradients and Laplace distributions with parameters according to Table 5.2.

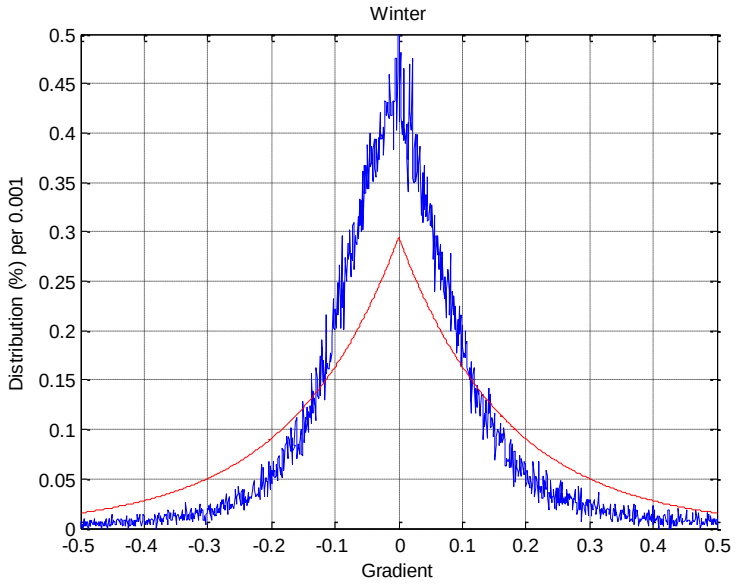

Fig. 5.7. Winter. Comparison between measurement and Laplace distribution with ø = 0.1696. Blue curve: Measurements, Red curve: Laplace distribution.

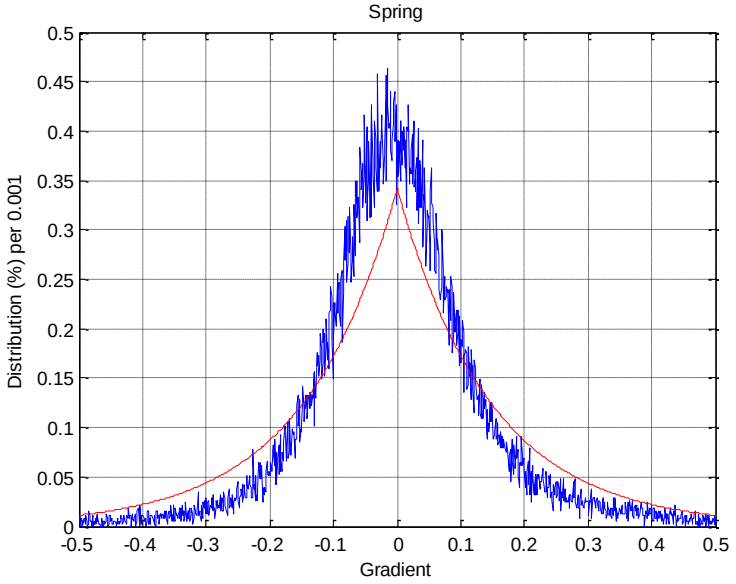

Fig. 5.8. Spring. Comparison between measurement and Laplace distribution with ø = 0.1462. Blue curve: Measurements, Red curve: Laplace distribution.

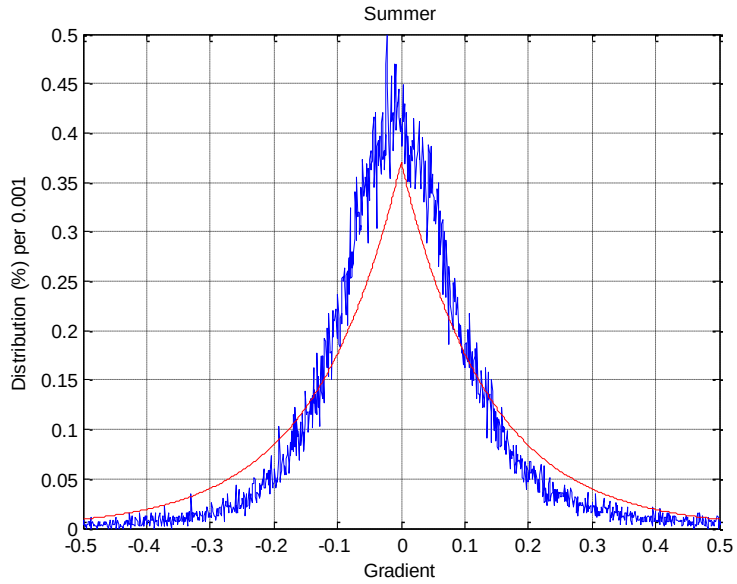

Fig. 5.9. Summer. Comparison between measurement and Laplace distribution with ø = 0.1349. Blue curve: Measurements, Red curve: Laplace distribution.

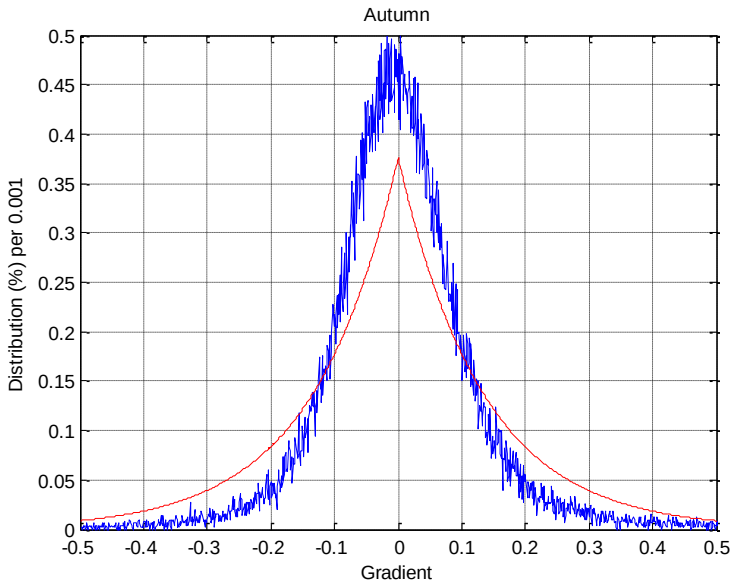

Fig. 5.10. Autumn. Comparison between measurement and Laplace distribution with ø = 0.1329. Blue curve: Measurements, Red curve: Laplace distribution.

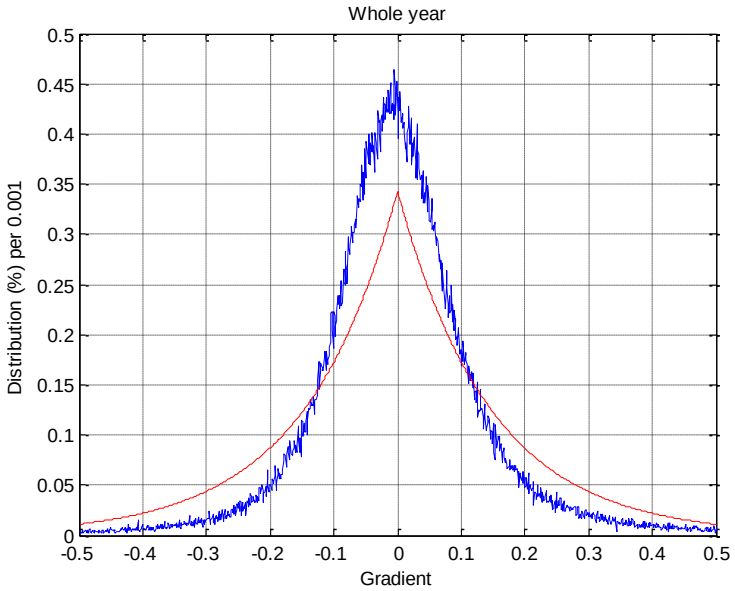

Fig. 5.11. Whole year. Comparison between measurement - Laplace distribution with ø = 0.1458. Blue curve: Measurements, Red curve: Laplace distribution.

5.2.4.5 Conclusion of the analysis

Parameter C_W in (5.2) is obtained by randomly drawing from a Laplace distribution. Laplace parameter ø has been assigned to different values depending on season or whole year. The analysis is based on measurements with a sampling frequency of 1 sample per 10 minutes. This has been considered appropriate in this case. As can be observed, the conformity between measurements and modelling according to a Laplace distribution is not quite perfect. One reason for deviation between measured distribution and calculated distribution is probably that the condition according to (4.42) is not quite fulfilled. However, the conformity is good enough for this work and its intention and the proposed model seems to be relevant.

5.2.5 Simulation routines

The routines in a simulation follow according to Fig. 5.12. The base component is updated 100 times during a simulation process and the noise component is updated each simulation step.

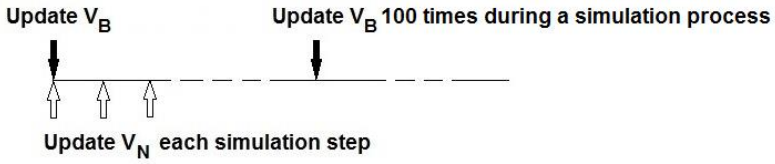

Fig. 5.12. The updating routine for V_B and V_N during a simulation process.

5.2.6 Example of simulated wind speeds

Fig. 5.13 shows an example of simulated wind speed during 1 year with the following input parameter values:

- Time resolution: 10 min
- A = 6.3, C = 1.9
- ø = 0.1458

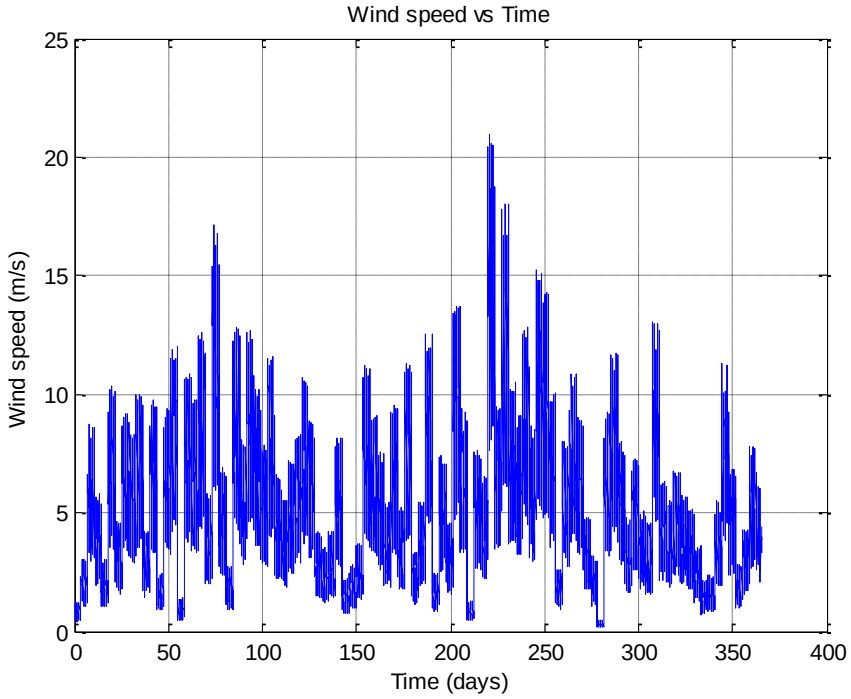

Fig. 5.13. An example of simulated wind speed.

Fig. 5.14 shows a more detailed part of Fig. 5.13 (some hours during day 243). The figure illustrates how the high frequency component is updated every 10 minutes.

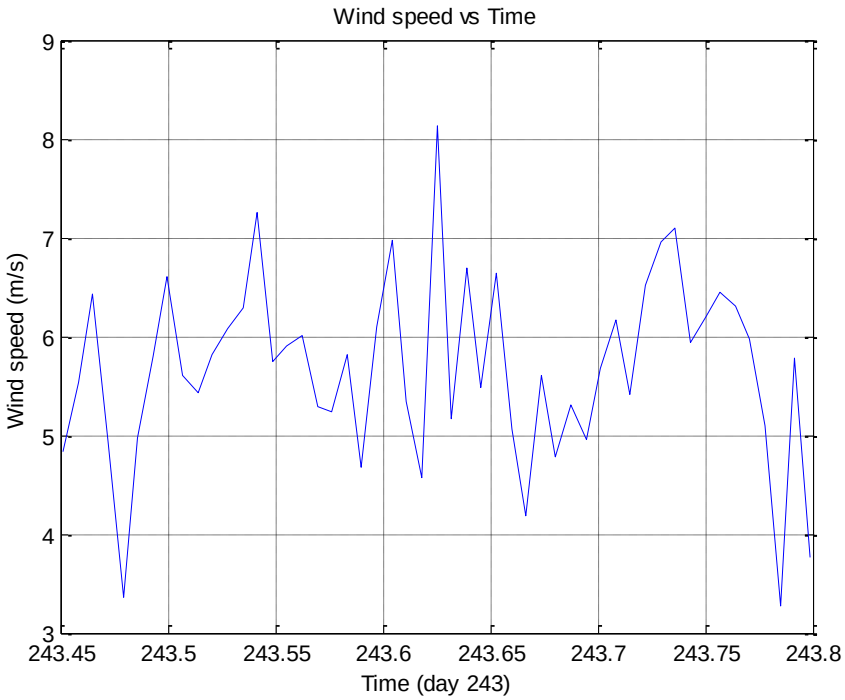

Fig. 5.14. Simulated wind speed during some hours, day 243. With reference to Fig. 5.13. The high frequency component is updated every 10 minutes.

5.2.7 The model in matrix form

The model can be expressed according to:

$$\mathbf{Wind} = \mathbf{V_{Bwind}} \times (\mathbf{M_E} + \mathbf{M_G}) \qquad (5.9)$$

Where:

Wind: N elements vector consisting of wind speeds. See).
$\mathbf{V_{Bwind}}$: N elements vector consisting of low frequency components of wind speed. See (5.12).
$\mathbf{M_E}$: N × N diagonal matrix. The main diagonal consists of "1". See (5.10).
$\mathbf{M_G}$: N × N diagonal matrix. The main diagonal consists of high frequency factors. See (5.11).
N: Number of simulation steps.

Suppose a simulation process corresponding to 365 days and a time resolution of 10 minutes. This means N = 52560.

See also (5.1) and (5.2).

$$\mathbf{M_E(N\times N)} = \begin{pmatrix} 1 & 0 & 0 & \vdots & \vdots & \vdots & 0 & 0 & 0 \\ 0 & 1 & 0 & \vdots & \vdots & \vdots & 0 & 0 & 0 \\ 0 & 0 & 1 & \vdots & \vdots & \vdots & 0 & 0 & 0 \\ \vdots & \vdots & \vdots & \vdots & \vdots & \vdots & \vdots & \vdots & \vdots \\ \vdots & \vdots & \vdots & \vdots & \vdots & \vdots & \vdots & \vdots & \vdots \\ \vdots & \vdots & \vdots & \vdots & \vdots & \vdots & \vdots & \vdots & \vdots \\ \vdots & \vdots & \vdots & \vdots & \vdots & \vdots & \vdots & \vdots & \vdots \\ 0 & 0 & 0 & \vdots & \vdots & \vdots & 1 & 0 & 0 \\ 0 & 0 & 0 & \vdots & \vdots & \vdots & 0 & 1 & 0 \\ 0 & 0 & 0 & \vdots & \vdots & \vdots & 0 & 0 & 1 \end{pmatrix} \tag{5.10}$$

$$\mathbf{M_G(N\times N)} = \begin{pmatrix} \mathrm{Cw}(1) & 0 & 0 & \vdots & \vdots & \vdots & 0 & 0 & 0 \\ 0 & \mathrm{Cw}(2) & 0 & \vdots & \vdots & \vdots & 0 & 0 & 0 \\ 0 & 0 & \mathrm{Cw}(3) & \vdots & \vdots & \vdots & 0 & 0 & 0 \\ \vdots & \vdots & \vdots & \vdots & \vdots & \vdots & \vdots & \vdots & \vdots \\ \vdots & \vdots & \vdots & \vdots & \vdots & \vdots & \vdots & \vdots & \vdots \\ \vdots & \vdots & \vdots & \vdots & \vdots & \vdots & \vdots & \vdots & \vdots \\ \vdots & \vdots & \vdots & \vdots & \vdots & \vdots & \vdots & \vdots & \vdots \\ 0 & 0 & 0 & \vdots & \vdots & \vdots & \mathrm{Cw}(\mathrm{N}-2) & 0 & 0 \\ 0 & 0 & 0 & \vdots & \vdots & \vdots & 0 & \mathrm{Cw}(\mathrm{N}-1) & 0 \\ 0 & 0 & 0 & \vdots & \vdots & \vdots & 0 & 0 & \mathrm{Cw}(\mathrm{N}) \end{pmatrix} \tag{5.11}$$

$\mathbf{V_{Bwind}(N)} = (V_B(1), V_B(2), V_B(3), \ldots\ldots, V_B(N\text{-}2), V_B(N\text{-}1), V_B(N))$ (5.12)

Wind(N) = (V(1), V(2), V(3), ... , V(N-2), V(N-1), V(N)) (5.13)

5.3 Compensation relating to height above ground

In order to compensate the obtained simulation results to wind speeds, correlated to various heights above ground, a method based on the so-called “Power Law” is used:

$$V2 = V1 \times \left(\frac{H2}{H1}\right)^{\alpha} \tag{5.14}$$

Where:

V1: Measured wind speed. Basic for the performed analysis
V2: New predicted wind speed. Compensated from basic data
H1: Height above ground when the wind speed was measured
H2: New height above ground corresponding to wind speed V2
α : Ground surface friction coefficient

The coefficient α has been determined on many occasions around the world. Estimated mean values for various terrain types are given in e.g. [14]. See Table 5.3.

Table 5.3. Estimated mean values for coefficient α.

Terrain type	**α**
Lake, ocean, smooth hard ground	0.10
Foot high grass on ground	0.15
Tall crops, hedges, shrubs	0.20
Wooded country with trees	0.25
Small town with some trees and shrubs	0.30
City with tall buildings	0.40

The following is applied in this work:

- H1 = 18.5 m
- α = 0.10

5.4 Summary

This chapter describes the development work of a wind speed model. The model is used as a module in the simulation system according to chapter 3.

The analysis is based on field measurements performed during a period of five years in total, from 2008 to 2012. All seasons during the year are represented. Measured sampling frequency used is 1 measured sample every 10 minutes.

The measure values have been analysed from a statistical perspective. The measurements have provided a basis for analysis of the wind speed outgoing from two aspects. This means that simulated wind speed has been divided into two components, a low frequency component and a high frequency component. The low frequency component aims on basic wind speed conditions during continuous periods of days. While the high frequency component is focused on temporary wind speed variations during periods of minutes. The high frequency component is superimposed on the low frequency component, with the latter as a base.

The basic assumption has been that the low frequency component can be described based on a Weibull distribution. Weibull parameters for the whole year respectively for individual seasons are calculated. This is done by comparing perfect Weibull distributions with measured wind speeds.

An interesting alternative, namely Rayleigh distribution instead of Weibull distribution, has been investigated.

The Weibull distribution and the Rayleigh distribution are focused on mean values of wind speed over long time intervals (days).

The high frequency components are treated as gradients superimposed on the low frequency components and can be seen in this context as wind speed noise.

The high frequency component (gradient) is generated by randomly drawing from a Laplace distribution. An update of this component occurs with each simulation step, usually corresponding to once per ten minutes in real time.

The wind speed model is equipped with an algorithm for adapting to different external conditions regarding terrain and height above ground.

The generation of wind speed during the simulation process has compactly been described by using matix formulations.

CHAPTER 6

ELECTRICAL LOAD

This chapter describes the development of a mathematical model to be used for statistical evaluation of power consumption with a focus on different consumers: Industrial areas (companies with workshop activities as well as office activities), commercial centres, residential areas and mixtures of industrial areas, commercial centres and residential areas. The model proposed is based on the results of a measurement campaign.

The measure values have been analysed from a statistical perspective. The measurements have provided a basis for analysis of electrical power consumption outgoing from two aspects, basic consumption during specific hours of the day, and temporary variations. This has resulted in statistical modelling of the electrical power consumption divided into two components, a low frequency component and a high frequency component.

The area in question, which has been an object for measurements, can be considered a reasonable representative of a small industrial estate.

A rough estimate has been made, namely that different industrial areas, regardless of size, have the same time-related power consumption patterns. This assumption implies that a scale factor proportional to the total annual consumption can be used as a model parameter for definition and modelling of a specific industrial estate. Based on this assumption, a general statistical model for an industrial estate has been developed.

A statistical model for a commercial centre has also been developed. This is based on the industrial area with focus on the statistical process during the weekend.

A statistical model for a residential area has been developed. A reasonable assumption regarding the internal dynamic process has been made. The statistical characteristics correspond to an industrial area during a weekend.

A mixture of an industrial area, a commercial centre and a residential area can be simulated.

6.1 Brief information about the measurements

Measurements of the electrical power consumption of an area consisting of a mixture of workshop and office activities have been performed. Total power consumption in the area have been divided into 18 part consumers. Their annual power consumption together with respective electrical fuse and voltage range are presented in Table 6.1. The measurement area can be considered a reasonable representative of a small industrial estate.

Table 6.1. Power consumption for the companies that were involved in the measurement campaign.

Part consumer	Power consumption (kWh/year)	Fuse (A)	Voltage (kV)
1	220929	315	10
2	266298	200	10
3	22900	35	0.4
4	111900	100	0.4
5	19400	63	0.4
6	121600	63	0.4
7	13100	25	0.4
8	3000	16	0.4
9	15300	16	0.4
10	41400	35	0.4
11	45700	63	0.4
12	67500	80	0.4
13	45600	35	0.4
14	102000	35	0.4
15	9300	25	0.4
16	11300	25	0.4
17	6600	25	0.4
18	150500	125	0.4
Total Consumption (kWh/year):	1274327		

- Test location: Almås, Lindome, Sweden
- Test period: 2005-10-25 to 2005-11-29
- Test equipment : Electricity network analyser “Unilyzer”, developed and delivered by the company “Unipower”
- Used sample frequency: 30 minutes
- The presented test results are focused on the consumed active power

6.2 Measurement results

Fig. 6.1 summarizes the measurement results from the entire measurement period.

Fig. 6.2 shows more in detail the results from the first 7 days. It is clear that the power consumption is significantly higher during the daytime compared to nighttime. It is also clear that the difference in power consumption differs significantly between a normal working day and a holiday. Days 4 and 5 in Fig. 6.2 are public holidays. A natural conclusion from this is to divide the upcoming analysis into different classes. The following breakdown is therefore:

- Power consumption during day time, working day
- Power consumption during night time, working day
- Power consumption during transition between daytime and nighttime, and vice versa, working day
- Power consumption during holiday

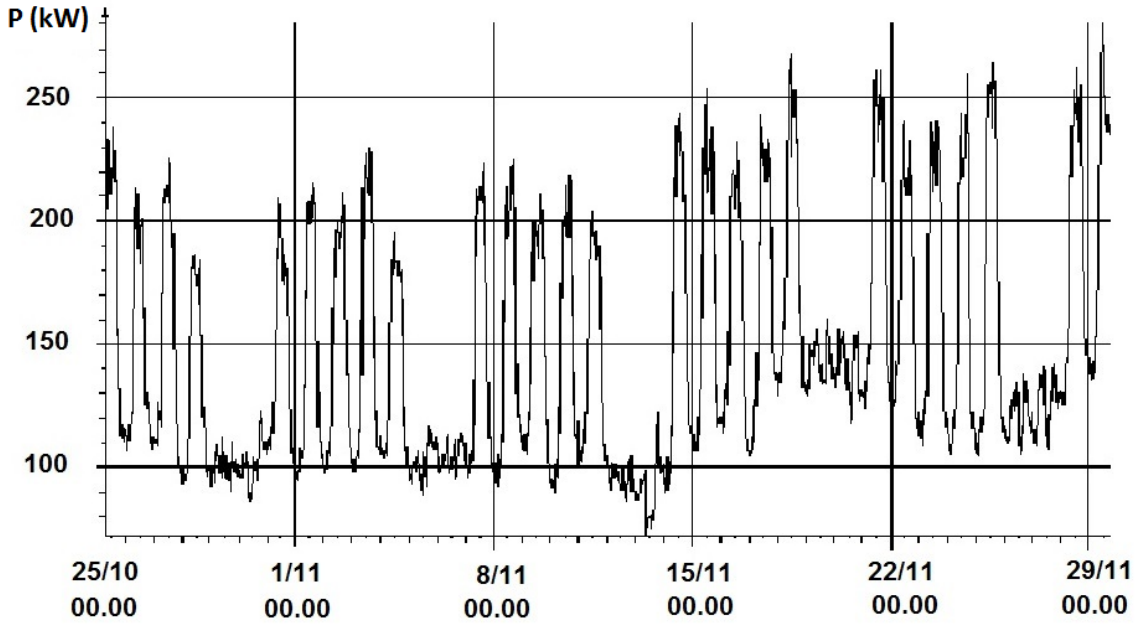

Fig. 6.1. Power consumption during entire measurement period.

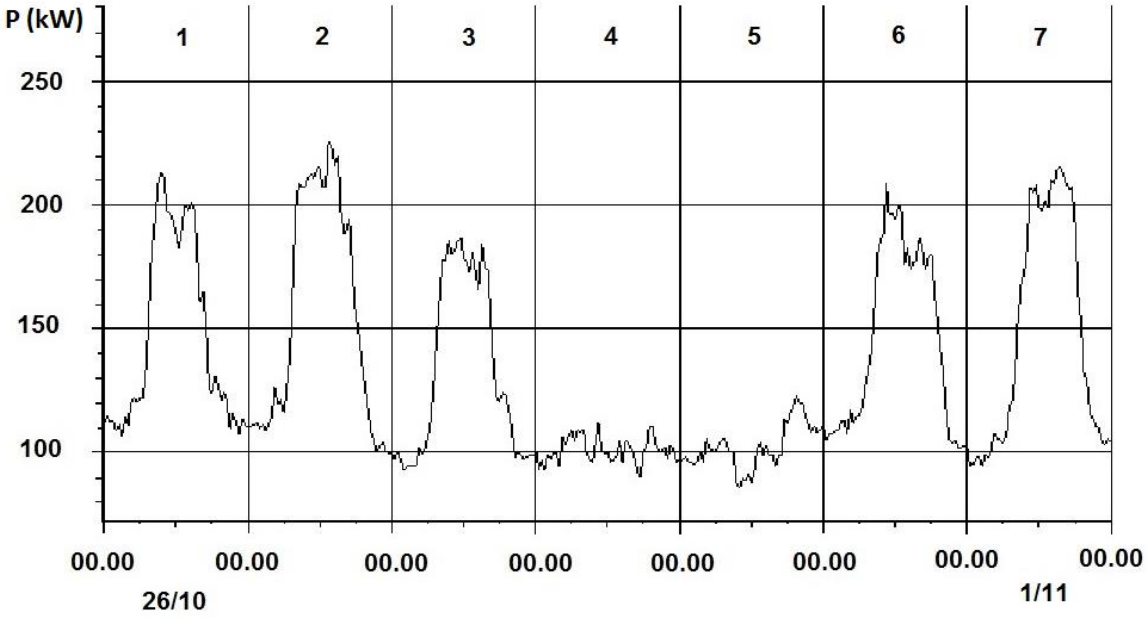

Fig. 6.2. Power consumption during the first 7 days.

Fig. 6.3 shows the mean consumption for all working days. The values represent the mean of consumption for all points in time. The corresponding mean values for the weekends is shown in Fig. 6.4.

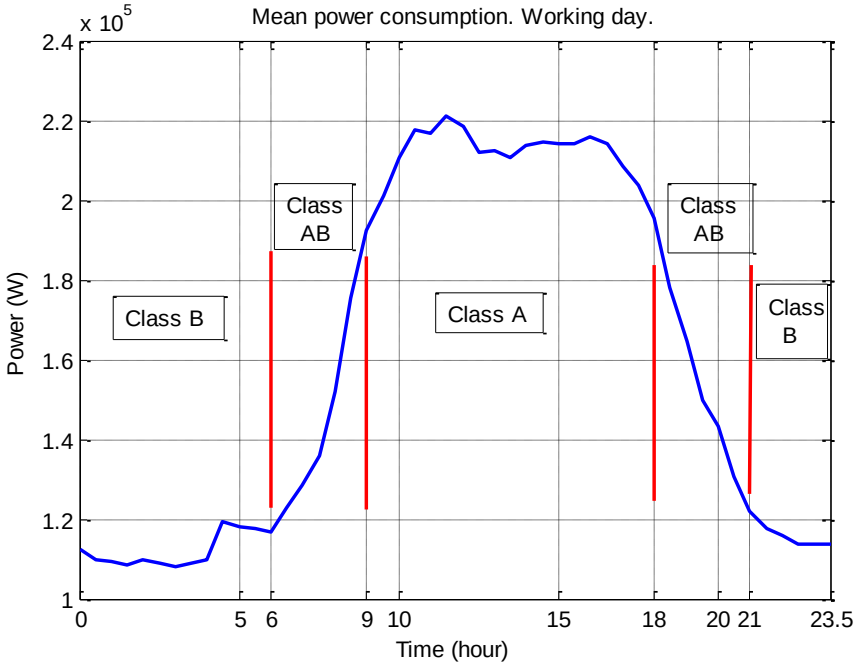

Fig. 6.3. Power consumption. Mean value for working days.

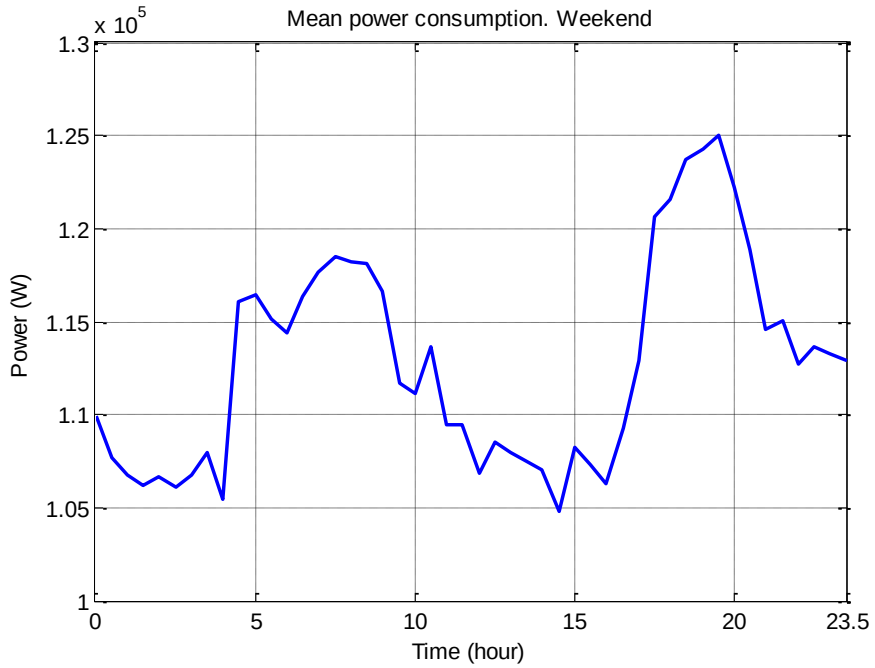

Fig. 6.4. Power consumption. Mean value for weekend days.

The results of the measurements make it reasonable to subdivide the days into different classes depending on points in time in question.

The following classification is made:

- Class A: Power consumption during day-time. Working day.
- Class B: Power consumption during evening-/night-time. Working day.
- Class AB: Power consumption during transition between day-time to evening-time and night-time to day-time. Working day.
- Class C: Power consumption during weekend

The following time intervals for the working day classes are defined:

- Time interval class A: 09.00 - 18.00
- Time interval class B: 00.00 – 06.00 and 21.00 – 00.00
- Time interval class AB: 06.00 – 09.00 and 18-00- 21.00

The power consumption can be divided into different frequency components. In the following analysis, two frequency components are used:

- Low frequency component
- High frequency component

(6.1) to (6.6) clarify certain details for the continued consideration of the topic.

$$S = P + jQ \tag{6.1}$$

$$P = |\mathbf{S}| \times \cos \varphi \tag{6.2}$$

$$Q = |\mathbf{S}| \times \sin \varphi \tag{6.3}$$

Where:

S: Apparent power
P: Active power
Q: Reactive power
φ: Phase angle

$|S|$ is divided into two components S_L and S_H

$$|S| = S_L + S_H \tag{6.4}$$

Where:

S_L: Low frequency power component
S_H: High frequency power component

$$S_L = F1 \tag{6.5}$$

$$S_H = F2 \times S_L \tag{6.6}$$

Where: F1 and F2 are statistical functions.

6.3 Principle for the model

The model shall simulate the statistical distribution of power consumption over a defined time period. This is done by using (6.4) - (6.6) in combination with the defined classes A, B, AB and C. According to (6.5), the statistical function, F1, gives the low frequency component. F1, depends on the class in question, resulting in F1(A), F1(B), F1(AB) and F1(C) according to:

F1(A): Defines low frequency component, day-time, working day.

F1(B): Defines low frequency component, evening-/night-time, working day.

F1(AB): Defines low frequency component, transition between night-time to day-time and day-time to evening-time.

F1(C): Defines low frequency component, weekend.

Fig. 6.5 illustrates how the low frequency components are functions of a point in time during a working day. F1(B)" in the figure defines the low frequency component, evening-/night-time, for a new 24-hour cycle. This will indicate that all functions F1 are updated every new 24-hour cycle.

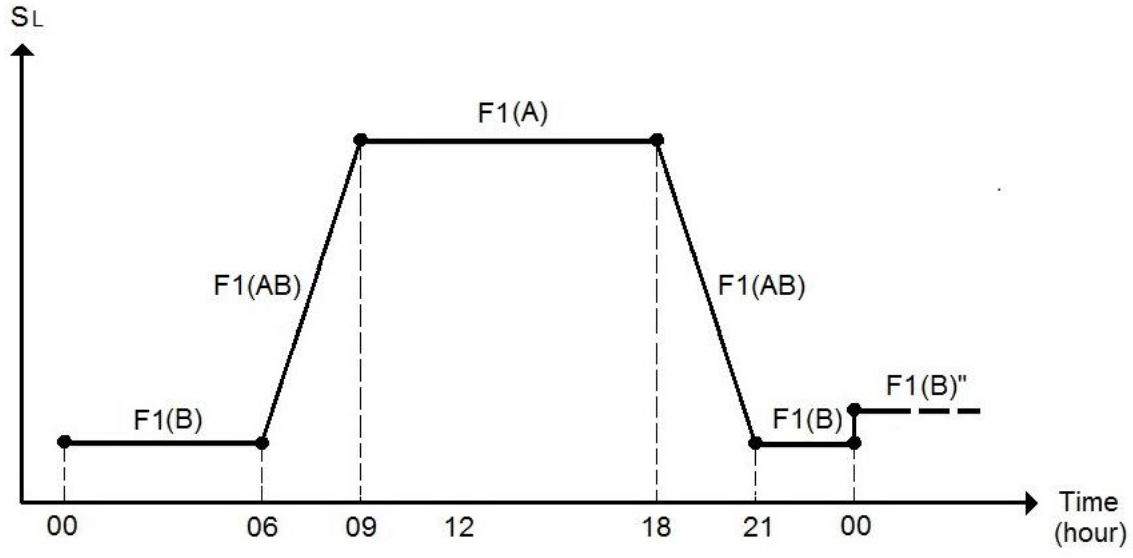

Fig. 6.5. Low frequency component as a function of time.

According to (6.6), the statistical function F2 results in the high frequency component. Like function F1, function F2 also depends on the class in question, resulting in F2(A), F2(B), F2(AB) and F2(C) according to:

F2(A): Defines high frequency component, day-time, working day.

F2(B): Defines high frequency component, evening-/night-time, working day.

F2(AB): Defines high frequency component, transition between night-time to day-time and day-time to evening-time, working day.

F2(C): Defines high frequency component, weekend.

F2(A), F2(B), F2(AB) and F2(C) are equivalent to gradient functions of the electrical load in the following. See the following sections.

6.4 Statistical analysis

6.4.1 Measurement vectors

Fig. 6.6 - Fig. 6.9 illustrate the measurements for class A, B, AB and C gathered in separated measurement vectors for each class.

Each vector was analysed with regard to low frequency and high frequency component. See sections 6.4.2 - 6.4.6.

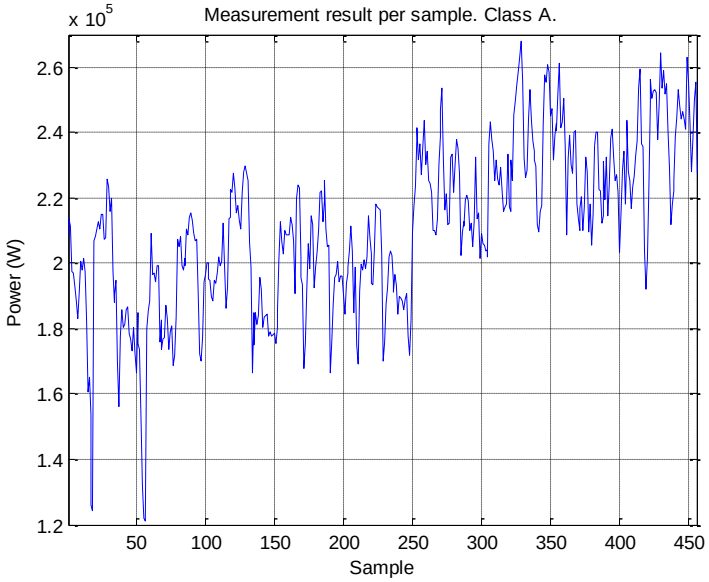

Fig. 6.6. Measurement result per sample. Class A. 456 samples. Min value = 120960 W. Max value = 267820 W.

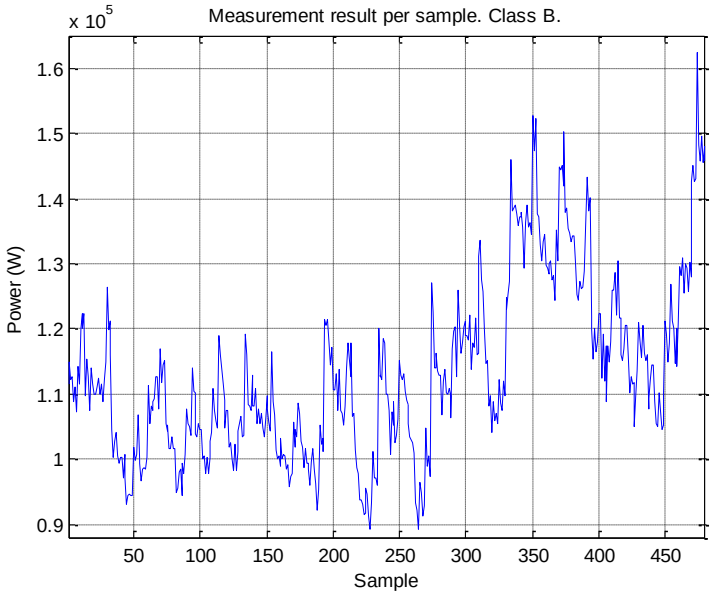

Fig. 6.7. Measurement result per sample. Class B. 480 samples. Min value = 89320 W. Max value = 162400 W.

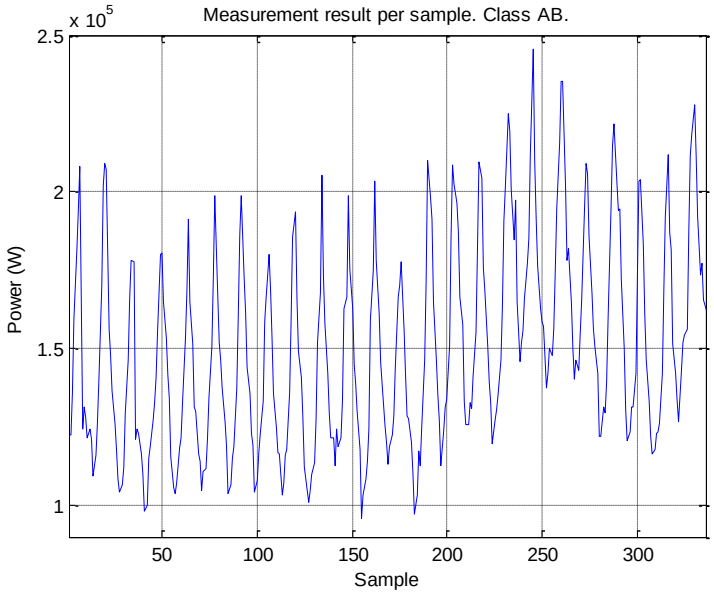

Fig. 6.8. Measurement result per sample. Class AB. 336 samples. Min value = 95900 W. Max value = 245420 W.

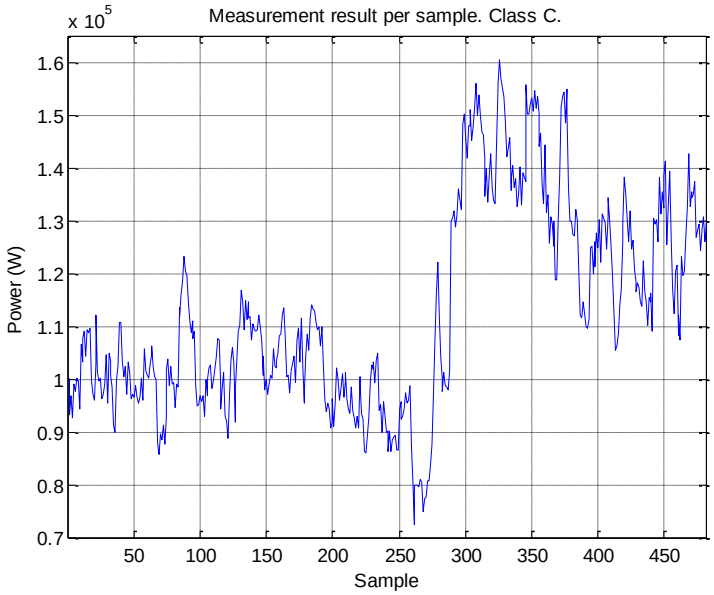

Fig. 6.9. Measurement result per sample. Class C. 481 samples. Min value = 72240 W. Max value = 160440 W.

6.4.2 Low frequency component. Class A, B and C

Measured values were analysed. The conclusion was to model the low frequency components as Gaussian distributed functions for class A, B and C. The distributions are shown in Fig. 6.10 - Fig. 6.12. The Gauss parameters are presented in the figures and in Table 6.2.

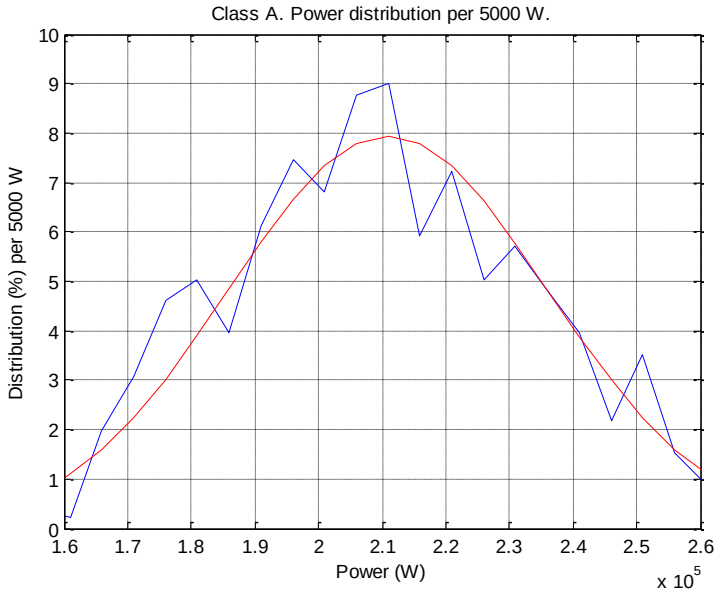

Fig. 6.10. Low frequency component. Class A. Power distribution per 5000 W. Blue curve: measured values. Red curve: Gauss distribution with $\mu = 2.1091 \times 10^5$ and $\sigma = 2.5107 \times 10^4$. See Table 6.2.

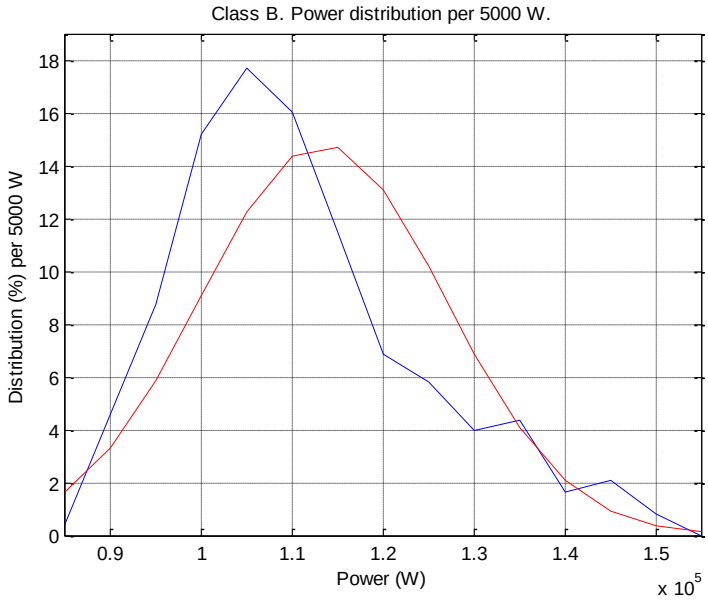

Fig. 6.11. Low frequency component. Class B. Power distribution per 5000 W. Blue curve: measured values. Red curve: Gauss distribution with $\mu = 1.1333 \times 10^5$ and $\sigma = 1.3462 \times 10^4$. See Table 6.2.

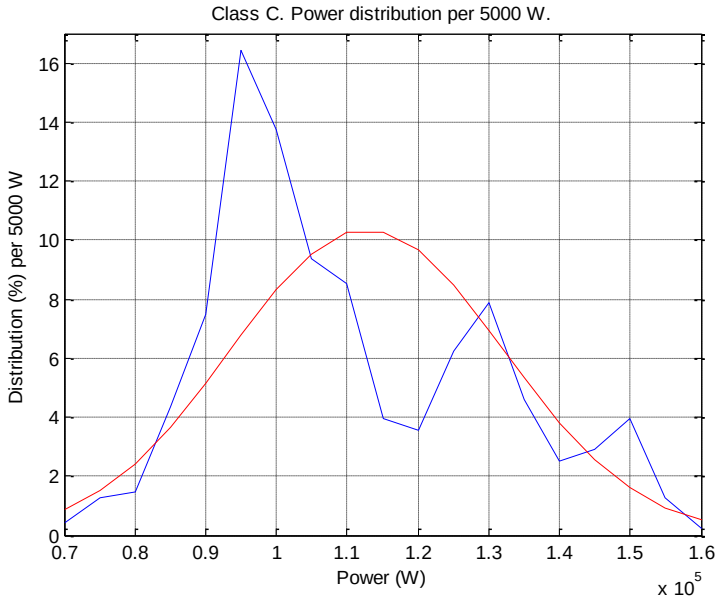

Fig. 6.12. Low frequency component. Class C. Power distribution per 5000 W. Blue curve: measured values. Red curve: Gauss distribution with $\mu = 1.1278 \times 10^5$ and $\sigma = 1.9269 \times 10^4$. See Table 6.2.

6.4.3 High frequency component. Class A, B and C

Measured values were analysed. The gradients between measurement samples were analysed. The conclusion was to model the gradients as Gaussian distributed functions to be used as bases for the high frequency components.

The gradient is defined according to:

$$\text{Grad (k)} = \frac{\text{Vect(k+1)} - \text{Vect(k)}}{\text{Vect(k)}} \qquad (6.7)$$

Where:

Grad(k): Gradient of sample k in measurement vector
Vect (k): Measurement value of sample k in measurement vector
Vect (k+1): Measurement value of k+1 in measurement vector

The distributions are shown in Fig. 6.13 - Fig. 6.15. The Gauss parameters are presented in the figures and in Table 6.2.

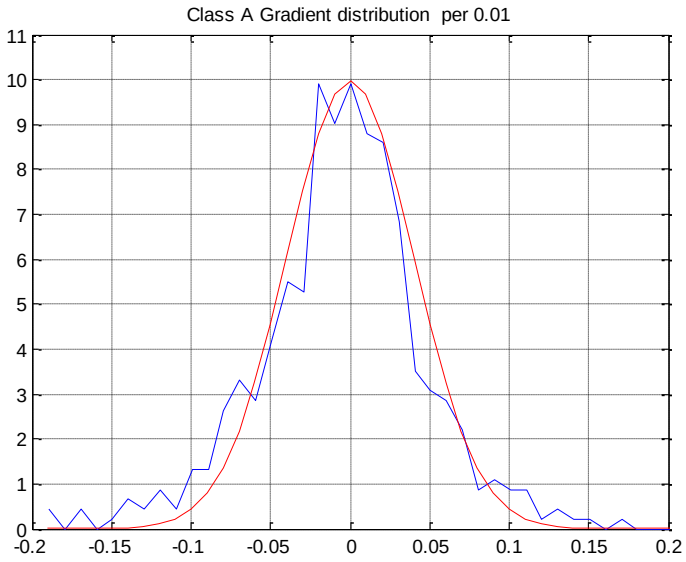

Fig. 6.13. Class A. Gradient distribution per 0.01. Blue curve: measured values. Red curve: Gauss distribution with μ = 0 and σ = 0.04. See Table 6.2.

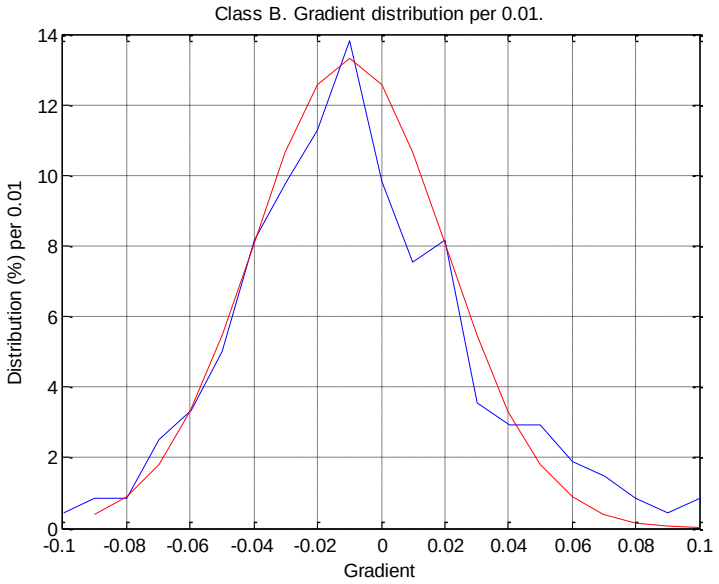

Fig. 6.14. Class B. Gradient distribution per 0.01. Blue curve: measured values. Red curve: Gauss distribution with μ = -0.01 and σ = 0.03. See Table 6.2.

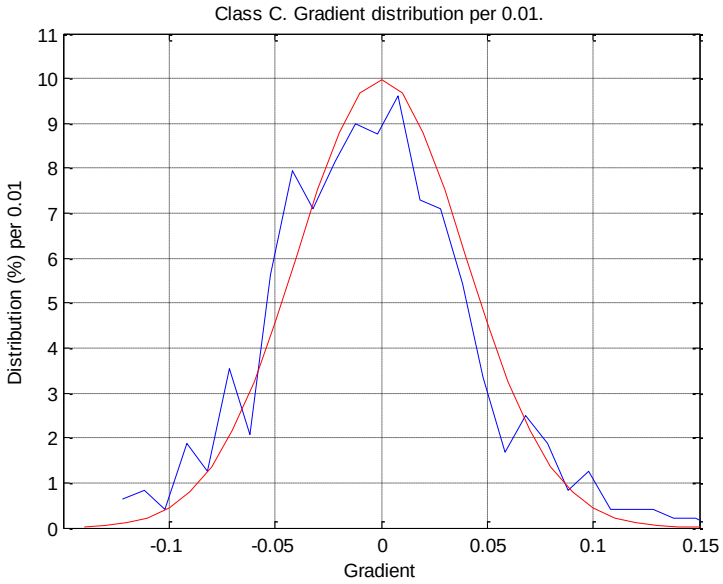

Fig. 6.15. Class C. Gradient distribution per 0.01. Blue curve: measured values. Red curve: Gauss distribution with μ = 0 and σ = 0.04. See Table 6.2.

6.4.4 Low frequency component. Class AB

Calculation of low frequency component for class AB is done for 2 separate time intervals.

Time interval 06 – 09:

$$F1(AB)\_1 = F1(B) + \frac{F1(A) - F1(B)}{N1} \times \Delta N \quad (6.8)$$

Where:

N1: Number of simulation steps in time region 06 – 09
ΔN: Simulation step in time region (1 - N1)

Time interval 18 – 21:

$$F1(AB)\_2 = F1(A) + \frac{F1(B) - F1(A)}{N2} \times \Delta N \quad (6.9)$$

where:

N2: Number of simulation steps in time region 18 – 21
ΔN: Simulation step in time region (1 - N2)

6.4.5 High frequency component. Class AB

Calculation of high frequency component for class AB is done according:

$$F2(AB) = F2(A) \quad (6.10)$$

This means that the high frequency component for class AB will be the same as for class A.

6.4.6 Conclusion of the analysis

Table 6.2 gives a conclusion of the Gauss parameters according to sections 6.4.2 - 6.4.5.

Function F1 is updated each 24-hour cycle, giving the low frequency component. Function F2 is updated each 30-minute cycle, giving the high frequency component.

Table 6.2. Statistical Gauss parameters per classes.

Class	**F1**		**F2**	
	Mean value (W)	*Standard deviation (W)*	*Mean value*	*Standard deviation*
A	2.1091×10^5	2.5107×10^4	0	0.04
B	1.1333×10^5	1.3462×10^4	-0.01	0.03
AB	Lines between F1(A) and F1(B)		0	0.04
C	1.1278×10^5	1.9269×10^4	0	0.04

According to (6.5) and (6.6):

- Low frequency power component: F1
- High frequency power component: F1 × F2

6.4.7 High frequency power component F2 alt gradient G_{NT}

The notations F2(A), F2(B), F2(AB) and F2(C) are also notated with corresponding gradients in the following, named $G_{NT}(n)$, where “n” is index for corresponding simulation step like:

High frequency power component = F1 × $G_{NT}(n)$ (6.11)

6.4.8 The model in matrix form

The model can be expressed according to:

$$\mathbf{P_L} = \mathbf{V_L} \times (\mathbf{M_E} + \mathbf{M_G}) \quad (6.12)$$

Where:

$\mathbf{P_L}$: N elements vector consisting of electrical load. See (6.23)
$\mathbf{V_L}$: N elements vector consisting of base components of electrical load. See (6.15)
$\mathbf{M_E}$: N × N diagonal matrix. The main diagonal consists of “1”. See (6.13)

M_G: N × N diagonal matrix. The main diagonal consists of electrical load gradients. See (6.14)
N: Number of simulation steps

Suppose a simulation corresponding to 356 days and a time resolution of 10 minutes. This means N = 52560.

$$\mathbf{M_E(N\times N)} = \begin{pmatrix} 1 & 0 & 0 & \cdots & 0 & 0 & 0 \\ 0 & 1 & 0 & \cdots & 0 & 0 & 0 \\ 0 & 0 & 1 & \cdots & 0 & 0 & 0 \\ \vdots & \vdots & \vdots & \vdots & \vdots & \vdots & \vdots \\ \vdots & \vdots & \vdots & \vdots & \vdots & \vdots & \vdots \\ \vdots & \vdots & \vdots & \vdots & \vdots & \vdots & \vdots \\ \vdots & \vdots & \vdots & \vdots & \vdots & \vdots & \vdots \\ 0 & 0 & 0 & \cdots & 1 & 0 & 0 \\ 0 & 0 & 0 & \cdots & 0 & 1 & 0 \\ 0 & 0 & 0 & \cdots & 0 & 0 & 1 \end{pmatrix} \quad (6.13)$$

(6.14) shows M_G corresponding to the first 24 simulation hours.

$$\mathbf{M_G} = \begin{pmatrix} \mathrm{Grad}(1) & 0 & 0 & 0\ 0\ 0\ 0 & 0 & 0 \\ 0 & \mathrm{Grad}(2) & 0 & 0\ 0\ 0\ 0 & 0 & 0 \\ 0 & 0 & \mathrm{Grad}(3) & 0\ 0\ 0\ 0 & 0 & 0 \\ \vdots & \vdots & \vdots & \vdots\ \vdots\ \vdots\ \vdots & \vdots & \vdots \\ \vdots & \vdots & \vdots & \vdots\ \vdots\ \vdots\ \vdots & \vdots & \vdots \\ \vdots & \vdots & \vdots & \vdots\ \vdots\ \vdots\ \vdots & \vdots & \vdots \\ \vdots & \vdots & \vdots & \vdots\ \vdots\ \vdots\ \vdots & \vdots & \vdots \\ 0 & 0 & 0 & 0\ 0\ 0\ 0 & \mathrm{Grad}(143) & 0 \\ 0 & 0 & 0 & 0\ 0\ 0\ 0 & 0 & 0 \\ 0 & 0 & 0 & 0\ 0\ 0\ 0 & 0 & \mathrm{Grad}(144) \end{pmatrix} \quad (6.14)$$

(6.15) shows V_L corresponding to the first 24 hours of a simulation.

$$\mathbf{V_L} = ([V_L(1) – V_L(36)], [V_L(37) – V_L(54)], [V_L(55) – V_L(108)], [V_L(109) – V_L(126)], [V_L(127) - V_L(144)]) \quad (6.15)$$

Where:

$V_L(1)$ to V(36) = F1(B) (6.16)

$V_L(37)$ to $V_L(54)$ = F1(B)+Fr_1×n, (n = 1,2, …, 18) (6.17)

$V_L(55)$ to $V_L(108)$ = F1(A) (6.18)

$V_L(109)$ to $V_L(126)$ = F1(A)+Fr_2×n, (n = 1,2, …, 18) (6.19)

$V_L(127)$ to $V_L(144)$ = F1(B) (6.20)

$$Fr\_1 = \frac{F1(A) - F1(B)}{N1} \quad (6.21)$$

$$Fr\_2 = \frac{F1(B) - F1(A)}{N2} \quad (6.22)$$

According to F1, F2 and Grad, see section 6.4.1- 6.4.7.

Applying (6.12) results in:

$\mathbf{P_L}$ = ([$P_L(1) – P_L(36)$], [$P_L(37) – P_L(54)$], [$P_L(55) – P_L(108)$], [$P_L(109) – P_L(126)$], [$P_L(127) - P_L(144)$]) (6.23)

Where:

$P_L(n)$ = F1(B)×(1+ Grad(n)) $1 \leq n \leq 36$ (6.24)

$P_L(n)$ = (F1(B)+Fr_1×(n-36))×(1+ Grad(n)) $37 \leq n \leq 54$ (6.25)

$$P_L(n) = F1(A)\times(1+ Grad(n)) \qquad 55 \leq n \leq 108 \qquad (6.26)$$

$$P_L(n) = (F1(A)+Fr\_2\times(n-108))\times(1+ Grad(n)) \qquad 109 \leq n \leq 126 \qquad (6.27)$$

$$P_L(n) = F1(B)\times(1+ Grad(n)) \qquad 127 \leq n \leq 144 \qquad (6.28)$$

6.5 Validation

6.5.1 Total energy over a year

A comparison is done between real consumed energy during a year according to Table 6.1 and corresponding energy based on mean values for the classes according to Table 6.2. The following assumption is made:

- Number of working days per year: 240
- Number of weekend/holidays per year: 125

Table 6.3 summarises the calculation.

Table 6.3. Calculation of daily energy consumption.

Class	**Hours per day**	**Mean value (kW)**	**Energy per day (kWh) (Hours per day × Mean value)**
A	9	210.91	1898.19
B	9	113.33	1019.97
AB	6	(210.91+ 113.33)/2	972.72
C	24	112.78	2706.72
Total energy per day, working day, all classes (kWh)			3890.88
Total energy per day, weekend/holiday (kWh)			2706.72

The calculated annual energy consumption is:

$$W_{annual} = N_{working\ day} \times W_{working\ day} + N_{weekend\ day} \times W_{weekend\ day} \qquad (6.29)$$

Where:

W_{annual}: annual energy consumption
$W_{working\ day}$: Energy per day, working day = 3890.88 kWh
$W_{weekend\ day}$: Energy per day, weekend/holiday = 2706.72 kWh
$N_{working\ day}$: Number of working days per year = 240
$N_{weekend\ day}$: Number of weekend/holidays per year = 125

This results in:

$W_{annual} = 1.272 \times 10^6$ kWh.

Measured annual energy according to Table 6.1 is 1.274×10^6 kWh.

Measured and calculated values differ by about 0.16 %.

This means that measurement and calculation match each other well.

6.5.2 Mean power and standard deviation

A validation is performed by comparing the result from the first 20 measured working days with corresponding simulation. The following have been compared:

Relation 1: Relation between mean power of measured working days and corresponding simulation.

Relation 2: Relation between standard deviation of measured working days and corresponding simulation.

This has been performed for 1000 simulation cycles. The result follows according to Fig. 6.16 and Fig. 6.17.

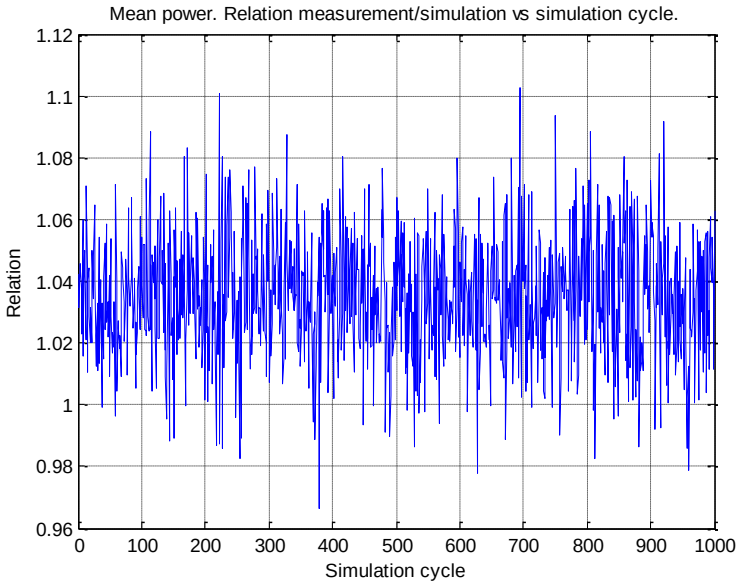

Fig. 6.16. Relation1. Mean power. Relation measurement to simulation vs simulation cycle.

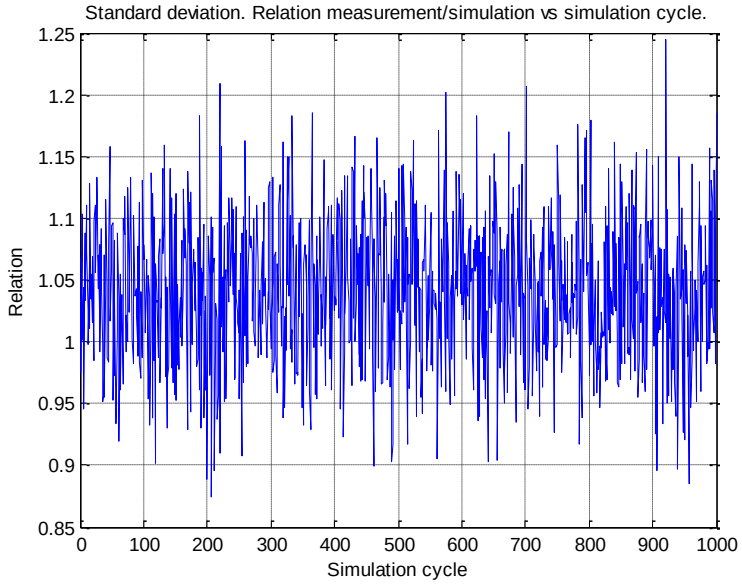

Fig. 6.17. Relation 2. Standard deviation of power. Relation measurement to simulation vs simulation cycle.

Table 6.4 gives the result of the comparison between measurement and simulation.

Table 6.4. Relation measurement to simulation.

Relation 1 (mean power)	Relation 2 (stand. dev. of power)
Mean relation 1 is 1.0350	Mean relation 2 is 1.0407
Stand. dev. relation 1 is 0.0198	Stand. dev. relation 2 is 0.0589

The comparisons show an acceptable consistency between measurements and simulations. The differences are:

- 3.5 % for mean power (with 2-σ limits +1.5 % to +5.5 %)
- 4 % for standard deviation (with 2-σ limits from -8 % to +16 %)

6.6 Simulation example

Fig. 6.18 illustrates a simulation example based on the modelling according to sections 6.2 - 6.4. The simulation covers 16 days with 12 working days and 4 weekend days.

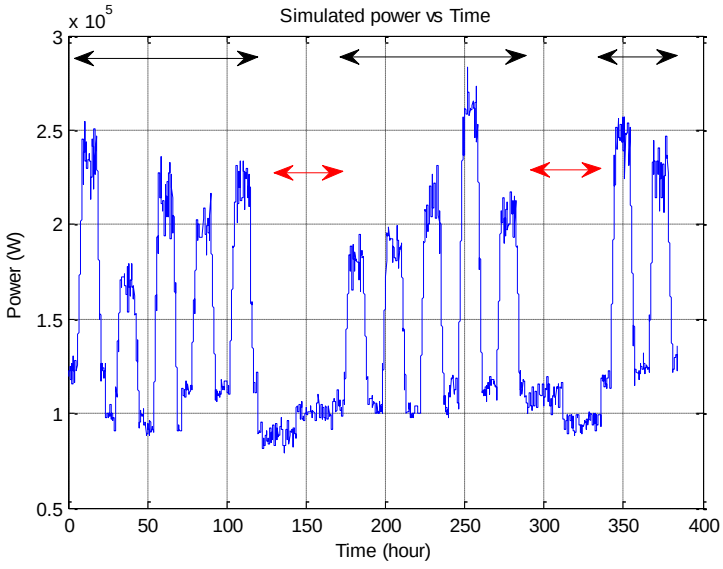

Fig. 6.18. Simulation example. 12 working days (black arrowed lines) and 4 weekend days (red arrowed lines).

6.7 Statistical model for a general industrial area

Sections 6.2 - 6.4 have dealt with a specific industrial area. In order to model the power consumption with regard to a general industrial area, some assumptions need to be made:

- The general industrial area has a power consumption that can be divided into the 4 classes A, B, C and AB according to Fig. 6.5. This refers to both power level and time limits
- The numeric relations between power for classes in the area, used above, is the same as corresponding relations in a general area. This refers to both low frequency component and high frequency component

Given the assumptions described above, it is possible to transform the statistical parameters from Table 6.2 to parameters that are valid for a general industrial area with any other optional annual power consumption. This is done by scaling the low frequency components in relation to the annual power consumption. The high frequency components are the same in all cases regardless of annual power consumption.

Note: This method for handling a general industrial area of course imposes restrictions. In reality, there are obviously a lot of variations of power consumption, depending on composition and kind of industrial areas. However, in the absence of more adequate measurements, this may be accepted as a method for providing reasonable information about the scenario in question.
The conclusion of that discussed above, implies the Gaussian parameters according to Table 6.5 and a general industrial area with annual power consumption as an optional parameter.

Table 6.5. Statistical Gauss parameters for a general industrial area.

Class	**F1**		**F2**	
	Mean value (W)	**Standard deviation (W)**	**Mean value (W)**	**Standard deviation (W)**
A	$K1 \times 2.1091 \times 10^5$	$K1 \times 2.5107 \times 10^4$	0	0.04
B	$K1 \times 1.1333 \times 10^5$	$K 1\times 1.3462 \times 10^4$	-0.01	0.03
AB	Straight line between F1(A) and F1(B)		0	0.04
C	$K1 \times 1.1278 \times 10^5$	$K1 \times 1.9269 \times 10^4$	0	0.04

Parameter K1 in Table 6.5 is defined according to:

$$K1 = E / 1.274 \times 10^6 \qquad (6.30)$$

Where: E: Annual power consumption (kWh).

The figure "1.274×10^6" in (6.30) corresponds to the annual power consumption for the industrial area, used in the analysis according to sections 6.2 - 6.4.

6.8 Statistical model for a commercial centre

6.8.1 Model basic

In order to model the power consumption with regard to a commercial centre, the following assumptions are made:

- Power consumption can be modelled by one single class, class A_{COM}
- Class A_{COM} has a low frequency component and a high frequency component. These components have same statistical properties as corresponding components in class C, industrial area

For the moment, and without specific statistics for commercial centres, these assumptions may be relevant. The reservations made concerning the general industrial area in section 6.7, however, also apply to a commercial centre.

The assumptions discussed above imply the Gaussian parameters according to Table 6.6.

Table 6.6. Statistical Gauss parameters for a commercial centre.

F1		**F2 (gradient)**	
Mean value (W)	Standard deviation (W)	Mean value (W)	Standard deviation (W)
$K2 \times 1.1278 \times 10^5$	$K2 \times 1.9269 \times 10^4$	0	0.04

Parameter K2 in Table 6.6 is defined according to (6.31).

$$K2 = \frac{E}{Eref} \tag{6.31}$$

Where:

E: Annual power consumption (Wh)
Eref: Annual power consumption (Wh) for class C, industrial area, according to (6.32).

$$Eref = 24 \times 365 \times 1.1278 \times 10^5 \tag{6.32}$$

The number "1.1278×10^5" corresponds to the mean value of F1 in class C, industrial area.

6.8.2 The model in matrix form

The model can be expressed according to (6.12). Suppose a time resolution of 10 minutes. This results in (corresponding 24 hours):

$$\mathbf{V_L} = ([V_L(1) - V_L(144)] = F1(A_{COM}) \quad (6.33)$$

Where $F1(A_{COM})$ corresponds to F1 in section 6.8.1.

The high frequency component follows the relation according to (6.11).

$$\mathbf{P_L} = ([P_L(1) - P_L(144)] = F1(A_{COM}) \times (1 + G_{NT}(n)) \qquad 1 \leq n \leq N \quad (6.34)$$

Where N is the number of simulation steps during 24 hours and a time resolution of 10 minutes.

6.9 Statistical model for a residential area

6.9.1 Model basic

Fig. 6.19 illustrates the low frequency components during a 24-hour cycle for a proposal of a load model consisting of a residential area.

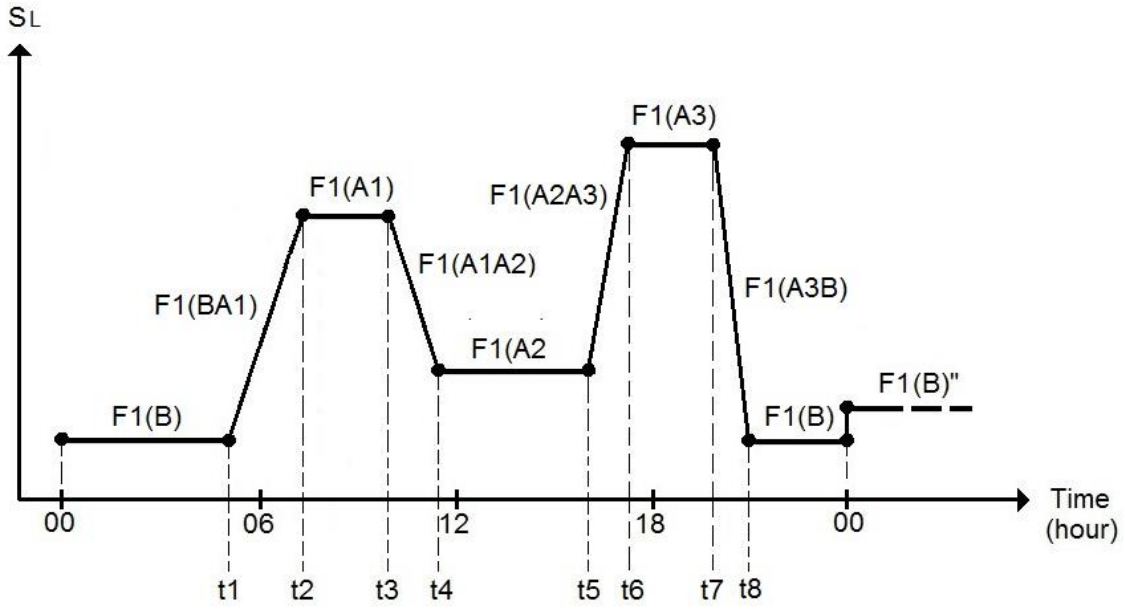

Fig. 6.19. Model for a residential area. Low frequency component.

The components are as follows:

- F1(B): low frequency component during time zones 00 – t1 and t8 – 00.
- F1(A1): low frequency component during time zone t2 – t3.
- F1(A2): low frequency component during time zone t4 – t5.
- F1(A3): low frequency component during time zone t6 – t7.
- F1(BA1): low frequency component during time zone t1 – t2.
- F1(A1A2): low frequency component during time zone t3 – t4.
- F1(A2A3): low frequency component during time zone t5 – t6.
- F1(A3B): low frequency component during time zone t7 – t8.

The transition between F1(B) – F1(A1), F1(A1) – F1(A2), F1(A2) – F1(A3) and F1(A3) – F1(B), corresponding to F1(BA1), F1(A1A2), F1(A2A3) and F1(A3B), follows the same principle as discussed in section 6.4.4.

The time zones t2 – t3 and t6 – t7 correspond to time zones with extra power consumption.
F1(B) is used as a reference for the low frequency components F1(A1), F1(A2) and F1(A3), according to Table 6.7.

Table 6.7. Low frequency components F1(A1), F1(A2) and F1(A13).

Low frequency component	Value
F1(A1)	n1 × F1(B)
F1(A2)	n2 × F1(B)
F1(A3)	n3 × F1(B)

Calculation of F1(B) is done according to:

$E_m = z1 \times m1 + z2 \times m2 + z3 \times m3 + z4 \times m4 + z5 \times m5 + z6 \times m6 + z7 \times m7 + z8 \times m8$ (6.35)

Where:

E_m: Mean energy corresponding to one day according to Fig. 6.19.

$z1 = 24 - t8 + t1$ (6.36)

$z2 = t2 - t1$ (6.37)

$z3 = t3 - t2$ (6.38)

$z4 = t4 - t3$ (6.39)

$z5 = t5 - t4$ (6.40)

$z6 = t6 - t5$ (6.41)

$z7 = t7 - t6$ (6.42)

$z8 = t8 - t7$ (6.43)

Where:

z1 - z8: time zones

$m1 = F1(B)$ (6.44)

$m2 = \frac{F1(B)+F1(A1)}{2}$ (6.45)

$$m3 = F1(A1) \tag{6.46}$$

$$m4 = \frac{F1(A1)+F1(A2)}{2} \tag{6.47}$$

$$m5 = F1(A2) \tag{6.48}$$

$$m6 = \frac{F1(A2)+F1(A3)}{2} \tag{6.49}$$

$$m7 = F1(A3) \tag{6.50}$$

$$m8 = \frac{F1(A3)+F1(B)}{2} \tag{6.51}$$

Where:

m1 - m8: Power with respect to time zones and power within time zones

$$E = 365 \times E_m \tag{6.52}$$

Where:

E: annual energy consumption (Wh)

$$E_m = K_{F1(B)} \times F1(B) \tag{6.53}$$

Where:

$K_{F1(B)}$: Factor as a result of factors n1 - n3 in Table 6.7 and time limits t1 - t8. See (6.35).

From (6.52) and (6.53) is obtained:

$$F1(B) = \frac{E}{365 \times K_{F1(B)}} \quad (6.54)$$

The statistical properties are assumed to be the same as for F1 and F2 in the industrial area, class C, and in relation to the power level in question. This assumption has not been validated. It is based only on the fact that workshop activities in an industrial area normally are quite low during the weekends. However, statistical properties of electrical consumption regarding office activities in an industrial area are assumed to be in parity with corresponding parameters for a residential area. See Table 6.8 and Table 6.9.

Table 6.8. Statistical Gauss parameters for a residential area. Low frequency component.

Low frequency component	Mean value (W)	Standard deviation (W)
F1(B)	F1(B)	$K2 \times 1.9269 \times 10^4$
F1(A1)	F1(B) × n1	$n1 \times K2 \times 1.9269 \times 10^4$
F1(A2)	F1(B) × n2	$n2 \times K2 \times 1.9269 \times 10^4$
F1(A3)	F1(B) × n3	$n3 \times K2 \times 1.9269 \times 10^4$

Parameter K2 in Table 6.8 is defined according to

$$K2 = \frac{F1(B)}{1.1278 \times 10^5} \quad (6.55)$$

The number "1.1278×10^5" corresponds to the mean value of F1 in class C, industrial area.

Table 6.9. Statistical Gauss parameters for a residential area. High frequency component.

High frequency component	Mean value (W)	Standard deviation (W)
F2(B)	0	0.04
F2(A1)	0	0.04
F2(A2)	0	0.04
F2(A3)	0	0.04

6.9.2 Parameters for time zones and low frequency components

6.9.2.1 Time zone limits

Time zone limits follow according to Table 6.10:

Table 6.10. Example of time zone limits.

Time zone	Limit (hour)
t1	5
t2	7
t3	10
t4	12
t5	15
t6	17
t7	21
t8	22

See Fig. 6.19.

6.9.2.2 Low frequency components

The low frequency components F1(A1), F1(A2) and F1(A3) are defined according to:

n1 = 2.5
n2 = 1.5
n3 = 3.5

See Table 6.7.

6.9.3 The model in matrix form

The model can be expressed according to (6.12). Suppose a time resolution of 10 minutes. This results for the first 24 hours in:

$$\mathbf{V_L} = ([V_L(1) – V_L(30)], [V_L(31) – V_L(42)], [V_L(43) – V_L(60)], [V_L(61) – V_L(72)], [V_L(73) - V_L(90)], [V_L(91) – V_L(102)], [V_L(103) – V_L(126)], [V_L(127) – V_L(132)], [V_L(133) – V_L(144)]) \quad (6.56)$$

Where:

$$V_L(1) \text{ to } V(30) = F1(B) \quad (6.57)$$

$V_L(31)$ to $V_L(42)$ = F1(B)+Fr_1×n, (n = 1,2, …, N1) (6.58)

$V_L(43)$ to V(60) = F1(A1) (6.59)

$V_L(61)$ to $V_L(72)$ = F1(B)+Fr_2×n, (n = 1,2, …, N2) (6.60)

$V_L(73)$ to V(90) = F1(A2) (6.61)

$V_L(91)$ to $V_L(102)$ = F1(B)+Fr_3×n, (n = 1,2, …, N3) (6.62)

$V_L(103)$ to V(126) = F1(A3) (6.63)

$V_L(127)$ to $V_L(132)$ = F1(B)+Fr_4×n, (n = 1,2, …, N4) (6.64)

$V_L(133)$ to V(144) = F1(B) (6.65)

Where:

N1: Simulation steps between t1 and t2. N1 = 12.
N2: Simulation steps between t3 and t4. N2 = 12.
N3: Simulation steps between t5 and t6. N3 = 12.
N4: Simulation steps between t7 and t8. N4 = 6.

$$Fr\_1 = \frac{F1(A1)-F1(B)}{N1} \quad (6.66)$$

$$Fr\_2 = \frac{F1(A2)-F1(A1)}{N2} \quad (6.67)$$

$$Fr\_3 = \frac{F1(A3)-F1(A2)}{N3} \quad (6.68)$$

$$Fr\_4 = \frac{F1(B) - F1(A3)}{N4} \tag{6.69}$$

P_L for the first 24 hours is according to:

$$\mathbf{P_L} = ([P_L(1) - P_L(30)], [P_L(31) - P_L(42)], [P_L(43) - P_L(60)], [P_L(61) - P_L(72)], [P_L(73) - P_L(90)], [P_L(91) - P_L(102)], [P_L(103) - P_L(126)], [P_L(127) - P_L(132)], [P_L(133) - P_L(144)]) \tag{6.70}$$

Where the elements in vector P_L are calculated according to the same principle as in (6.24) to (6.28).

The high frequency component follows the relation according to (6.11).

6.9.4 An example of a residential area

Fig 6.20 illustrates the simulation result during 24 hours based on the model and an annual energy consumption of 1000 GWh.

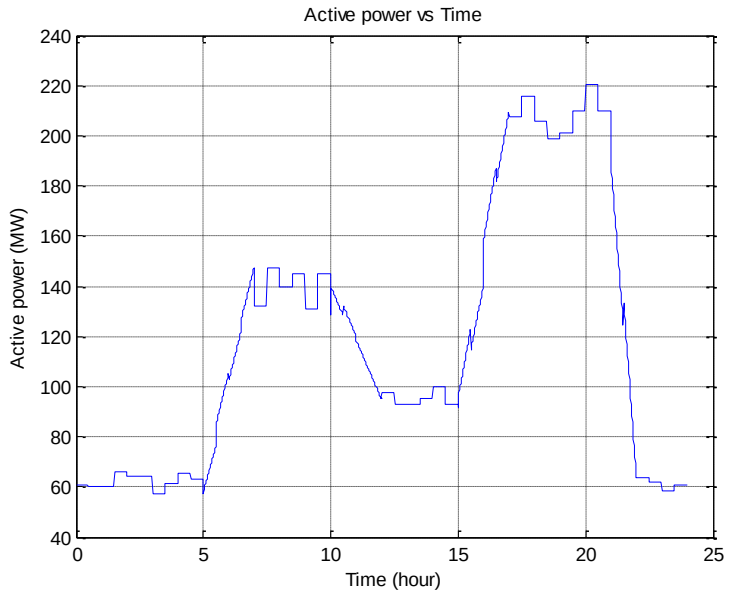

Fig. 6.20. Simulation example for a residential area.

6.10 Statistical model for an area consisting of a mix of industries, commercial centres and residential areas

Fig. 6.21 shows an area consisting of 4 industrial complexes, 1 commercial centre and 12 residential complexes.

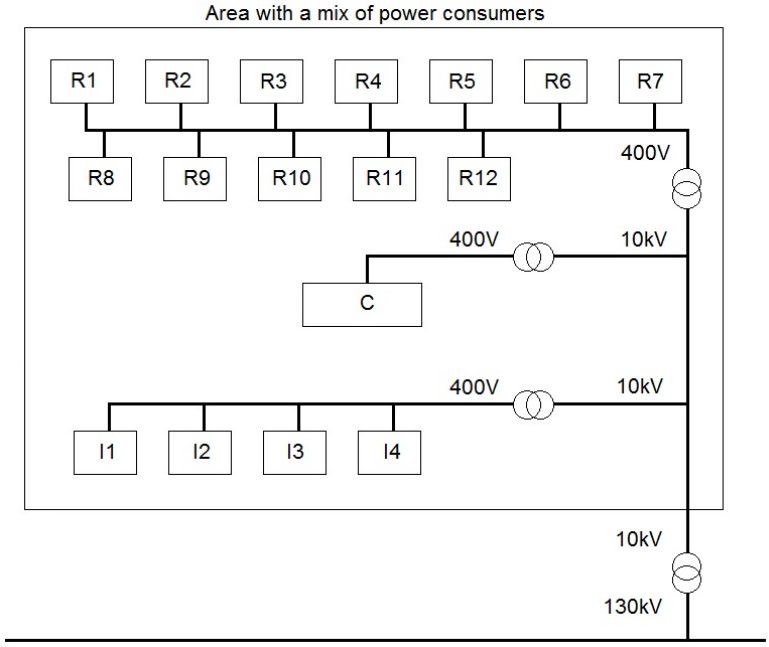

Fig. 6.21. A region consisting of a mix of power consumers.

Abbreviations in Fig. 6.21:

- I1 – I4: 4 industrial complexes
- C: Commercial centre
- R1 –R12: 12 residential complexes

A simulation is done with the following assumptions:

Industrial area, I1 – I4

- Model as in section 6.7. Annual power consumption: 1 GWh

Commercial centre, C

- Model as in section 6.8. Annual power consumption 0.5 GWh

Residential area, R1 – R12

- Model as in section 6.9. Annual power consumption 2 GWh

The simulation results for 3 simulation processes corresponding10 days are illustrated in Fig. 6.22 - Fig. 6.24. The figures clearly show the great statistical spread over time.

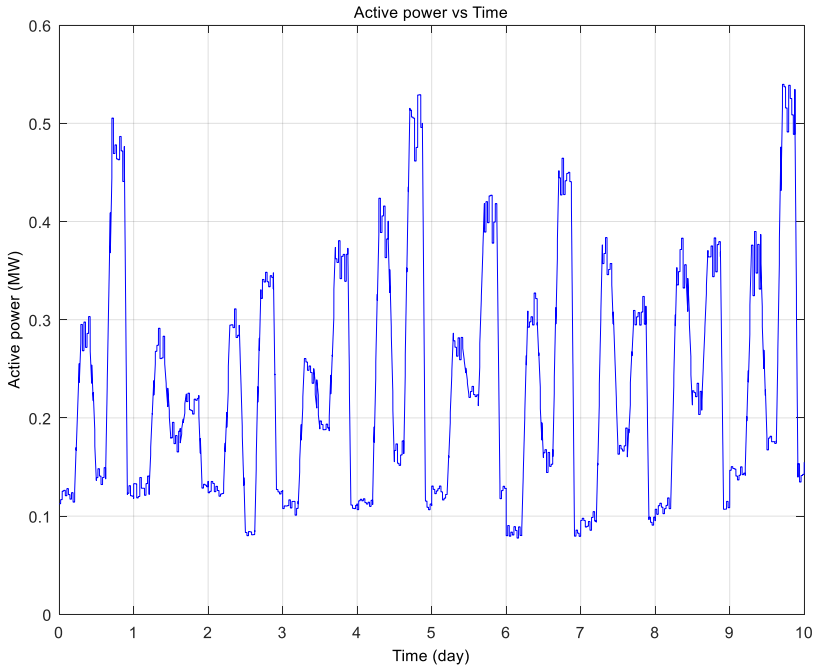

Fig. 6.22. Simulation 1. Simulated active power consumption during 10 days for the area of mixed power consumers.

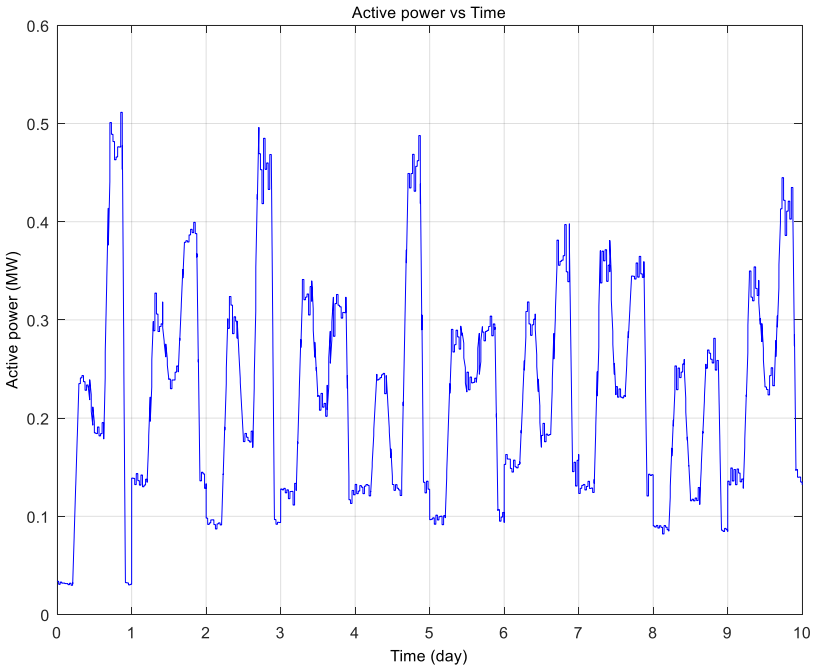

Fig. 6.23. Simulation 2. Simulated active power consumption during 10 days for the area of mixed power consumers.

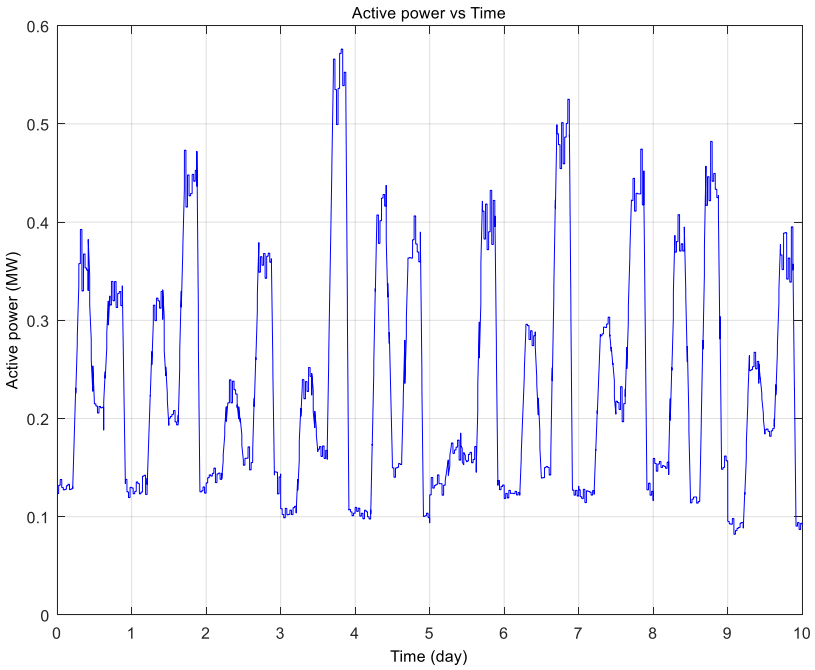

Fig. 6.24. Simulation 3. Simulated active power consumption during 10 days for the area of mixed power consumers.

6.11 Summary

This chapter describes the development work of a model for statistical simulation of different kinds of electrical power load. The model is used as a module in the simulation system according to chapter 3.

The analysis work is based on field measurements performed during a period of 36 days. The measurement object was an industrial area, consisting of different companies with a mixture of workshop and office activities.

The measurement values have been analysed based on a statistical perspective. The measurements have provided the basis for analysis of the electrical power load during longer periods (days) but has also given information about the temporary load changes that will be present in a load region. This has resulted in statistical modelling of the electrical power consumption divided into two components, a low frequency component and a high frequency component. The low frequency component is aimed on time periods on a number of hours, while the high frequency component is focused on the temporary power load variations, as is present during intervals of for example 10 minutes. The high frequency component is superimposed on the low frequency component, with the latter as a base.

The basic assumption has been that the low frequency component can be described based on a Gaussian distribution. This distribution is very consistent with measurements made. An update of this component is done at the beginning of the time interval in question. See below regarding different time classes.

The high frequency components are treated as gradients superimposed on the low frequency components and can in this context be seen as power consumption noise.

The high frequency component (gradient) is generated by randomly drawing from a Gaussian distribution. An update of this component is done, for example, every 10 minutes in real time.

The power load region, as has been the object for measurements, can be considered a reasonable representative for a small industrial estate.

As the average power consumption varies greatly depending on the time point of day and also between a working day and weekend day, it has been useful to define separate time classes. For the industrial area, the following classification has been made:

- Class A: Power consumption during day-time. Working day.
- Class B: Power consumption during evening-/night-time. Working day.
- Class AB: Power consumption during transition between day-time to evening- time and night-time to day-time. Working day.
- Class C: Power consumption during weekend

The following time intervals for the working day classes are defined:

- Time interval class A: 09.00 - 18.00
- Time interval class B: 00.00 – 06.00 and 21.00 – 00.00
- Time interval class AB: 06.00 – 09.00 and 18-00- 21.00

Statistical parameters for all classes have been defined based on performed measurements.

A rough model validation has been carried out. This involves comparing the obtained statistical parameters regarding measurements and simulations. A simulation test consisting of 1000 simulation rounds was performed. Mean value and standard deviation, based on all simulation rounds, were compared with mean value and standard deviation of measurements. The consistency between simulation results and measurement results were found to be very good.

A rough estimate has been made, namely that different industrial areas, regardless of size, have the same time-related power consumption patterns. This assumption implies that a scale factor proportional to the total annual consumption can be used as a model parameter for definition and modelling of a specific industrial estate. Based on this assumption, a general statistical model for an industrial estate has been developed.

A statistical model for a commercial centre has been developed. This is based on the industrial area with a focus on the statistical process during the weekend.

A statistical model for a residential area has been developed. A reasonable assumption regarding the internal dynamic process has been made. The statistical characteristics correspond to an industrial area during a weekend.

A mixture of industrial areas, commercial centres and residential areas can be modeled.

The different models have been compactly described by using matrix formulations.

CHAPTER 7

OPTIMUM ANGLE RELATIVE TO ZENITH AND SOUTH. SOLAR TRACKING

When planning the design of a photovoltaic system, the geometric orientation of solar cell panels towards the sun is of great importance. This chapter deals with analysis of the design with a focus on how solar panel angles relative to the sun has an impact on the produced power.

Two angles have been defined where the normal direction of solar panel surfaces acts as a reference direction: angle relative to south and angle relative to zenith.

Two design variants have been studied:

- Fixed installed solar cell panels. The panels are installed with fixed angles relative to zenith and to south.
- Solar tracking. The panels automatically follow the direction to the sun.

Five geographical locations have been investigated: Kiruna and Göteborg in Sweden, München in Germany, Malaga in Spain and Nairobi in Kenya.

The study will investigate the effect and sensitivity in relation to deviation from the optimal angle to south, that is zero. In this case Göteborg is taken as an example.

In respect of the angle relative to zenith, the location of the power plant has an important significance. Optimal angle for the five locations will be tested.

The technology with solar tracking can provide a great positive effect on energy production. The effect is, however, dependent on the location of the power plant. This will be studied and even compared with the case of fixed mounted panels.

The study described is performed by using the simulation system according to chapter 3.

7.1 Tasks of the study

The tasks of the study are the following:

- Find out the optimum angle Ω_Z for different latitudes
- Compare the annual produced solar energy for the 5 locations

- Test solar tracking and compare the result with corresponding result without solar tracking, but with optimum use regarding angle Ω_Z and angle Ω_S
- Test the effect when angle Ω_S differs from the optimum value zero.

7.2 Locations, cloudiness and angles

Five geographical locations are to be investigated:

Table 7.1 Locations and corresponding coordinates.

Location	Latitude (degrees)	Longitude (degrees)
Kiruna, Sweden	67.8	20.2
Göteborg, Sweden	57.7	12.0
München, Germany	48.8	11.3
Malaga, Spain	36.7	-4.4
Nairobi, Kenya	-1.3	36.8

The different degrees of cloudiness at the five locations are estimated according to section 4.2. The values are given in Table 4.3.

Two angles are defined:

- Angle between solar cell surface normal direction relative to south. This angle is denoted Ω_S
- Angle between solar cell surface normal direction relative to zenith. This angle is denoted Ω_Z

The angles Ω_Z and Ω_S are defined according to Fig. 2.4 and Fig. 2.5.

7.3 Annual energy vs Ω_Z (direction to zenith)

The optimum angles for the different locations and corresponding annual produced energy per m^2 follow according to Table 7.2. Angle Ω_Z has been varied with an angular resolution of 5º.

Table 7.2 Optimum angle Ω_Z vs location and corresponding produced annual energy.

Location	**Simulated Optimum angle Ω_Z (º)**	**Annual Produced energy (kWh/m^2) with Optimum angle Ω_Z**
Kiruna	50	56.31
Göteborg	40	76.47
München	35	98.16
Malaga	30	166.1
Nairobi	0	178.7

Fig. 7.1 illustrates the graph for Optimal angle Ω_Z vs latitude. As can be noted, the relation in principle follows a straight line. The simulated values have been adapted to a first order polynomial according to:

$$\Omega_Z\_opt(\beta) = C_0 + C_1 \times \beta \qquad (7.1)$$

Where:

Ω_Z_opt: Optimal value on Ω_Z according to adaptation (º)
C_0 = 1.6 (º)
C_1 = 0.7
β: Latitude (º)

Table 7.3 shows the optimal Ω_Z according to adaptation vs location.

Table 7.3. Optimal Ω_Z according to adaptation vs location.

Location	**Adapted Optimal angle Ω_Z_opt (º)**
Kiruna	49.1
Göteborg	42.0
München	35.8
Malaga	27.3
Nairobi	0.7

Adapted values are plotted together with the simulated ones in Fig. 7.1.

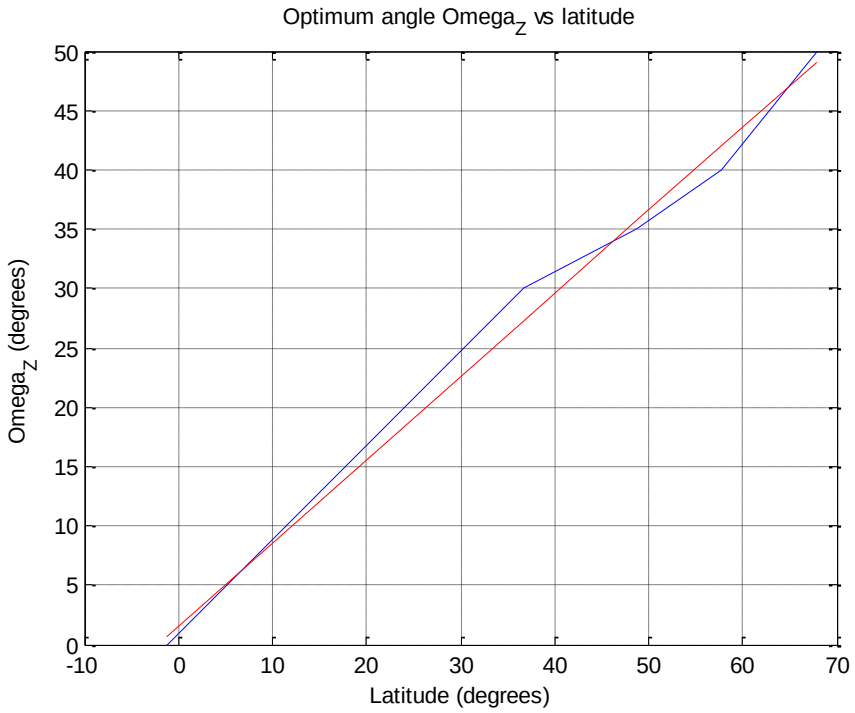

Fig. 7.1. Optimum angle Ω_Z vs latitude. Blue curve: Simulated values. Red curve: Adapted values. The blue curve represents simulation results. The reason that this curve is not continuous depends on the fact that simulations were performed with an angular resolution of 5º with respect to angle Ω_Z.

Fig. 7.2 – Fig. 7.4 illustrate the annual produced energy per m^2 for the five locations.

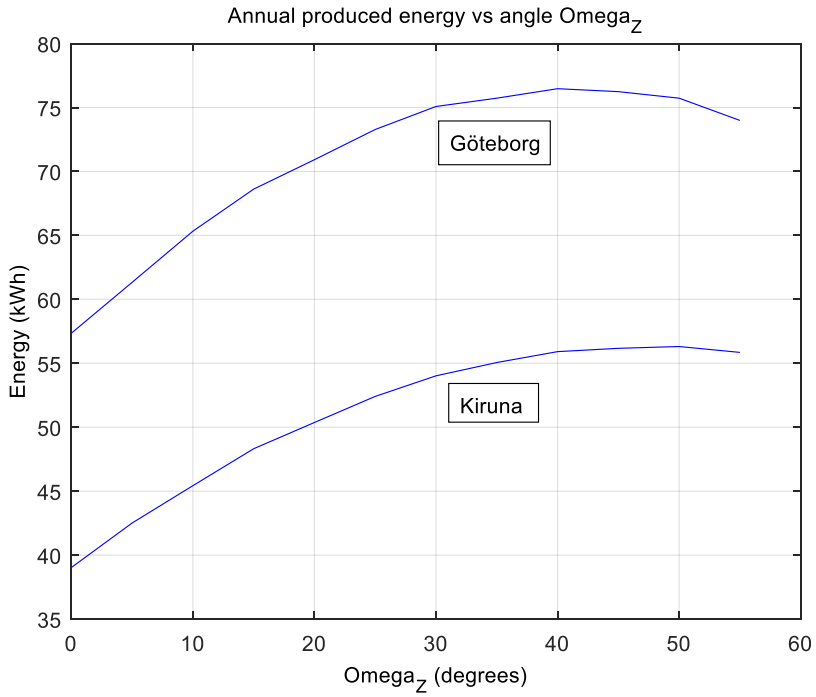

Fig. 7.2. Göteborg and Kiruna. Annual produced energy vs angle $\Omega_{Z.}$

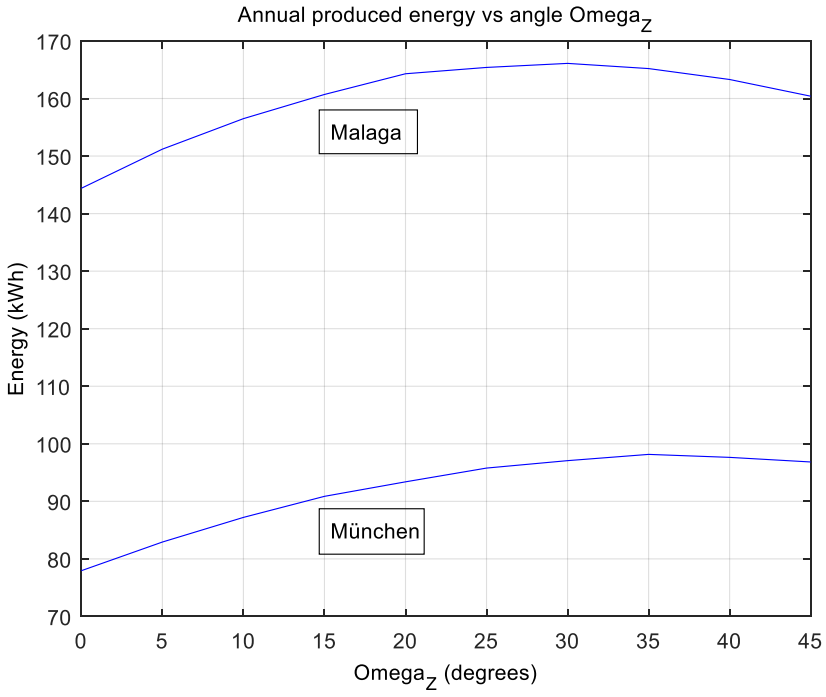

Fig. 7.3. München and Malaga. Annual produced energy vs angle $\Omega_{Z.}$

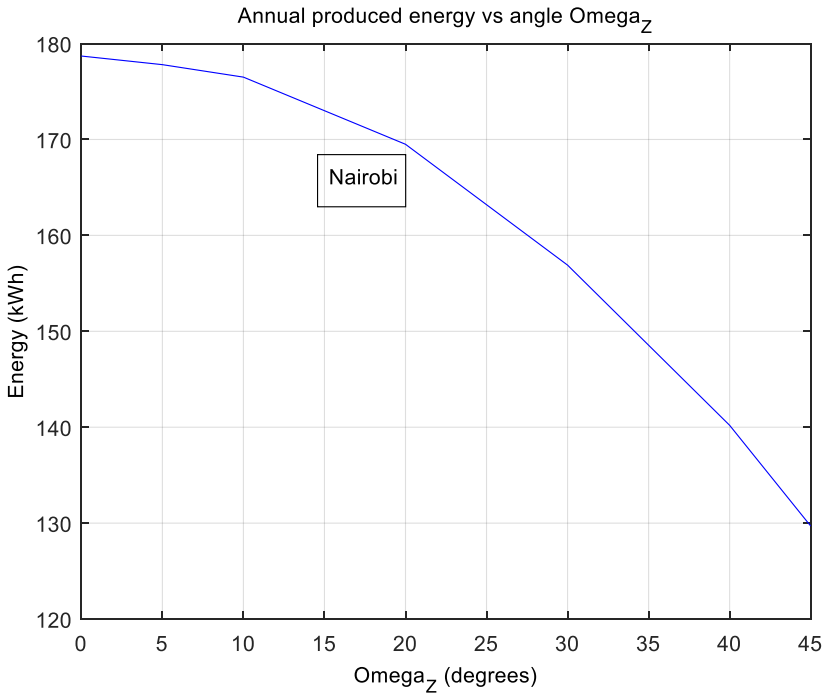

Fig. 7.4. Nairobi. Annual produced energy vs angle $\Omega_{Z.}$

The tests demonstrate that a deviation of about ± 5º from optimum angle Ω_Z can be acceptable, if a decrease of the annual produced energy of around 1 % can be accepted.

The annual produced solar energy is compared with Nairobi as reference in Fig. 7.5. Optimum angles Ω_S and Ω_Z are used.

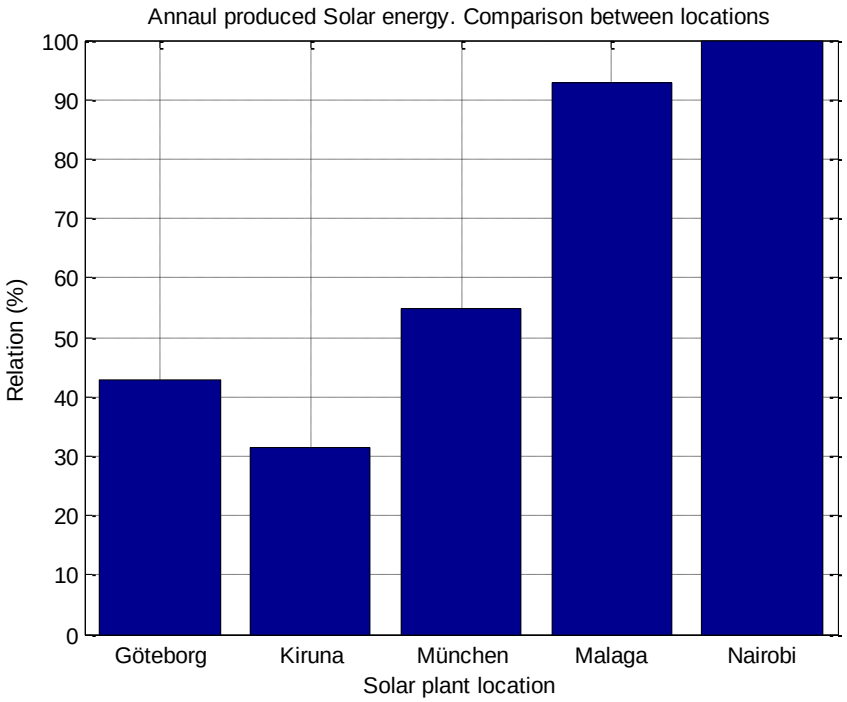

Fig. 7.5. Annually produced solar energy. Comparison between locations. Optimum angles Ω_S and Ω_Z are used.

7.4 Annual energy vs Ω_S (direction to south)

Angle Ω_S shall be adjusted in the position zero, in order to achieve optimum annual energy production.

To study the power reduction, affected by deviations from optimal value of angle towards south, Ω_S, a simulation work has been carried out. Investigated power farms are located in Kiruna, Göteborg, München and Malaga. Angle Ω_Z has in this section been chosen according to Table 7.2. That is, optimal Ω_Z-values for the respective locations. The reason for excluding Nairobi from the study is based on the fact that optimal angle Ω_Z at this location is zero. Solar energy production is of course independent of angle Ω_S for the case $\Omega_Z = 0$.

The results are presented in Table 7.4 - Table 7.7.

Table 7.4. Annual solar energy vs angle Ω_S. Relation to optimum angle. Kiruna.

Angle Ω_S (º)	**Solar energy in relation to optimum angle**
0	1.0000
15	0.9883
30	0.9402
45	0.8771
60	0.7869
75	0.6840
90	0.5748

Table 7.5. Annual solar energy vs angle Ω_S. Relation to optimum angle. Göteborg.

Angle Ω_S (º)	**Solar energy in relation to optimum angle**
0	1.0000
15	0.9886
30	0.9499
45	0.8932
60	0.8154
75	0.7225
90	0.6277

Table 7.6. Annual solar energy vs angle Ω_S. Relation to optimum angle. München.

Angle Ω_S (º)	**Solar energy in relation to optimum angle**
0	1.0000
15	0.9900
30	0.9595
45	0.9083
60	0.8410
75	0.7681
90	0.6864

Table 7.7. Annual solar energy vs angle Ω_S. Relation to optimum angle. Malaga.

Angle Ω_S (º)	Solar energy in relation to optimum angle
0	1.0000
15	0.9923
30	0.9703
45	0.9346
60	0.8855
75	0.8297
90	0.7693

The relative annual solar energy vs angle Ω_S is presented in Fig. 7.6.

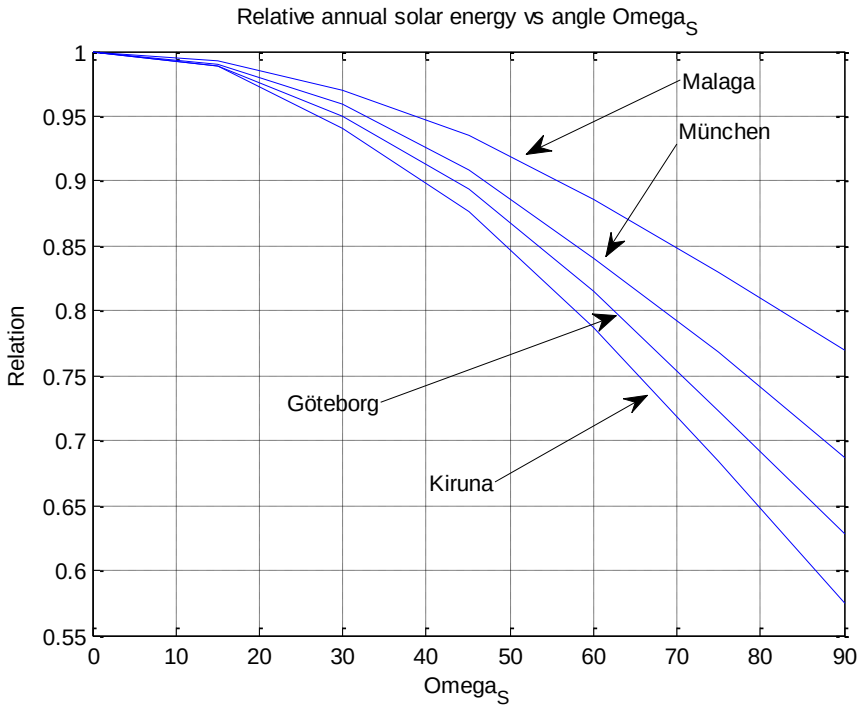

Fig. 7.6. Relative annual solar energy vs angle Ω_S.

As can be noted, a small deviation from zero is not very sensitve. Up to an angle deviation of 15 degrees, the decrease of energy production is about 1 % for all locations. Then the curve tends to drop down more. Especially for the 2 most northern sites, Kiruna and Göteborg. It is clear that the northern latitudes are more sensitive regarding the optimum or near optimum angle Ω_S than those of southern latitudes. This is illustrated in Fig. 7.7 by comparison between Kiruna and Malaga. Blue bar: Kiruna. Blue + red bar: Malaga

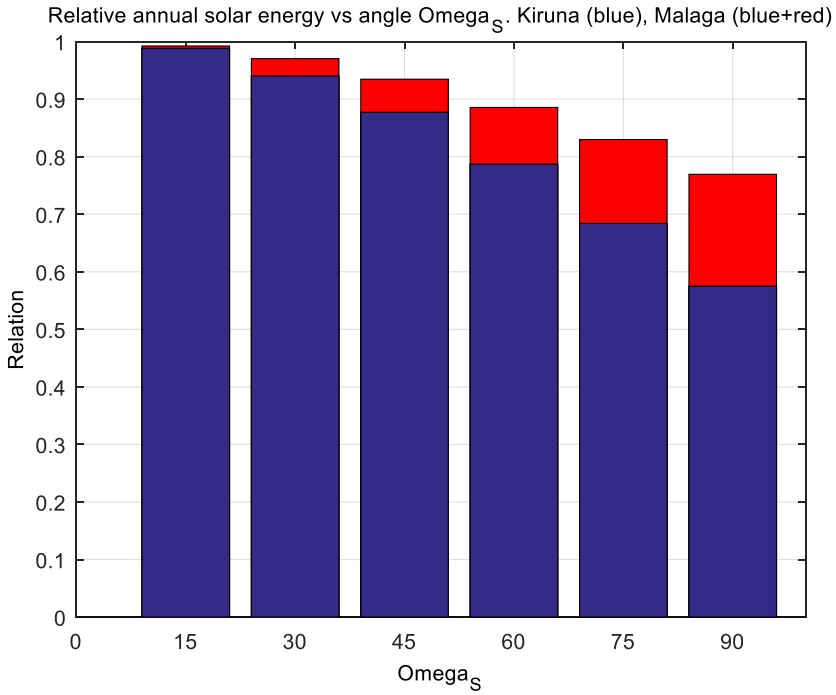

Fig. 7.7. Relative annual solar energy vs angle Ω_S. Comparison between Kiruna and Malaga. Blue bar: Kiruna. Blue + Red bar: Malaga.

7.5 Solar tracking

Annual solar production for solar tracking and for no solar tracking (optimum angles Ω_Z and Ω_S), are listed in Table 7.8 . The table also shows the relative increase of annual solar production if solar tracking is used.

Table 7.8 Annual produced energy vs location. Solar tracking and no solar tracking.

Location	Annual Produced energy (kWh/m^2). Solar tracking	Annual Produced energy (kWh/m^2). No solar tracking	Relative increase if solar tracking is used (%)
Kiruna	80.12	56.31	42
Göteborg	103.8	76.47	36
München	131.1	98.16	34
Malaga	221.4	166.1	33
Nairobi	235.8	178.7	32

Fig. 7.8 – Fig. 7.12 illustrate the annual produced energy per m^2 for solar tracking together with the results when no solar tracking is used. Produced energy for optimum angle is marked in the figures.

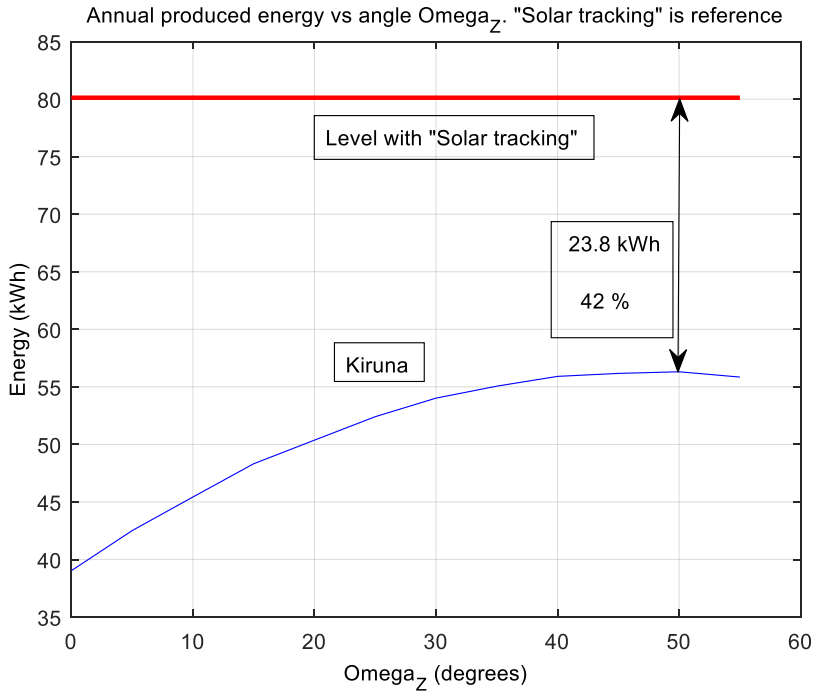

Fig. 7.8. Kiruna. Annual produced energy vs angle $\Omega_{Z.}$ Produced annual energy with and without solar tracking.

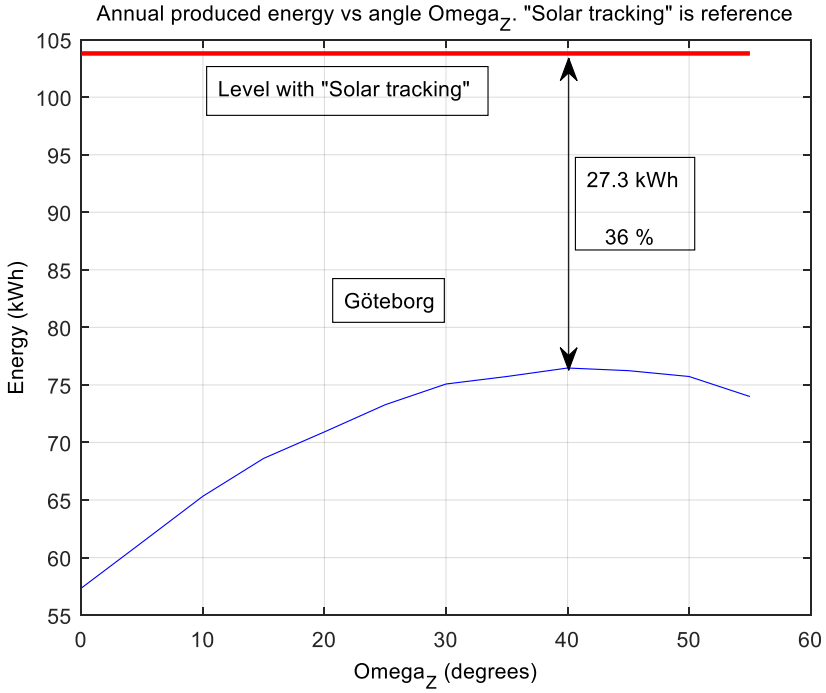

Fig. 7.9. Göteborg. Annual produced energy vs angle $\Omega_{Z.}$ Produced annual energy with and without solar tracking.

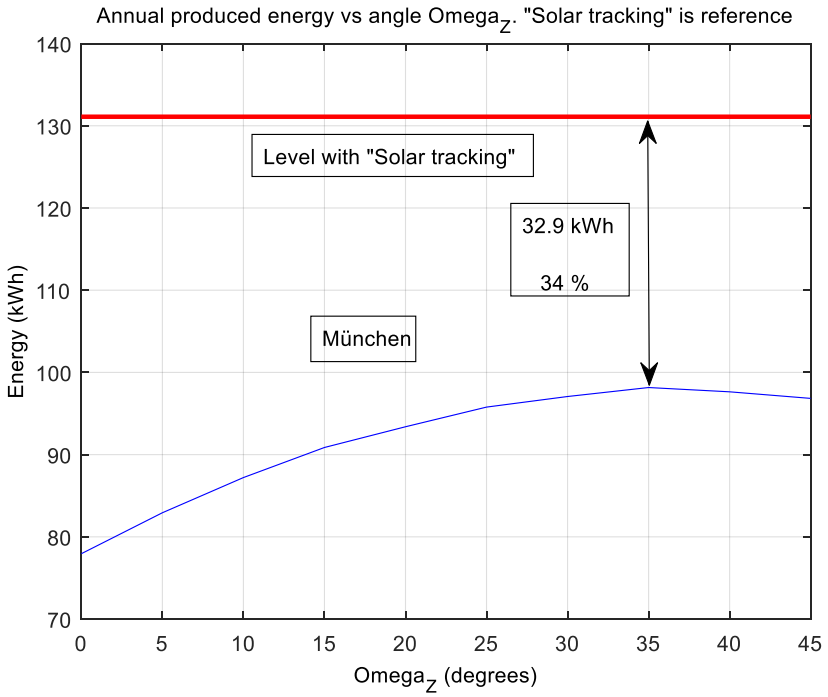

Fig. 7.10. München. Annual produced energy vs angle Ω_Z. Produced annual energy with and without solar tracking.

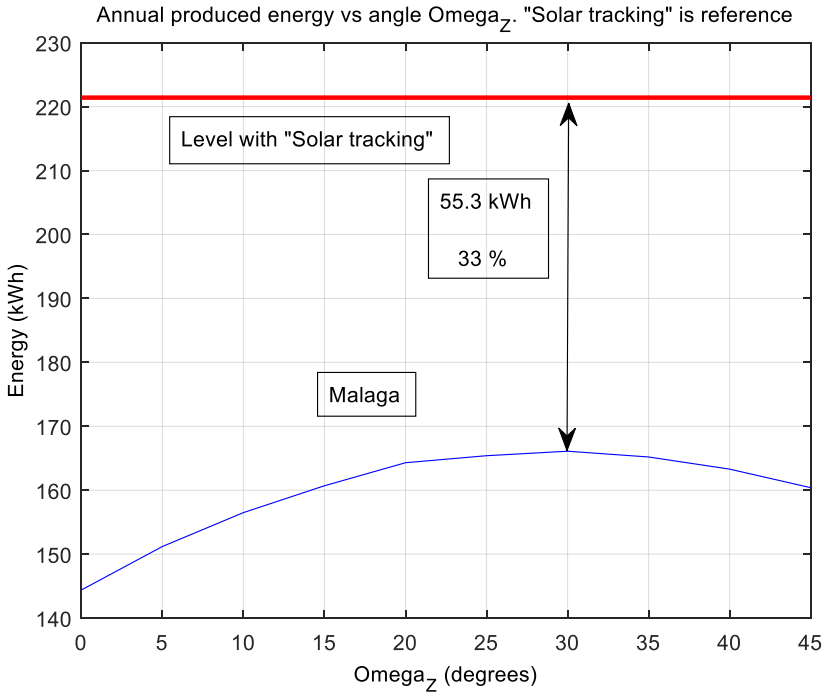

Fig. 7.11. Malaga. Annual produced energy vs angle Ω_Z. Produced annual energy with and without solar tracking.

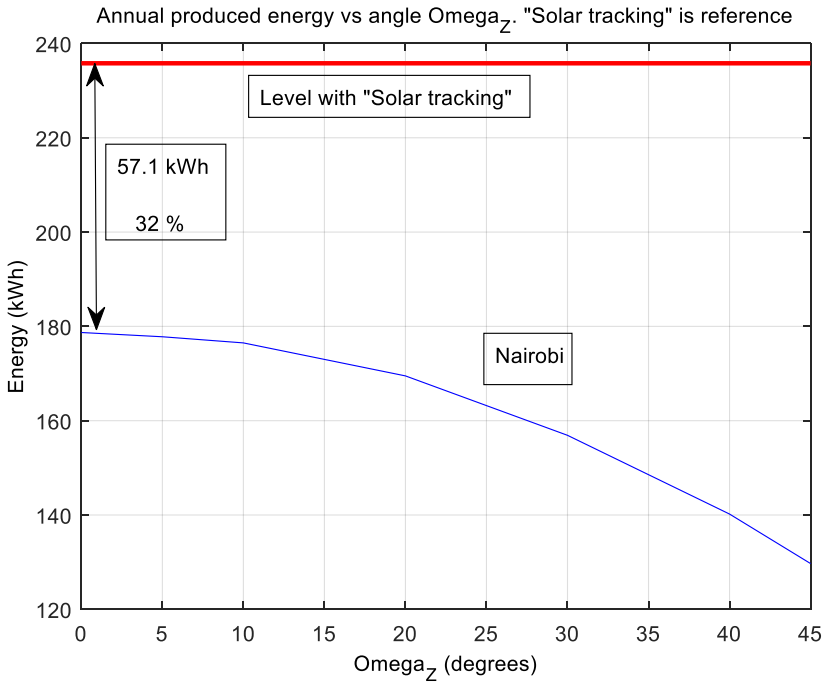

Fig. 7.12. Nairobi. Annual produced energy vs angle Ω_Z. Produced annual energy with and without “Solar tracking”.

Fig. 7.13 illustrates the graph for “Increase” relative to fix angle for solar tracking vs latitude. As can be noted, the rate of increase tends to increase versus latitude. See also Table 7.8.

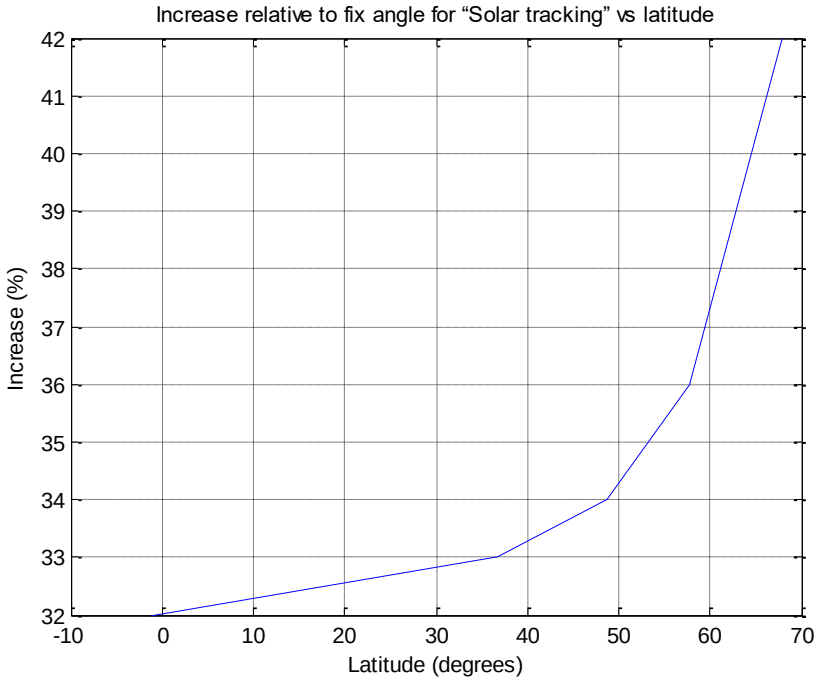

Fig. 7.13. Increase relative to fix angle for “Solar tracking” vs latitude.

7.6 Summary

The chapter deals with a study to clarify the importance of optimally mounted photovoltaic panels when it comes to the geometric orientation towards the sun. The study is performed by using the simulation system according to chapter 3. Five geographical locations have been investigated: Kiruna and Göteborg in Sweden, München in Germany, Malaga in Spain and Nairobi in Kenya. The different degrees of cloudiness at these locations have been estimated according to chapter 4.

Two solar cell panel angles have been defined: Angle relative to zenith and angle relative to south. In both cases with surface normal of solar panels as reference direction.

- Angle relative to zenith named Ω_Z
- Angle relative to south named Ω_S

Two design variants have been studied:

- Fixed installed solar cell panels. This means that the panels are installed with fixed angles relative to zenith and to south.
- Solar tracking. This means that the panels automatically follow the direction to sun.

As the geographical location of a solar plant determines the optimal angle Ω_Z, five locations have been investigated: Kiruna and Göteborg in Sweden, München in Germany, Malaga in Spain and Nairobi in Kenya.

Optimum values of angle Ω_Z have been calculated for the five locations. The results confirm a linear relationship between optimum angle Ω_Z and geographical latitude of the solar cell plant.

Tests with varying angle Ω_Z were performed. It was found that a deviation of about $\pm$ 5 º from optimum angle Ω_Z may be acceptable. This is provided that a reduction of around 1 % relative maximum value of annual produced energy is acceptable. However, for large deviations from optimum angle, the decrease is noticeable. For example, for Göteborg, a deviation of 20 degrees will reduce the energy by about 7 %.

Tests with various deviations from the optimal angle for Ω_S (that is zero) show that northern positioned photovoltaic plants are more sensitive regarding the optimum angle than more southern located photovoltaic plants. A deviation of 20 degrees results, for example in Malaga, in an energy reduction of about 1.5 %, while the corresponding deviation in Kiruna results in almost double that reduction. An angle deviation of up to 10 degrees, decreases the energy production for all locations less than 1 %.

A comparison regarding annually produced solar energy between the five locations was done. The annual energy produced differs markedly between sites. The annual production of energy in Nairobi and Malaga, for example, is about three times the corresponding production in Kiruna. The difference is partly due to different latitudes and partly due to the cloud presence.

Solar tracking is an effective method for increasing the energy produced. It was shown that an increase of more than 30% up to more than 40%, depending on the latitude in question, is achievable with this technology. Solar tracking is more effective as a method at higher latitudes than at lower latitudes.

CHAPTER 8

SMALL COMBINED SOLAR AND WIND POWER SYSTEMS

This chapter deals with the analysis of small electrical power systems, intended for use in households.

The power system is built up as a combined electrical power system according to Fig. 2.1.

The study is based on simulations where solar radiation, wind speed and electrical load are generated stochastically under given prerequisites.

In this study, wind power turbine “Skystream 3.7”, manufactured by Xzeres, USA, has been used for wind power production. This turbine can be regarded as a good example of powerful turbines for private usage and is an aerodynamic stall controlled turbine.

The solar panels are supposed to be designed with ordinary silicon solar cells. The panels are fixed mounted regarding angles relative to sun.

Regarding devices for energy storage, the design of these has not been specified.

The local power system is connected to the utility grid.

The study will try to find out the optimal number of wind turbines and the optimal size of the solar cell area. Optimal refers in this case to the point where the curve: "imported energy vs production capacity" tends to flatten out. This means that the absolute value of the second derivative of the function: "imported energy vs. production capacity" is below a certain value. This point is not very obvious. Several factors affect the criteria for this, e.g. the current power price, investment costs for turbines and solar panels, etc. The results regarding “optimal number of wind turbines and optimal size of solar cell area”, should be seen as approximate guide values.

The study makes analyzes regarding the benefits of combinations of wind power, solar power and energy storage.

Location for the power plant in question is Göteborg in Sweden.

The study is consistently based on simulations corresponding to a time period of one year (365 days). This means that the study is focused on the annual result for all cases studied. Results in the form of, for example, imported/exported energy mean annual amounts.

8.1 Tasks of the study

Some questions to be investigated:

- Optimal number of Wind power turbines
- Optimal Solar cell area
- Advantage of combining Wind power and Solar power
- Advantage of combining Wind power, Solar power and Energy storage

To get an answer to the questions, the frequency of energy shortage during the year has been a key parameter. This means that the need to import power or to use the power back-up has been a reference. In the study, "need to import power" as well as "need to use the power back-up" are both grouped together under the resulted rubric "imported energy". The terms "need to import power" and "need to use the power back-up" have also been assigned the designation “energy shortage”.

8.2 Basic specifications

8.2.1 Power plant location

Göteborg, Sweden.

8.2.2 Wind Power

8.2.2.1 Wind power system

- Wind power turbine: “Skystream 3.7”
- Maximum power per turbine: 2.4 kW
- Wind power efficiency: 80 %. This includes generator and power electronics, but excludes the impact of the power coefficient Cp. See section 3.3.2
- Rotor diameter: 3.72 m
- Maximum output power from turbine: 2.4 kW
- Minimum wind speed for output power: 3.5 m/s
- Maximum wind speed has been limited to 19 m/s
- Turbine height above ground: 10 m

- Aerodynamic stall controlled
- Number of turbines: To be tested

8.2.2.2 Wind speed

Weibull parameters

- A = 6.3
- C = 1.9

This results in:

- Wind speed mean value: 6.45 m/s
- Wind speed standard deviation: 0.35 m/s

See Table 5.1.

Adjustment relating to turbine height above ground

According to section 5.3.

8.2.3 Solar Power

8.2.3.1 Solar power system

The solar power system is structured according to the following specification:

- Photovoltaic solar cell panels
- Total effective solar cell area: To be tested
- Total efficiency for solar power system: 13.54 %. This includes:
  - Solar cell efficiency: 15 %
  - Maximum Power Point (MPP) efficiency: 95 %
  - Power electronics efficiency: 95 %
- Solar cell material: Silicon
- Position of angle $\Omega_Z = 40^o$. See Table 7.2
- Position of angle $\Omega_S = 0^o$

8.2.3.2 Cloudiness

Cloudiness probability: 64 %. See Table 4.3.

8.2.4 Energy Storage

The absolute and relative storage capacity (ESC abs and ESC rel) is defined according to (2.4) and (2.5).

8.2.5 Local Electrical Load

The following applies to the electrical load:

- Type of load: Residential
- Annual energy consumption: 10 000 kWh

8.3 Simulations

8.3.1 Tests with varying number of turbines

Simulations have been performed with varying numbers of turbines.

- No energy storage
- No solar power

Table 8.1 lists the simulation results.

Table 8.1. Simulation results with varying values of wind turbines. No solar power. No energy storage.

Number of turbines	Exported energy (kWh)	Imported energy (kWh)	Exported energy - Imported energy (kWh)
0	0	9994	-9994
1	344	7326	-6982
2	1831	6122	-4291
3	3899	5471	-1572
4	6199	5088	1111
5	8648	4788	3860
6	11400	4509	6891
7	13640	4393	9247

Fig. 8.1 shows imported energy vs number of turbines.

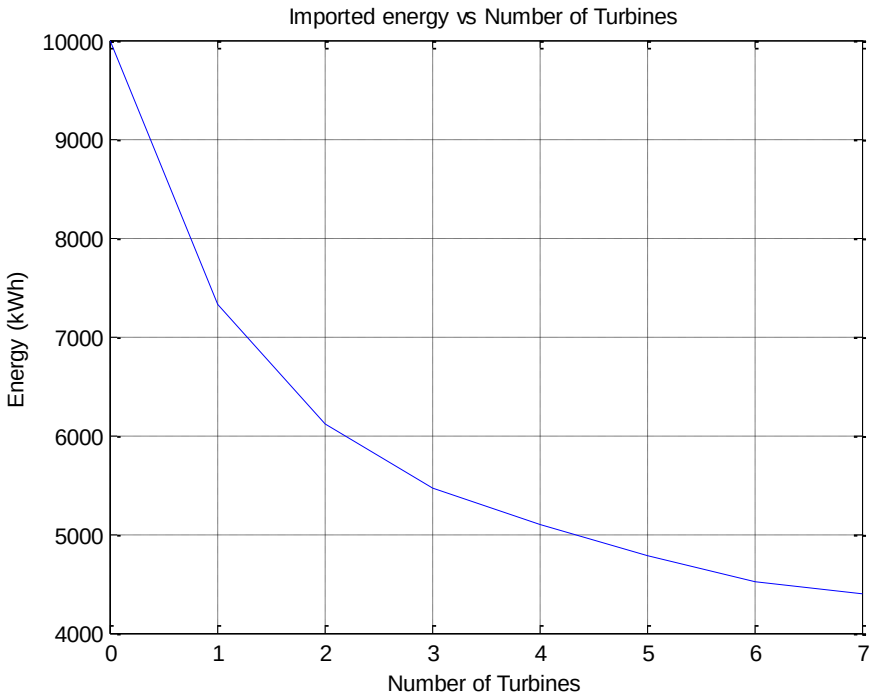

Fig. 8.1. Imported energy vs number of turbines.

The study is primarily focused on the need to import energy or the need to use power back-up as a function of wind turbines. Fig. 8.1 shows the annually imported energy vs number of wind turbines. As can be observed, the curve drops quickly in the region 0 to 3 turbines. It tends to flatten out at about 6 turbines. This can be a hint regarding the optimal number of turbines in respect of energy shortage. The annually produced wind power, with 6 turbines, is simulated to about 16700 kWh.

Produced wind energy with 6 turbines in relation to consumed energy is:

$$\text{Rel\_wind\_load} = \frac{16700\ \text{kWh}}{10000\ \text{kWh}} = 1.67 \tag{8.1}$$

Where:

Rel_wind_load: Produced wind energy relative to consumed energy

The value of Rel_wind_load is approximated to 1.7.

8.3.2 Tests with varying area of solar cells

Simulations have been performed with varying area of solar cells.

- No energy storage
- Number of wind turbines = 6 (see section 8.3.1)

Table 8.2 lists the simulation results.

Table 8.2. Simulation results with varying area of solar cells. 6 wind power turbines. No energy storage.

Solar cell area (m^2)	Exported energy (kWh)	Imported energy (kWh)	Exported energy - Imported energy (kWh)
0	11340	4559	6781
25	12460	3967	8493
50	14030	3741	10289
100	17880	3549	14331
200	24860	3469	21391
400	39540	3369	36171

Fig 8.2 shows imported energy vs solar cell area.

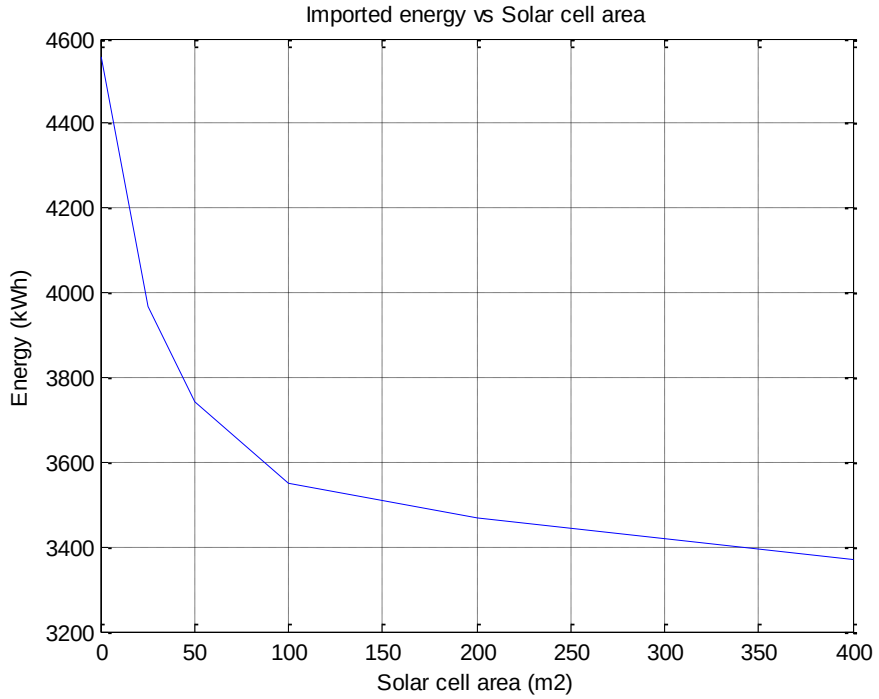

Fig. 8.2. Annual imported energy vs solar cell area.

The study is primarily focused on the need to import energy or the need to use power back-up as a function of solar cell area. Fig. 8.2 shows the annual imported energy vs number of solar cell area. As can be observed, the curve drops quickly in the region 0 to 100 m^2. It tends to flatten out at about 200 m^2. This can be a hint regarding the optimal solar cell area in respect of energy shortage. 200 m^2 solar cell area corresponds to an annual production of about 15000 kWh.

Produced solar energy with 200 m^2 solar cell area in relation to consumed energy is:

$$\text{Rel\_solar\_load} = \frac{15000\ \text{kWh}}{10000\ \text{kWh}} = 1.5 \tag{8.2}$$

Where:

Rel_solar_load: Produced solar energy relative to consumed energy

For the case of 6 wind power turbines, supplemented with solar power from 200 m^2 solar cells, the annual imported energy is decreased from 4509 kWh to 3469 kWh, i.e. a decrease of 23 %. The difference “Exported power - Imported power” is more than 3 times larger. An increase from 6891 kWh to 21391 kWh.

Fig. 8.3 illustrates the difference between Exported power and Imported power vs Solar cell area. The case of 6 turbines and no Solar power is plotted as reference. See also Table 8.2.

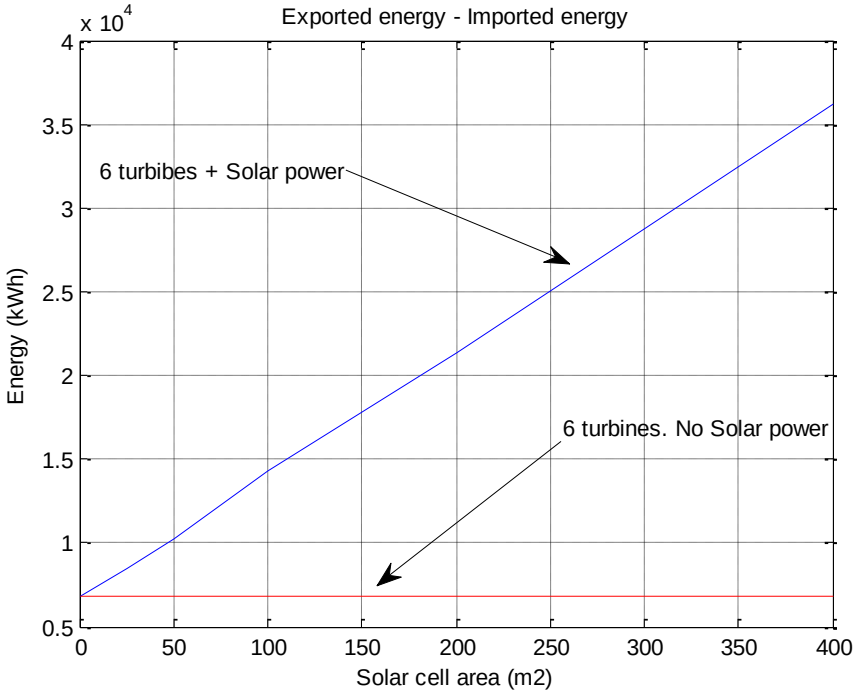

Fig. 8.3. Exported energy - Imported energy. Comparison with 6 turbines and no Solar Power. Also see Table 8.2.

Completed tests give a clear result in terms of whether a combination of wind and solar energy reduces the risk of energy shortages and strengthens the difference between exported and imported energy.

8.3.3 Tests with varying Energy storage capacity

Simulations have been performed with varying energy storage capacity. Two cases regarding energy source have been tested. Wind power as an energy source and Wind power + Solar power as an energy source.

Regarding the designation ESC rel, see (2.5).

8.3.3.1 Energy storage and Wind power

- Number of wind turbines = 6 (see section 8.3.1)
- No solar power

Table 8.3 lists the simulation results.

Table 8.3. Simulation result with Energy storage and Wind power.
The probability of energy shortage has been listed.

Energy storage (ESC rel)	Energy storage (kWh)	Exported energy (kWh)	Imported energy (kWh)	Probability of energy shortage (%)
1	27.4	10210	3338	100
3	82.2	8620	2112	100
5	137.0	8032	1443	100
10	274.0	7217	532.2	98
15	411.0	6946	199.9	70.5
20	547.9	6396	104.2	46
30	821.9	6169	23.29	14
40	1095.9	6005	6.1	4.5
50	1369.9	5841	1.8	1
60	1643.8	5618	0.43	0.5
70	1917.8	5503	0	0

8.3.3.2 Energy storage and Wind power + Solar power

- Number of wind turbines = 6 (see section 8.3.1)
- Annually produced solar power: 15000 kWh (see section 8.3.2)

Table 8.4 lists the simulation results.

Table 8.4. Energy storage and Wind power + Solar power.

Energy storage (ESC rel)	Energy storage (kWh)	Exported energy (kWh)	Imported energy (kWh)	Probability of energy shortage (%)
1	27.4	22710	1234	100
3	82.2	21850	422.2	100
5	137.0	21610	239.0	95.5
10	274.0	21240	70.02	46
15	411.0	21230	13.86	12
20	547.9	21310	4.771	3.5
30	821.9	20880	0.1915	0.5
40	1095.9	20790	0	0

Fig. 8.4 compares the results from section 8.3.3.1 and section 8.3.3.2 in respect of Imported energy vs Energy storage (ESC rel). As can be noted, the difference between the curves is quite large. Fig. 8.5 shows the relation between the curves. The relation increases rapidly when the Energy Storage increases.

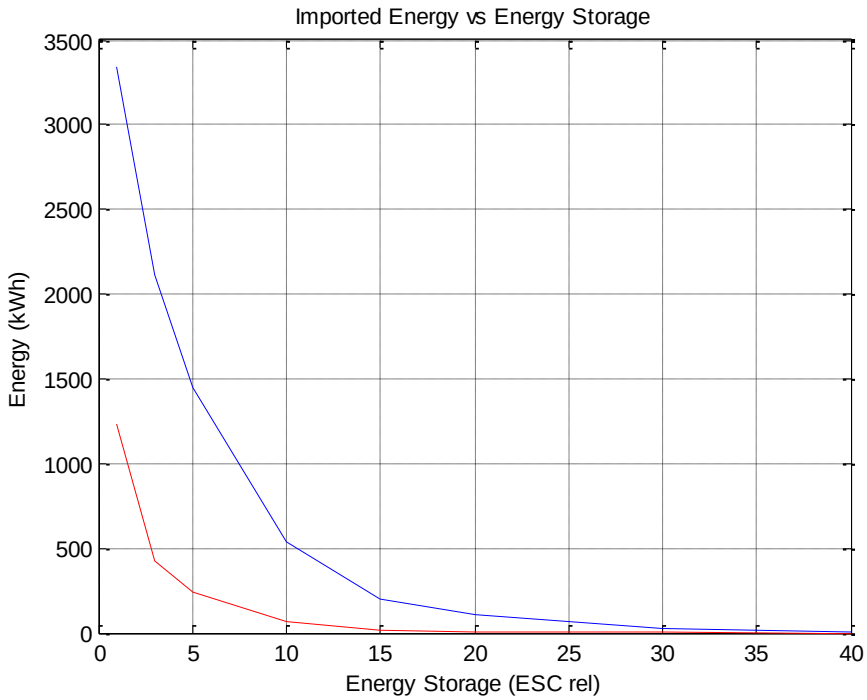

Fig. 8.4. Imported Energy vs Energy Storage.
Blue curve: Wind + Energy storage. Red curve: Wind + Solar + Energy storage.

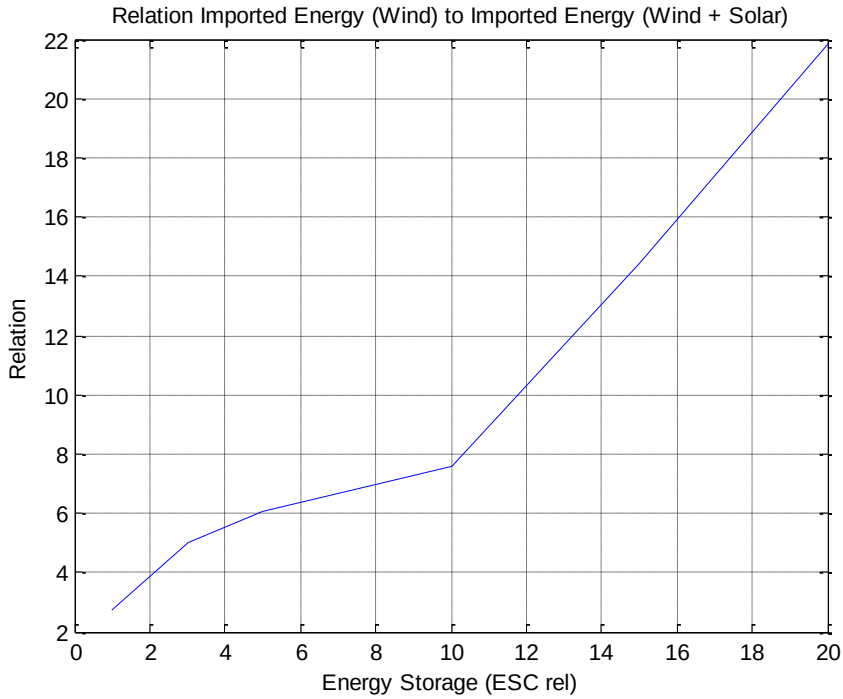

Fig. 8.5. Relation Imported Energy (Wind) to Imported Energy (Wind + Solar) vs Energy Storage.

Fig. 8.6 compares the results from section 8.6.3.1 and section 8.6.3.2 in respect of Probability of energy shortage vs Energy storage (ESC rel). As can be noted, the

difference between the curves is quite large. Fig. 8.7 shows the relation between the curves. The relation increases rapidly when the Energy Storage increases over ESC = 10.

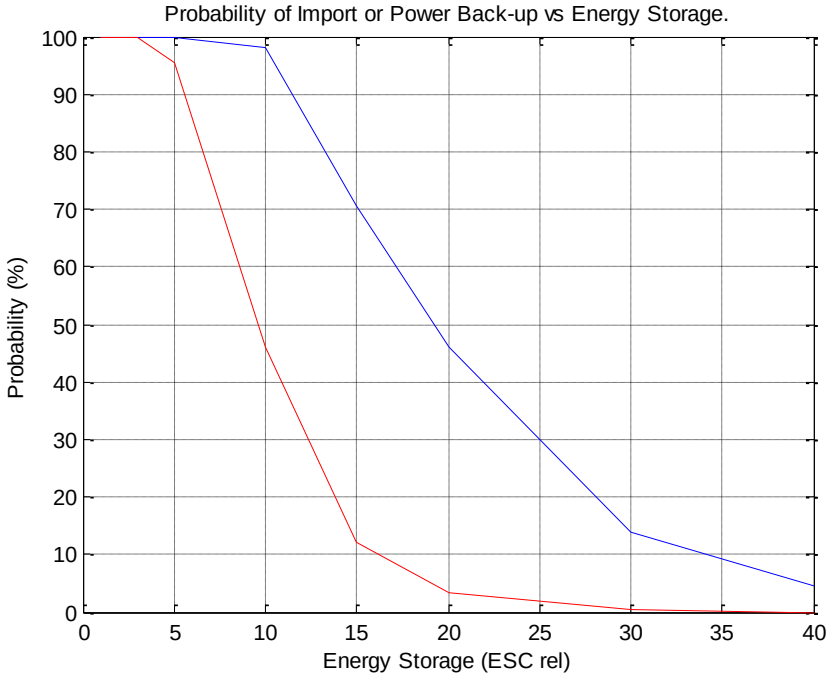

Fig. 8.6. Probability for need of Energy Import or Power Back-up vs Energy Storage. Blue curve: Wind + Energy storage. Red curve: Wind + Solar + Energy storage.

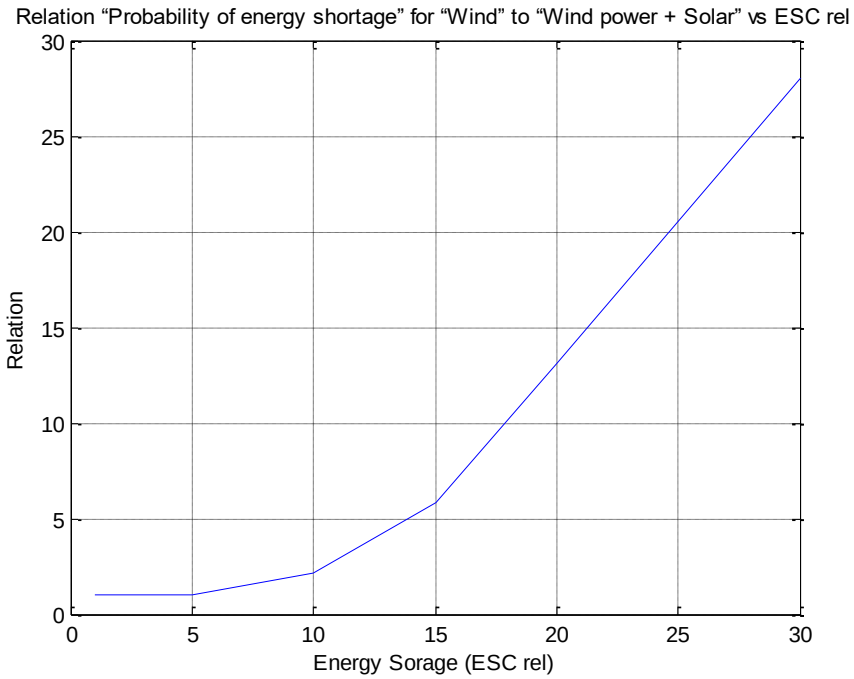

Fig. 8.7. Relation “Probability of energy shortage” for “Wind power” to “Wind power + Solar power” as Energy source vs Energy Storage.

As can be noted, the advantage with a combination of wind power and solar power is very significant compared with only wind power as an energy source if energy storage is used. For example, for the case ESC rel = 25, the probability of energy shortage with only wind power is about 21 times the corresponding probability with the combination wind power and solar power. See Fig. 8.7.

8.4 Summary

A small electrical power system intended for use in a pivate household is analysed. The power system consists of a combination of wind and solar power units. The study is performed by using the simulation system according to chapter 3. The electrical load is defined as a residential area according to section 6.9, with an annual consumption of 10 000 kWh.

Tests with a varying number of wind turbines and varying solar cell areas are performed. This is with the aim of finding an appropriate balance between production of wind power, solar power, and annual consumption of electricity. The analysis showed that the relationship between annual wind power production and annual power consumption should be about 1.7. This is assuming wind power conditions according to section 8.2.2. A suitable dimensioning of the solar power system should be a relationship between annually produced solar power and annual power consumption of approximately 1.5. This is assuming a combination with wind power and solar power conditions according to section 8.2.3 and power plant location at Göteborg.

The studies regarding dimensioning of wind power and solar power capacity are focused on the corresponding effect on the need to import energy or need to use power back-up. There is a large difference between a case where no solar power and only wind power is used and a case where wind power is supplemented with solar power. A complementation with solar power decreases the need of annual power import by about 25 %. The difference "exported annual energy – imported annual energy" is in this case more than three times larger compared with the case where no solar power is used.

Tests with varying energy storage capacity are performed. The tests are done with energy storage and only wind power and separately with energy storage and wind power in combination with solar power. The storage capacity is here defined with the term “ESC rel”, that is the quota between absolute storage capacity (kWh) and mean daily energy consumption (kWh). For the case with only wind power as an internal power source, the risk of energy shortage is 98 % when parameter ESC rel is 10. If ESC rel is increased to 50, the corresponding risk of energy shortage will be reduced to 1 %. The term "energy shortage" here refers to the need to import energy or the need to use power back-up. If wind power as a power source is combined with solar power, the risk of energy shortage is 46 % when parameter ESC rel is 10. An increase of ESC rel to 40 will reduce the risk of energy shortage to 0 %. ECS rel = 40 corresponds in this case to about 1.1 MWh.

CHAPTER 9

LARGE COMBINED SOLAR AND WIND POWER SYSTEMS

This chapter deals with simulation of large combined power systems, where solar and wind act as power sources. The solar radiation, wind speed and load are generated stochastically. The power system can be equipped with an energy storage device. The system is connected to the utility grid to balance the power. Fig. 2.1 shows the main components in the power system.

Wind power turbines with a maximised defined power capacity are used.

The solar panels are supposed to be designed with ordinary silicon solar cells. The panels are fixed mounted in terms of angles relative to sun.

Regarding devices for energy storage, the design of these has not been specified.

The electrical load is a combination of industrial area, commercial centre and residential area.

Five geographic locations for power plants will be studied: Kiruna and Göteborg in Sweden, München in Germany, Malaga in Spain and Nairobi in Kenya.

Produced solar energy per season (quarter) is to be analysed. The energy density in the form of produced energy per m^2 solar cell area will be studied and used as a measure of utilisation of the solar power systems at the location in question.

The design guide-lines regarding production capacity of wind- and solar energy, which were obtained in chapter 8, will be tested.

The combination Solar – Wind – Energy storage will be analysed. The probability of energy shortage is a key parameter in this case.

An economic analysis of the power plants will be performed.

The study is consistently based on simulations where each simulation process consists of 200 cycles (parameter N in fig. 3.1).

9.1 Tasks of the study

Some questions to be investigated:

- Produced solar energy distribution per season (quarter)
- Utilization of the solar power systems
- Optimal capacity of wind- and solar power production *)
- The probability of energy shortage with the combination of wind – solar – energy storage
- The power production costs

*) Optimal refers in this case to the point where the curve: "imported energy vs. production capacity" tends to flatten out. This means that the absolute value of the second derivative of the function: "imported energy vs. production capacity" is below a certain value. This point is not very obvious. Several factors affect the criteria for this, e.g. the current power price, investment costs for turbines and solar panels, etc. The results regarding “optimal number of wind turbines and optimal size of solar cell area”, should be seen as approximate guide values.

“Imported energy” indicates basic information about the power system and its vulnerability to energy deficit. For this reason, the goal is to get a dimensioning of the power capacity to a level that gives a reasonable compromise between imported energy cost and investment cost. The method used is to assess the point where the correlation curve between imported energy and increased power capacity tends to flatten out.

This study should be seen in light of a combined system with the possibility of energy storage and as far as possible, make the system autonomous. See sections 9.4.3 - 9.4.4.

9.2 Geographic locations of the power plants

Five geographical locations are to be investigated:

Table 9.1 Locations and corresponding coordinates.

Location	Latitude (degrees)	Longitude (degrees)
Kiruna, Sweden	67.8	20.2
Göteborg, Sweden	57.7	12.0
München, Germany	48.8	-11.3
Malaga, Spain	36.7	-4.4
Nairobi, Kenya	-1.3	36.8

9.3 Basic specifications

9.3.1 Wind Power

9.3.1.1 Wind power system

- Maximum power per turbine: 2000kW
- Wind power efficiency: 85 %. This includes generator and power electronics, but excludes the impact of the power coefficient Cp. See section 3.3.1
- Rotor diameter: 80 m
- Maximum rotation speed: 30 rpm
- Minimum wind speed for output power: 4 m/s
- Maximum wind speed for power 25 m/s
- Turbine height above ground: 80 m
- Variable speed controlled
- Number of turbines: To be tested
- Annual wind power production: 34.7 GWh (with wind speed according to section 9.3.1.2)
- λ_{ref} (λ-value that gives Cp – max): 9

9.3.1.2 Wind speed

<u>Weibull parameters</u>

- A = 6.3
- C = 1.9

This results in:

- Wind speed mean value: 6.45 m/s
- Wind speed standard deviation: 0.35 m/s

See Table 5.1.

<u>Adjustment relating to turbine height above ground</u>

According to section 5.3.

9.3.2 Solar Power

9.3.2.1 Solar power system

- Photovoltaic solar cell panels
- Total efficiency for solar power system: 13.54 %. This includes:
  - Solar cell efficiency: 15 %
  - Maximum Power Point (MPP) efficiency: 95 %
  - Power electronics efficiency: 95 %
- Solar cell material: Silicon
- Solar cell area: The solar cell area depends on the location in question. See Table 9.3
- Position of angle Ω_Z: Optimum angle. This depends on geographic location. See Table 9.2
- Position of angle $\Omega_S = 0^o$

9.3.2.2 Position of angle Ω_Z

The position of angle Ω_Z depends on the location in question, and follows according to Table 9.2.

Table 9.2. Optimum angle Ω_Z vs locations and corresponding produced annual energy.

Location	**Annual Produced energy (kWh/m^2) with Optimum angle Ω_Z**
Kiruna	56.31
Göteborg	76.47
München	98.16
Malaga	166.1
Nairobi	178.7

9.3.2.3 Solar cell area

The needed solar cell area to produce a certain amount of annual energy, depends on the location in question. Table 9.3 lists the required solar cell area to produce 1.5 × 20 GWh. The listed areas corresponds to 1.5 A_equ units. The unit A_equ units is defined as:

1 A_equ units = Required solar cell area to produce E_annual (9.1)

Where:

E_annual: Annual produced solar energy

Table 9.3. Solar cell area corresponding to 1.5 A_equ units.

Location	**Required solar cell area $\times 10^6$ (m^2)**
Kiruna	0.53277
Göteborg	0.39231
München	0.30562
Malaga	0.18061
Nairobi	0.16788

9.3.2.4 Cloudiness

Cloudiness probability: Depends on geographic location. See Table 4.3.

9.3.3 Energy Storage

The absolute and relative storage capacity (ESC abs and ESC rel) is defined according to (2.4) and (2.5).

- ESC rel: To be tested

9.3.4 Local Electrical Load

An area with a mix of power consumers with the following annual power consumption (see section 6.10):

- Industrial area, annual power consumption: 5 GWh
- Commercial centre, annual power consumption: 5 GWh
- Residential area, annual power consumption: 10 GWh

9.4 Solar- and Wind power

9.4.1 Introduction

This section is investigating a combination of solar power and wind power systems, located in Kiruna, Göteborg, München, Malaga and Nairobi. No energy storage has been used.

Note! The values regarding parameters “Wind energy” and “Solar energy” differ slightly between the presented cases. This is a result of ordinary statistical variation.

9.4.2 Produced solar energy per quarter

Table 9.4 lists produced solar energy for the 5 locations in question. The information is divided into the 4 quarters of the year. The production is based on solar cell areas of 1.5 A_equ. See Table 9.3.

Table 9.5 lists the energy density for the 5 locations. The energy density is defined according to:

$$\text{Energy density} = \frac{\text{Produced energy}}{\text{Solar cell area}} \tag{9.2}$$

Where: Solar cell area is the real area in m^2 for the location in question, converted from area unit A_equ = 1.5.

Table 9.4. Produced solar energy per quarter and annual production.

Time period	Kiruna Solar energy (GWh)	Göteborg Solar energy (GWh)	München Solar energy (GWh)	Malaga Solar energy (GWh)	Nairobi Solar energy (GWh)
Jan – Mar	2.179	3.654	4.815	6.037	7.528
Apr – Jun	14.39	12.52	10.96	9.336	7.149
Jul – Sep	12.10	11.28	10.14	9.014	7.390
Oct – Dec	0.6131	1.895	3.321	5.122	7.375
Annual	29.282	29.349	29.236	29.509	29.442

Table 9.5. Energy density. Solar cell kWh/m^2. Per quarter and annual.

Time period	Kiruna Energy density (kWh/m^2)	Gbg Energy density (kWh/m^2)	München Energy density (kWh/m^2)	Malaga Energy density (kWh/m^2)	Nairobi Energy density (kWh/m^2)
Jan – Mar	4.0899	9.3141	15.7549	33.4256	44.8416
Apr – Jun	27.0098	31.9135	35.8615	51.6915	42.5840
Jul – Sep	22.7115	28.7528	33.1785	49.9086	44.0195
Oct – Dec	1.1508	4.8304	10.8664	28.3594	43.9302
Annual	54.9620	74.8107	95.6613	163.3852	175.3753

Fig. 9.1 – 9.2 compare produced electrical solar energy per quarter for the 5 locations:

- Kiruna (Ki)
- Göteborg (Gö)
- München (Mü)
- Malaga (Ma)
- Nairobi (Na)

The following two observations can be made:

1) Time period October to March. This corresponds fairly close to the period from autumn equinox to spring equinox.
   Observation: Produced electrical solar energy is increased for falling latitude

2) Time period April to September. This corresponds fairly close to the period from spring equinox to autumn equinox.
   Observation: Produced electrical solar energy is decreased for falling latitude

Produced electrical solar energy is relatively low during the time between autumn- and spring equinox at northern geographic locations. This is compensated during the time between spring- and autumn equinox when the produced solar energy is high. This fact also shows that the solar systems have relatively low utilization rate during the "dark" part of the year, regarding northern located facilities.

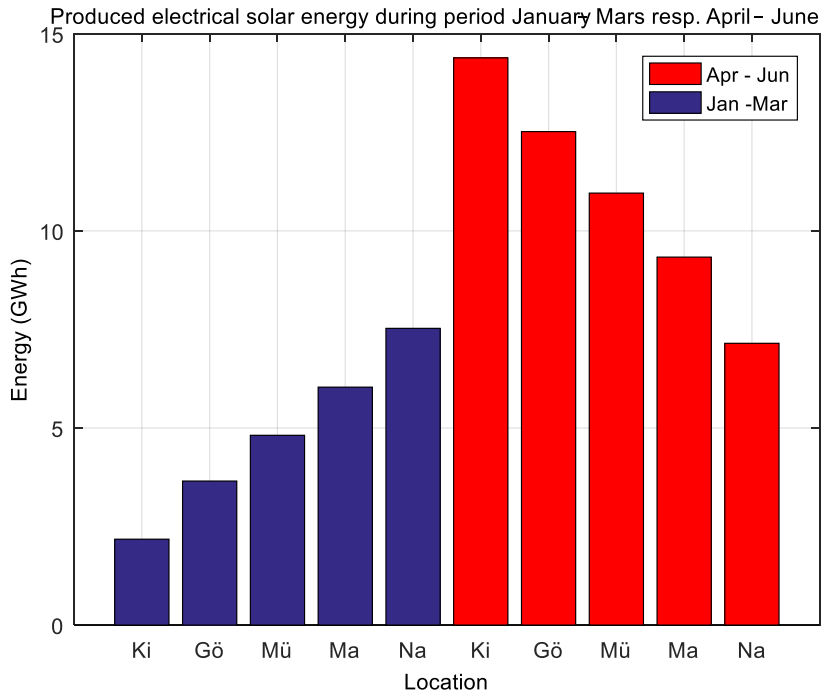

Fig. 9.1. Produced electrical solar energy during period January – March and April – June.

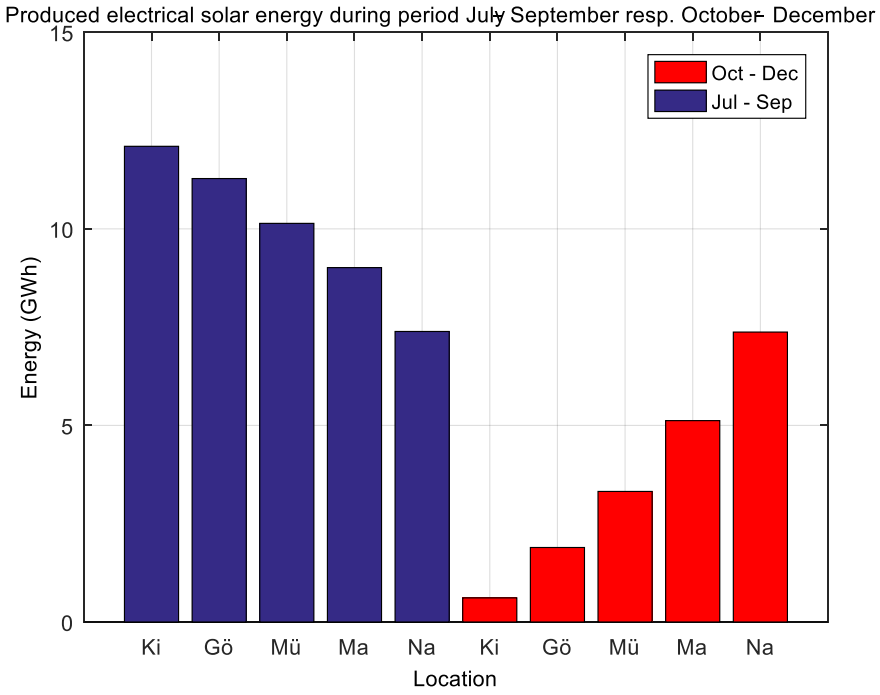

Fig. 9.2. Produced electrical solar energy during period July – September and October – December.

The energy density, defined according to (9.2), is plotted in Fig. 9.3 – 9.4. This illustrates the difference between geographic locations regarding produced energy per unit area solar cell. The following can be noted:

- Kiruna, Göteborg and Munchen: The energy density is increased with decreasing latitude.
- Malaga and Nairobi: The correlation between energy density and latitude is not the same as for Kiruna, Göteborg and München. For the period between spring- and autumn equinox, the density is higher at Malaga than at Nairobi. This is an effect of the low cloudiness at Malaga (35 % at Malaga and 44 % at Nairobi).

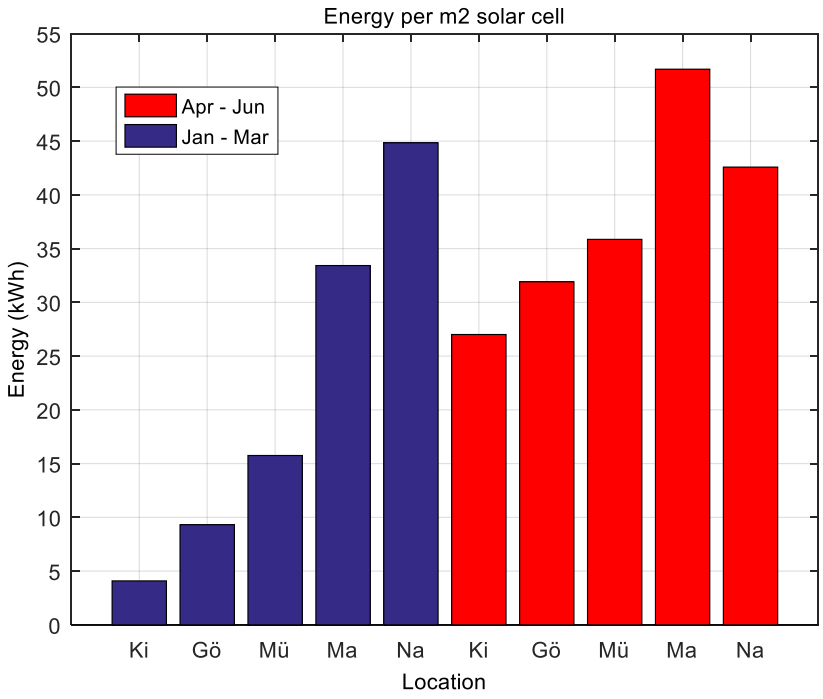

Fig. 9.3. Electrical solar energy per m^2 solar cell. Period January – March and April – June.

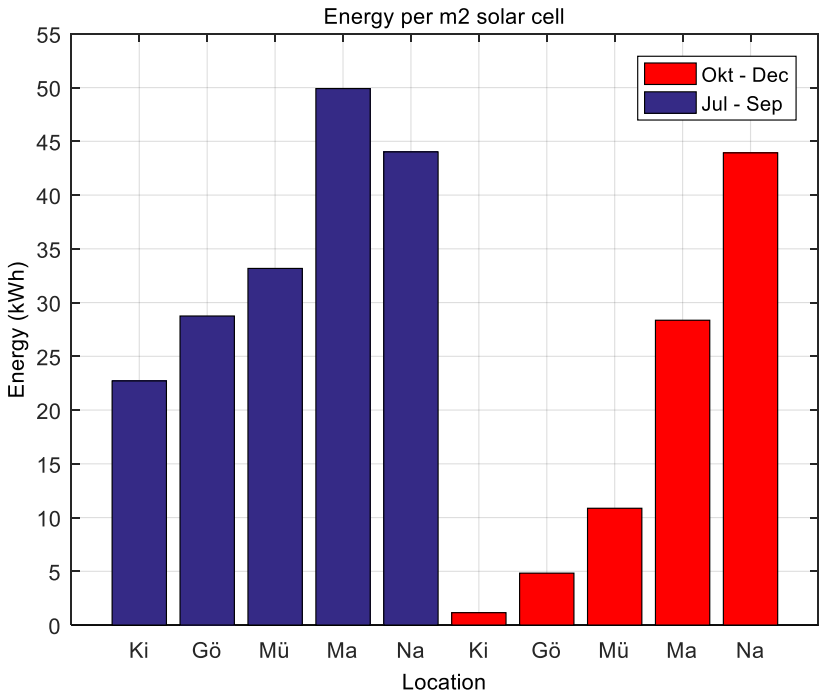

Fig. 9.4. Electrical solar energy per m^2 solar cell. Period July – September and October – December.

Fig. 9.5 – 9.10 clearly illustrate the difference regarding energy produced and energy density for the four quarters and for respective geographic positions.

Q1: January – March
Q2: April – June
Q3: July – September
Q4: October – December

A rough classification regarding utilization of the solar power systems per quarter and location could be done according to Table 9.6.

Table 9.6. Rough classification regarding solar power utilization per quarter Q1 – Q4.

Location	**Q1. Utilization**	**Q2. Utilization**	**Q3. Utilization**	**Q4. Utilization**
Kiruna	Low	High	High	Low
Göteborg	Low	High	High	Low
München	Low	High	High	Low
Malaga	High	High	High	High
Nairobi	High	High	High	High

According to Table 9.6, the utilization is high for all locations during quarter Q2 and Q3, but high during all quarters only at Malaga and Nairobi. The fact that the utilization is high during half of the year for all locations is a clear indication that solar energy makes an important contribution to the total energy production, even at high geographical latitudes.

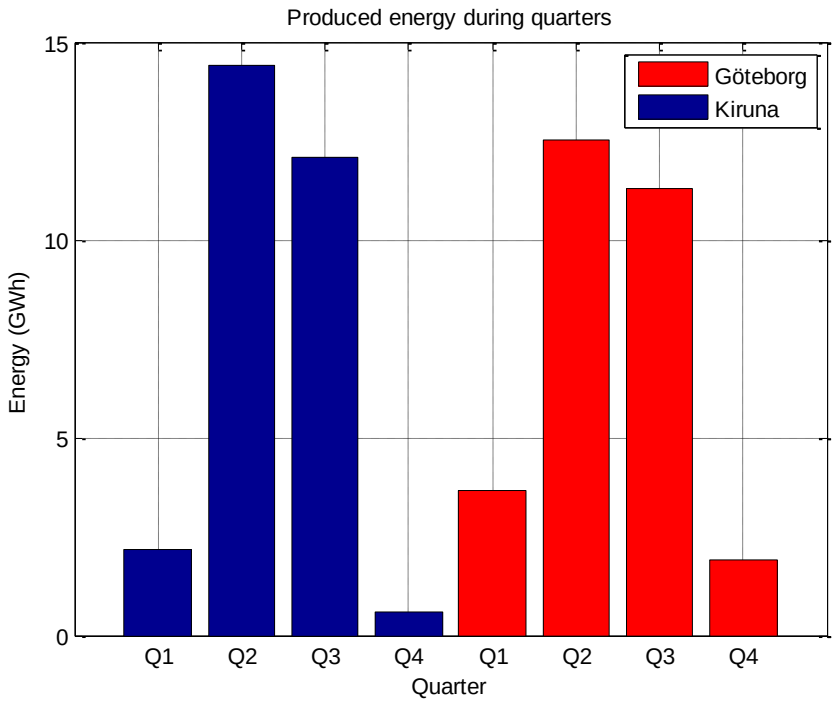

Fig. 9.5. Produced electrical solar energy during periods January – March, April – June, July – September and October – December. Kiruna and Göteborg.

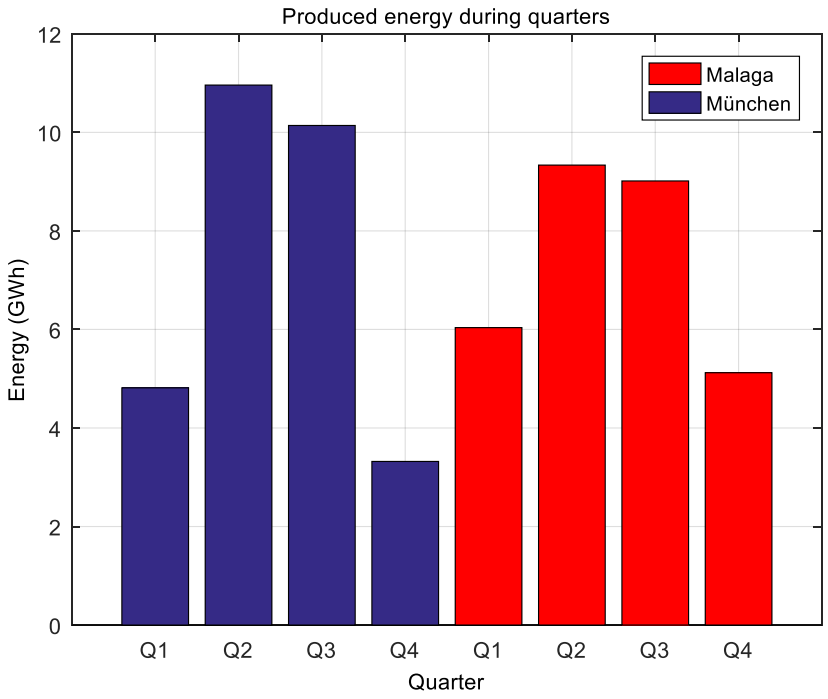

Fig. 9.6. Produced electrical solar energy during periods January – March, April – June, July – September and October – December. München and Malaga.

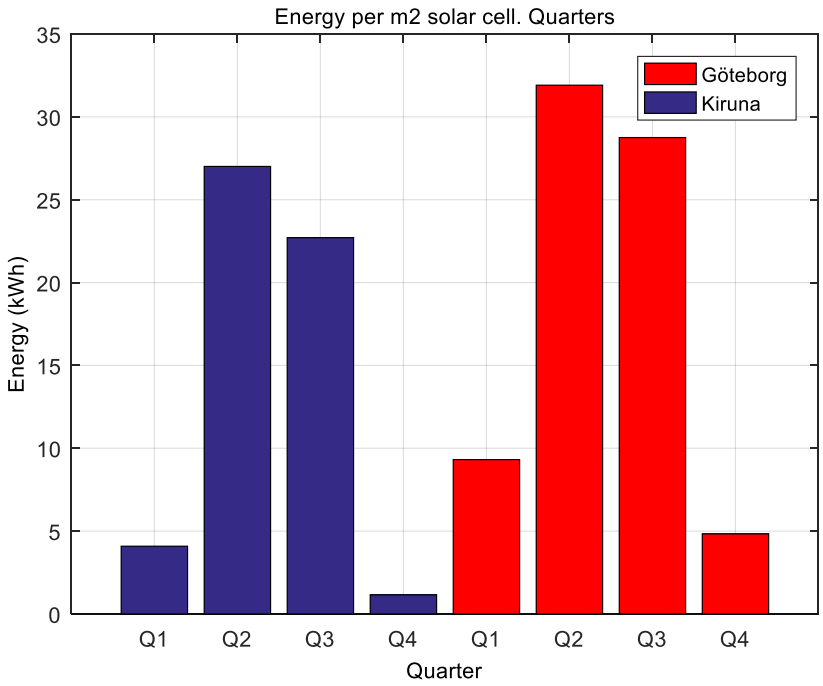

Fig. 9.7. Electrical solar energy per m^2 solar cell. Periods January – March, April – June, July – September and October – December. Kiruna and Göteborg.

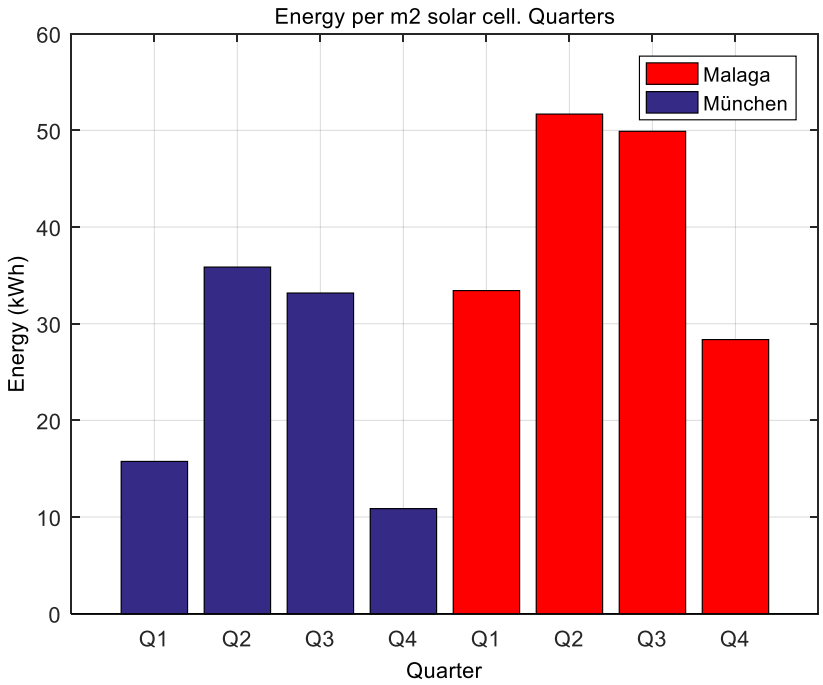

Fig. 9.8. Electrical solar energy per m^2 solar cell. Periods January – March, April – June, July – September and October – December. München and Malaga.

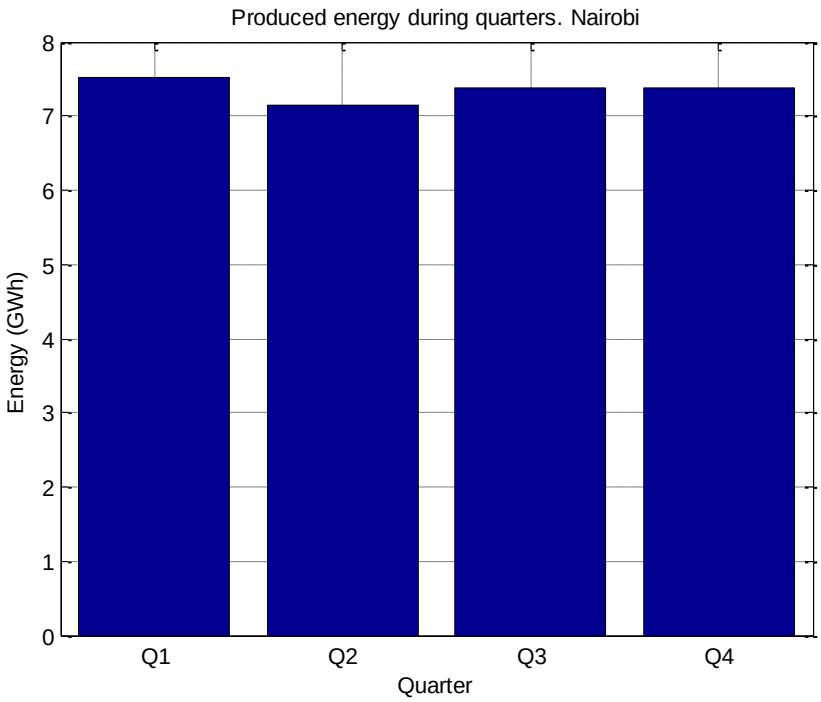

Fig. 9.9. Produced electrical solar energy during periods January – March, April – June, July – September and October – December. Nairobi.

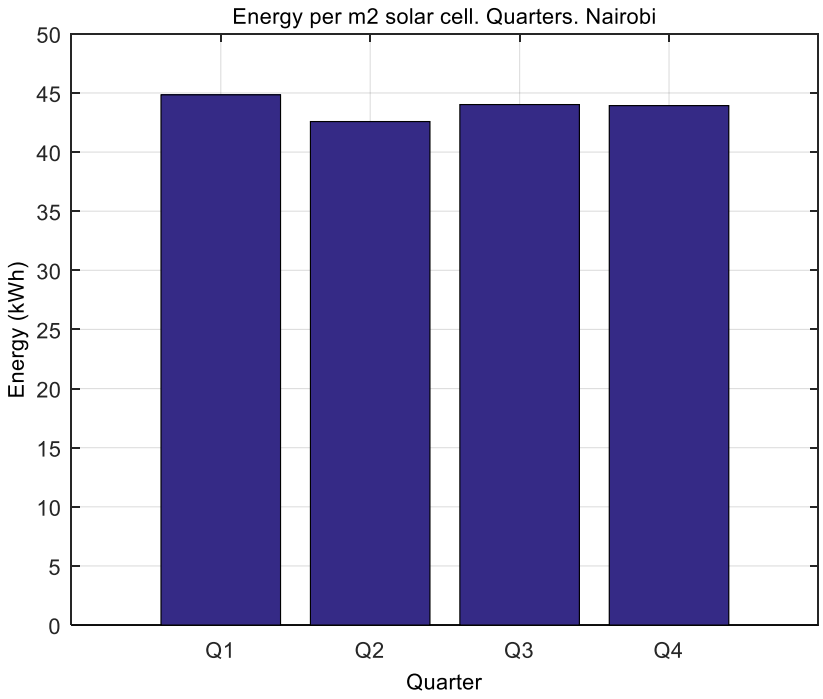

Fig. 9.10. Electrical solar energy per m^2 solar cell. Periods January – March, April – June, July – September and October – December. Nairobi.

9.4.3 Wind power capacity. Design guideline

According to chapter 8, the following guide-line was found:

- Annual energy production from the wind power system = 1.7 × annual consumed energy from the local electrical load

In this section, this guide-line will be further checked.

Table 9.7 lists simulation results for a varying number of wind power turbines. No solar power is used.

Parameter "-ΔIp/ΔTb" is defined according to:

$$\frac{\Delta Ip}{\Delta Tb} = - \frac{\text{Decreased imported energy}}{\text{Increased number of turbines}} \quad \text{(GWh/turbine)} \tag{9.3}$$

Where "ΔI_P (GWh)" corresponds to an decreasing need of imported energy when the number of turbines are increased ΔTb.
Example. See Table 9.7:

- Number of turbines 1 → 2
- Imported energy 16.32 GWh → 13.98 GWh
- ΔIp = - 2.34 GWh
- ΔTb = 1
- -ΔIp/ΔTb = 2.34

"-ΔIp/ΔTb" is used as a reference to predict a usable guideline for wind power capacity.

Table 9.7. Varying number of wind turbines.

Number of turbines	**Wind energy (GWh)**	**Exported energy (GWh)**	**Imported energy (GWh)**	**- ΔIp/ΔTb (GWh/turbine)**
0	0	0	20	-
1	3.852	0.1	16.32	3.6800
2	7.610	1.505	13.98	2.3400
3	11.43	3.834	12.50	1.4800
5	19.27	9.741	10.55	0.9750
7	26.81	16.14	9.403	0.5735
9	34.39	22.94	8.642	0.3805
12	46.31	33.95	7.721	0.3070
15	58.19	45.26	7.156	0.1883
18	70.29	57.10	6.899	0.0857

Fig. 9.11 and Fig. 9.12 show imported energy and parameter - ΔIp/ΔTb vs number of turbines.

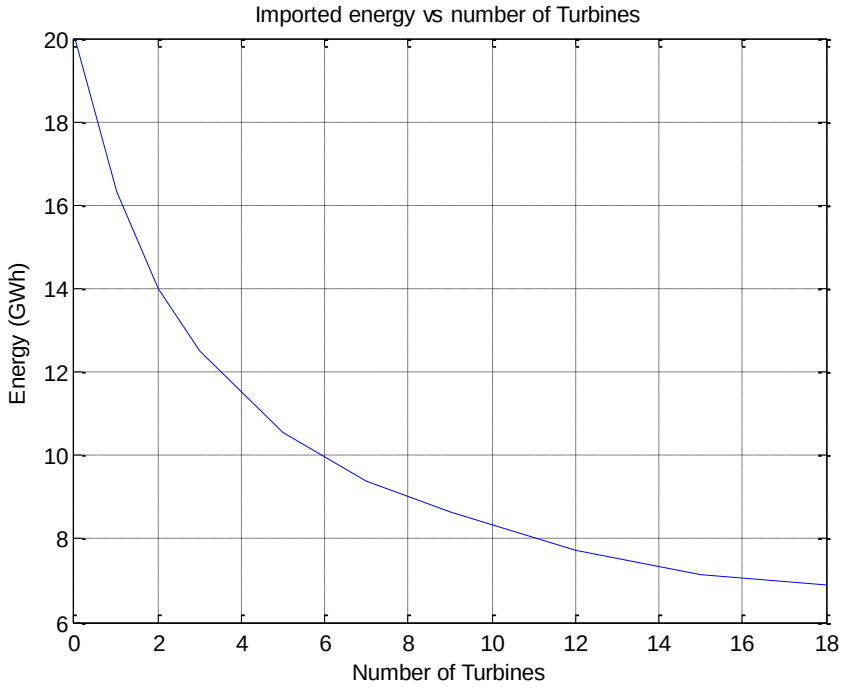

Fig. 9.11. Imported energy vs number of turbines.

As can be observed in Fig. 9.11, the curve tends to flatten out in the region between 9 – 18 turbines.

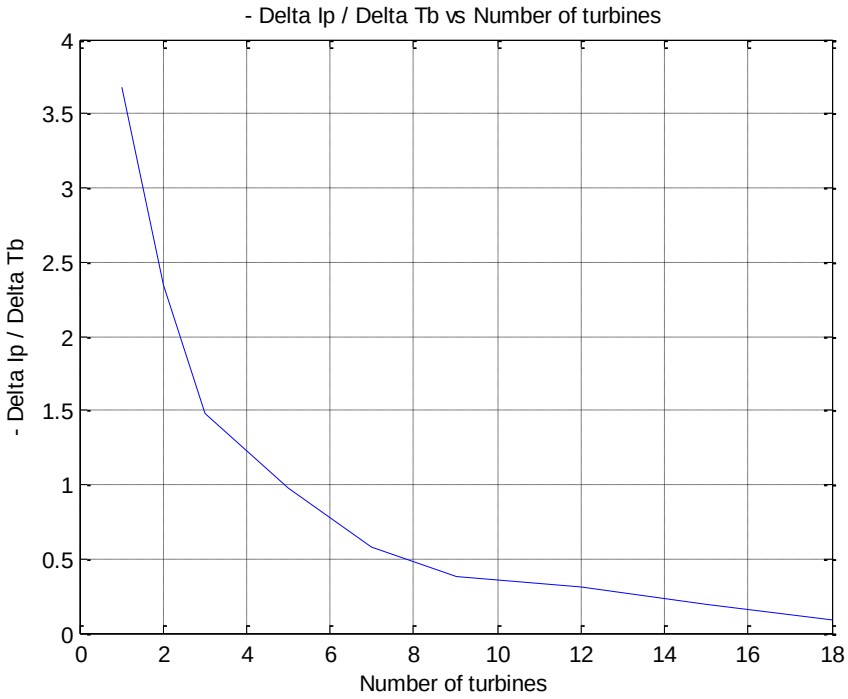

Fig. 9.12. - ΔIp/ΔTb vs Number of turbines.

A reasonable basic principle for selection of appropriate number of turbines is as follows:

9 turbines imply that parameter - ΔIp/ΔTb = 0.3805. See Table 9.7 and Fig. 9.12.

A check with (9.3) results in the conclusion that 9 turbines is a good choice in relation to design guideline.

This agrees well with the guide-line from chapter 8. Annual consumed energy = 20 GWh. 1 wind power turbine produces, with the current specification, an annual energy of 3.83 GWh. To produce 1.7 × 20 GWh (guideline from chapter 8), 8.88 turbines are required, which is rounded up to 9 turbines.

9.4.4 Solar power capacity. Design guide-line

According to chapter 8, the following guide-line was found:

- Annual energy production from the solar power system = 1.5 × annual consumed energy from the local electrical load

In this section, this guide-line will be further checked.

Table 9.8 - Table 9.12 are listing simulation results for the 5 locations in question. The wind power is fixed and corresponds to power produced from 9 wind power turbines. Solar cell area A_equ for the different location is defined according to Table 9.3.

Parameter "- ΔIp/ΔA" is defined according to:

$$\frac{\Delta \mathrm{Ip}}{\Delta \mathrm{A}} = \frac{\text{Decreased imported energy}}{\text{Increased solar cell area}} \quad \text{(GWh/A\_equ)} \tag{9.4}$$

Where:

Decreased imported energy (GWh) corresponds to an decreasing need of imported energy when the solar cell area is increased ΔA (A_equ units). See (9.1).

Example. See Table 9.8:

- Solar cell area 0.2 A_equ → 0.5 A_equ
- Imported energy 7.494 GWh → 7.218 GWh
- ΔIp = - 0.276 GWh

- ΔA = 0.3 A_equ
- - ΔIp/ΔA = 0.92 GWh/ A_equ

"-ΔIp/ΔA" is used as a reference to predict a usable guideline for solar power capacity.

Table 9.8. Kiruna. Simulation results. Varied solar cell area. Fixed wind power.

Solar cell area (A_equ)	Wind energy (GWh)	Solar energy (GWh)	Exported energy (GWh)	Imported energy (GWh)	- ΔIp/ΔA (GWh/A_equ)
0	34.92	0	23.35	8.514	-
0.2	34.47	3.976	25.87	7.494	5.1000
0.5	34.39	9.976	31.49	7.218	0.9200
1.0	34.73	20.01	41.57	6.913	0.6100
1.5	34.91	29.80	51.42	6.801	0.2240
2.0	35.14	39.93	61.78	6.786	0.0300
3.0	34.28	59.65	80.60	6.754	0.0320

Table 9.9. Göteborg. Simulation results. Varied solar cell area. Fixed wind power.

Solar cell area (A_equ)	Wind energy (GWh)	Solar energy (GWh)	Exported energy (GWh)	Imported energy (GWh)	- ΔIp/ΔA (GWh/A_equ)
0	34.92	0	23.35	8.514	-
0.2	34.67	3.981	25.85	7.278	6.1800
0.5	34.24	10.03	31.16	6.973	1.0167
1.0	34.47	20.01	41.00	6.584	0.7780
1.5	34.39	29.96	50.73	6.478	0.2120
2.0	34.47	40.02	60.77	6.348	0.2600
3.0	34.67	59.71	80.52	6.221	0.1270

Table 9.10. München. Simulation results. Varied solar cell area. Fixed wind power.

Solar cell area (A_equ)	Wind energy (GWh)	Solar energy (GWh)	Exported energy (GWh)	Imported energy (GWh)	- ΔIp/ΔA (GWh/A_equ)
0	34.92	0	23.35	8.514	-
0.2	34.39	3.984	25.46	7.183	6.6550
0.5	34.73	9.969	31.15	6.530	2.1767
1.0	34.91	19.97	40.99	6.195	0.6700
1.5	35.14	29.93	51.06	6.077	0.2360
2.0	34.67	39.79	60.33	5.951	0.2520
3.0	35.14	59.85	80.73	5.819	0.1320

Table 9.11. Malaga. Simulation results. Varied solar cell area. Fixed wind power.

Solar cell area (A_equ)	Wind energy (GWh)	Solar energy (GWh)	Exported energy (GWh)	Imported energy (GWh)	- ΔIp/ΔA (GWh/A_equ)
0	34.92	0	23.35	8.514	-
0.2	34.24	4.000	25.10	6.938	7.8800
0.5	34.28	9.985	30.30	6.125	2.7100
1.0	34.69	19.97	40.24	5.672	0.9060
1.5	34.72	29.96	50.06	5.481	0.3820
2.0	34.54	40.00	59.85	5.404	0.1540
3.0	34.42	59.95	79.59	5.301	0.1030

Table 9.12. Nairobi. Simulation results. Varied solar cell area. Fixed wind power.

Solar cell area (A_equ)	Wind energy (GWh)	Solar energy (GWh)	Exported energy (GWh)	Imported energy (GWh)	- ΔIp/ΔA (GWh/A_equ)
0	34.92	0	23.35	8.514	-
0.2	34.40	3.998	25.04	6.731	8.9150
0.5	35.30	10.01	31.16	5.941	2.6333
1.0	34.79	19.96	40.42	5.754	0.3740
1.5	34.48	29.97	49.96	5.595	0.3180
2.0	34.35	39.89	59.67	5.514	0.1620
3.0	34.52	59.92	79.72	5.359	0.1550

Fig. 9.13 shows imported energy vs solar cell area for the 5 locations. As can be observed, the 5 curves tend to flatten out in the region around 1.5 A_equ.

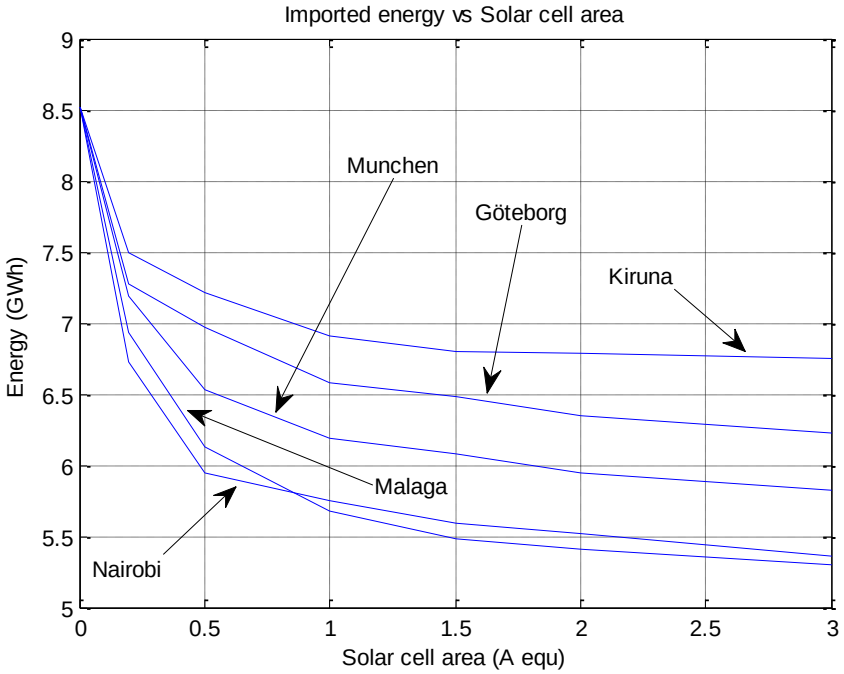

Fig. 9.13. Imported energy vs Solar cell area. Kiruna, Göteborg, München, Malaga and Nairobi.

Parameter - ΔIp/ΔA vs solar cell area is plotted in Fig. 9.14 – Fig. 9.16.

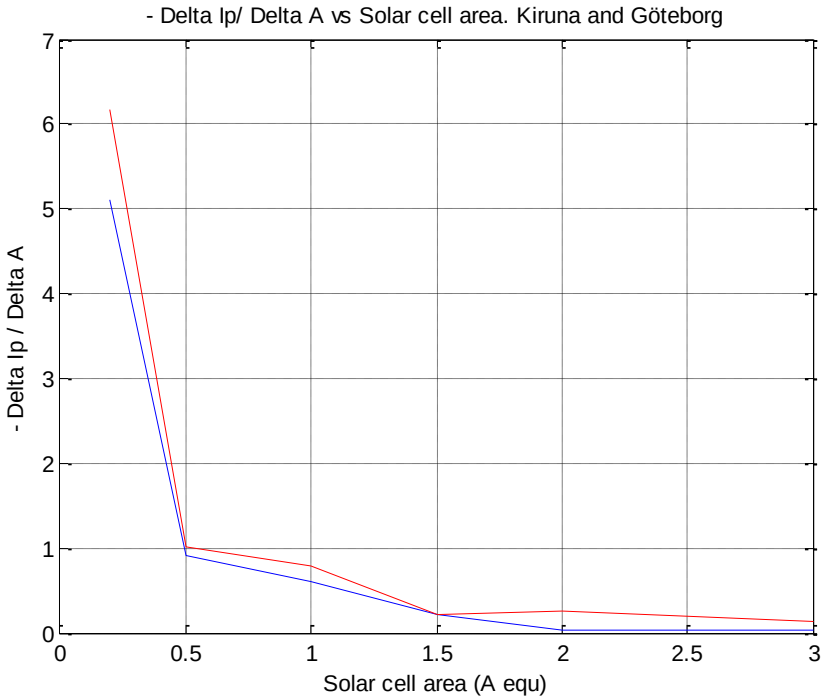

Fig. 9.14. - ΔI/ΔA vs Solar cell area. Kiruna and Göteborg.
Blue curve: Kiruna. Red kurve: Göteborg.

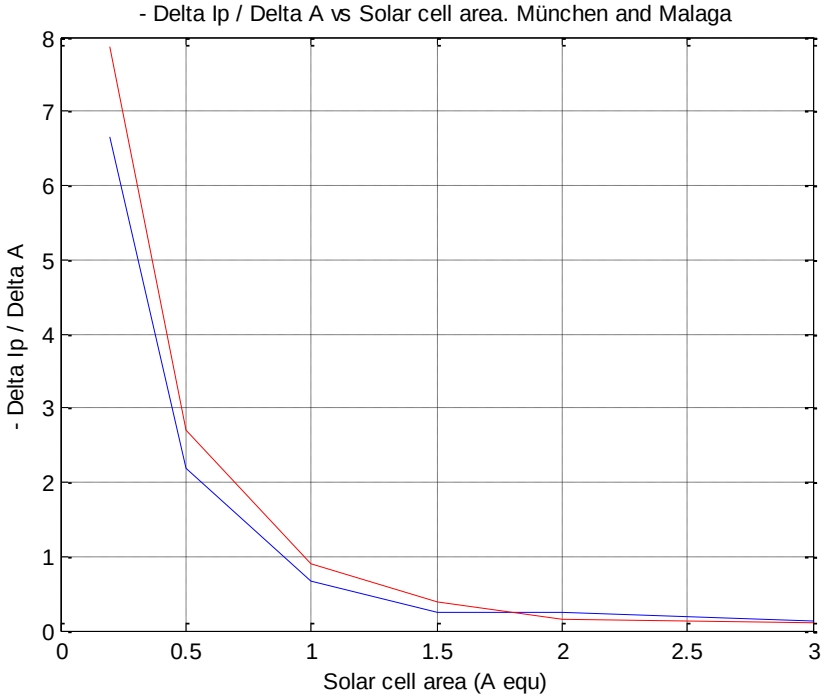

Fig. 9.15. - ΔI/ΔA vs Solar cell area. München and Malaga.
Blue curve: München. Red curve: Malaga.

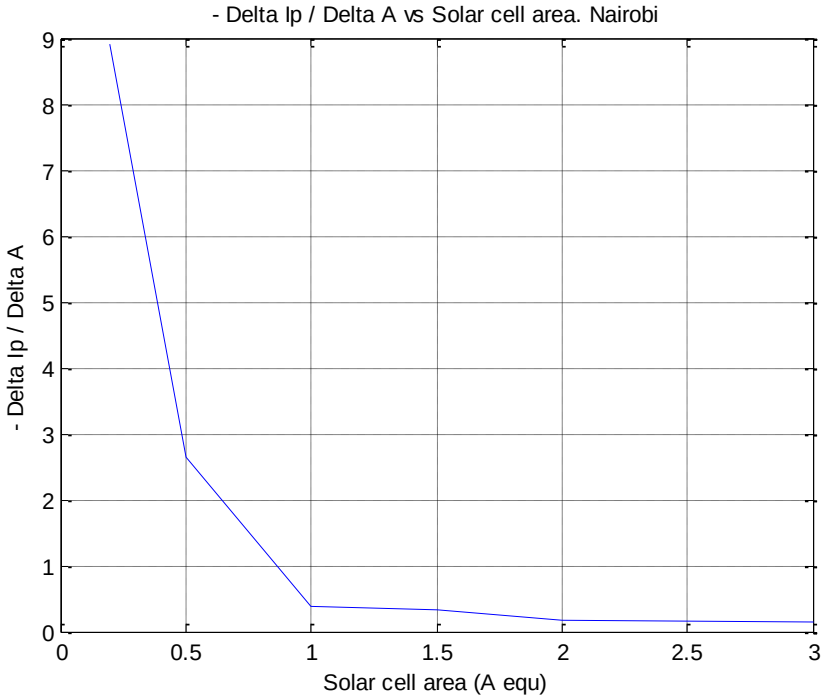

Fig. 9.16. - ΔI/ΔA vs Solar cell area. Nairobi.

Area A_equ = 1.5 implies parameter - ΔIp/ΔTb according to Table 9.13. See Table 9.8 - Table 9.12 and Fig. 14 – Fig. 16.

Table 9.13. - ΔIp/ΔA for A_equ = 1.5.

Location	**- ΔIp/ΔA**
Kiruna	0.2240
Göteborg	0.2120
München	0.2360
Malaga	0.3820
Nairobi	0.3180

The conclusion is that the guideline from chapter 8 can be accepted.

9.5 Solar- and Wind power in combination with Energy storage

Simulations have been performed with varying energy storage capacity in combination with solar- and wind power. Regarding parameters “ESC rel” and “ESC abs”, see section 9.3.3 and (2.4) - (2.5). The power capacities for wind and solar have been dimensioned in accordance with the design guidelines according to sections 9.4.3 and 9.4.4.

Two effects of the combination with energy storage are studied according to:

- Decrease of imported energy
- Probability of energy shortage

The simulation results are presented in Table 9.14 - Table 9.18. The parameters “Exported energy” and “Imported energy” are presented according to:

$$\text{Exported energy Rel} = \frac{\text{Exported energy (GWh) with energy storage}}{\text{Exported energy (GWh) without energy storage}} \quad (9.5)$$

$$\text{Imported energy Rel} = \frac{\text{Imported energy (GWh) with energy storage}}{\text{Imported energy (GWh) without energy storage}} \quad (9.6)$$

With energy shortage in the tables is meant in this context one of the following:

- The power system imports energy via the utility grid
- The power system starts up the back-up unit

Table 9.14. Energy storage, Wind power and Solar power. Kiruna.

Energy storage ESC rel	Energy storage ESC abs (GWh)	Exported energy Rel (%)	Imported energy Rel (%)	Probability of energy shortage (%)
5	0.2740	88.4675	17.7474	100
7	0.3836	87.7091	12.5143	99
10	0.5479	88.5842	7.3298	84
15	0.8219	87.2034	3.8347	46
20	1.0959	86.4644	2.6305	36.5
25	1.3699	87.1840	1.5233	14
30	1.6438	86.9506	0.9055	11.5
35	1.9178	87.0089	0.5018	7
40	2.1918	86.1727	0.1117	3
50	2.7397	86.2505	0.1532	2
60	3.2877	87.0867	0.0810	1.5
65	3.5616	85.8421	0.0876	0.5
70	3.8356	86.9895	0	0

Table 9.15. Energy storage, Wind power and Solar power. Göteborg.

Energy storage ESC rel	Energy storage ESC abs (GWh)	Exported energy Rel (%)	Imported energy Rel (%)	Probability of energy shortage (%)
3	0.1644	89.7299	14.4288	100
5	0.2740	89.0203	9.4211	98.5
7	0.3836	88.1333	6.8324	88
10	0.5479	88.0741	2.9870	56.5
15	0.8219	87.8179	1.2989	27
20	1.0959	87.1674	0.6269	12.5
25	1.3699	87.9953	0.2081	4
30	1.6438	87.2856	0.1318	2
35	1.9178	87.6996	0.0788	1
40	2.1918	88.8232	0	0

Table 9.16. Energy storage, Wind power and Solar power. München.

Energy storage ESC rel	Energy storage ESC abs (GWh)	Exported energy Rel (%)	Imported energy Rel (%)	Probability of energy shortage (%)
1	0.0548	90.8735	28.1060	100
3	0.1644	89.3655	5.1703	98
5	0.2740	87.3286	1.9697	70.5
7	0.3836	87.1915	1.0439	39.5
8	0.4384	87.1524	0.6564	30
10	0.5479	86.6236	0.4543	17
11	0.6027	86.7998	0.2546	10
12	0.6575	86.9174	0.0751	4.5
15	0.8219	87.3090	0.0579	2
20	1.0959	86.5452	0.0061	0.5
25	1.3699	87.2503	0	0

Table 9.17. Energy storage, Wind power and Solar power. Malaga.

Energy storage ESC rel	Energy storage ESC abs (GWh)	Exported energy Rel (%)	Imported energy Rel (%)	Probability of energy shortage (%)
1.5	0.0822	89.4127	2.3791	100
2	0.1096	89.3927	0.6393	72.5
2.5	0.1370	88.7135	0.2166	37.5
3	0.1644	89.1131	0.1145	17.5
3.5	0.1918	88.4938	0.0508	7
4	0.2192	89.0931	0.0242	3.5
4.5	0.2466	88.2341	0.0221	2
5	0.2740	88.2341	0.0140	1.5
5.5	0.3014	88.2141	0.0004	0.5
6	0.3288	89.0132	0	0

Table 9.18. Energy storage, Wind power and Solar power. Nairobi.

Energy storage ESC rel	**Energy storage** ESC abs **(GWh)**	**Exported energy Rel (%)**	**Imported energy Rel (%)**	**Probability of energy shortage (%)**
1.7	0.0932	89.5717	1.6652	100
2	0.1096	90.1922	0.5871	96.5
2.2	0.1205	88.9512	0.1930	74
2.3	0.1260	89.1513	0.1035	56
2.4	0.1315	88.5308	0.0407	34
2.5	0.1370	89.2314	0.0128	15.5
2.6	0.1425	89.4516	0.0036	7
2.7	0.1479	90.6725	0.0014	1
2.8	0.1534	89.4315	0	0

9.5.1 Decrease of imported energy

As shown in Table 9.14 - Table 9.18, the energy storage has a dramatic impact on the total import of energy. Even relatively small storages will substantially reduce the need for energy import. Fig. 9.17 illustrates an example with ESC rel = 5 for Kiruna, Göteborg, München and Malaga and ESC rel = 2.5 for Nairobi.

Note! The reductions are rounded to the nearest tenth of a percent. This means that Malaga and Nairobi do not have a reduction of exactly 100%, but very close to this value.

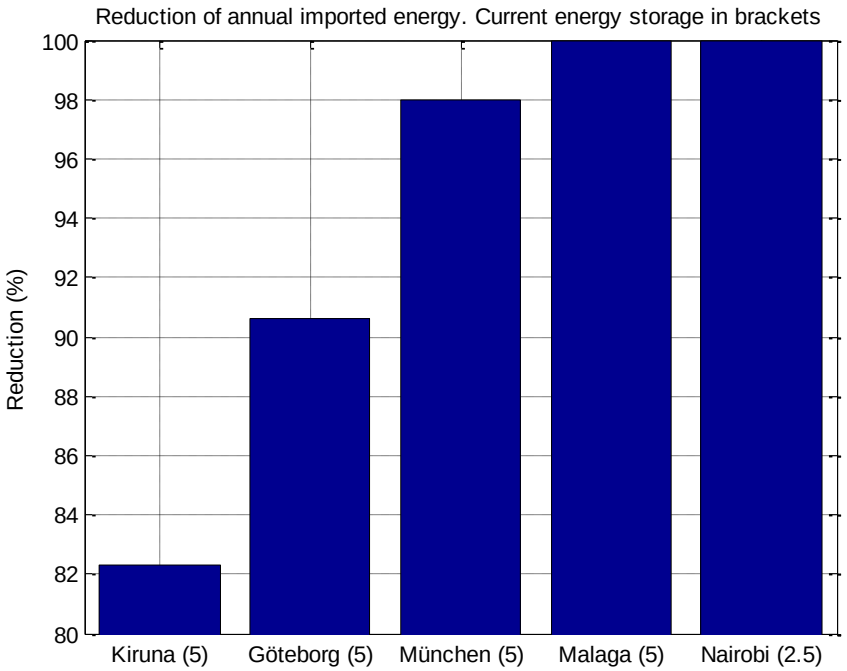

Fig. 9.17. Reduction of annual imported energy. Current energy storage (ESC rel) in brackets.

Fig. 9.18 – 20 illustrate the relative decrease of imported energy vs energy storage for the 5 locations.

It can be noted that the energy storages for Kiruna, Göteborg and München have to be in the order between ESC rel = 20 (München) to about 65 (Kiruna), to get a reduction of imported energy close to 100 %. This is to compare with Malaga (ESC rel = 5) and Nairobi (ESC rel = 2.5).

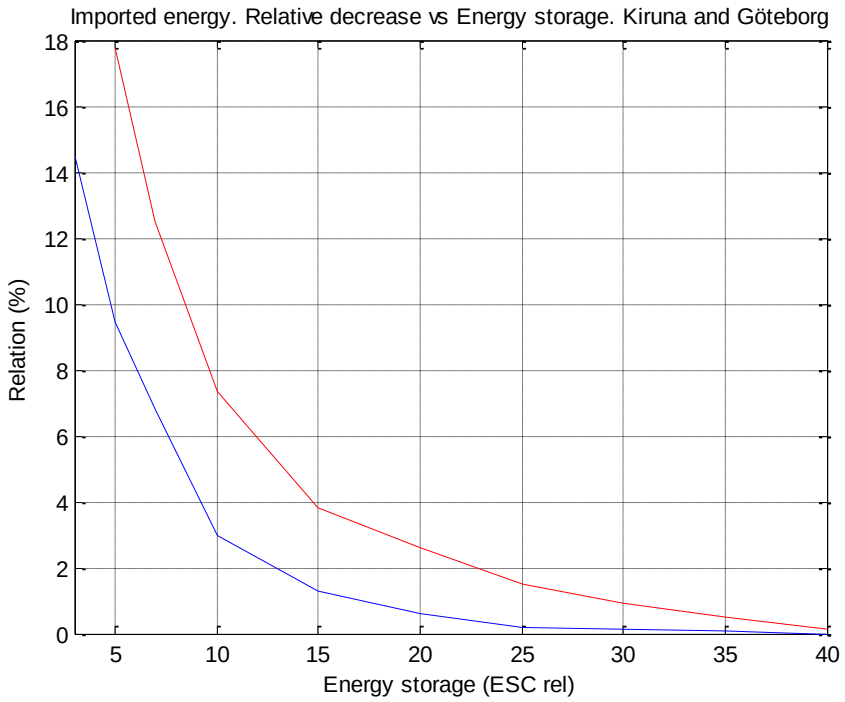

Fig. 9.18. Imported energy. Relative decrease vs Energy storage. Red curve: Kiruna. Blue curve: Göteborg.

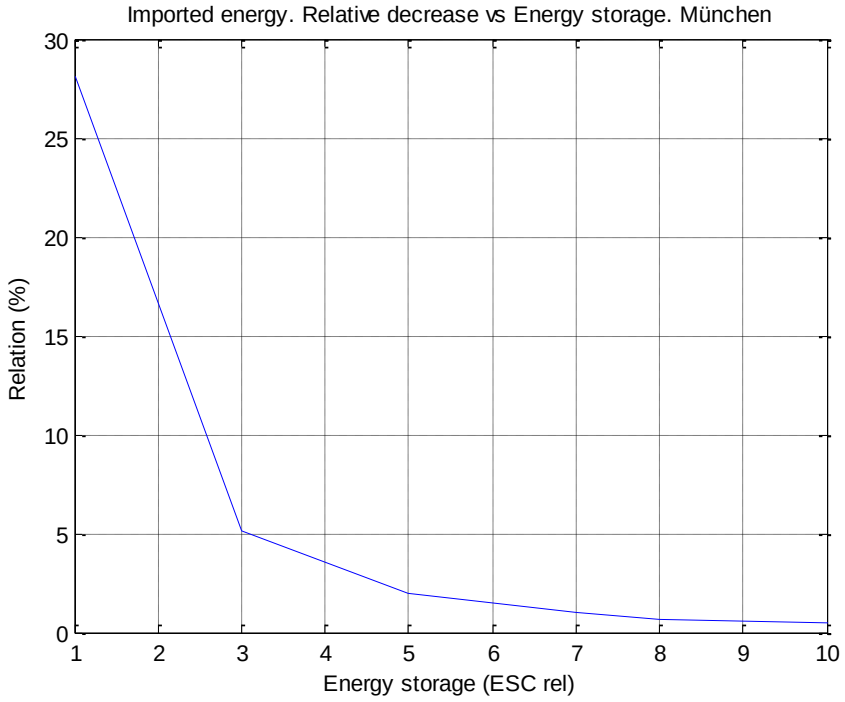

Fig. 9.19. Imported energy. Relative decrease vs Energy storage. München.

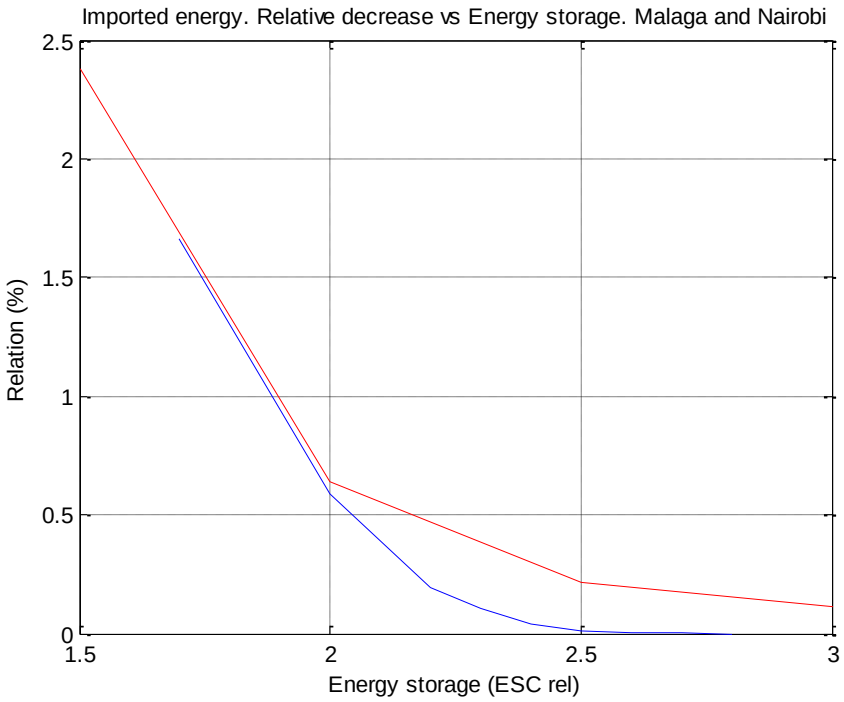

Fig. 9.20. Imported energy. Relative decrease vs Energy storage.
Red curve: Malaga. Blue curve: Nairobi.

9.5.2 Probability of energy shortage

Fig. 9.21 – 25 illustrate the probability of energy shortage for the 5 locations. The blue curves are direct simulation results, while the red curves represent adaptation between certain points by using the least square method.

As an example, it can be noted that the probability of energy shortage is about 20% if ESC rel = 10 in München. Corresponding probability of energy shortage will be obtained for ESC rel = 25 in Kiruna and for ESC rel less than 3 in Malaga and Nairobi.

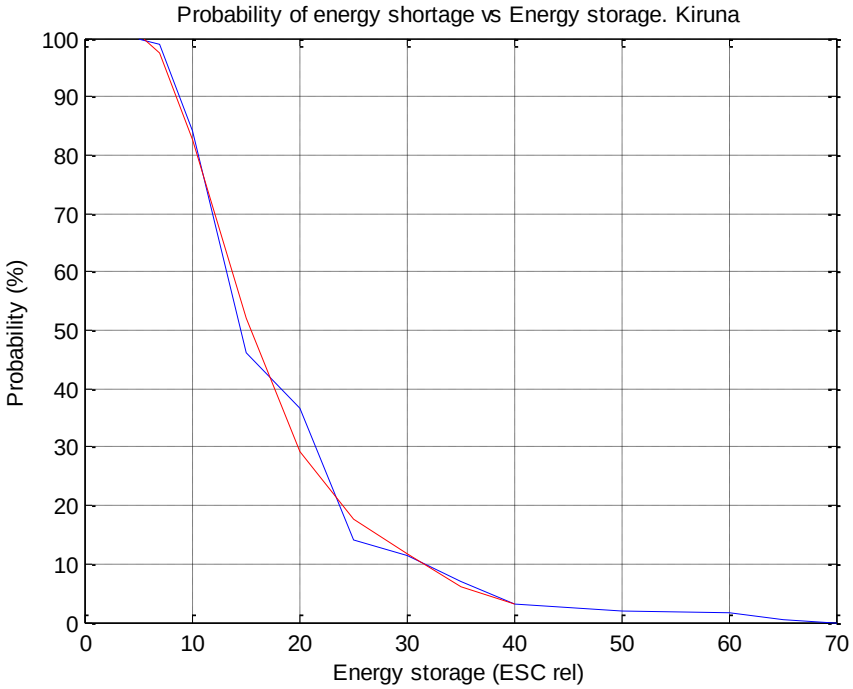

Fig. 9.21. Probability of energy shortage vs Energy storage. Kiruna.
Blue curve: Simulated values. Red curve: Adapted values.

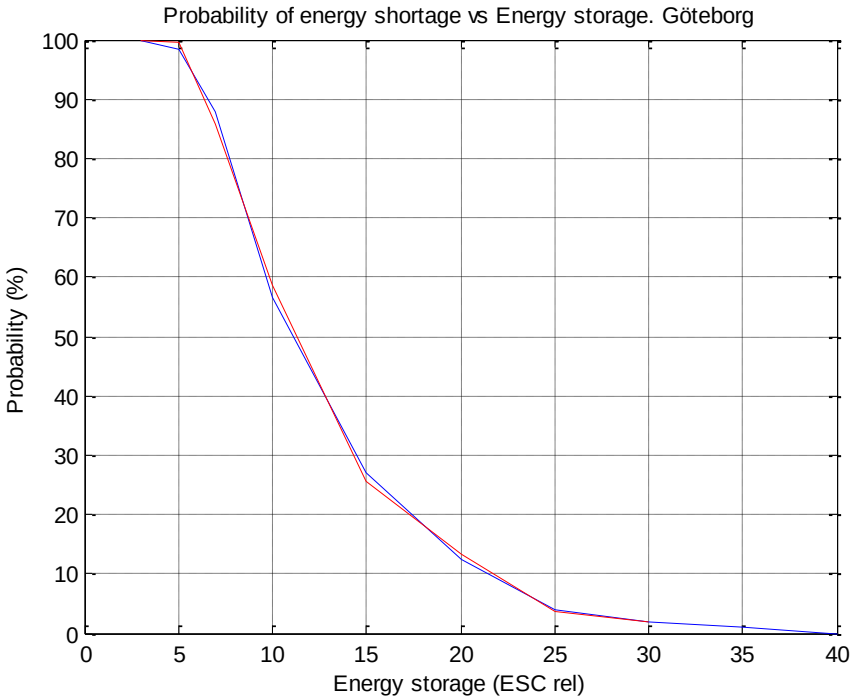

Fig. 9.22. Probability of energy shortage vs Energy storage. Göteborg.
Blue curve: Simulated values. Red curve: Adapted values.

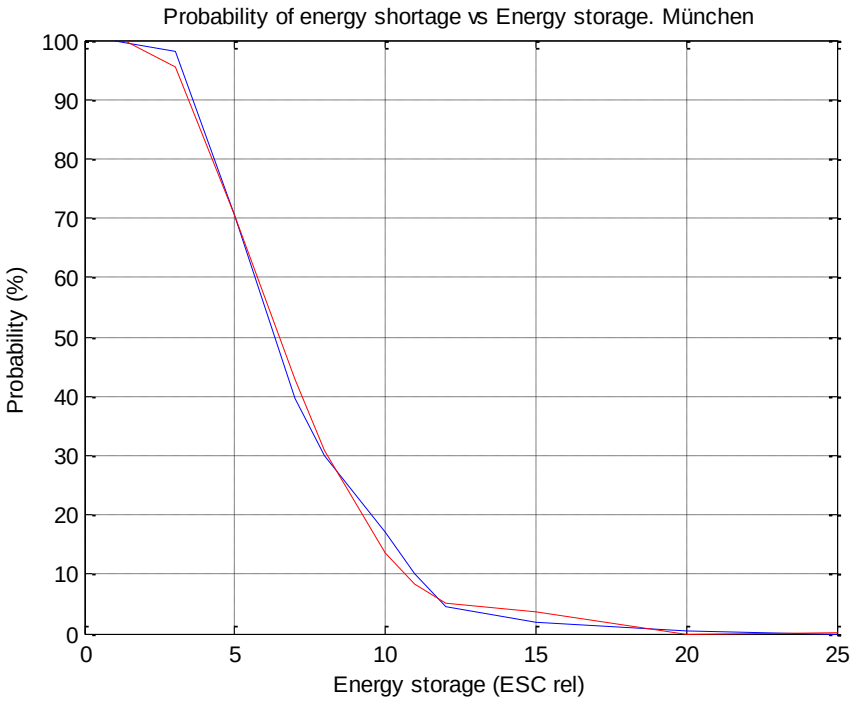

Fig. 9.23. Probability of energy shortage vs Energy storage. München. Blue curve: Simulated values. Red curve: Adapted values.

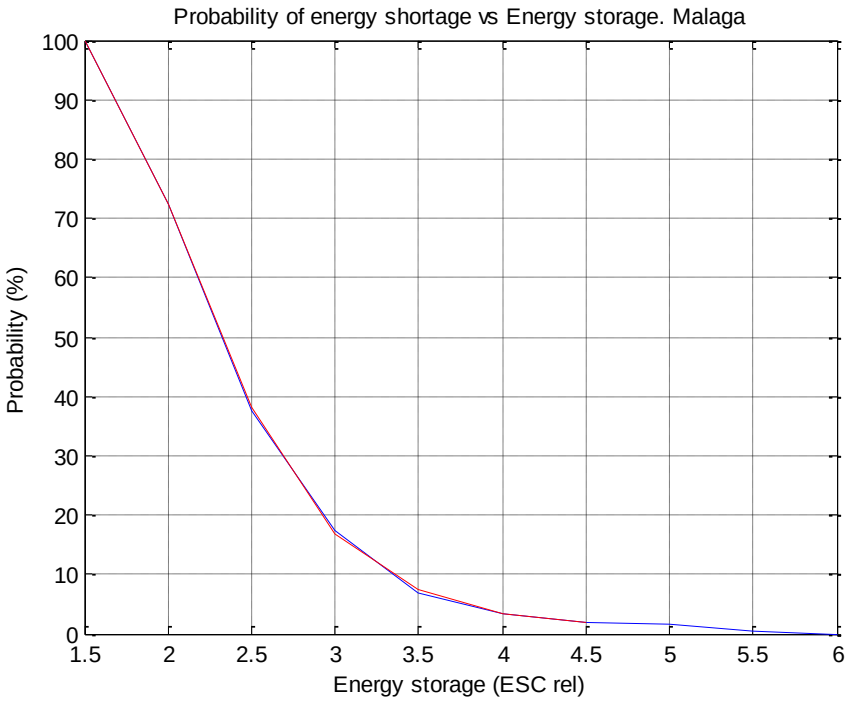

Fig. 9.24. Probability of energy shortage vs Energy storage. Malaga. Blue curve: Simulated values. Red curve: Adapted values.

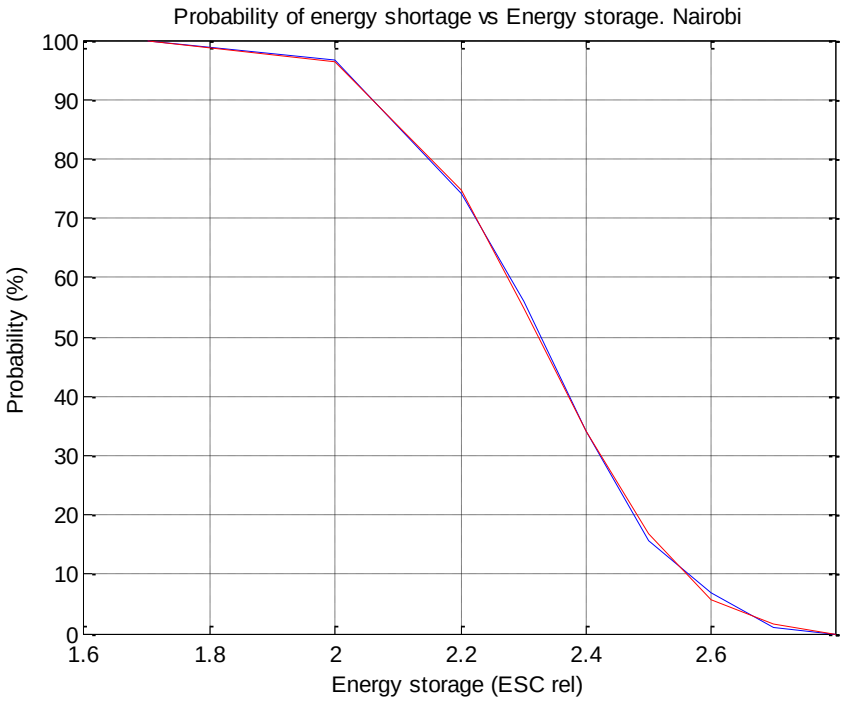

Fig. 9.25. Probability of energy shortage vs Energy storage. Nairobi. Blue curve: Simulated values. Red curve: Adapted values.

9.5.3 10 % and 50 % probability of energy shortage

The term “energy shortage” has in this study been used to denote a situation where there is a need to import power via utility grid or, alternatively, to use a power back-up unit. A probability of 10 % energy shortage can be taken as an example of a reasonable goal. The study has resulted in a different need for energy storage, depending on geographic location of the power plants. Table 9.19 and Table 9.20 show the minimum energy storage needed to meet requirements of maximum10 % and 50 % probability of energy shortage. See Fig. 9.21 – Fig. 9.25.

Table 9.19. Energy storage needed to meet the requirement of maximum probability of 10 % energy shortage.

Location	Energy storage, ESC rel	Energy storage, ESC abs (GWh)	Square root of required solar cell area (m)
Kiruna	32	1.7534	730
Göteborg	22	1.2055	626
München	11	0.6027	553
Malaga	3.4	0.1863	425
Nairobi	2.6	0.1425	410

Table 9.20. Energy storage needed to meet the requirement of maximum probability of 50 % energy shortage.

Location	Energy storage, ESC rel	Energy storage, ESC abs (GWh)	Square root of required solar cell area (m)
Kiruna	16	0.8767	730
Göteborg	12	0.6575	626
München	7	0.3836	553
Malaga	2.4	0.1315	425
Nairobi	2.4	0.1315	410

In order to get a comparison of the requirement for energy storage at different locations “Kiruna” is taken as a reference. Table 9.21 gives the relations for required energy storage and different locations with Kiruna as reference.

Table 9.21. Energy storage to meet the requirement of maximum probability of 10 % and 50 % energy shortage. Relation to energy storage for Kiruna and 10 % probability ofenergy shortage.

Location	Energy storage relation. Probability of 10 % energy shortage	Energy storage relation. Probability of 50 % energy shortage
Kiruna	1.0000	0.5000
Göteborg	0.6875	0.3750
München	0.3438	0.2188
Malaga	0.1063	0.0750
Nairobi	0.0813	0.0750

Fig. 9.26 and Fig. 9.27 illustrate the relations of energy storage requirements according to Table 9.21 between the 5 locations studied. Relation to energy storage for Kiruna and 10 % probability of energy shortage.

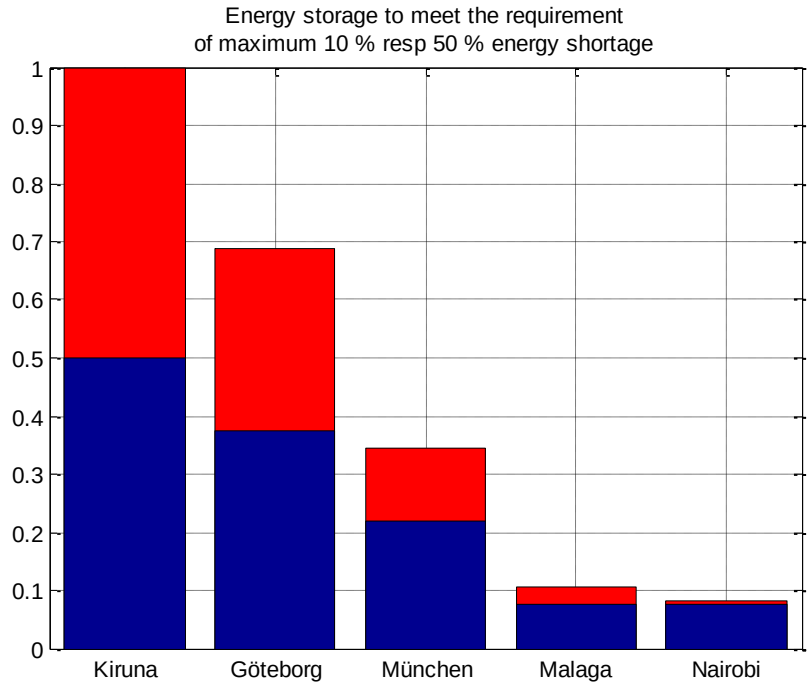

Fig. 9.26. Energy storage. 5 power farm locations.
Red + blue bars: To meet the requirement of maximum 10 % energy shortage.
Blue bars: To meet the requirement of maximum 50 % energy shortage.
For Malaga and Nairobi see enlarged section in Fig. 9.27.

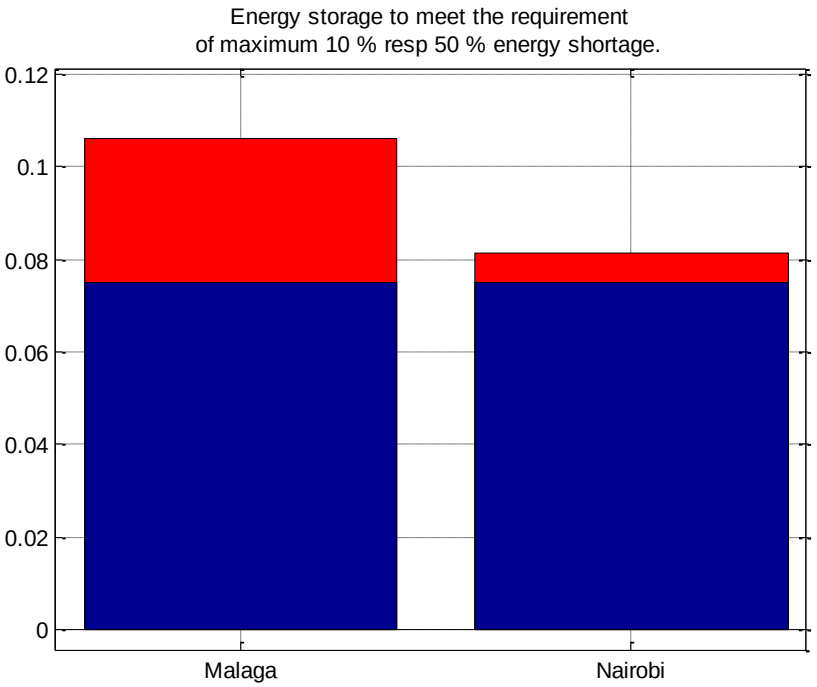

Fig. 9.27. Enlarged section of Fig. 9.26.

9.6 Required solar cell area. Different locations

Kiruna is taken as a reference in this section. The intention is to compare the required solar cell area to produce the same, unspecified amount of solar power at different locations. Table 9.22 gives these relations. The area requirement is based on the assumption according to section 9.3.2.3.

Table 9.22. Required solar cell area and relation to case “Kiruna”.

Location	**Solar cell area × 10^6 (m^2). Annual production 30 GWh**	**Relation to case “Kiruna”**
Kiruna	0.53277	1.0000
Göteborg	0.39231	0.7364
München	0.30562	0.5736
Malaga	0.18061	0.3390
Nairobi	0.16788	0.3151

Fig. 9.28. illustrates the relations according to Table 9.22. These relations reflect directly the difference between the production costs for varying power plant locations. See section 9.7.2.

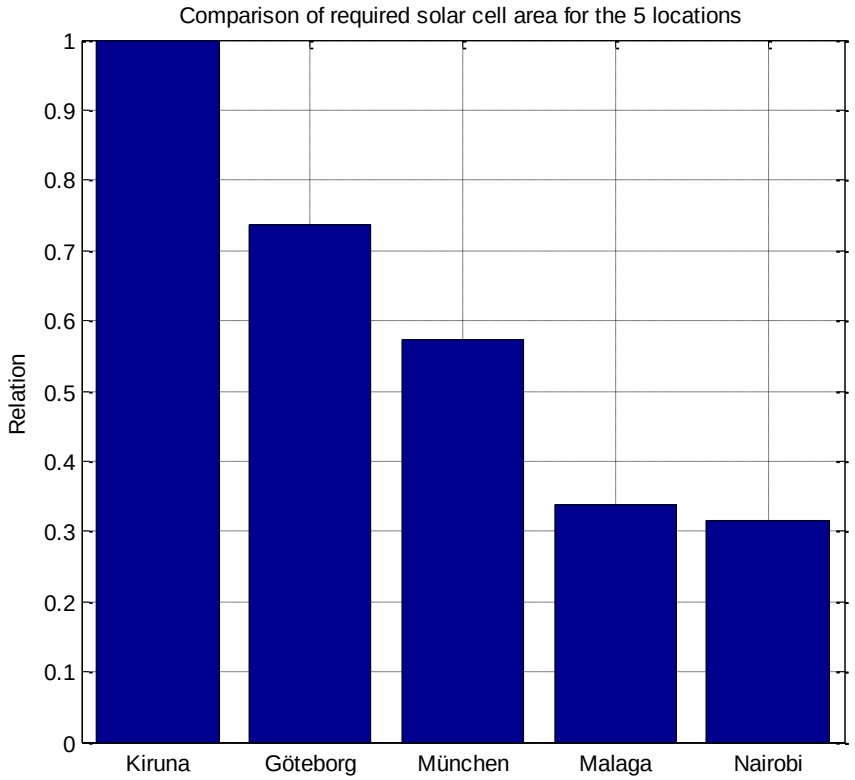

Fig. 9.28. Comparison of required solar cell area with “Kiruna” as reference. The relations reflect the difference regarding required solar cell area to produce a certain amount of solar energy at the 5 locations.

9.7 Cost analysis

A simple cost analysis regarding wind- and solar power systems will be done. The power capacities for wind and solar have been dimensioned in accordance with the design guide-lines according to sections 9.4.3 and 9.4.4. Information presented in [24] and [25] will be used.

9.7.1 Wind power cost

Annual costs regarding turbines are calculated according to:

$$T_{cost} = \frac{1}{Y} \times (T_{Ref} \times P_{Max} \times N_{Turb} + Cost_{Inf} \times P_{Max}) \quad (9.7)$$

Where:

T_{cost}: Total annual turbine costs including infrastructure costs
Y: Expected life time
T_{Ref}: Reference turbine cost / max power
P_{Max}: Maximum power / turbine
N_{Turb}: Number of turbines
$Cost_{Inf}$: Infrastructure cost / max power

Annual cost for operation and maintenance are calculated according to:

$$OM_{Tot} = OM \times Prod \quad (9.8)$$

Where:

OM_{Tot}: Total annual cost for operation and maintenance
OM: Cost for operation and maintenance / produced energy
Prod: Annual produced energy

According to [24], the following is applied:

- Reference turbine cost: 9 MSEK / MW
- Infrastructure cost: 3 MSEK / MW
- Operation and Maintenance: 0.15 SEK / kWh

For the power plants in question, the following is valid:

- Maximum power per turbine: 2MW
- Number of turbines: 9
- Annual produced wind energy: 3.83 GWh × 9 = 34.47 GWh

Expected life-time: 20 years

Total annual cost for wind power is calculated according to:

$$Wind_{cost} = T_{cost} + OM_{Tot} \quad (9.9)$$

Where:

$Wind_{cost}$: Total wind power cost for the plant

The information above results in the following annual wind power cost for the plant:

$Wind_{cost}$ = 13.57 MSEK

9.7.2 Solar power cost

A simplified assumption is made in this analysis: Cost of solar power plant is linearly dependent on size of solar cell area. The cost is then calculated according to:

$$Solar_{cost} = Area_{cost} \times Area \quad (9.10)$$

Where:

$Solar_{cost}$: Total annual cost for solar power plant
$Area_{cost}$: Annual cost/m^2
Area: Total solar cell area (m^2)

According to [25], the annual cost in southern Germany for solar power is estimated to be about:

$$Solar_{cost} = 8.4\ ct_{EUR} / kWh \times Prod \quad (9.11)$$

Where:

Prod: Annual produced energy (kWh)

München can be regarded as a typical example of a place in southern Germany.

For the “München case” according to section 9.5, the following is valid:

Prod = 30×10^6 kWh

Area = 0.30562×10^6 See Table 9.3

By applying (9.11), the following will be obtained with respect to München:

$Solar_{cost}$ = 2.52 MEuro

By applying (9.10), the following will be obtained:

$Area_{cost}$ = 8.2455 Euro / m^2

Total annual solar power costs of plants, located in Kiruna, Göteborg, Malaga and Nairobi are obtained by using the information about solar cell areas given in Table 9.3. See Table 9.23.

Table 9.23. Total annual cost for solar power plants.

Location	**$Solar_{cost}$ (MEuro)**	**Production cost (ct_{EUR} / kWh)**
Kiruna	4.39	14.6
Göteborg	3.23	10.8
München	2.52	8.4
Malaga	1.49	5.0
Nairobi	1.38	4.6

9.7.3 Solar power cost. Difference of module temperature

According to section 9.3.2.1, the solar power efficiency was adopted to be the same for all power plants, regardless of location. However, the temperature can have an impact on the result. If the cell temperature is increasing, the produced power of silicon cells will be decreasing about 0.45 % per K. See [25]. Table 9.24 shows the impact if the annual mean temperature is taken into account regarding the production cost. The cost for München has been taken as reference. The correction has been done according to:

Cost after correction = Cost before correction × Correction factor (9.12)

Correction factor = $(1 + \Delta T \times \frac{0.45}{100})$ (9.13)

Where:

Δ T: Difference of annual mean temperature (day-time) relative to München

Table 9.24. Production cost for solar power plants. Before and after correction for difference of module temperature. München is reference.

Location	Annual mean temperature relative to München (K)	Correction factor	Production cost before correction (ct_{EUR} / kWh)	Production cost after correction (ct_{EUR} / kWh)
Kiruna	- 9.9	0.9555	14.6	14.0
Göteborg	-2.1	0.9906	10.8	10.7
München	-	-	8.4	-
Malaga	10.6	1.0477	5.0	5.2
Nairobi	12.3	1.0554	4.6	4.9

As is shown in the table, the effect of the correction is quite marginal: Nairobi +6%, Malaga +5%, Göteborg -1% and Kiruna -4%.

In this context, Malaga can be regarded as representative for southern Spain. According to [25], the production cost (2014) for southern Spain has been predicted as 5.4 ct_{EUR} / kWh. This can be compared with Malaga in Table 9.24: 5.0 ct_{EUR} / kWh before temperature correction and 5.2 ct_{EUR} / kWh after temperature correction.

For additional information regarding solar power cost, see [25] and [55].

9.7.4 Power plant cost

The annual costs for the 5 locations are calculated according to:

$$\text{Annual power plant cost} = Solar_{cost} + Wind_{cost} \quad (9.14)$$

The costs for energy storages are not included in this calculation.

$Wind_{cost}$ = 13.57 MSEK See section 9.7.1

Conversion from MSEK to MEuro is approximatively according to:

10 MSEK ≈ 1 MEuro

This means: $Wind_{cost} \approx$ 1.4 MEuro

Annual power plant costs for the 5 locations are according to Table 9.25.

Table 9.25. Annual power plant costs. ($Solar_{cost}$ + $Wind_{cost}$).

Location	Annual power plant cost (MEuro)
Kiruna	5.7900
Göteborg	4.6300
München	3.9200
Malaga	2.8900
Nairobi	2.7800

Fig. 9.29 illustrates the power plant costs, with and without wind power.

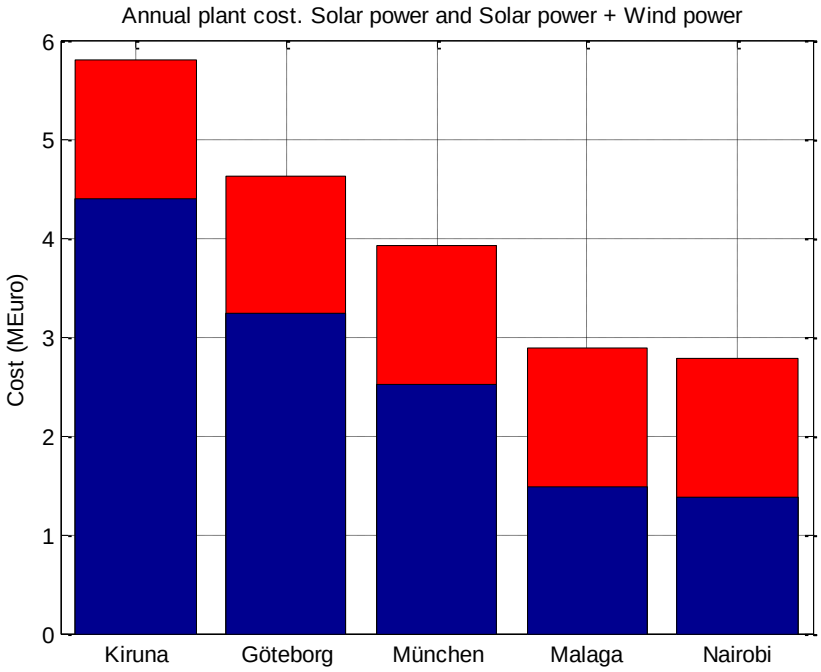

Fig. 9.29. Annual power plant costs. Blue bars: Only solar power.
Blue + Red bars: Solar power + Wind power.

9.8 Summary

Large combined power systems with solar power and wind power as power sources have been analysed. Present solar radiation and wind speed as well as electrical load are stochastically generated. The electrical load is a combination of industrial area, commercial centre and resident area. The power systems are connected to the utility grid to balance the power and can also be equipped with energy storage devices. 5 combined power plants have been investigated. The plants are located at Kiruna, Göteborg, München, Malaga and Nairobi.

Produced solar energy per quarter is analysed and is compared regarding power plant locations.

The utilization of the solar power system in respect of plant location is studied.

Design guide-lines regarding appropriate annual energy production of wind power systems and solar power systems are analysed. The guide-lines refer to the number of wind turbines with given power output and size of solar cell area.

The combination Solar power – Wind power – Energy storage is analysed. The effect of the combination is studied in the form of reduced need for imported energy or reduced probability of energy loss. The analysis compares current output depending on the geographic location of the power system.

Minimum solar cell panel area required vs power plant geographic location and a certain total produced annual solar energy is illustrated. The comparison reflects the difference between production costs for varying power plants in respect of geographic locations.

Annual wind power cost for a plant is calculated.

Annual solar power cost is calculated for the 5 locations.

An estimated correction for solar power costs based on differences of module temperature for the 5 locations is made.

Total annual power plant cost for the 5 locations is calculated.

CHAPTER 10

ANALYSIS OF A SOLAR POWER SYSTEM FOR HOUSEHOLD USAGE

A photovoltaic power system for household usage has been analysed. The system is located at Onsala close to Göteborg. Annual produced solar energy has been measured at 8400 kWh. See [68].

The power system is divided into two subsystems according to:

Table 10.1. Specification of the two subsystems.

Power system	Solar cell area (m^2)	Solar cells direction to south (º)	Solar cells direction to zenith (º)
Subsystem 1	44	20	30
Subsystem 2	22	-70	30

The system has been the subject of comparative simulations with the following approach regarding the solar cell system:

- Solar cell material: Silicon
- Total efficiency for solar power system: 13.54 %. This is based on the following assumptions (see section 2.2):
  - Solar cell efficiency = 15 %
  - Maximum Power Point (MPP) efficiency = 95 %
  - Power electronics efficiency = 95 %.

The observed annual energy production of 8400 kWh is based on information during one single year and can not be expected as a typical value for the power system. Annual variation from mean cloudiness for the location in question will have an impact on the result. The same is valid for the atmospheric attenuation, which can vary during a specific year relative to the typical condition.

The solar power system is located close to Göteborg with an annual calculated cloudiness of 64 %. See Table 4.3. This value has been assumed as a reference. In order to compare the impact as a result of cloudiness, simulations have been performed with different mean values of cloudiness. The mean cloudiness varies during the year. In order to test the impact of this, two methods have been objects for simulations and cloud statistics:

- Simulations based on whole-year statistics
- Simulations based on half-year statistics

The atmospheric attenuation in a clear sky is represented by parameter ε_B according to (4.31). In the simulation model, this parameter has been assigned to 0.43 as a mean value. To compare the impact of atmospheric attenuation, simulations have also been performed with varied mean values of ε_B.

10.1 Extinction coefficient and the probability density

Current available measurement data are the basis for the statistical model regarding the extinction coefficient that is used in this work. It should be noted that the measurements are limited to a specific time of the year, and also to a relatively short time period. The extinction coefficient is a critical parameter regarding solar power. It is dependent on different factors. Aerosols in the air, different kinds of gases in the air, clouds and so on.

Calculations of the extinction coefficient are realised with a focus on two separated modes, mode 1 and mode 2. See section 4.7.

Mode 1 (clouds do not impact solar radiation). According to section 4.7.1, a Gaussian statistic model has been used for the extinction coefficients. This seems to be a relevant choice and the measurements give no reason to doubt this. However, in respect of mean value and standard deviation, this ought to be a point for further investigation. Even without clouds in the sky, the transmission of sun radiation can vary from time to time and between different locations. Temperature, humidity, air pollution and aerosols are factors that can change the atmospheric transmission of radiation. This means that these parameters have an impact regarding choice of mean value as well as standard deviation for the Gaussian model. Values for mean and standarddeviation in the basic model are 0.43 and 0.048 respectively.

.

Mode 2 (clouds impact solar radiation). According to section 4.7.2, a trapezoidal distribution has been found to be a relevant statistical model for the extinction coefficients. Although the measurements are relatively unambiguous, they are limited in time. The impact of clouds is very complex. Thin layer clouds and thick clouds are, for example, quite different regarding attenuation of solar radiation. See also section 11.6.2. Further measurements are needed in this case.

In this chapter, alternative tests have been realized regarding the extinction coefficients related to mode 1 and mode 2 respectively. This means that parameter ε_B according to (4.31) has been varied for comparative simulations in section 10.2 to 10.3. Parameter ε_B is associated with mode 1. In section 10.4, tests have been realized with a focus on mode 2. This section presents simulation

results with a Gaussian distribution model as an alternative to a trapezoidal distribution.

10.2 Cloudiness based on whole-year statistics

Simulations with season-independent cloudiness have been performed with cloudiness of 50 %, 57 % and 64 % (reference).

Parameter εB has been assigned to the alternative values 0.20, 0.30 and 0.43 (reference).

Simulation results with annual produced energy follow according to

Table 10.2 to Table 10.4. The tables show the results for different cloudiness conditions and with varied mean values of parameter ε_B. The energy is presented for the single subsystems and for the total system.

Table 10.2. Annual simulated energy. Cloudiness 50%.
Varied mean values of parameter ε_B.

Power system	**ε_B, mean 0.20 Annual energy (kWh)**	**ε_B, mean 0.30 Annual energy (kWh)**	**ε_B, mean 0.43 Annual energy (kWh)**
Subsystem 1	6137	5055	4026
Subsystem 2	2514	2061	1642
Total energy (kWh)	8651	7116	5668

Table 10.3. Annual simulated energy. Cloudiness 57%.
Varied mean values of parameter ε_B.

Power system	**ε_B, mean 0.20 Annual energy (kWh)**	**ε_B, mean 0.30 Annual energy (kWh)**	**ε_B, mean 0.43 Annual energy (kWh)**
Subsystem 1	5458	4524	3630
Subsystem 2	2217	1841	1481
Total energy (kWh)	7675	6365	5111

Table 10.4. Annual simulated energy. Cloudiness 64%.
Varied mean values of parameter ε_B.

Power system	**ε_B mean 0.20 Annual energy (kWh)**	**ε_B mean 0.30 Annual energy (kWh)**	**ε_B mean 0.43 Annual energy (kWh)**
Subsystem 1	4746	3971	3246
Subsystem 2	1925	1604	1310
Total energy (kWh)	6671	5575	4556

Table 10.5 lists the annual simulated energy relative to measured energy of 8400 kWh.

Table 10.5. Annual simulated energy relative to 8400 kWh.
Varied cloudiness and mean values of parameter ε_B.

Relation to 8400 kWh								
Cloudiness 50 %			**Cloudiness 57 %**			**Cloudiness 64 %**		
ε_B mean 0.20	**ε_B mean 0.30**	**ε_B mean 0.43**	**ε_B mean 0.20**	**ε_B mean 0.30**	**ε_B mean 0.43**	**ε_B mean 0.20**	**ε_B mean 0.30**	**ε_B mean 0.43**
103 %	85 %	67 %	91 %	76 %	61 %	79 %	66 %	54 %

Fig. 10.1 illustrates simulated annual energy vs cloudiness and with varied mean values of parameter ε_B. Fig. 10.2 illustrates simulated annual energy relative to 8400 kWh vs cloudiness and with varied values of parameter ε_B.

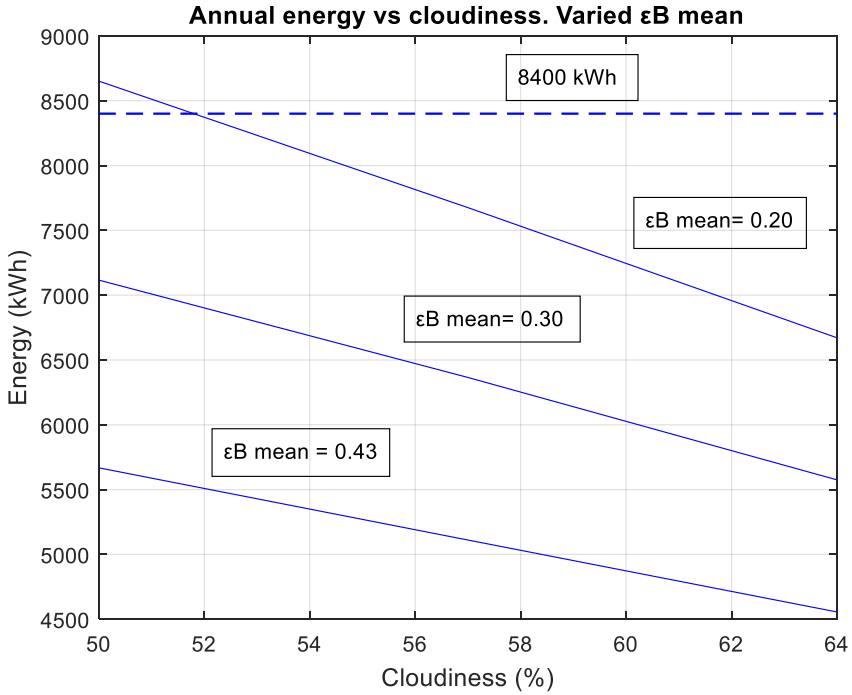

Fig. 10.1. Simulated annual energy vs cloudiness. Varied mean values of parameter ε_B.
Dashed line: Measured annual energy.

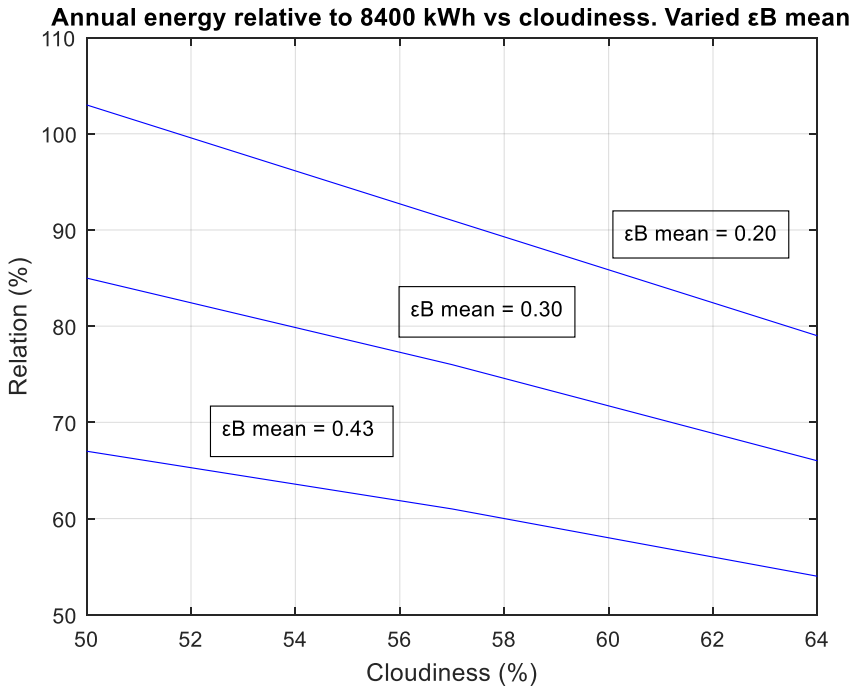

Fig. 10.2. Simulated annual energy relative to 8400 kWh vs cloudiness. Varied mean values of parameter $\varepsilon_{B.}$

Fig. 10.1 and Fig. 10.2 show a difference between measured annual energy production relative to corresponding simulations. The deviations can be explained by different reasons.

According to Fig. 10.1 and Fig. 10.2, an ε_B-value of 0.20 and a mean cloudiness of about 52 % will result in a compliance between simulations and measurements. For ε_B = 0.30 and a cloudiness of 50 %, the deviation between measurements and simulations is 15 %.

10.3 Cloudiness based on half-year statistics

Simulations with the season-dependent cloudiness have been conducted focusing on the division into separate half years.

To calculate the cloudiness for a specific season, the method according to section 4.2 has been used. Separated calculations have been performed for the following time periods:

- October – December
- January – March
- April – June

- July – September

Table 10.6 and Table 10.7 are valid for Göteborg (also see Table 4.1):

Table 10.6. Average number of daily hours of sunshine.

Month	**Mean sunshine per day (hours)**	**Month**	**Mean sunshine per day (hours)**
October	3	January	1
November	2	February	2
December	1	March	3
Sum	6	**Sum**	6

Table 10.7. Average number of daily hours of sunshine.

Month	**Mean sunshine per day (hours)**	**Month**	**Mean sunshine per day (hours)**
April	5	July	8
May	7	August	7
June	8	September	5
Sum	20	**Sum**	20

The values in Table 10.8 are results from simulations by using the simulation model according to chapter 3.

Table 10.8. Total number of hours per time interval when sun is over horizon.

Time interval	**Sun over horizon (hours)**
October -December	742
January – March	836
April – June	1440
July – September	1357

The cloudiness will in this section be analysed with the full year divided into two half-year periods:

Half-year period 1: October – March
Half-year period 2: April – September

Application of (4.21) and information according to Table 10.6 to Table 10.8 results in average cloudiness values according to Table 10.9.

Table 10.9. Calculated cloudiness per time interval season and half-year period.

Season	Cloudiness (%)	Half year period	Cloudiness (%)
Oct – Dec	75	Oct - Mar	77
Jan – Mar	78	Apr - Sep	56
Apr – Jun	58		
Jul – Sep	55		

Reference values for cloudiness and the two half-year periods are assigned according to case 1 (below). The values are based on Table 10.9 with information for the half-year periods rounded to the nearest "5 unit".

Case 1 (reference)

October – March: 55 %
April – September: 75 %

In order to analyse the impact of cloudiness, simulations are also conducted with 10 % reduction of the cloudiness according to the following case 2:

Case 2

October – March: 45 %
April – September: 65 %

Simulations have been performed with mean values of ε_B assigned to 0.2, 0.3 and 0.43 (reference).

Table 10.10 to Table 10.13 present the simulation results with cloudiness according to case 1 and case 2 per half year and for whole year respectively with varied values of parameter ε_B.

Table 10.10. Simulated energy half year case 1 (regarding cloudiness). Varied mean values of parameter ε_B.

Power system	**October - March Cloudiness 75 %**			**April - September Cloudiness 55 %**		
	ε_B mean 0.20 Energy (kWh)	**ε_B mean 0.30 Energy (kWh)**	**ε_B mean 0.43 Energy (kWh)**	**ε_B mean 0.20 Energy (kWh)**	**ε_B mean 0.30 Energy (kWh)**	**ε_B mean 0.43 Energy (kWh)**
Subsystem 1	785.8	577.7	403.7	4299	3716	3106
Subsystem 2	258.7	190.3	135.4	1859	1583	1302
Total energy (half year) (kWh)	1044.5	768.0	539.1	6158	5299	4408
Distribution of annual production (%)	14.50	12.66	10.90	85.50	87.34	89.10

Table 10.11. Simulated energy whole year and case 1 (regarding cloudiness). Varied mean values of parameter ε_B.

Power system	**ε_B, mean 0.20 Annual energy (kWh)**	**ε_B, mean 0.30 Annual energy (kWh)**	**ε_B, mean 0.43 Annual energy (kWh)**
Subsystem 1	5084.8	4293.7	3509.7
Subsystem 2	2117.7	1773.3	1437.4
Total energy (whole year) (kWh)	7202	6067	4947

Table 10.12. Simulated energy half year case 2 (regarding cloudiness). Varied mean values of parameter ε_B.

Power system	October - March Cloudiness 65 %			April - September Cloudiness 45 %		
	ε_B mean 0.20 Energy (kWh)	ε_B mean 0.30 Energy (kWh)	ε_B mean 0.43 Energy (kWh)	ε_B mean 0.20 Energy (kWh)	ε_B mean 0.30 Energy (kWh)	ε_B mean 0.43 Energy (kWh)
Subsystem 1	1075	777.0	532.3	5021	4295	3547
Subsystem 2	351.8	256.8	178.0	2174	1832	1498
Total energy (half year) (kWh)	1426.8	1033.8	710.3	7195	6127	5045
Distribution of annual production (%)	16.55	14.44	12.34	83.45	85.56	87.66

Table 10.13. Simulated energy whole year and case 2 (regarding cloudiness). Varied mean values of parameter ε_B.

Power system	ε_B, mean 0.20 Annual energy (kWh)	ε_B, mean 0.30 Annual energy (kWh)	ε_B, mean 0.43 Annual energy (kWh)
Subsystem 1	6096	5072	4079.3
Subsystem 2	2525.8	2088.8	1676
Total energy (whole year) (kWh)	8621.8	7160.8	5755.3

Table 10.11 and Table 10.12 show how the total annual energy produced is distributed over each half year respectively. This is illustrated in Fig.10. 3, where energy distributions for case 1 (red bars) and case 2 (blue bars) in combination with the two seasons (October - March and April - September) are shown. The results are presented for each of the three values of parameter εB mean (0.20, 0.30 and 0.43).

As is evident, the energy contribution during the "dark" half of the year, i.e. October to March, is quite small relative to the corresponding contribution during the "bright" half of the year, i.e. April to September. The energy contribution during the "bright" half of the year is about five to eight times the energy contribution during the "dark" half of the year. The ratio increases with decreasing conditions regarding solar radiation. The maximum ratio (i.e. = 8.2) at the simulations is thus

at case 1 (cloudy 55%, 75%) and εB mean = 0.43. The minimum ratio (i.e. = 5.0) is obtained at case 2 (cloudiness 45%, 65%) and εB mean = 0.20.

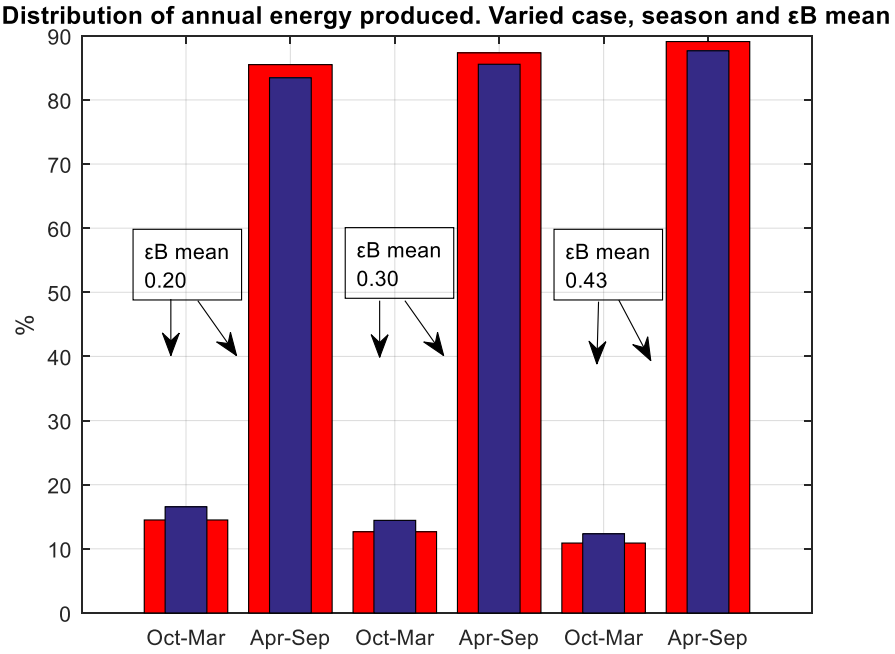

Fig. 10.3. Part of annual production. Varied case, season and ε_B mean.
Red bars: Cloudiness 55 %, 75 % (case 1).
Blue bars: Cloudiness 45 %, 65 % (case 2).

Simulated energy corresponding to whole year at case 1 and case 2 relative to 8400 kWh and with varied mean values of parameter ε_B follows in Table 10.14.

Table 10.14. Simulated energy whole year. Case 1 and case 2 (regarding cloudiness) relative to 8400 kWh. Varied mean values of parameter ε_B.

Relation to 8400 kWh					
Cloudiness 55 %, 75 % (case 1)			**Cloudiness 45 %, 65 % (case 2)**		
ε_B mean 0.20	**ε_B mean 0.30**	**ε_B mean 0.43**	**ε_B mean 0.20**	**ε_B mean 0.30**	**ε_B mean 0.43**
86 %	72 %	59 %	103 %	85 %	69 %

Fig. 10.4 illustrates the results according to Table 10.14. The results in accordance with section 10.2 are plotted in the same figure. As shown in the figure, case 2 (solid blue) largely corresponds to a mean annual cloudiness of 50 % (dotted red). Case 1 (solid red) corresponds to a mean annual cloudiness of between 57 % (dotted black) and 64 % (dotted blue).

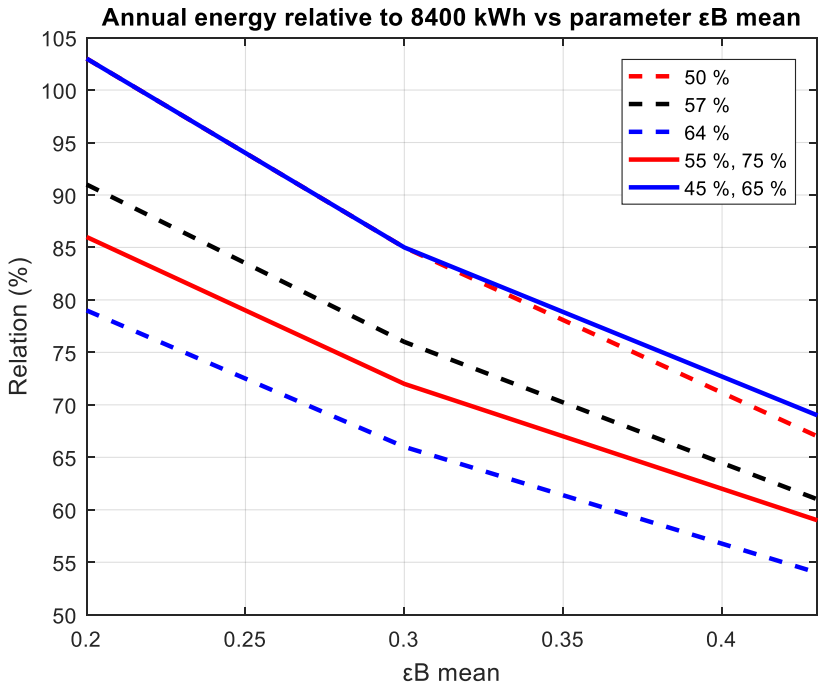

Fig. 10.4. Simulated energy production whole year relative to 8400 kWh vs ε_B mean.
Red solid line: Case 1. Blue solid line: Case 2.
Dotted lines correspond to the results in accordance with section 10.2.

As identified in accordance with section 10.2, there is a deviation between measured and simulated energy production. According to the simulation model and corresponding calculated annual energy production, the calculated values are underestimated in relation to measured values. The reason for this can be of a statistical as well as local nature.

According to Fig. 10.4, an ε_B-value of 0.20 and a mean cloudiness as in case 2 will result in a compliance between simulations and measurements. For ε_B = 0.30 and a cloudiness as in case 2, the deviation between measurements and simulations is 15 %.

Assigned parameter ε_B for “typical” Göteborg is based on measurements conducted during a very limited time. See section 4.3. This means that it is not yet verified whether the applied value of ε_B can be regarded as a representative value for “typical” Göteborg. And in addition to this, it has not been verified whether the mean atmospheric condition for the geographic location of the analysed power system is the same as the corresponding condition for “typical” Göteborg. In addition to this, statistical deviations can have impacts on parameter ε_B.

Fig. 10.5 illustrates how incoming solar radiation to the ground varies as a function of the extinction coefficient with a solar angle above the horizon of 50 º. According to the figure, the irradiance at ground level decreases from about 1050 W/m^2 to about 780 W/m^2 when the extinction coefficient increases from 0.20 to 0.43.

The mean value, μ, and the standarddeviation, σ, in the basic model are 0.43 and 0.048 respectively. This means that band-limits ”2.5× σ” is located within interval 0.31 to 0.55. In the Gaussian distribution, 98.76 % of total area is distributed within these band-limits. Extinction coefficients within interval 0.31 to 0.55 (i.e. 2.5× σ limits) correspond to solar irradiance to ground and when solar angle above the horizon is 50 º, in the interval 912 W/m^2 down to 667 W/m^2.

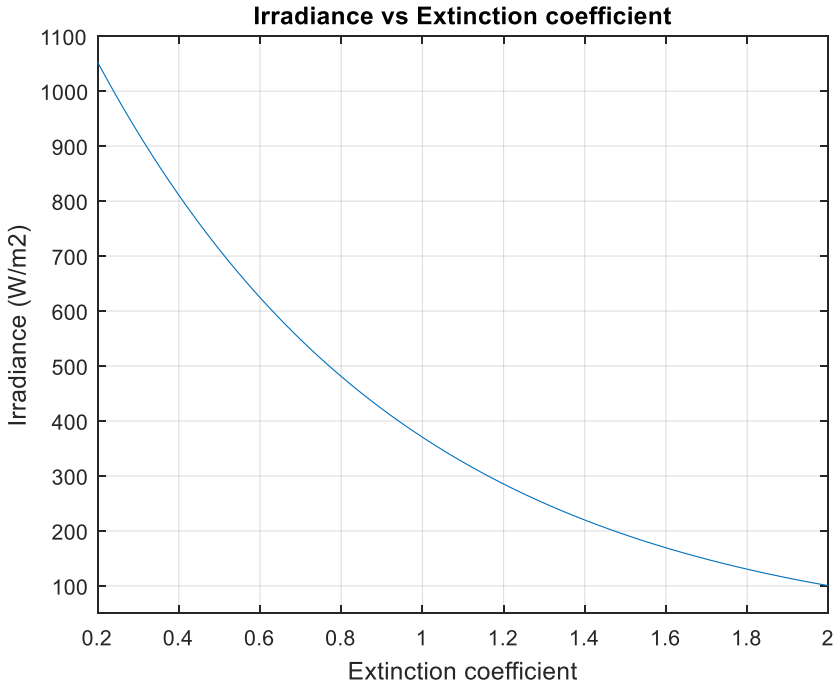

Fig. 10.5. Irradiance as a function of Extinction coefficient.

Assigned parameter regarding cloudiness is based on the assumption that Göteborg is representative regarding cloudiness for the geographic location of the analysed power system. Whether this is correct is not verified. Local deviations may occur. In addition to this, statistical deviations may have impacts on the cloudiness.

Fig. 10.6 illustrates calculated cloudiness as a function of sun hours factor. Three graphs are shown according to different bases of calculation, based on whole year or based on separated half year. The sun hours factor is defined as:

$$\text{Mean\_sun\_h\_perday\_month\_alt (m)} = \text{Sun\_h\_factor} \times \quad (10.1)$$

$$\times \text{ Mean\_sun\_h\_perday\_month(m)}$$

Where:

Mean_sun_h_perday_month_alt (m):	Alternative average number of sunshine hours per day during a specific month, m
Sun_h_factor:	Sun hours factor
Mean_sun_h_perday_month (m):	Average number of sunshine hours per day during a specific month, m

Parameter "Mean_sun_h_perday_month (m)" is defined according to Table 10.6 and Table 10.7. Parameter "Mean_sun_h_perday_month_alt (m)" is an alternative value for calculation of cloudiness according to section 4.2. In expression (4.18), parameter "Mean_sun_h_perday_month (m)" is in this case replaced by parameter "Mean_sun_h_perday_month_alt (m)". This implies that the sun hours factor indicates the correlation between number of sunshine hours per day and corresponding cloudiness. According to Fig. 10.6, this correlation differs between the two half-year periods. The graph for April to September drops more steeply compared with the period October to March. Even small variations of the sun hours factor for the period April to September impacts the cloudiness.

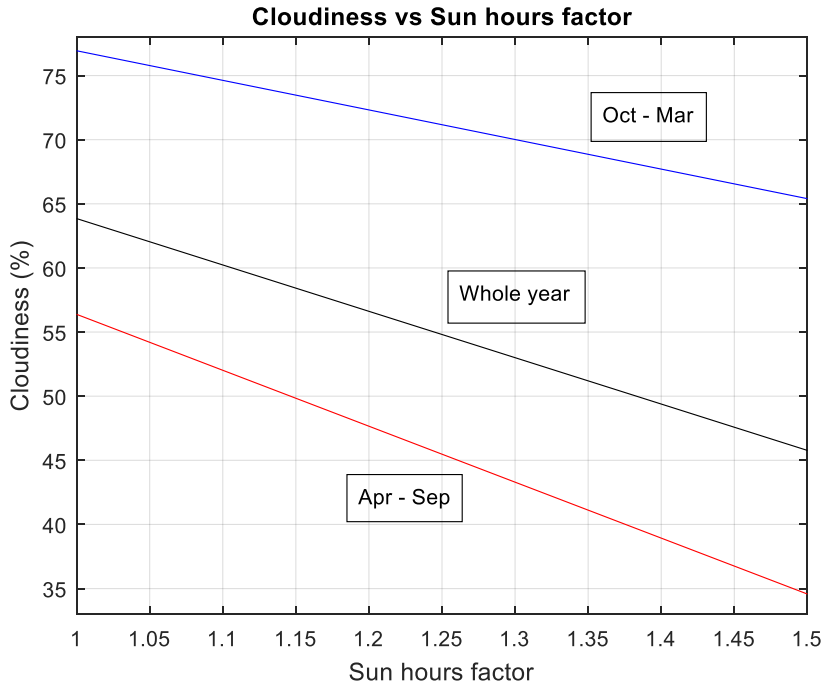

Fig. 10.6. Calculated cloudiness as a function of sun hours factor. Whole year and divided into half-year periods.

For a cloudiness according to case 2, the following is valid regarding the sun hours factor:

- Sun hours factor, period October to March: 1.5
- Sun hours factor, period April to September: 1.25

This means an increase relative to mean values in Table 10.6 and Table 10.7 from 2 hours to 3 hours during October to March and from 6.7 hours to 8.3 hours during April to September as mean values for number of sun hours per day.

The sun hours factors according to the above of 1.5 (October to March) and 1.25 (April to September) indicates a corresponding deviation from expected effective solar radiation. However, this deviation can in this case be regarded as reasonable and may be a result of variations regarding time and geographic location. This means that the difference regarding cloudiness at case 2 relative to case 1 can be explained as a difference located within the statistical error margin. This together with the possibility for geographic variations that can impact the cloudiness.

10.4 Extinction coefficient mode 2. Alternative distribution model

This section presents simulation results based on an alternative distribution model regarding the extinction coefficient in mode 2. Instead of the original, a trapezoidal distribution, a Gaussian distribution has been used. Three mean values of the Gaussian distribution have been compared. The cloudiness parameters are according to case 1 and case 2 respectively. See section 10.3. Regarding the Gaussian distribution function, see also (4.28).

Table 10.15 shows simulated energy production for case 1 and mode 2 with a Gaussian probability distribution. Mean values (ε_H mean) are 0.65, 1.00 and 1.50. Standard deviation is consistently 0.05.

Regarding parameter ε_B mean (mode 1), the value of 0.43 is used consistently.

Table 10.15. Simulated energy half year case 1 (regarding cloudiness).
Varied mean values of parameter ε_H. Mode 2 with Gaussian distribution.

Power system	**October – March Cloudiness 75 %**			**April – September Cloudiness 55 %**		
	ε_H mean 0.65 Energy (kWh)	**ε_H mean 1.00 Energy (kWh)**	**ε_H mean 1.50 Energy (kWh)**	**ε_H mean 0.65 Energy (kWh)**	**ε_H mean 1.00 Energy (kWh)**	**ε_H mean 1.50 Energy (kWh)**
Subsystem 1	814.1	510.9	373.4	4682	3769	3110
Subsystem 2	270.1	170.5	124.8	1969	1582	1309
Total energy (half year) (kWh)	1084.2	681.4	498.2	6651	5351	4419

Table 10.16. Simulated energy whole year case 1 (regarding cloudiness).
Varied mean values of parameter ε_H. Mode 2 with Gaussian distribution.

Power system	**ε_H mean 0.65 Annual energy (kWh)**	**ε_H mean 1.00 Annual energy (kWh)**	**ε_H mean 1.50 Annual energy (kWh)**
Subsystem 1	5496.1	4279.9	3483.4
Subsystem 2	2239.1	1752.5	1433.8
Total energy (whole year) (kWh)	7735.2	6032.4	4917.2
Total energy relative to 8400 kWh (%)	92.1	71.8	58.5

Table 10.17. Simulated energy half year case 2 (regarding cloudiness).
Varied mean values of parameter ε_H. Mode 2 with Gaussian distribution.

Power system	**October – March Cloudiness 65 %**			**April – September Cloudiness 45 %**		
	ε_H mean 0.65 Energy (kWh)	**ε_H mean 1.00 Energy (kWh)**	**ε_H mean 1.50 Energy (kWh)**	**ε_H mean 0.65 Energy (kWh)**	**ε_H mean 1.00 Energy (kWh)**	**ε_H mean 1.50 Energy (kWh)**
Subsystem 1	883.1	620.3	504.4	4845	4101	3563
Subsystem 2	291.6	206.4	167.7	2040	1723	1498
Total energy (half year) (kWh)	1174.7	826.7	672.1	6885	5824	5061

Table 10.18. Simulated energy whole year case 2 (regarding cloudiness).
Varied mean values of parameter ε_H. Mode 2 with Gaussian distribution.

Power system	**ε_H mean 0.65 Annual energy (kWh)**	**ε_H mean 1.00 Annual energy (kWh)**	**ε_H mean 1.50 Annual energy (kWh)**
Subsystem 1	5728.1	4721.3	4067.4
Subsystem 2	2331.6	1929.4	1665.7
Total energy (whole year) (kWh)	8059.7	6650.7	5733.1
Total energy relative to 8400 kWh (%)	95.9	79.2	68.3

Simulated energy production for case 1 and case 2 relative to 8400 kWh according to Table 10.16 and Table 10.18 is shown in Fig. 10.7. The dotted lines represent energy production for case 1 and case 2 relative to 8400 kWh for a trapezoidal distribution at mode 2 and correspond to simulation results according to Table 10.14 and ε_B mean 0.43. These lines are references to show the impact of the alternative distribution at mode 2.

As shown in Fig. 10.7, the simulated energy production increases significantly in connection with the alternative distribution and for values of ε_H mean in the interval 0.65 to 1.0. For ε_H mean assigned to the value 1.5, then the energy production with alternative distribution and original distribution coincide.
The performed tests underscore the importance of appropriate distribution function regarding mode 2.

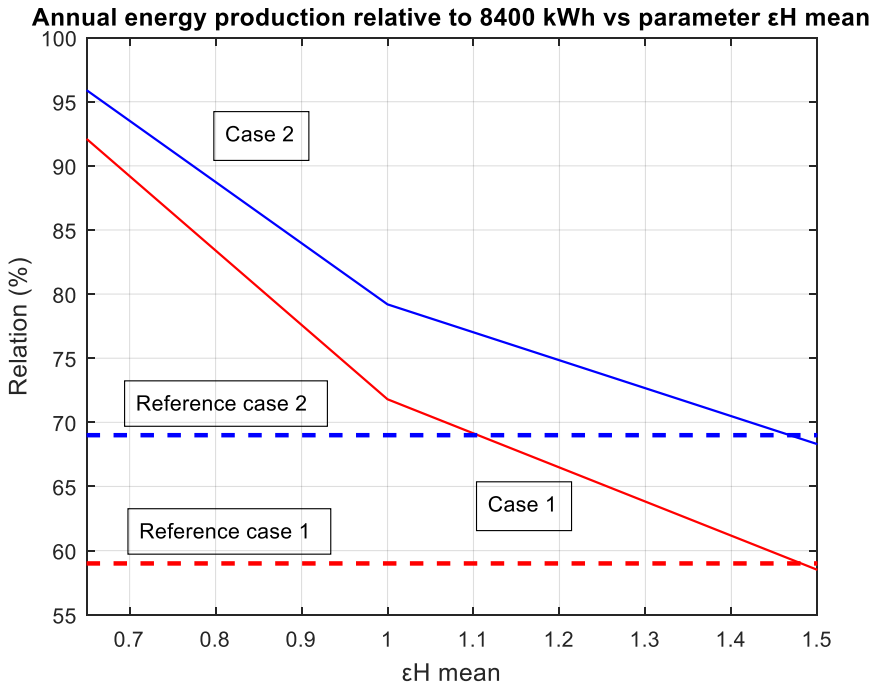

Fig. 10.7. Simulated energy production whole year relative to 8400 kWh vs parameter ε_H mean. Case 1 (solid red) and case 2 (solid blue) relate to assigned conditions for cloudiness. The dotted lines are references, where original distribution (trapezoidal) at mode 2 is used.

10.5 Summary

Measurements on an existing PV system for household usage have been performed. The corresponding PV system is analysed by simulations. Annual production based on simulations is compared with measured production. The comparison shows a difference between measured annual energy production relative to corresponding simulations if reference values regarding cloudiness and atmospheric attenuation for a clear sky are assigned as input parameters to the simulation model. Reference values in this case referring to mean value of annual cloudiness in Göteborg and mean value of assigned value of parameter ε_B. The deviation can be explained by local and annual statistical fluctuations and by the fact that assigned parameter ε_B for “typical” Göteborg is based on measurements completed in a very limited time.

Tests with varied values of cloudiness and parameter “ε_B mean” have been performed. A suitable combination of cloudiness and parameter “ε_B mean” results in simulation results that are quite similar to measured results.

In addition to tests with varied values of cloudiness and parameter “ε_B mean”, tests have also been carried out with a Gaussian distribution function as an alternative to the original trapezoidal distribution function regarding the extinction coefficient at mode 2 (clouds have impact on solar radiation). These tests indicate a strong correlation between mean value of the Gaussian function and corresponding simulation results.

The reason for deviation between simulations and measurements is probably a mix of geographic local variations and statistical variations regarding cloudiness and parameter “ε_B mean” and even a distribution function at mode 2 that is not fully perfect.

CHAPTER 11

SOLAR POWER. BASIC ANALYSIS

This chapter deals with theoretical analysis of some basic questions, which are central regarding the production of solar energy. The chapter is intended to give support to the performed calculations regarding extinction coefficients of chapter 4 and to demonstrate the possibilities for future theoretical calculations of these coefficients. In addition, an analysis regarding the possible development potential for solar cells is given in this chapter.

Theoretical calculation of extinction coefficients can conveniently be done by means of specially developed software for atmospheric attenuation. The method is introduced here. Regarding the development of various photovoltaic cells, possibilities of alternative wavelength ranges in combination with alternative materials are analysed here.

At the end of the chapter, it is demonstrated how the atmospheric visibility affects the extinction coefficient. In addition, the effect of different kinds of cloud categories is studied.

The chapter is divided into five sections:

- Solar radiation
- Atmospheric transmittance
- Solar cell current
- Wave-length bands
- Extinction coefficient

Regarding solar radiation, some fundamental theoretical principles for “black-body” objects will be discussed. Based on this theory, the spectral solar irradiance will be calculated

The atmospheric transmittance is dependent on molecular absorption and molecular scattering, but also on particle scattering. In respect of molecular absorption/scattering, 2 examples of defined scenarios, namely “Mid-latitude summer”and “US Standard”, will be studied. The particle scattering will be analysed in a more general form, with a focus on fog and clouds.

Based on information on spectral solar radiation and spectral transmittance, the spectral solar radiation after passing the atmosphere will be calculated .

The spectral solar cell current will be studied based on a typical responsivity curve for a silicon PV cell.

An analysis regarding appropriate wave-length bands related to photovoltaics will be done. This will be performed in combination with technical properties of the solar cells.

Calculations of extinction coefficients are to be done. The calculations will be performed based on two types of atmospheres, “Mid-latitude summer" and “US Standard”. Alternative extinction coefficients, in order to represent cases with clouds and fog, will be calculated. Calculated coefficients are to be compared with corresponding coefficients used in the model. These “model coefficients” are based on measurements performed in Göteborg, and represent the attenuation in an atmosphere that differs from the case “Mid-latitude summer" and “US Standard”. See chapter 4.

11.1 Solar radiation

11.1.1 Black-body radiation

A black-body is an idealized body, with the ability to totally absorb all incoming radiation. That is, no reflection is emitted from the body.

The radiation from a black-body can be calculated by Planck’s radiation law according to:

$$W_B(\lambda,T) = \frac{C1}{\lambda^5 \left(e^{\frac{C2}{\lambda T}} - 1\right)} \quad (W/m^2/m,sr) \tag{11.1}$$

$$C1 = 2\pi c^2 h \quad (W/m^2) \tag{11.2}$$

$$C2 = \frac{h c}{k} \tag{11.3}$$

Where:

$W_B(\lambda,T)$: Black-body irradiance per wave-length unit and per steradian
λ: Wave-length (m)
T: Temperature (K)
c: Speed of light in vacuum, 2.99792×10^8 m/s
h: Planck’s constant, 6.62608×10^{-34} Js
k: Boltzmann’s constant, 1.38066×10^{-23} J/K

λ: Wave-length (m)

C1 and λ can be adapted to dimensions according to:

C1: W/m^2 per µm (wave length)
λ: µm

This results in C1 = 3.74177×10^8 and C2 = 14.38769×10^3.

11.1.2 Sun as a black-body

To calculate the sun's radiation, the sun can be regarded as a "black-body", with a space angle of 2.1749×10^5 (sr)

The space angle is calculated according to:

$$\Omega_S = \pi \frac{Rs^2}{Ds^2} \quad \text{(sr)} \tag{11.4}$$

Where:

Ω_S: Space angle of sun (sr)
R_S: Equivalent sun radius = 3.936×10^5 km
D_S: Distance between sun and earth = 1.496×10^8 km

Equivalent sun radius is about 56.5 % of the real sun radius. The reason for using an equivalent radius in this case depends on the different temperature variations at the sun's surface.

To use the equivalent radius, the sun can be regarded as a black-body with a temperature of 5770 K. A more detailed description of the different components inside the sun that have an effect on the radiation can be found in [31].

The spectral sun irradiance outside the earth's atmosphere is calculated according to:

$$L(\lambda)_{NA} = W(\lambda, 5770) \times \Omega_S \quad (W/m^2) \tag{11.5}$$

Where:

$L(\lambda)_{NA}$: Spectral sun irradiance (W/m^2) outside the earth's atmosphere
W(λ, 5770)): Black-body radiation according to (11.1) and temperature = 5770 K

11.1.3 Total solar radiation

Sun radiation over the total wave-length spectrum is calculated according to:

$$L_{NA\ tot} = \int_0^{\infty} L(\lambda)_{NA}\ d\lambda \quad (11.6)$$

Where:

$L_{NA\ tot}$: Total incoming irradiance (W/m^2) from sun before atmospheric attenuation

The total irradiation of a black-body, over total wave-length spectrum, can be calculated by means of Stefan-Boltzmann law, which states:

$$L_{tot} = \sigma_{SB} \times T^4 \times \Omega_S \quad (11.7)$$

Where:

L_{tot}: Total irradiation of the black-body
σ_{SB}: Stefan-Boltzmann constant = 5.6705×10^{-8} ($W/m^2/T^4$)

By applying (11.7), T = 5770K and Ω_S as above, is obtained:

- $L_{NA\ tot} = 1367\ W/m^2$

$L_{NA\ tot}$ corresponds to the Solar constant. See section 4.1.

11.2 Atmospheric transmittance

The spectral irradiation from the sun after atmospheric attenuation is calculated according to:

$$L(\lambda)_A = \tau(\lambda) \times L(\lambda)_{NA} \quad (11.8)$$

Where:

$L(\lambda)_A$: Spectral sun irradiance (W/m^2) after atmospheric attenuation
$\tau(\lambda)$: Spectral transmittance in the atmosphere

Transmittance values for the case Mid-latitude summer in the range of 200 nm to 2600 nm, and in steps of 0.025 µm, have been estimated from information in [56]. Transmittance values for the case US Standard in the range of 200 nm to 2600 nm, and in steps of 0.1 µm, have been estimated from information in [49]. The original information is calculation results obtained by "Modtran" for case Mid-latitude summer and by "Lowtran" for case US Standard. Modtran and Lowtran are software for calculation of atmospheric transmittance and are delivered by Ontar Corporation, USA. Descriptions of Modtran and Lowtran can be found in [27], [43] and [57]. More about atmospheric transmission can be found in e.g. [28], [39] and [46]. In [28] a basic description is given of the concept of atmospheric transmission. In [39], Modtran is applied for modelling both direct and scattered spectral solar radiation. The wave band between 280 nm to 4000 nm, with focus on a direct satellite to ground link is studied in [46]. Regarding wave band see section 11.5.

Spectral resolution for software expressed in wave number:

- Modtran: 2 cm^{-1}
- Lowtran: 20 cm^{-1}

Conversion between wave number [cm^{-1}] and corresponding wave length [µm] is:

$$v = 10^4 \times \boldsymbol{\lambda} \qquad (11.9)$$

Where:

v: wave number [cm^{-1}]
λ: wave length [µm]

The wave length interval 0.200 - 1.150 µm (ordinary silicon solar cell) corresponds for example to the wave number interval 2000 – 11500 cm^{-1}.

Specified conditions for case Mid-latitude summer are among others:

- Latitude: 45 ° north
- Time: July
- Air temperature at ground level: 21.0 ºC

Specified temperature condition for case US Standard atmosphere:

- Air temperature at ground level: 15.0 ºC

Predicted transmittance values for Mid-latitude summer and US Standard atmosphere are listed in Table 11.1 and Table 11.2 respectively.

Table 11.1. Transmittance vs wave-length. Mid-latitude summer. 200 – 2600 nm. Zenith angle = 20 º.

λ (nm)	τ	λ (nm)	τ	λ (nm)	τ	λ (nm)	τ	λ (nm)	τ
200	0.00	700	0.67	1200	0.76	1700	0.90	2200	0.87
225	0.00	725	0.64	1225	0.85	1725	0.87	2225	0.90
250	0.00	750	0.77	1250	0.89	1750	0.80	2250	0.89
275	0.00	775	0.56	1275	0.82	1775	0.49	2275	0.87
300	0.00	800	0.77	1300	0.84	1800	0.20	2300	0.87
325	0.22	825	0.68	1325	0.57	1825	0.00	2325	0.81
350	0.31	850	0.79	1350	0.26	1850	0.00	2350	0.73
375	0.37	875	0.81	1375	0.00	1875	0.00	2375	0.70
400	0.43	900	0.63	1400	0.00	1900	0.00	2400	0.61
425	0.48	925	0.66	1425	0.05	1925	0.00	2425	0.40
450	0.52	950	0.37	1450	0.10	1950	0.10	2450	0.42
475	0.56	975	0.71	1475	0.24	1975	0.47	2475	0.23
500	0.58	1000	0.84	1500	0.68	2000	0.62	2500	0.03
525	0.61	1025	0.85	1525	0.83	2025	0.34	2525	0.00
550	0.63	1050	0.87	1550	0.91	2050	0.78	2550	0.00
575	0.64	1075	0.86	1575	0.89	2075	0.68	2575	0.00
600	0.64	1100	0.70	1600	0.92	2100	0.87	2600	0.00
625	0.68	1125	0.14	1625	0.90	2125	0.88		
650	0.70	1150	0.30	1650	0.91	2150	0.91		
675	0.72	1175	0.71	1675	0.90	2175	0.89		

Table 11.2. Transmittance vs wave-length. US Standard atmosphere. 200 – 2600 nm. Zenith angle = 20 º.

λ (nm)	τ	λ (nm)	τ	λ (nm)	τ	λ (nm)	τ	λ (nm)	τ
200	0	700	0.7827	1200	0.8855	1700	0.8902	2200	0.9042
300	0	800	0.8248	1300	0.7967	1800	0.2570	2300	0.9322
400	0.5304	900	0.8131	1400	0	1900	0.0187	2400	0.5561
500	0.6589	1000	0.8598	1500	0.7103	2000	0.5000	2500	0.3084
600	0.7173	1100	0.8668	1600	0.9065	2100	0.9112	2600	0

The values in Table 11.1 are valid for a zenith angle of 20º. A correction to 0º is made as:

$$\tau_0 = e^{\ln(\tau_{20} \times \cos 20^\circ)} \quad (11.10)$$

Where:

τ_0: Transmittance at 0º

τ_{20}: Transmittance at 20º

Transmittance vs wave-length is plotted in Fig. 11.1. The figure shows values for zenith angle 0º and 20º for Mid-latitude summer and for angle 0º for US Standard. As can be observed, the difference between 0º and 20º is quite small. The spectral resolution is 0.025 µm for Mid-latitude summer and 0.1 µm for US Standard.

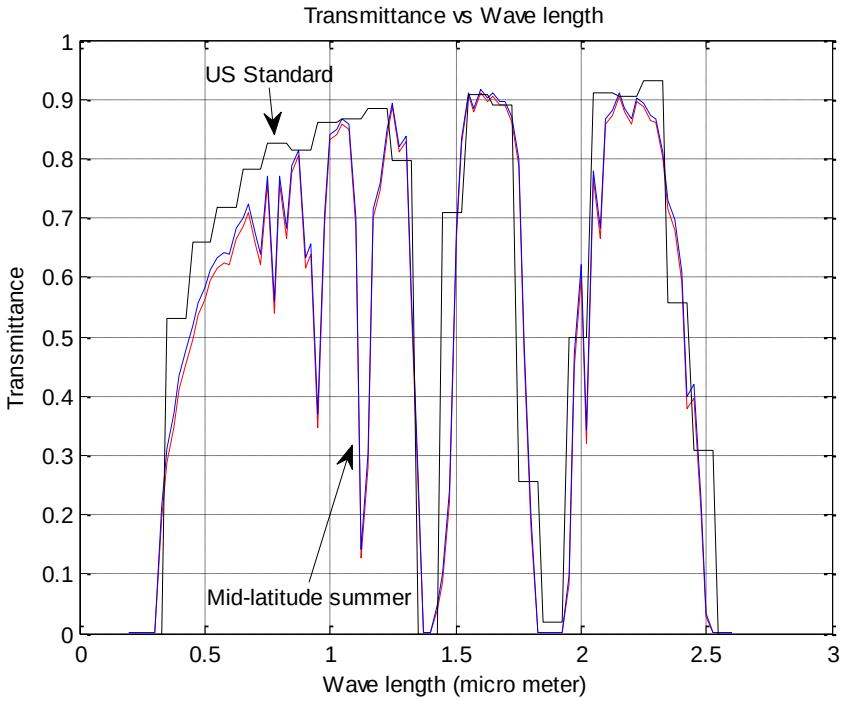

Fig. 11.1. Atmospheric transmission coefficient vs Wave length. Red curve: Zenith angle = 20 º, Mid-latitude summer. Blue curve: Zenith angle 0 º, Mid-latitude summer. Black curve: Zenith angle 0 º, US Standard.

Sun irradiation outside the earth's atmosphere and after atmospheric attenuation has been calculated as described in section 11.1 and (11.8). The result is illustrated in Fig. 11.2. Transmittances according to Table 11.1, Mid-latitude summer, and Table 11.2, US Standard with correction to zenith angle 0 º, have been used.

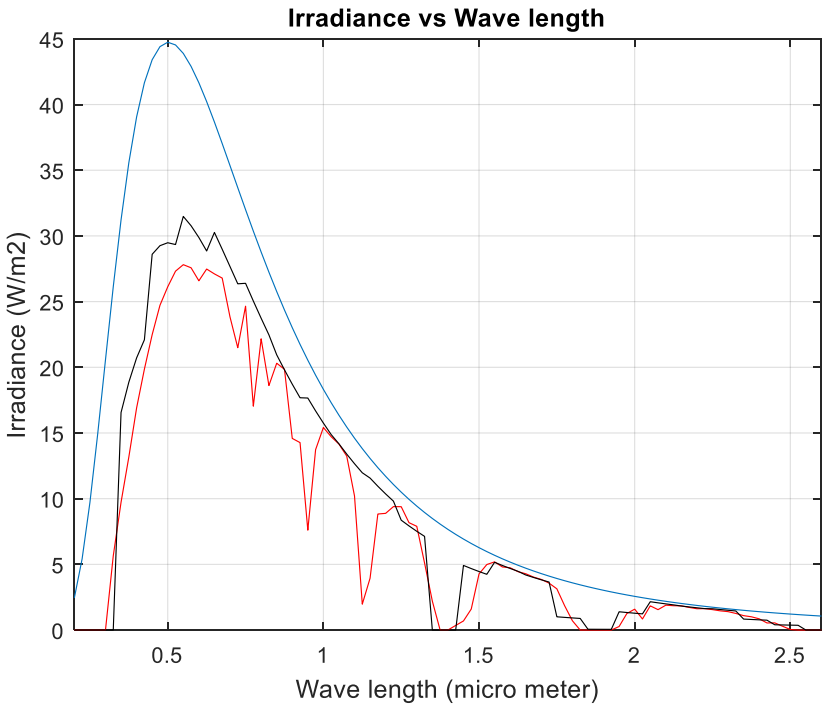

Fig. 11.2. Solar irradiance vs wave-length. Blue: Without atm attenuation. Red: With atm. attenuation. Mid-latitude summer. Zenith angle 0 º. Black: With atm. attenuation. US Standard. Zenith angle 0 º.

The curves in Fig. 11.2 correspond to the following atmospheric transmittances:

- Mid-latitude summer: Atmospheric transmittances = 0.58
- US Standard: Atmospheric transmittances = 0.67

11.3 Solar cell current

Performance for a specific solar cell is usually related to air mass 1.5. See Fig. 4.1. The designation “air mass”, corresponds in Fig. 4.1 to the relation between the atmospheric depths h and h0. Air mass = 1.5 corresponds to:

$$\frac{h}{h0} = 1.5 \qquad (11.11)$$

This results in (see Fig. 4.1):

$$\alpha = 41.8^{\circ} \qquad (11.12)$$

For more information about “Air mass 1.5”, see [58].

The spectral characteristics of the atmosphere are often related to the defined case “US Standard atmosphere”. See section 11.2.

Fig. 11.3 illustrates the responsivity curve of a typically mono-crystalline silicon solar cell. The curve is taken from information given in [30].

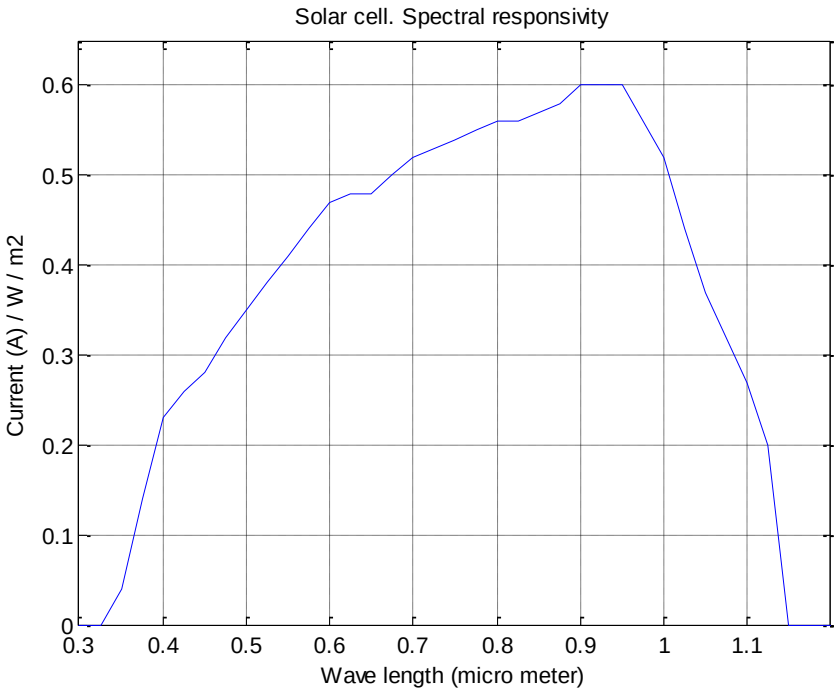

Fig. 11.3. Solar cell. Spectral responsivity.

Fig 11.4 shows the spectral current density for a solar cell with the responsivity according to Fig. 11.3 after atmospheric attenuation by US Standard atmosphere and an air mass of 1.5. See above, (11.11) and (11.12).

Integrated current density over whole spectra (short-circuit current) is 274.5 A/m^2. Solar irradiance after atmospheric attenuation is 766.8 W/m^2. Performance for a specific solar cell is usually related to an illumination of 1000 W/m^2. With this illumination, the integrated current density is:

$$J_{SC\ Ref} = \frac{L_{Ref}}{L} \times J_{SC} \qquad (11.13)$$

Where:

$J_{SC\ Ref}$: Reference short circuit current density (A/m^2)
L_{Ref}: Reference irradiance = 1000 W/m^2
L: Calculated irradiance = 766.8 W/m^2
J_{SC}: Calculated short circuit current 274.5 A/m^2

Applying (11.13):

$J_{SC\ Ref}$ = 358.0 A/m^2.

358.0 A/m^2 corresponds to 3.58 A/100 cm^2.This value can be compared with corresponding value 3.66 A/100 cm^2 in Table 4.4, as was used for calculation of extinction coefficients according to chapter 4.

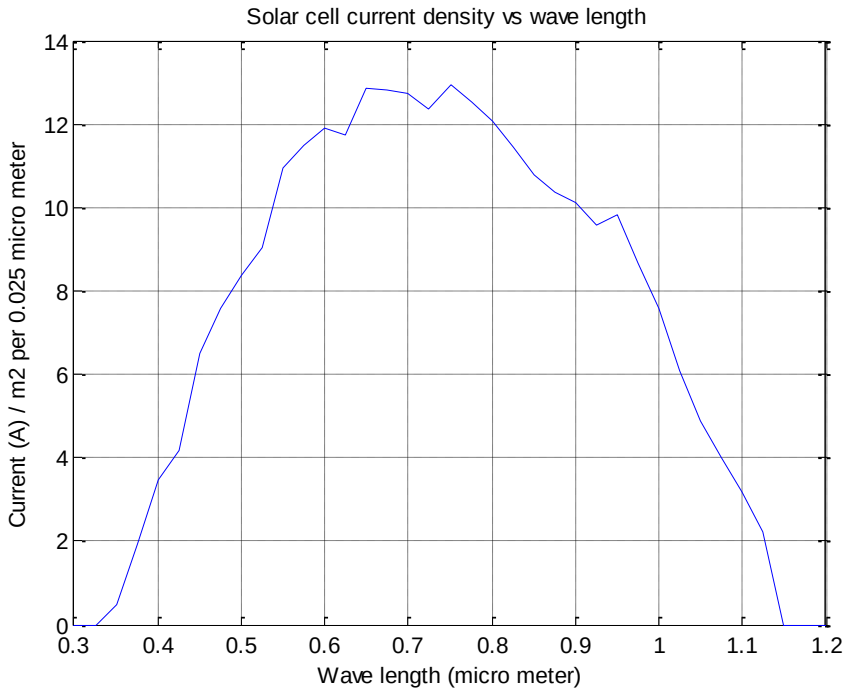

Fig. 11.4. Solar cell current vs wave-length.

11.4 Responsivity in relation to Mid-latitude summer and US-Standard

The “effective transmittance” has been calculated for the two atmospheric models Mid-latitude summer and US-Standard. With the term “effective transmittance” is mean the atmospheric transmittance when the influence of the spectral responsivity of the PV-cell is included. Fig. 11.5 illustrates the spectral current density for a silicon PV-cell. The figure shows the current density before atmospheric attenuation and after atmospheric attenuation with the two atmospheric models Mid-latitude summer and US-Standard.

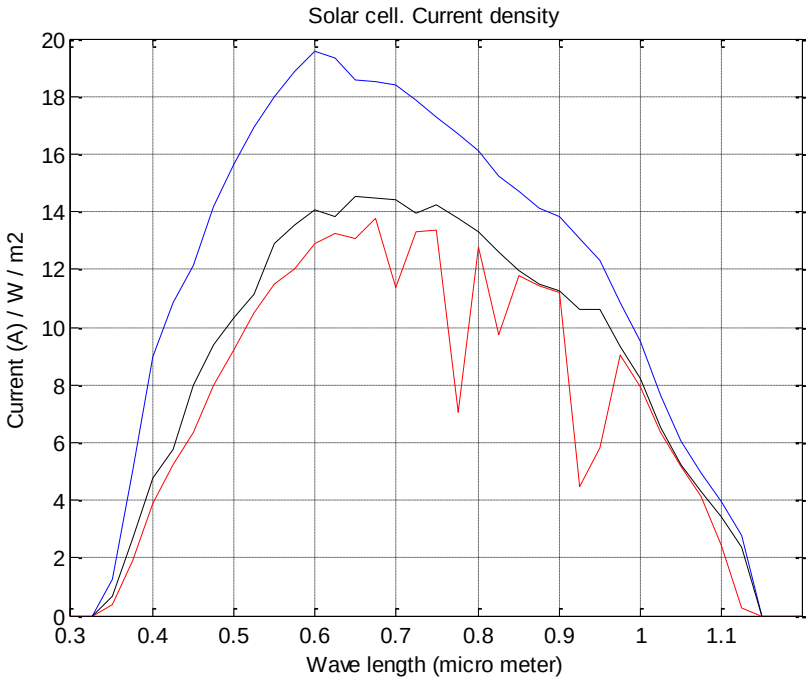

Fig. 11.5. Solar cell. Spectral current density. Comparison between Mid-latitude summer and US-Standard. Zenith angle = 0. Blue curve: Without atmospheric attenuation. Black curve: US-Standard. Red curve: Mid-latitude summer.

The curves according to Fig. 11.5 correspond to the following effective atmospheric transmittances:

- Mid-latitude summer. Effective transmittance: 0.65
- US-Standard. Effective transmittance: 0.76

11.5 Wave-length bands

11.5.1 Analysis of four wave-length bands

A definition of 4 wave-length bands has been done according to Table 11.3. Band 1 represents a silicon PV cell according to Fig. 11.3. The wave-length interval for a silicon PV cell is sometimes defined as 0.20 to 1.15 µm. However, as a consequence of the strong radiation attenuation in the ozone layer, the useful lower wavelength band limit for a silicon PV cell is about 300 nm. This means that the solar cell according to Fig. 11.3 is well adapted to reality.

Table 11.3. Definition of wave-length bands.

Wave-length band (designation)	Wave-length band (µm)
Wb 1	0.200 - 1.150
Wb 2	0.200 - 1.375
Wb 3	0.200 - 1.825
Wb 4	0.200 - 2.600

Calculation of sun irradiation has been performed using the theory in section 11.1 and section 11.2 relating to mid-latitude summer. Table 11.4 presents irradiances before and after atmospheric attenuation and different relations.

Table 11.4. Irradiance bofore and after atmospheric attenuation (mid-latitude summer) vs wave-length band. Different relations.

Wave-length band (designation)	Irradiance before atmospheric attenuation, L_{NA} (W/m^2)	Irradiance after atmospheric attenuation, L_A (W/m^2)	Relation L_{NA} to Solar constant, $L_{REL\ 1}$	Relation L_A to Solar constant, $L_{REL\ 2}$
Wb 1	1079	621	0.79	0.45
Wb 2	1170	681	0.86	0.50
Wb 3	1264	733	0.92	0.54
Wb 4	1324	761	0.97	0.56

According to Table 11.4 $L_{REL\ 1}$(Wb 4) is 0.97. This means that just around 3 % of the total solar radiation is outside band Wb 4. This also implies that $L_{REL\ 2}$(Wb 4) is a relevant measure of the total atmospheric transmittance, τ_atm. This means that $L_{REL\ 2}$(Wb 4) $\approx$ τ_atm.

Table 11.5 presents irradiances before and after atmospheric attenuation and corresponding wave-length transmittances.

Table 11.5. Irradiance bofore and after atmospheric attenuation (mid-latitude summer) vs wave-length band. Transmittances.

Wave-length band (designation)	**Irradiance before atmospheric attenuation, L_{NA} (W/m^2)**	**Irradiance after atmospheric attenuation, L_A (W/m^2)**	**Transmittance $\tau 1 - \tau 4$ (L_A / L_{NA})**
Wb 1	1079	621	$\tau 1 = 0.58$
Wb 2	1170	681	$\tau 2 = 0.58$
Wb 3	1264	733	$\tau 3 = 0.58$
Wb 4	1324	761	$\tau 4 = 0.57$

As can be noted in Table 11.5, the differences between $\tau 1$, $\tau 2$, $\tau 3$ and τ 4 are quite small. It is even evident that the differences between $\tau 1$, $\tau 2$, $\tau 3$, τ 4 and τ_atm (see above) are quite small. The fact that $\tau 1$ can be considered a relevant approximation to τ_atm is an important prerequisite for the calculation principle of the extinction coefficient according to chapter 4.

Table 11.6 gives the percentage increase of solar irradiation for Wb 2, Wb 2 and Wb 4, relative to Wb 1. The digits intend comparison between sun irradiation after atmospheric attenuation. The table shows that an extension of the available wavelength range can increase the efficiency significantly.

Table 11.6. Increase of solar irradiation relative to Wb 1.

Wave-length band (designation)	**Increase (%)**
Wb 2	9.7
Wb 3	18.0
Wb 4	22.5

Calculation results according to Table 11.4 regarding $L_{REL\ 1}$ and $L_{REL\ 2}$ are illustrated in Fig. 11.6.

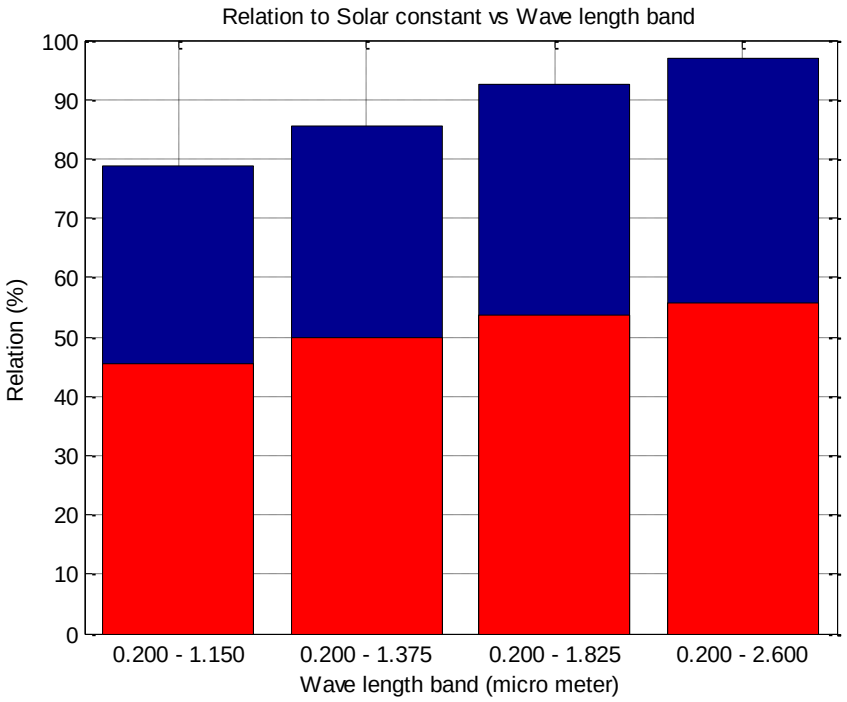

Fig. 11.6. Irradiation relative to solar constant vs wave-length band. Blue + red bars: Before atmospheric attenuation. Red bars: After atmospheric attenuation.

An extension of the available wavelength range band, compared with the ordinary band for silicon solar cells, can be done by combining silicon material with other materials or to use other materials instead of silicon. Another interesting method is to apply nano-technology.
In [44], work is presented around use of the combination ZnO-ZnSe-Si-Ge in a tandem solar cell. [41] deals with a very complex tandem cell consisting of different combinations/alternatives of AlAs, AlGaAs, GaAs, GaGe, Ge.
[33] and [35] deal with different kinds of solar cell designs and compares corresponding features. In these reports, nano-technology and use of “quantum dots” is discussed together with more conventional technologies.

11.5.2 Quantum dots

The quantum dots (QDs) technology is a part of nano-technology. The quantum dot is a small piece in the range of nanometers (some hundreds of atoms). By adjusting the size of the quantum dot, it is possible to tune the band gap of the material. On the other hand, this results in a tuning of corresponding PV wave band. If a solar cell is designed as a tandem cell, consisting of layers of tuned quantum dots, it is possible to broaden the original wave band, and also corresponding efficiency of the cell. Because of the ability to tune bandgaps, quantum dots have been referred to as “artificial atoms”.

More information regarding nano-technology and “quantum dots”, can be found in e.g. [32], [34], [36] and [63] - [66].

If the spectrum of incoming radiation corresponds to an energy that is greater than the bandgap between the valence band and the conduction band for the solar cell material, bound electrons in the valence band can be excited to the conduction band. Excited electrons form the current in the electrical circuit of the solar cell. The relation between bandgap and maximum wave-length is:

$$h \times f > E_g \tag{11.14}$$

$$f = \frac{c}{\lambda} \tag{11.15}$$

Where:

h: Planck’s constant = 4.1357×10^{-15} eVs
f: Radiation frequency
E_g: Bandgap (eV)
c: Speed of light in vacuum = 2.99792×10^{8} m/s
λ: Wave-length (m)

Fig. 11.7 illustrates the band gap between the energy condition of the free electrons in the conduction band and the energy condition of the bounded electrons in the valence band. The electrons in the conduction band can be used in the power production of the solar cell.

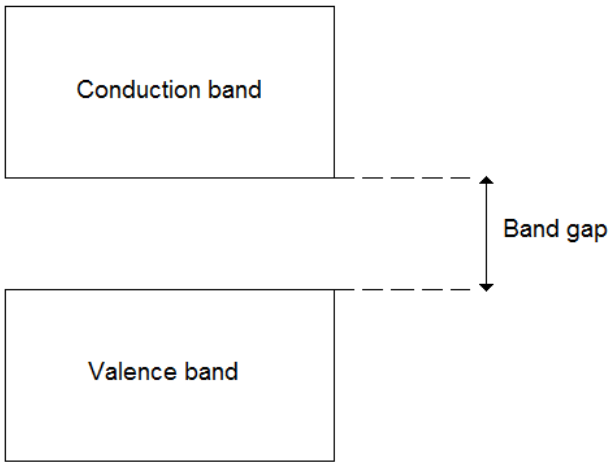

Fig. 11.7. Valence band, conduction band and band gap in a semiconductor.

For silicon quantum dots, the bandgap can be calculated according to (11.16). For more information about this, see [65].

$$E_g = 1.12 + \frac{3.98}{d^{1.36}} - \frac{0.19}{d} \quad (11.16)$$

Where:

d: Silicon quantum dot diameter (nm)

Table 11.7 shows bandgap and corresponding maximum wave-length for silicon, silicon quantum dots with varying dot diameter and germanium. λmax in the table corresponds to maximum wave-length as fulfill (11.14) for the bandgap in question. Bandgap and λmax vs diameter of silicon QD given by applying (11.14) - (11.16).

Table 11.7. Bandgap and corresponding maximum wave-length for silicon, germanium and silicon quantum dots.

Material	**Bandgap (eV)**	**λmax (μm)**
Silicon	1.12	1.11
Silicon, QD. Diameter = 10 nm	1.27	0.97
Silicon, QD. Diameter = 6 nm	1.44	0.86
Silicon, QD. Diameter = 4 nm	1.68	0.74
Silicon, QD. Diameter = 2 nm	2.58	0.48
Silicon, QD. Diameter = 1 nm	4.91	0.25
Germanium	0.67	1.85

Fig. 11.8 illustrates λmax vs diameter of silicon QD by applying (11.14) - (11.16). As can be noted according to Fig. 11.3, the responsivity curve of a silicon solar cell has its maximum at a wave-length of about 0.9 μm. The curve starts to decrease when the wave-lengths get shorter. With a combination of an ordinary silicon solar cell and a solar cell made of silicon quantum dots in a tandem cell, the silicon quantum dots cell can take over the absorption when the ordinary silicon cell starts to fall out. According to Fig. 11.8, a dot-diameter of 7 nm results in a maximum wave-length of 0.9 μm. This is a hint about the dot size, that may be suitable in this case.

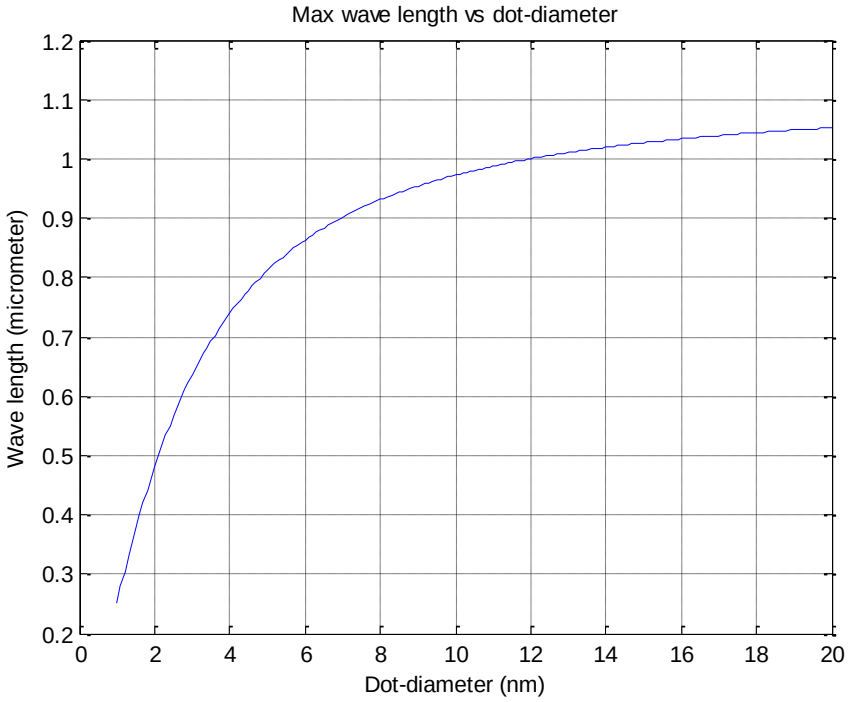

Fig. 11.8. Maximum wave-length for silicon dots vs dot diameter.

Fig. 11.9 illustrates a road map to increase the efficiency of a solar cell by using the QD technology. The figure is based on information given in [63]. The process described starts with an ordinary standard silicon solar cell to the left with n-resp. p-doped silicon. The efficiency in this step has been adopted to 18%. In the second step, the ordinary n-doped silicon layer has been replaced with a QD-layer of n-type. The efficiency has increased to 22 %. The arrangement according to step 3 is a tandem cell with an ordinary standard silicon solar cell connected to a silicon cell in QD design. The efficiency is 28 %. In step 4, the combination of silicon QD and germanium QD has been used to build up a tandem cell. This design results in an efficiency of 30 %.

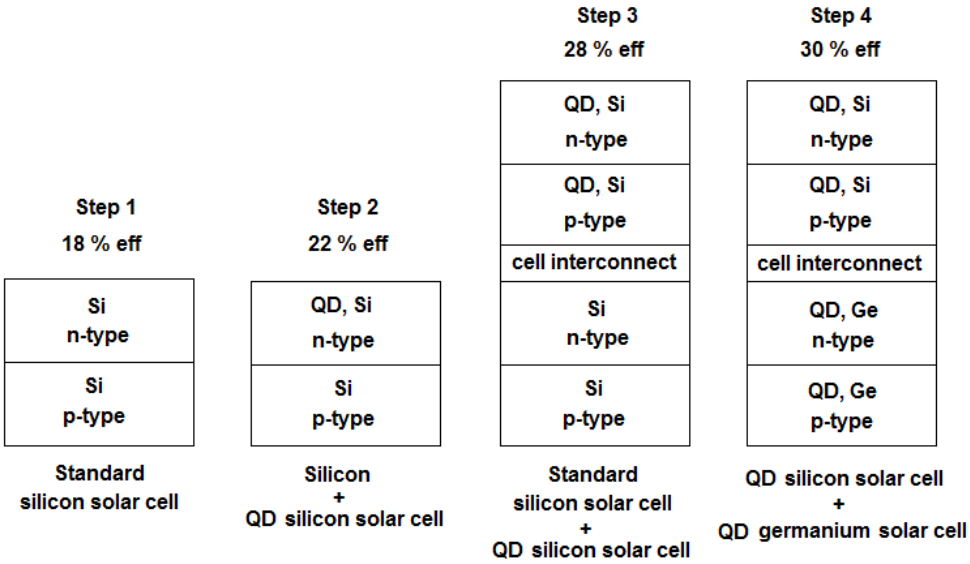

Fig. 11.9. A road map to increase the efficiency of a solar cell.

11.6 Extinction coefficient

Regarding the extinction coefficient, see also chapter 4.

Based on the results in sections 11.3 - 11.5, corresponding extinction coefficients are calculated. By definition according to section 4.1, the extinction coefficient can be calculated as:

The extinction coefficient is composed of two components:

- Absorption coefficient
- Scattering coefficient

See (4.2).

Absorption coefficient

The absorption coefficient is a function of molecular absorption. In wave-length region 0.2 – 1.15 µm, it is primarily water that has an influence. In wave-length region 0.2 – 0.3 µm, ozone and oxygen also have an influence on the transmittance.

If the concentration of air particles is low, e.g. low concentration of dust particles, it can be assumed that it is mainly absorption that has an influence on the extinction coefficient in mode 1. On the other hand, if high particle content is present, as is the case in some industrial areas, then the scatter effect has a significant effect also in mode1.

Scattering coefficient

The scattering coefficient is a function of scattering from molecules and particles. In the region of a silicon cell, it is primarily particles that have influence. Different particles can cause scattering: particles from industrial emissions, dust particles, water particles etc.

11.6.1 Extinction coefficient. Mode 1

The extinction coefficient for mode 1 (no clouds affect solar radiation) is calculated for the 2 cases Mid-latitude summer and US Standard atmosphere.

With reference to sections 11.2 and 11.5:

- US Standard: Atmospheric transmittances = 0.67
- Mid-latitude summer: Atmospheric transmittances = 0.58

This gives:

- US Standard atmosphere: Extinction coefficient = 0.40
- Mid-latitude summer: Extinction coefficient = 0.54

Comparison with model parameter according to section 4.7.1:

Extinction coefficient based on measurements (simulation model)

- 2.5σ – limit min = 0.31
- 2.5σ – limit max = 0.55
- Mean = 0.43
- Standard deviation = 0.048

Extinction coefficient based on calculations

- US Standard atmosphere: Extinction coefficient = 0.40
- Mid-latitude summer: Extinction coefficient = 0.54

This means that the simulation parameter is close to the calculated parameter for US Standard atmosphere.

Irradiances at ground level and air mass 1.5 (see section 4.1 and 11.3)

- Simulation model (mean extinction coeffient). Irradiance at ground level: 717 W/m^2
- US Standard atmosphere. Irradiance at ground level: 750 W/m^2
- Mid-latitude summer. Irradiance at ground level: 608 W/m^2

11.6.2 Extinction coefficient. Mode 2

11.6.2.1 Calculation of scattering

In mode 2, it is mainly scattering in cloud layers that affects the extinction coefficient. The contribution from molecular absorption is small in relation to the scattering effect. When calculating the scattering effect, there are 3 different methods that are in question, depending on the kind of scattering:

- Rayleigh scattering
- Mie scattering
- Optical scattering

The scattering type in question depends on the dimension of the scattering particles. A size parameter is defined according to:

$$\alpha = \frac{2\pi r}{\lambda} \qquad (11.17)$$

Where:

- α: Size parameter
- r: Radius of the scattering particle (µm)
- λ: Wave-length (µm)

The following is valid regarding scattering type:

- Rayleigh scattering: $\alpha < 0.5$
- Mie scattering: α in the region 0.5 - 10
- Optical scattering: $\alpha > 10$

Scattering in cloud layers is caused by water particles of different sizes in fog. The diameter of these particles is located in the region 1 – 20 µm. See e.g. [38]. According to (11.17) and a wave-length interval from 0.3 – 1.15 µm, this results in:

$2.7 < \alpha < 209$

This means that calculation methods regarding optical scattering (geometric optics) in combination with calculation methods regarding Mie scattering will be in question primarily. Methods for Mie scattering will be used in region $2.7 < \alpha < 10$ and methods for optical scattering will be used in region $10 < \alpha < 209$. However, the calculation methods regarding Mie scattering can be used with sufficient accuracy, even when α is greater than 10. See e.g. [51], [53] and [54]. Consequently, the following calculations relate to scattering in cloud layers, will be focused on the methods of Mie scattering.

The basic Mie theory for calculation requires detailed information regarding particle size distribution and optical properties. The theory is rather complex and implies solution of Maxwell's equations with associated boundary conditions. An alternative method for calculating the scattering effect has been developed by Koschmieder and Kruse. See [29], [47] and [48]. The method is based on information regarding the visibility in the atmosphere. The following expression is used according to this method:

$$k(\lambda) = \frac{3.912}{V} \times \left(\frac{\lambda}{550}\right)^{-q} \tag{11.18}$$

Where:

k(λ): Scattering coefficient
V: Visibility (Km)

The coefficient q is dependent on the visibility according to:

$$q = \begin{cases} 1.6 & \text{if } V > 50 \text{ km} \\ 1.3 & \text{if } 6 \text{ km} < V < 50 \text{ km} \\ 0.16\,V + 0.34 & \text{if } 1 \text{ km} < V < 6 \text{ km} \\ V - 0.5 & \text{if } 0.5 \text{ km} < V < 1 \text{ km} \\ 0 & \text{if } V < 0.5 \text{ km} \end{cases} \tag{11.19}$$

Calculation using (11.18) and (11.19) has been done with different visibility distances. The results are presented in Fig. 11.10 which shows a plot with scattering coefficient vs visibility.
For further studies regarding this topic, see e.g. [26].

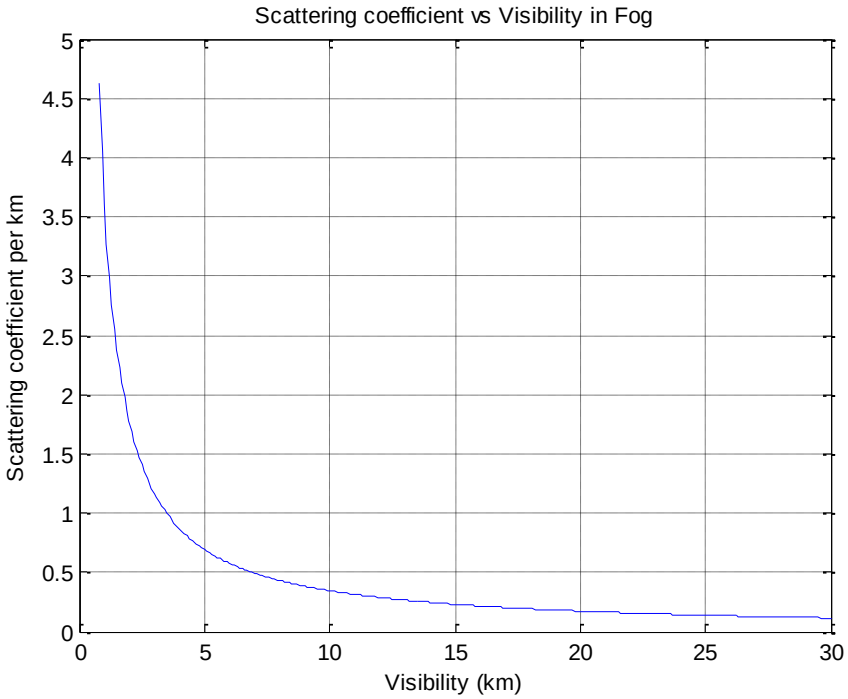

Fig. 11.10. Scattering coefficient per km air mass as a result of particle scattering vs visibility.

The scattering coefficient according to Fig. 11.10 is calculated as the mean value in respect of wave-length region 0.3 µm – 1.15 µm.

The scattering coefficient thus increases from 0.12/km to 3.60/km if the visibility decreases from 30 to 1 km.

As can be noted, the scattering coefficient falls rapidly in the region below a visibility of about 3 km. Then in the region over 3 km, the curve tends to flatten out.

Table 11.8 shows the International code of visibility range. See [40].

Table 11.8. International code of visibility range.

Visibility range (m)	**Description**
< 40	Dense fog
40 – 200	Thick fog
200 – 1000	Fog
1000 - 2000	Mist (mainly due to water droplets)

11.6.2.2 Low and middle level clouds

To calculate the visibility in a cloud, (11.20) can be used.

$$V = \frac{1.002}{(\mathrm{LWC} \times \mathrm{N})^{0.6473}} \qquad (11.20)$$

Where:

LWC: Liquid water content (g/m $^{-3}$)
N: Cloud number concentration (cm $^{-3}$)

Using (11.20) results in the visibility values according to Table 11.9. N, LWC and (11.20) are taken from [59].

Table 11.9. N and LWC for different clouds.

Cloud Type	N (cm $^{-3}$)	LWC (g/m $^{-3}$)	Visibility (km)	Comment
Cumulus	250	1.0	0.028	Low clouds < 2000 m
Stratus	250	0.29	0.063	
Stratocumulus	250	0.15	0.096	Middle clouds 2000 – 7000 m
Altostratus	400	0.41	0.037	
Nimbostratus	200	0.65	0.043	
Cirrus	0.025	0.06405	65	High clouds > 7000 m
Thin Cirrus	0.5	0.0003138	291	

The scattering coefficients for different cloud types are calculated by using (11.18). The result follows in Table 11.10. Five examples of approximated cloud thickness are given in the table. Also see [61] and [62].

Table 11.10. Scattering coefficient for different clouds.

Cloud Type	Scattering coefficient, k (1/km)	Approximated thickness (km)
Cumulus	140	2 (see [61])
Stratus	62	0.6 (see [61])
Stratocumulus	41	-
Altostratus	106	-
Nimbostratus	91	0.8 (see [61])
Cirrus	0.05	1.5 (see [62])
Thin Cirrus	0.01	1.5 (see [62])

As can be noted according to Table 11.8, “low level clouds” and “mid level clouds” correspond to dense fog or thick fog. The scattering coefficient for these clouds is also very high. The examples of thickness in combination with corresponding scattering coefficients indicate that in reality all solar radiation is scattered away. No radiation arrives to the solar cells as direct radiation. The received radiation consists at these cases of diffuse radiation.

An approximate method for calculating the diffuse radiation at different cloud heights is given in [18]. Some examples below:

Low clouds:

$$L_R = 0.14 \times L_{Clear} \quad (11.21)$$

Mid-level clouds:

$$L_R = 0.25 \times L_{Clear} \quad (11.22)$$

Where:

L_R: Diffuse irradiation to solar cells (W/m^2) with cloudy sky. This corresponds to mode 2
L_{Clear}: Irradiation to solar cells with clear sky (W/m^2). This corresponds to mode 1

Scattering coefficient based on (11.21) and (11.22):

$$k_{Cloud} = - \ln(C) \quad (11.23)$$

Where:

k_{Cloud}: Scattering coefficient as an effect of clouds

C = 0.14 if low clouds in sky
C = 0.25 if mid-level clouds in sky

This gives:

$k_{Cloud\_low\ clouds} = 1.97$
$k_{Cloud\_mid\text{-}level\ clouds} = 1.39$

Suppose the following:

ε, mode 2 = k_{Cloud_mean} (11.24)

Where:

ε, mode 2: extinction coefficient mode 2
k_{Cloud_mean}: mean value of $k_{Cloud\_low\ clouds}$ and $k_{Cloud\_mid\text{-}level\ clouds}$

This gives a mean value for low clouds and mid-level clouds as:

ε, mode 2 = 1.68

This can be compared with the simulation model, mode 2. The distribution function is in this case a trapezoidal function in the interval 0.55 – 4.55 and with an expected value of 2.00.

Irradiances at ground level and air mass 1.5 (see section 4.1 and 11.3)

- Simulation model (expected value of extinction coeffient). Irradiance at ground level: 68 W/m^2
- Low clouds and mid-level clouds (mean extinction coeffient): 110 W/m^2

Equivalent fog

According to the simulation model, mode 2, the expected value for the extinction coefficient is 2.0. For this high value, the extinction coefficient is equivalent to the scattering coefficient.

If the scattering coefficient in this case is regarded in the term of “equivalent fog” with an air mass of 1 km, the visibility is about 1.8 km. See Fig. 11.10.

11.6.2.3 High-level clouds

The high-level clouds result in a low scattering coefficient. For cirrus clouds the scattering coefficient is just about 0.05 / km. See Table 11.10. Measurements have estimated the distance from bottom to top of these clouds. See [62]. The maximum distance was measured up to 2 km, with a mean value of about 1.5 km. This means that high-level clouds just marginally contribute to the total extinction coefficient. However, these clouds are probably one reason for the variation of the irradiation at ground level. High-level clouds can be present even if they are not discovered and noted. The following example illustrates this effect:

- Mean value of extinction coefficient in the simulation model, mode 1 = 0.43. This corresponds to the absorption coefficient
- Scattering coefficient of a cirrus cloud, depth 2 km = 2 × 0.05

Using (4.2) results in ε = 0.53 when the cirrus cloud has an impact.

Irradiances at ground level and air mass 1.5 (see section 4.1 and 11.3)

- No clouds. Extinction coefficient: 0.43. Irradiance at ground level: 717 W/m^2
- Cirrus cloud, depth 2 km has an impact. Extinction coefficient: 0.53. Irradiance at ground level: 617 W/m^2

The example illustrates how a cirrus cloud can reduce the irradiance at ground level with 100 W/m^2. This means in this case a reduction of 14 %.

11.7 Summary

The radiation from a black-body has been discussed with reference to Planck's radiation law.

The solar radiation has been analysed. It is found that this radiation can be regarded as an effect of radiation from a black-body, where the sun is the black-body with a temperature of 5770 K.

The "solar constant", 1367 W/m^2, has been verified.

Spectral transmittance values in wave-length region 0.2 – 2.6 µm have been estimated. This is performed with reference to two typical atmospheric models: Mid-latitude summer and US Standard atmosphere.

Based on solar radiation characteristics regarding black body radiation in combination with calculated atmospheric transmittance, the spectral solar radiation after attenuation in the atmosphere has been calculated.

The responsivity curve for a typical silicon PV cell has been illustrated.

The short circuit current density for a solar illuminated silicon PV cell has been calculated. The solar illumination is based on an atmospheric attenuation of solar radiation after passing an atmosphere corresponding to US Standard atmosphere and an air mass of 1.5.

A reference value of short circuit current (typical silicon PV) has been calculated based on reference irradiance = 1000 W/m^2 and US Standard atmosphere, air mass 1.5. The reference value was compared with the value used for calculation of extinction coefficients in chapter 4.

Different wave-length bands for PV use have been studied and compared with and without atmospheric attenuation.

The quantum dots technology and its usage in solar cell development has been discussed.

The extinction coefficients have been calculated based on atmospheric attenuation corresponding to the cases Mid-latitude summer and US Standard atmosphere. The calculated coefficients are compared with corresponding model coefficients according to chapter 4.

The effect on extinction coefficients under influence of different kinds of fog and clouds have been discussed.

A simplified method for calculation of the scattering coefficient (see (4.2)) based on the visibility in atmosphere have been introduced. Examples with scattering coefficients vs visibility have been illustrated.
Extinction coefficients for a cloudy sky have been calculated in the cases of low-level clouds, mid-level clouds and high-level clouds. The results were compared with corresponding model coefficients according to chapter 4.

It has been demonstrated how a cirrus cloud can reduce the incoming solar irradiance.

It has been shown that the effective solar irradiation against a solar cell at full cloudy sky just consists of diffuse radiation. The direct irradiation can be ignored in this case.

CHAPTER 12

INTERCONNECTION OF A NUMBER OF COMBINED POWER SYSTEMS

As a result of the flexible module structure of the simulation system, the software easily can be adapted for an efficient analysis of a combination of a large number of interconnected individually combined power systems. Fig. 12.1 shows an example of how the basic system can be expanded and adapted. The figure illustrates how N combined power systems are interconnected by the utility grid via power nodes. The main control unit is used to balance the power flow to the utility grid. Each individual combined power system may have a specific combination of individual parameters regarding wind power unit, solar power unit, local electrical load, energy storage, power back-up, and conditions regarding wind speed and solar radiation.
The parameters S(x) and ΔS(x) are control signals and correspond to "actual power" that is produced by combined power system x, and desired "target power" that must be produced by combined power system x respectively.

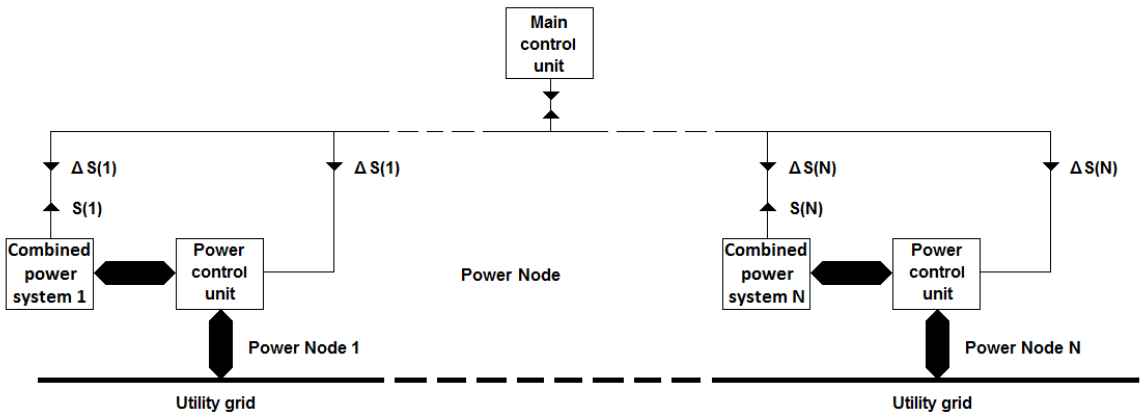

Fig. 12.1. N locally separated combined power systems connected to the utility grid. The combined power systems and the power control units are controlled by a main control unit.

Three power vectors are calculated, “actual power vector”, “target power vector” and “deviation vector”. The relationship is as:

$$\mathbf{S(N)} = (S(1), S(2), \ldots\ldots, S(N-1), S(N)) \quad (12.1)$$

$$\mathbf{Sd(N)} = (Sd(1), Sd(2), \ldots\ldots, Sd(N-1), Sd(N)) \quad (12.2)$$

$$\mathbf{\Delta S} = \mathbf{Sd} - \mathbf{S} \quad (12.3)$$

$$\mathbf{\Delta S(N)} = (\Delta S(1), \Delta S(2), \ldots\ldots, \Delta S(N-1), \Delta S(N)) \quad (12.4)$$

Where:

S: Vector containing actual apparent power for the power nodes, Node 1 to Node N
Sd: Vector containing desired apparent power for the power nodes, Node 1 to Node N
ΔS: Vector containing deviation regarding desired apparent power relative to actual apparent power for the power nodes, Node 1 to Node N

The elements in vector **S** and vector **ΔS** are used as control signals between main control unit, the combined systems and the power control units according to Fig. 12.1.

“Node x” corresponds to element number “x” in the respective vector.

The apparent power consists of active and reactive power. These are defined according to (6.1) to (6.3).

Based on the power vectors, the power control units at the respective power node will convert the output power to the utility grid according to:

$$\mathbf{Sd} = \mathbf{S} + \mathbf{\Delta S} \quad (12.5)$$

For the individual elements, the following applies:

$$S(x) = P(x) + jQ(x) \quad (12.6)$$

$$Sd(x) = Pd(x) + jQd(x) \quad (12.7)$$

$$\Delta P(x) = Pd(x) - P(x) \quad (12.8)$$

$$\Delta Q(x) = Qd(x) - Q(x) \quad (12.9)$$

Where:

P(x): Actual active power node x (element x in vector)
Pd(x): Desired active power node x (element x in vector)
Q(x): Actual reactive power node x (element x in vector)
Qd(x): Desired reactive power node x (element x in vector)
ΔP(x): Deviation regarding desired active power relative to actual active power node x (element x in vector)
ΔQ(x): Deviation regarding desired reactive power relative to actual reactive power node x (element x in vector)

The combined power systems send information regarding actual apparent power to the main control unit. The main control unit is prepared with information about the level of desired apparent power. This is based on information about the overall condition in the utility grid. A calculation of possible need for power correction relative to actual power is performed. The main control unit sends a reply to each node x with possible correction information in the form of parameter ΔP(x) or ΔQ(x). Since the active power from wind power farms and solar power farms constantly varies, a continuous updating of vector **ΔS** must be done. The update frequency can be varied from each simulation step to longer time intervals depending on the situation in question.

The active power will primarily be modified by adjusting the power flow to the energy storages and the power back-up units. The reactive power will be modified by the power control units.

By controlling the output apparent power at individual power nodes, it is possible to use each individual combined power system to get an optimal utilization of available apparent power at the utility grid. An appropriate application of the system according to Fig. 12.1 can, for example, be to test out different configurations, applications and control algorithms in combination with so-called “smart grids”. Regarding the topic smart grids, see e.g. [70] and [71].

CHAPTER 13

SUMMARY OF CHAPTER 2 TO CHAPTER 12

Chapter 2. This thesis has presented the work around a combined electrical power system with wind power and solar power as energy sources. The combined power system is featured with an energy storage unit and is also connected to the utility grid. The energy storage unit and the connection to the utility grid enable energy balancing. As an extra unit, a power back-up device is installed in the system.

Chapter 3. The work includes development of a simulation system for analysis of a combined power system. It is three modules in particular in this system that have been important parts in the development work: the module for simulation of atmospheric attenuation, the module for simulation of wind speed and the module for simulation of electrical power consumption.

Chapter 4. The module for simulation of atmospheric attenuation is developed based on performed measurements. The parameter “extinction coefficient” is used as a measure of the atmospheric attenuation regarding solar radiation. This parameter has been modelled in order to enable a statistical processing of the damping effect. The program module distinguishes between two modes depending on condition of cloudiness, "solar radiation is not damped by clouds" and "solar radiation is damped by clouds". In practice, a mix of these modes is present and has a corresponding impact on the solar radiation. The relation between the modes is controlled by the parameter “cloudiness”, which informs about the probability of "cloud attenuation" regarding the solar radiation.

Chapter 5. The module for simulation of wind speed is developed based on performed measurements and is modelled to enable a statistical processing of the wind speed. The model generates statistical wind speeds typical for each of the four seasons or for the total year.

Chapter 6. The module for simulation of electrical power consumption is developed based on performed measurements. Four kinds of power consumers are modelled: industrial area, commercial centre, residential area and a mixture of these three. The models generate statistical power consumption.

Chapter 7. The simulation model is used to analyse the impact of solar cell direction relative to zenith and south.

The tests were focused on two special mechanical installation types, fixed mounted panels relative to sun direction and the installation when the panels follow sun direction, so-called “solar tracking. For fixed mounted panels, the optimal zenith angles and south angles of the panels was studied for various geographical locations. The case of “solar tracking” was analysed and compared with fixed mounted panels in relation to energy production.

Chapter 8. “Tests on a small combined power system” aimed to study the performance of the system with wind power as the only power source and with wind- and solar power in combination. These tests were performed with and without energy storage.
The studies resulted in preliminary guide-lines regarding optimal power capacity of the wind- and solar power units.
The tests also demonstrated the advantage of the combination of wind- and solar power if an energy storage unit is installed in the system. The probability of power shortage for varying capacity of the energy storage was predicted.

Chapter 9. “Tests on large combined power systems” were devoted largely to the study of the geographic difference regarding solar energy production. Five geographical locations were investigated, Kiruna and Göteborg in Sweden, München in Germany, Malaga in Spain and Nairobi in Kenya. The production of solar energy was compared between the different sites. Comparison was made for the whole year and also divided into seasons (quarter).
The economic picture was clarified when it comes to the production of solar electricity and comparison between different locations.
The total power plant cost (wind and solar) for the five locations was estimated.
Another important point of the chapter was to analyse the effect of using an energy storage device in the system. The probability of power shortage as a function of capacity of the energy storage device was studied.
The preliminary guide-lines for optimum power capacity of wind and solar power units, which have been developed in the chapter on a small combined power system, were verified.

Chapter 10. “Analysis of a solar power system for household usage”. A small solar power system was analysed in respect of produced annual energy production. The simulation results were compared with corresponding measured production. The possible reasons for deviation between simulations and measurements were analysed and discussed.

Chapter 11. This chapter was devoted to theoretical analysis of some key areas in the field of solar energy. The chapter was devoted to solar radiation, atmospheric transmittance, solar cell current, wave-length bands and extinction coefficient.
For calculation of spectral solar radiation, basic black-body theory was applied.
The atmospheric transmittance was exemplified with two defined reference atmospheres, mid-latitude summer and US standard atmosphere.

Based on information about spectral solar radiation and spectral atmospheric transmittance, the spectral solar radiation, after atmospheric attenuation, was calculated.
By applying calculated solar radiation on a reference solar cell, corresponding short circuit current was calculated. A typical silicon solar cell and its spectral responsivity curve were used as reference. The result was compared with the short circuit current, used for evaluation of earlier measurements regarding extinction coefficients.
Different wavelength bands were analysed regarding the ability to increase the generated energy of a solar cell. The analysis was focused on the spectral solar radiation after atmospheric attenuation, and shows one of the possibilities for increasing the solar cell efficiency. The key point in this regard is the development of suitable solar cells adapted for broader wavelength bands. The issue is still at the experimental stage.
Estimates of the extinction coefficients were made on the basis of two cases, "solar radiation is not damped by clouds" and "solar radiation is damped by clouds". These cases correspond to mode 1 and mode 2 respectively in the simulation model.
Calculations for mode 1 were based on the two reference atmospheres mid-latitude summer and US standard atmosphere. The result was compared with the corresponding values used in the simulation model.
Calculations for mode 2 were based on an atmosphere influenced by fog. This was applied to various types of clouds. The corresponding extinction coefficients were calculated. It was found that only thin cirrus clouds provide the ability to directly transmit solar radiation. The radiation that reaches a solar cell is for other clouds an effect of diffuse radiation. The effective solar radiation, based on different cloud height, has been estimated in other contexts. On that basis, calculations were made of the corresponding extinction coefficients. These estimated values were compared with the corresponding values in the simulation model. It was shown that the effective solar irradiation against a solar cell at full cloudy sky just consists of diffuse radiation. The direct irradiation can be ignored in this case.

Chapter 12. As a result of the flexible module structure of the simulation system, the software can easily be adapted for an efficient analysis of interconnected combined power systems. This was discussed in this chapter.

CHAPTER 14

CONCLUSION

A simulation model with the intention to show the potential of systems consisting of wind power and solar power as energy sources has been developed. The systems can be entirely stand-alone or connected to utility grids and also be equipped with an energy storage or an auxiliary device in the form of, for example, a diesel generator.

The presented simulation system has the flexibility of analysing a wide range of combined power generation systems. From small systems for domestic use to large systems intended for national purposes. Four categories of electrical load may be simulated: “industrial area”, “commercial centre”, “residential area” and a “mixture” of these three cases.

As a result of the flexible module structure of the simulation system, the software can easily be adapted for an efficient analysis of a combination of a large number of interconnected individually combined power systems into a common larger power grid. Each individual combined power system may have a specific combination of individual parameters regarding wind power, solar power, local electrical load, energy storage, power back-up and location. By controlling the output power from each individual combined power system, it is possible to get an optimal utilization of available power of the large common grid. The total complex system can be simulated in order to test out different configurations, applications and control algorithms in combination with so-called “smart grids”.

A key feature of the simulation system is its emphasis on statistical analysis. The statistics are related to solar radiation, wind speed and electrical load. Analyses of performed measurements have enabled well-founded starting points for statistical models.

The work introduces the use of "extinction coefficient" as an important parameter for calculation of effective solar radiation. This parameter is a measure of the attenuation of the solar radiation when passing through the atmosphere. By utilizing this parameter, a very good opportunity to calculate the solar radiation affecting a photovoltaic cell is provided. It has been shown that this parameter may be calculated using information from measurements but also from information resulting from specific software intended for transmittance calculations. The calculations are in this case based on different atmospheric conditions regarding

molecular concentration, temperature, humidity, air pressure, aerosols, pollution, rain, fog, etc.

It has been demonstrated that the usage of "number of sun hours" at a certain location to predict solar energy is a very uncertain method. The effective solar radiation that impacts a solar cell can vary a lot in full sunshine depending on temporary and/or local variation of the actual atmospheric attenuation.

The development potential of photovoltaic devices is discussed based on spectral analysis of incoming solar radiation. The conclusion of this analysis is that the efficiency of solar cells can be increased significantly by using alternative solar cell materials and production methods.

A number of simulation cases have been analysed. As examples of important observations from these analyses can be noted:

- The combination of wind power and solar power in a power plant increases the availability of energy significantly
- It is possible to define reasonable installed capacity of wind power and solar power at a power plant
- If a combined power system is equipped with an energy storage, then the availability of energy is increased significantly and it also reduces the need to use power back-up or importing energy from connected utility power grid.
- A combined power system with wind and solar power as energy sources must be supplemented by some form of energy reserve. This energy reserve can be an energy storage, an auxiliary device (e.g. diesel generator) or the possibility to connect the system to the utility grid.
- Solar tracking as a complement to a solar power system increases the produced solar power most significantly.
- To make it possible to plan an optimal location for a solar power plant, it is important to get information about local variations regarding the extinction coefficient

CHAPTER 15

FUTURE WORK

Future work should primarily focus on the following:

- Studies of the atmospheric transmission
- Studies of the high frequency components for the modeling of extinction coefficients and wind speeds. See sections 4.7.6 and 5.2.4
- To supplement the existing simulation model with hardware-oriented structures
- To prepare the model for studies of a number of interconnected combined power systems
- Continue the initiated work on simulations with a focus on:
  - Hardware applications
  - Interconnected combined power systems

Regarding PV-related issues, the following points should be included:

- Theoretical studies of the atmospheric transmission
- Studies concerning usage of the extinction coefficient for prediction of the effective solar radiation that impacts a solar cell. These studies shall even include methods to predict the extinction coefficient at certain locations.
- Measurements on PV cells

The results from these activities are material to validate and to complement the present simulation model.

Regarding the expansion of the model with hardware functions, the focus should be on the opportunity to study dynamic features. With an updated simulation model in respect of hardware functions, the possibility to analyse the dynamics in a power grid is increased. It is very interesting to prepare the model for analysis of a larger number of interconnected combined power systems. This make it possible, for instance, to study the benefits of smart grids as parts of utility grids.

15.1 Studies of the atmospheric transmission

15.1.1 Calculation. Clear sky

Spectral transmittance values shall be calculated by using Modtran (see [27], [43] and [57]). Transmittance values should be calculated for these defined cases:

- Tropical
- Midlatitude summer
- Midlatitude winter
- Subarctic summer
- Subarctic winter
- U. S. Standard

15.1.2 Calculation. Decreased visibility

This moment is focused on conditions where the visibility is decreased as a result of environmental contamination.

Spectral transmittance values shall be calculated by using Modtran (see [27], [43] and [57]).

15.1.3 Diffuse and direct radiation

Measurements of the direct and diffuse radiation shall be performed during varying condition of cloudiness.

15.1.4 Prediction of extinction coefficient at specified locations

In order to make it possible to plan an optimal location for a solar power plant, it is important to get information about local variations regarding the extinction coefficient. This means that a closer study of this topic needs to be performed. The study shall be done in the form of a combination of local measurements and the results from sections 15.1.1 - 15.1.3.

15.2 Heigh frequency components. Extinction coefficient and wind speed

See sections 4.7.6 and 5.2.4. The algorithms for modeling of the high frequency components should be further analyzed. This to improve the possibilities of good transient analysis in connection with a complement of hardware features in the model. See section 15.4. The task includes both extinction coefficient and wind speed.

15.3 Measurements

Extended measurements should be performed. The measurements shall be focused on validation and complementation of the present model. The following parameters are to be recorded:

- Short circuit current of PV cells
- Temperature of PV cells
- Date and time
- Incoming solar irradiation
  - Direct radiation
  - Diffuse radiation
- Air temperature
- Cloudiness

15.4 Expansion of the model with hardware functions

The present model is partly equipped with functions for dynamic evaluations. To fully implement such studies, some expansions of the model are needed. Fig. 15.1 illustrates a proposal of a total simulation model, expanded with Matlab functions, Simulink and Plecs.

The intention is to make it possible to perform dynamic tests relating to, for example, power quality, MPP-algorithms and power electronics.

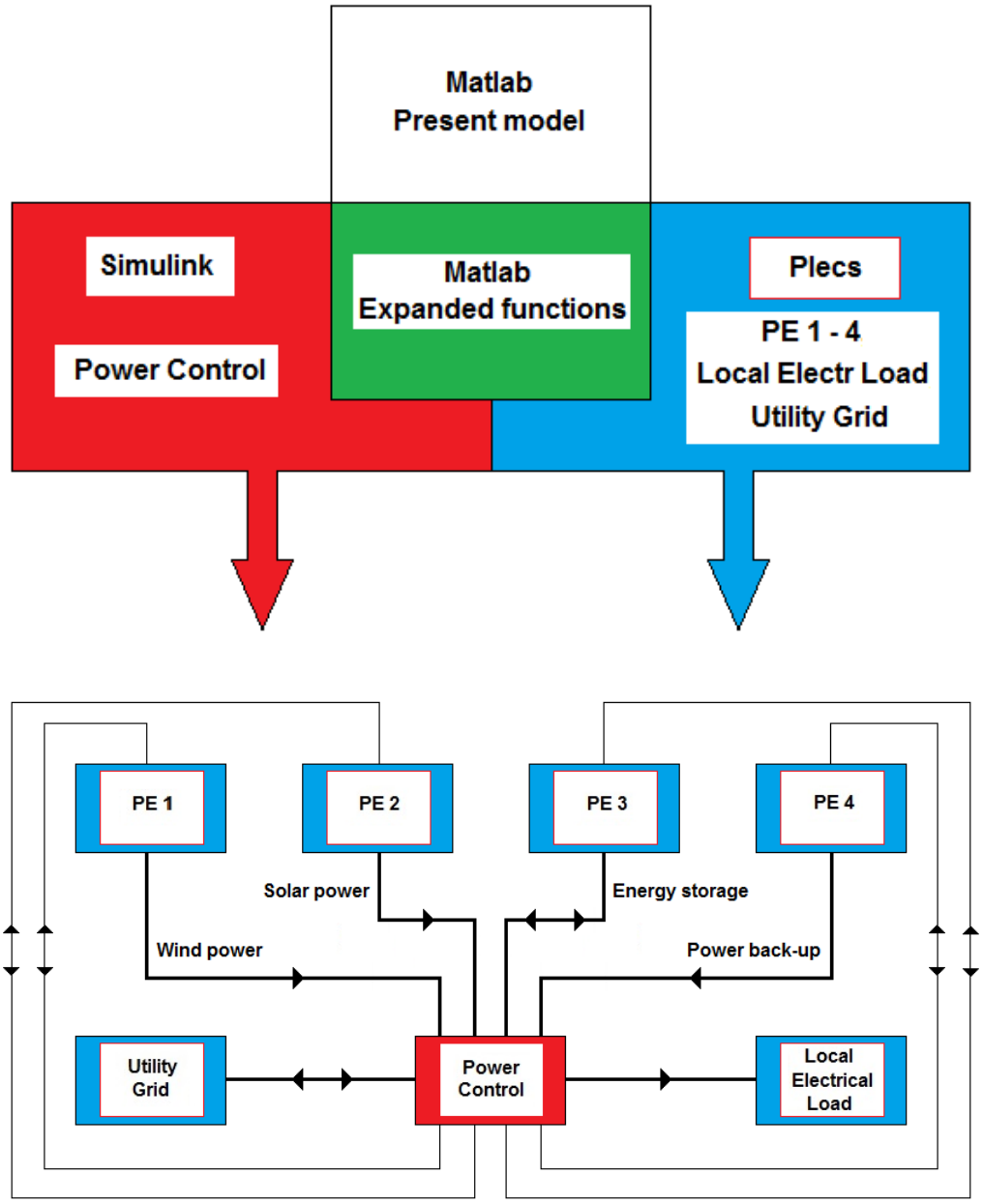

Fig. 15.1. Expanded simulation model with the combination of Matlab, Simulink and Plecs.

15.5 Preparing the model for a number of combined power systems

In chapter 12, the principle to expand the simulation model with a function for analysis of a larger number of interconnected combined power systems was discussed. Such an extension of the model makes it possible to study the benefits of including smart grids in the utility grids.

15.6 Further simulations

The performed simulations that are presented in chapter 7 to chapter 10 are a good basis for further simulations. Additional simulations with an updated simulation model are proposed for the purposes of:

- Analysis of the dynamic characteristics of different combined power systems
- Analysis of obtained results when using smart grids in ordinary power grids

REFERENCES

[1] Mathiasson I. “Simulation of autonomous electric power systems”. Chalmers University of Technology, 2015.

[2] Mathiasson I. “Solar power. Statistical analysis of extinction coefficients”. Chalmers University of Technology, 2015.

[3] Mathiasson I. “Modelling of an electrical load”. Chalmers University of Technology, 2015.

[4] Mathiasson I. “Wind power. Statistical analysis of wind speed”. Chalmers University of Technology, 2015.

[5] Mathiasson I. “Solar and Wind Power”. Chalmers University of Technology, 2016.

[6] Mathiasson I. “Simulation of a solar power farm”. Chalmers University of Technology, 2015.

[7] Mathiasson I. “Simulation of a wind power farm”. Chalmers University of Technology, 2015.

[8] Mathiasson I. “Simulation of a combined solar and wind power farm. Economic analysis.” Chalmers University of Technology, 2015.

[9] Mathiasson I, Carlson O. ”Prediction of solar power by using the extinction coefficient”. 5th Solar Integration Workshop, International Workshop on Integration of Solar Power into Power Systems, 2015.

[10] Mathiasson I. “Stochastic modelling of extinction coefficients for solar power applications”. Chalmers University of Technology, 2007.

[11] Mathiasson I. “Investigation of a Wind Power Generator. Part 1”. Chalmers University of Technology, 2005.

[12] Mathiasson I. “Investigation of a Wind Power Generator. Part 2”. Chalmers University of Technology, 2005.

[13] Schlyter P, based on T. van Flandern's and K. Pulkkinen's paper "Low precision formulae for planetary positions. Algorithms to calculate planetary positions for Sun, Moon and major planets". Published in the Astrophysical Journal Supplement Series, 1980.

[14] Yeh T, Wang L. "A study on generator capacity for wind turbines under various tower heights and rated wind speeds using Weibull distribution". IEEE TRANSACTIONS ON ENERGY CONVERSION, 2008.

[15] Madapati K, Ellsén M. "Hönö wind resource assessment. A statistical report on Chalmers wind turbine station data". Chalmers University of Technology, 2014.

[16] Messenger R. A, Ventre J. "Photovoltaic systems engineering", second edition. CRC Press, 2003.

[17] Markvart T. "Solar electricity", second edition. University of Southampton, UK, John Wiley & Sons, LTD, 2006.

[18] Liljequist G. H. "Meteorologi: Strålning". Uppsala Universitet, 1979.

[19] Chauhan A, Saini R. P. "Statistical analysis of wind speed data using Weibull distribution parameters". 1st International Conference on Non Conventional Energy, 2014.

[20] Haque M.H, Jayaratne K.G, Bernardo C.W. "Estimation of annual energy delivered by a variable speed wind generating system using historical wind data". 3rd International Conference on the Developments in Renewable Energy Technology, 2014.

[21] G. M. Masters, "Renewable and efficient electric power systems", John Wiley & Sons, Inc, 2004.

[22] "Experimental test site for small wind turbines of Narbonne. Test Report no. 15 version 4 of March, 25 2010. Skystream Grid Connected Wind Turbine". Sud Eoliennes Technologie, 2010.

[23] "Marknadsöversikt små vindkraftverk i Sverige". Svensk Vindkraftförening (SVIF), co-funded by Energimyndigheten, 2013.

[24] Westin P, Stenkvist M. "Produktionskostnadsbedömning för vindkraft i Sverige". Statens energimyndighet, ER 2014:16, ISSN 1403-1892.

[25] Mayer J. N. et al. "Current and future cost of photovoltaics". Fraunhofer-Institute for Solar Energy Systems (ISE), 2015.

[26] Rahman A. K et al. ”Study of rain attenuation with diversity of wavelengths propagation transmission in tropical rainforest region”**.** 2008 International Conference on Electronic Design, 2008.

[27] McClatchey R. A et al. ”Optical properties of the atmosphere”. Air Force Cambridge Research Laboratories, 1992.

[28] Thomas M. E, Duncan D. D. ”Atmospheric transmission”. The Infrared and Electro-Optical Systems Handbook, Volyme 2: Atmospheric Propagation of Radiation, Chapter 1, Infrared Information Analysis Center and Spie Optical Engineering Press, 1996.

[29] Shah S, Mughal S, Memon S. “Theoretical and empirical based extinction coefficients for fog attenuation in terms of visibility at 850 nm”. International Conference on Emerging Technologies (ICET), 2015.

[30] Chander S et al. “A study on spectral response and external quantum efficiency of mono-crystalline silicon solar cell”. INTERNATIONAL JOURNAL of RENEWABLE ENERGY RESEARCH, 2015.

[31] Milone E F, Wilson W J F. “Solar system astrophysics”. Springer New York Heidelberg Dordrecht London, 2014.

[32] Chen L, Yin Y, Ho, T, Chen Y. “Sensitized solar cells via nanomaterials: A recent development in quantum dots-based solar cells”. IEEE Journals & Magazines, 2014.

[33] Manna T K, Mahajan S M. “Nanotechnology in the development of photovoltaic cells”. International Conference on Clean Electrical Power, 2007.

[34] Honsberg C B, Barnett A M, Kirkpatric D. “Nanostructured solar cells for high efficiency photovoltaics”. IEEE 4th World Conference on Photovoltaic Energy Conference, 2006.

[35] Morgera A F, Lughi V. “Frontiers of photovoltaic technology: A review”. International Conference on Clean Electrical Power, 2015.

[36] Giannoccaro G, Muciaccia T, Passaro V M N. “Evaluation of the absorption spectrum in quantum dots for efficient solar cells”. Fotonica AEIT Italian Conference on Photonics Technologies, 2014.

[37] Nann S, Riordan C. “Solar spectral irradiance under overcast skies”. Conference record of the twenty first ieee photovoltaic specialists conference, 1990.

[38] Elkamchouchi H M, El-Shimy M A. “Monte carlo simulation of light propagation through the troposphere for free space optical communication”. Proceedings of the Twenty Third National Radio Science Conference, 2006.

[39] Choi J, Kim T. “Study on spectral transmission characteristics of the reflected and self-emitted radiations through the atmosphere”. IEEE International Conference on Multisensor Fusion and Integration for Intelligent Systems, 2008.

[40] Khan M S et al. “Selecting a distribution function for optical attenuation in dense continental fog conditions”. International Conference on Emerging Technologies, 2009.

[41] Varonides A C, Spalletta R A. “Full spectrum absorption through 1ev-tuning in a p-i (mqw)-n high efficiency solar cell”. 34th IEEE Photovoltaic Specialists Conference, 2009.

[42] Bernstein L S, Berk A, Fox M J, Sundberg R L. “An extended-wavelength exoplanet spectral model based on modtran 5”. 2nd Workshop on Hyperspectral Image and Signal Processing: Evolution in Remote Sensing, 2010.

[43] Qiang F et al. “Study of a mixture programming software on atmosphere transmission”. 12th IEEE International Conference on Communication Technology, 2010.

[44] Shivaganaik H, Jangamshetti S H. “Modeling and analysis of multi-junction solar cells”. International Conference on Emerging Trends in Electrical and Computer Technology, 2011.

[45] Cole I R, Betts T R, Gottschalg R. “Solar profiles and spectral modeling for CPV simulations”. IEEE Journal of Photovoltaics, 2012.

[46] Jooshesh A, Gulliver T A, Uysal S. “Space to ground optical power transmission”. Seventh International Conference on Broadband, Wireless Computing, Communication and Applications, 2012.

[47] Rammprasath K, Shanthi P. “Analyzing the cloud attenuation on the performance of free space optical communication”. International Conference on Communication and Signal Processing, 2013.

[48] Brazda V, Fiser O. “Long-term analysis of atmospheric effects on free space optical links”. SBMO/IEEE MTT-S International Microwave & Optoelectronics Conference, 2013.

[49] Fenn R W et al. “Optical and infrared properties of the atmosphere”. Handbook of Geophysics and Space Environment, Chapter 18, Air Force Research Laboratory, 1985.

[50] Partain L, Fraas L. “Displacing California's coal and nuclear generation with solar PV and wind by 2022 using vehicle-to-grid energy storage”. IEEE 42nd Photovoltaic Specialist Conference, 2015.

[51] Naimullah B S et al. “Comparison of wavelength propagation for free space optical communications”. ICED 2008. International Conference on Electronic Design, 2008.

[52] Fiser O, Rejfek L, Brazda V. “On forward and backward scattering from fog and rain drops”. 13th Conference on Microwave Techniques, 2013.

[53] Zhuanhong Jia, Qinglin Zhu, Faliang Ao. “Atmospheric attenuation analysis in the FSO link”. International Conference on Communication Technology, 2006.

[54] Fiser O, Schejbal V. “Comparison of formulas estimating fog attenuation on free space optics links”. Proceedings of the Fourth European Conference on Antennas and Propagation, 2010.

[55] Burger B et al. “Photovoltaics report”. Fraunhofer Institute for Solar Energy Systems, ISE with support of PSE AG, 2016.

[56] Clark R N. “Spectroscopy of rocks and minerals, and principles of spectroscopy”. Chapter 1, Manual of Remote Sensing, John Wiley and Sons, Inc, 1999.

[57] Kneizys F X et al. “The MODTRAN 2/3 Report and LOWTRAN 7 MODEL”. Ontar Corporation, 1996.

[58] Riordan C, Hulstrom R. “WHAT IS AN AIR MASS 1.5 SPECTRUM?”. Conference Record of the Twenty First IEEE Photovoltaic Specialists Conference, 1990.

[59] Nadeem F, Leitgeb E, Kandus G. “Comparing The Cloud Effects on Hybrid Network Using Optical Wireless and GHz Links”. 7th International Symposium on Communication Systems Networks and Digital Signal Processing, 2010.

[60] Capsoni C, Luini L, Nebuloni R. “Prediction of Cloud Attenuation on Earth-space Optical Links”. 6th European Conference on Antennas and Propagation, 2012.

[61] Capsoni C, Luini L, Nebuloni R. “Site Diversity: A Promising Technique to Counteract Cloud Attenuation on Earth-Space Optical Links”. International Workshop on Optical Wireless Communications, 2012.

[62] Sydney D P. “Investigation of cirrus clouds using the Calipso lidar data”. IEEE International Geoscience and Remote Sensing Symposium, 2010.

[63] Flood D J. “Quantum Dot Solar Cells: A Potential Game Changer For World Energy Production”. Natcore Technology, Inc., 2013.

[64] Rühle S, Shalom M, Zaban A. “Quantum-Dot-Sensitized Solar Cells”. Wiley-VCH Verlag GmbH & Co, 2010.

[65] Lee J, Goodnick S M, Honsberg C B. “Limiting efficiency of silicon based nanostructure solar cells for multiple exciton generation”. IEEE 39th Photovoltaic Specialists Conference, 2013.

[66] Tian J, Cao G. “Semiconductor quantum dot-sensitized solar cells”. Nano Reviews, 2013.

[67] Rudemo M, Råde L. “Sannolikhetslära och statistik med tekniska tillämpningar. Del 1”. Biblioteksförlaget. Stockholm, 1965.

[68] Carlson O. ”Hand written information regarding performance of a small solar power system”. Chalmers University of Technology, 2016.

[69] MittResVäder. http://www.mittresvader.se

[70] Pazheri F.R, Khan H, Ahamed I. ”Smart grid implementation across the globe: A survey”. IEEE PES Innovative Smart Grid Technologies - India (ISGT India), 2011.

[71] Blaabjerg F, Guerrero J M. “Smart grid and renewable energy systems”. International Conference on Electrical Machines and Systems (ICEMS), 2011.

[72] Ellsén M, Mathiasson I, Carlson Ola. “Series and Parallel Compensation for the Permanent Magnet Synchronous Generator at Chalmers Test Wind Turbine”. NORDIC WIND POWER CONFERENCE, 2006.

APPENDIX A CALCULATION OF SOLAR POSITION

This section is a summary of the expressions used for prediction of solar position in the sky. The expressions are taken from [13].

Input data for the calculations is:

- Geographic location in the form of latitude and longitude
- Time of the year and time of the day

Output data is:

- Solar position in the form of angle over horizon (alpha) and angle relative to south (az)

Used expressions follow according to (A 1) - (A 28).

$$UT = star\_hour + time\_counter/60 \times count\_interval \quad \text{(A 1)}$$

Where:

- UT: ”Universal Time” expressed in hours + decimals
- start_hour : Start hour for simulation (0 if the simulation will start at midnight)
- time_counter : Simulation step in question. This parameter will step from 1 up to an uper limit named time_counter_limit
- count_interval : Simulation interval per step. This parameter is specified in minutes or parts of a minute

$$time\_counter\_limit = 60 \times (stop\_hour - start\_hour) / count\_interval \quad \text{(A 2)}$$

Where:

- time_counter_limit: upper limit for simulation steps

- *stop_hour* : stop hour for the simulation (24 if the simulation is to be performed during 24 hours, 240 if the simulation is to be performed during 10 days, and so on)

$$d = 367 \times y - \text{floor}(7 \times (y + \text{floor}((m + 9) / 12)) / 4) + \\ + \text{floor}(275 \times m / 9) + D - 730530 + UT / 24 \quad \text{(A 3)}$$

Where:

- d: day number from 2000, Jan 01
- y: year in question (e.g. 2015)
- *m*: month in question (month number)
- *D*: date (day number in the month)

Note: floor(x) rounds “x” down to the nearest integer.

$$ecl = 23.4393 - 3.563 \times 10^{-7} \times d \quad \text{(A 4)}$$

Where:

- ecl: “the obliquity of the ecliptic”, i.e. the “tilt” of the Earth’s axis of rotation (currently approx. 23.4 degrees and slowly decreasing)

<u>Orbital elements of the Sun. These elements are partly used in the calculation of the sun’s position</u>:

- *N*: longitude of the ascending node
- *i*: inclination to the ecliptic (plane of the Earth’s orbit)
- *w*: argument of perihelion
- *a*: semi-major axis, or mean distance from Sun
- *e*: eccentricity (0=circle, 0-1=ellipse, 1=parabola)
- *M*: mean anomaly (0 at perihelion; increase uniformly with time)

In this case, the following is valid:

- $N = 0.0$

- $i = 0.0$
- $a = 1.0$

$$w = 282.9404 + 4.70935 \times 10^{-5} \times d \quad \text{(A 5)}$$

$$e = 0.016709 - 1.15 \times 10^{-9} \times d \quad \text{(A 6)}$$

$$M = 356.0470 + 0.9856002585 \times d \quad \text{(A 7)}$$

Compute the eccentric anomaly *E* from the mean anomaly *M* and from the eccentricity *e* (*E* and *M* in degrees):

$$E = M + e \times \left(\frac{180}{\pi}\right) \times \sin\left(\frac{M}{180}\right) \times (1.0 + e \times \cos\left(\frac{M}{180}\pi\right)) \quad \text{(A 8)}$$

Compute the Sun's distance r and its true anomaly v from:

$$Xv = r \times \cos\left(\frac{v}{180}\pi\right) = \cos\left(\frac{E}{180}\pi\right) - e \quad \text{(A 9)}$$

$$Yv = r \times \sin\left(\frac{v}{180}\pi\right) = \sqrt{1.0 - e^2} \times \sin\left(\frac{E}{180}\pi\right) \quad \text{(A 10)}$$

$$v = \text{atan2}(Yv, Xv) \times \frac{180}{\pi} \quad \text{(A 11)}$$

Note: atan2 is a function that converts a coordinate pair to the correct angle in all four quadrants.

$$r = \sqrt{Xv^2 + Yv^2} \quad \text{(A 12)}$$

Compute the Sun's true longitude, lonsun:

$$lonsun = v + w \quad \text{(A 13)}$$

Convert lonsun and r to ecliptic rectangular geocentric coordinates Xs and Ys

$$Xs = r \times \cos\left(\frac{lonsun}{180}\pi\right) \quad \text{(A 14)}$$

$$Ys = r \times \sin(\frac{\mathbf{lonsun}}{\mathbf{180}}\boldsymbol{\pi}) \quad \text{(A 15)}$$

As Sun is in the ecliptic plane, Zs is zero. Xs and Ys is the Sun's position in a coordinate system in the plane of the ecliptic.

Convert to equatorial, rectangular, geocentric coordinates:

$$Xe = Xs \quad \text{(A 16)}$$

$$Ye = Ys \times \cos(\frac{\mathrm{ecl}}{180}\pi) \quad \text{(A 17)}$$

$$Ze = Ys \times \sin(\frac{\mathrm{ecl}}{180}\pi) \quad \text{(A 18)}$$

Compute Sun's Right Ascension (RA) and Declination (Dec):

$$RA = \mathrm{atan2}(Ye, Xe) \times \frac{180}{\pi} \quad \text{(A 19)}$$

$$Dec = \mathrm{atan2}(Ze, \sqrt{Xe^2 + Ye^2} \times \frac{180}{\pi} \quad \text{(A 20)}$$

Compute Sun's mean longitude, L:

$$L = M + w \quad \text{(A 21)}$$

Compute "the Sidereal Time at Greenwich", GMST0, at 00:00 "Universal Time":

$$GMST0 = L + 180 \quad \text{(A 22)}$$

GMST0 is expressed in degrees to simplify the computations. GMST0 = 360 degrees corresponds to 24 hours, i.e. each hour corresponds to 15 degrees.

Compute Local Sidereal Time, LST:

$$LST = GMST0 + UT \times 15.0 + long \quad \text{(A 23)}$$

Where:

- UT: ”Universal Time” expressed in hours + decimals
- Long: local longitude in degrees. East longitude counts as positive and west longitude as negative

Compute Sun’s Local Hour Angle, LHA, i.e. the angle the Earth has turned since the Sun was last in south:

LHA = LST - RA (A 24)

Compute Sun’s altitude above the horizon, alpha:

sin_alpha = $\cos(\frac{\mathrm{Dec}}{180}\pi) \times \cos(\frac{\mathrm{lat}}{180}\pi) \times \cos(\frac{\mathrm{LHA}}{180}\pi) + \sin(\frac{\mathrm{Dec}}{180}\pi) \times \sin(\frac{\mathrm{lat}}{180}\pi)$ (A 25)

where:

lat : the latitude in question

alpha = arcsin(sin_alpha) (A 26)

(radians)

Compute Sun’s azimuth, az:

$\mathrm{cos\_az} = \frac{\cos(\frac{\mathrm{Dec}}{180}\pi)\times\sin(\frac{\mathrm{lat}}{180}\pi)\times\cos(\frac{\mathrm{LHA}}{180}\pi)-\sin(\frac{\mathrm{Dec}}{180}\pi)\times\cos(\frac{\mathrm{lat}}{180}\pi)}{\cos(\mathrm{alpha})}$ (A 27)

az = arccos(cos_az) (A 28)

(radians)